



Characterization of binding mechanisms and mobility of metals and metalloids under the influence of increased carbon dioxide in mofette soils

Dissertation

zur Erlangung des akademischen Grades
einer Doktorin der Naturwissenschaften (Dr. rer. nat.)
an der Fakultät für Biologie, Chemie und Geowissenschaften
der Universität Bayreuth

vorgelegt von:

Judith Mehlhorn
(MSc. Geoökologie)

geboren in Gera

Bayreuth, November 2018

Die vorliegende Arbeit wurde in der Zeit von Oktober 2014 bis November 2018 in Bayreuth am Lehrstuhl Umweltgeochemie unter Betreuung von Frau Professorin Dr. Britta Planer-Friedrich angefertigt.

Vollständiger Abdruck der von der Fakultät für Biologie, Chemie und Geowissenschaften der Universität Bayreuth genehmigten Dissertation zur Erlangung des akademischen Grades einer Doktorin der Naturwissenschaften (Dr. rer. nat.).

Dissertation eingereicht am: 15.11.2018

Zulassung durch die Promotionskommission: 05.12.2018

Wissenschaftliches Kolloquium: 08.02.2019

Amtierender Dekan: Prof. Dr. Stefan Peiffer

Prüfungsausschuss:

Prof. Dr. Britta Planer-Friedrich (Gutachterin)

Prof. Dr. Thilo Rennert (Gutachter)

Prof. Dr. Martin Obst (Vorsitz)

Prof. Dr. Egbert Matzner

ACKNOWLEDGEMENTS

First of all, I would like to thank my doctoral advisor Prof. Dr. Britta Planer-Friedrich for giving me the opportunity to continue my work on metal(loid)s in mofette soils after my master thesis. I am sincerely grateful for her constant and intense scientific support, especially, for the numerous helpful discussions and for the guidance I received during this work. Furthermore, I would like to thank her for the various opportunities to broaden my scientific horizon, also beyond the topic of my PhD thesis, by enabling me the participation in sampling campaigns, field trips, and scientific conferences.

I acknowledge financial support from the German Academic Scholarship Foundation for a three-year PhD stipend and the financial support from University of Bayreuth Graduate School for a three-month 'Feuerwehrfonds' as well as for travel grants to the EuCheMS conference 2014 in Istanbul and to the Goldschmidt Conference 2015 in Prague.

Special thanks also go to my collaborators. For their support with XAS data collection and interpretation as well as for their helpful contributions to the manuscript on copper in mofettes, I would like to thank Prof. Dr. Ruben Kretzschmar from ETH Zürich, Prof. Dr. Jon Petter Gustafsson from SLU Uppsala, my colleague Johannes Besold, and Dr. Juan Lezama Pacheco from Stanford University. I am grateful to Prof. Dr. Andreas Kappler and Dr. James Byrne from Tübingen University for conducting Mössbauer spectroscopy and for their helpful contributions to the manuscript on short-term mobilization processes in mofettes.

Many thanks of course go to all my present and former colleagues from the Environmental Geochemistry Group, who accompanied me during my PhD. I am especially grateful to Dr. Regina Lohmayer, Dr. Sinikka Hinrichsen, Dr. Maria Ullrich, Dr. Julia Arndt, Carolin Kerl, Johannes Besold, Dr. Jörg Schaller, and Dr. Samer Bachmaf for their support and helpful advices as well as for their interest in my work. Thanks go to Stefan Will for assistance with ICP-MS analyses. I would also like to thank my supervised bachelor students Rouven Metz and Lukas Gerber as well as my Hiwis Nadja Knauer, Esther Breuninger, and Kai Jansen for their great cooperation.

I acknowledge helpful discussions with Prof. Dr. Egbert Matzner, Prof. Dr. Martin Obst, and Prof. Dr. Marcus Horn.

Furthermore, I am sincerely grateful to the numerous people, who contributed to this work by providing equipment or access to instruments, conducting analyses, or helping with data interpretation, namely, Dr. Benjamin Gilfedder, Silke Hammer, Martina Rohr, Jutta Eckert, and Heidi Zier from the Hydrology Department, the staff from the Geo workshop, Dorothea Wiesner and Dr. Tiziana Boffa Ballaran from BGI, Dr. Oliver Schmidt, Ralf Mertens, and Anita Gössner from ÖMIK, Beate Bojer from AC III, Dr. Stefan Schwarz and Anna-Maria Dietel from AC II, Manfred Fischer from

Geomorphology, Prof. Dr. Ruth Freitag and Nicolas Weithmann from Process Biotechnology, Helga Rupp, and the staff from SSRL. I also thank Prof. Dr. Andreas Kappler, Dr. Tina Gauger, Wiebke Ruschmeier, and Dominik Wimmer for providing microbial cultures and for help with their cultivation. Furthermore, I would like to thank everyone, who participated in the 2014 drilling campaign in Czech Republic, even if the obtained data were unfortunately not coherent enough to be included in this thesis. Special thanks go to Dr. Horst Kämpf from the GFZ Potsdam for organizing this drilling campaign, as well as to Dr. Jörg Schaller and Benedikt Werner for their help with the collection and stabilization of samples.

For proof-reading, I am thankful to Dr. Regina Lohmayer, Dr. Boris Plüschke, and Dr. Daniel Forberg.

Last but not least, I would like to thank my family, especially my parents and my partner, who always motivated me and helped me to overcome hard times. Without your support this would not have been possible.

ABSTRACT

Mofettes are natural exhalation sites of geogenic carbon dioxide (CO₂), which mainly occur in seismically active regions. Soil conditions at such sites are strongly influenced by extreme CO₂ partial pressure. The soil is anoxic up to the surface and CO₂ dissolution in pore water causes soil acidification. Formation of pedogenic iron (oxyhydr)oxides is inhibited and decomposition of organic material is decelerated in such soils leading to accumulation of poorly degraded soil organic matter (SOM). These changes in soil conditions can affect metal(loid) binding mechanisms and thus the mobility of metal(loid)s in soil. Carbon dioxide triggered mobilization may become dangerous if large amounts of potentially toxic metal(loid)s are mobilized into aquifers, while immobilization can constitute a risk for plants and soil organisms by limitation of essential trace elements.

The aim of the present thesis was to investigate CO₂-induced changes in binding processes and the mobility of several (trace) metal(loid)s. Besides aluminum (Al), cadmium (Cd), cobalt (Co), chromium (Cr), nickel (Ni), and zinc (Zn), special attention was paid to the elements iron (Fe), arsenic (As), manganese (Mn), and copper (Cu). The studied mofette site is located in the Cheb Basin in northwestern Czech Republic.

In a first study, the spatial distribution of the mentioned metal(loid)s around a main degassing feature of the mofette site was investigated both for soil and pore water. Sequential extraction of selected soil samples was used to assign distinct groups of metal(loid) binding. The spatial distribution and mobility of Fe and As were mainly determined by the presence of Fe (oxyhydr)oxides, which could form as soon as traces of oxygen were available. Aluminum and Cr were predominantly incorporated into aluminosilicates and showed almost no mobilization. Depletion around the main degassing center could be explained by decreased mineral contents due to SOM accumulation. The metals Co, Mn, and Ni were depleted within the whole CO₂-influenced area due to release from increased weathering of silicates and leaching, following long-term CO₂-induced soil acidification. The only elements that showed enrichment directly in the degassing center were Cd, Cu, and Zn. Effective sequestration of these chalcophilic metals was attributed to the formation and (co-)precipitation of sulfidic minerals. The highest metal(loid) pore water concentrations correlated with dissolved organic carbon concentrations and were observed close to the degassing center for Al, As, Cr, Cu, Fe, and Zn. Due to anoxic conditions, poorly degraded, easily mobilized SOM accumulates in mofettes. Complexation with dissolved organic matter (DOM) prevents re-adsorption and leads to increased mobility of these metal(loid)s.

In a second study, short-term mobilization processes of Fe, As, Mn, and Cu following CO₂ intrusion into a hitherto non-CO₂-influenced soil were studied in laboratory batch experiments, using non-CO₂-influenced soil from close vicinity of the mofette. Fast, abiotic mobilization of metal cations (shown

for Mn) occurred due to surface protonation, however, overall mobilization remained low. After depletion of other electron acceptors, microbially triggered reductive dissolution of Fe (oxyhydr)oxides began, mobilizing large amounts of Fe and incorporated metal(loid)s like As.

In a last study, Cu mobility was investigated both by studying a transect over the mofette site and by conducting a Cu-spike experiment with natural, SOM-rich topsoil from this transect. Sorption isotherms for Cu were determined and Cu solid-phase speciation was investigated using X-ray absorption spectroscopy. Copper mobility was highest in soils from the transition between oxic (reference) and anoxic (mofette) conditions, while strong Cu sequestration and high adsorption coefficients were determined for soil from the degassing center. Solid-phase speciation revealed that Cu reduction and precipitation of Cu sulfides was the main sequestration process in the permanently anoxic degassing center. In transition and reference soils, Cu binding to SOM was the dominating process. The lower degradation state of SOM in the mofettes has a negative effect on SOM stability, which could be seen by an increasing dissolved-to-solid-phase ratio of organic carbon with increasing CO₂. Thus, also Cu mobility increased with increasing CO₂ influence since Cu both complexed with DOM and solid-phase SOM. Mobility was highest in some meters distance from the degassing center, where micro-oxic conditions prevented Cu sulfide precipitation.

Overall, both metal(loid) mobilization and immobilization were found to occur in CO₂-influenced soils, necessitating risk assessment with regard to potential ground water contamination or trace element limitations at such sites. Desorption and mineral dissolution are the main mobilization processes while sulfide mineral precipitation of chalcophilic metals is the main immobilizing process in mofette soils. Carbon dioxide influence on these processes is primarily indirect, via soil acidification and creation of anoxic conditions. Fast metal(loid) mobilization via desorption and reductive dissolution of Fe (oxyhydr)oxides are dominating processes on a short-term scale. Ongoing CO₂ exhalation will induce further metal(loid) release via silicate weathering and subsequent leaching. The highest mobilization risk on a long-term scale arises from metal(loid) complexation with DOM, which can exhibit strongly elevated concentrations close to the degassing center.

ZUSAMMENFASSUNG

Mofetten sind natürliche Austrittsstellen von geogenem Kohlenstoffdioxid (CO₂). Sie treten vor allem in seismisch aktiven Regionen auf. Die extremen CO₂-Konzentrationen beeinflussen maßgeblich die Bodenbedingungen, die um Mofetten herum herrschen. So ist der Boden bis an die Oberfläche anoxisch und CO₂-Lösung im Porenwasser bewirkt eine fortschreitende Bodenversauerung. Die Bildung pedogener Eisen(oxyhydr)oxide ist in Mofettenböden ebenso gehemmt wie die Streuzersetzung, was zur Anreicherung von organischer Bodensubstanz (SOM) führt. All diese Änderungen der Bodenbedingungen können sich maßgeblich auf Bindungsmechanismen und somit auf die Mobilität von Metall(oid)en auswirken. Eine CO₂-induzierte Mobilisierung kann gefährlich werden, wenn potenziell toxische Metall(oid)e ins Grundwasser gelangen, wohingegen eine Immobilisierung essenzieller Spurenelemente ein Risiko für Pflanzen und Bodenorganismen darstellt.

Ziel der vorliegenden Arbeit war es, CO₂-induzierte Änderungen in den Bindungsmechanismen und der Mobilität einiger ausgewählter Metal(oid)e zu untersuchen. Neben Aluminium (Al), Cadmium (Cd), Kobalt (Co), Chrom (Cr), Nickel (Ni) und Zink (Zn) wurde ein besonderes Augenmerk auf die Elemente Eisen (Fe), Arsen (As), Mangan (Mn) und Kupfer (Cu) gelegt. Das untersuchte Mofettengebiet befindet sich im Egerbecken im Nordwesten der Tschechischen Republik.

In einer ersten Studie wurde die räumliche Verteilung der genannten Metall(oid)e um eine CO₂-Entgasungsstelle sowohl für die Bodenfestphase als auch im Porenwasser untersucht. Mit Hilfe einer sequenziellen Extraktion konnten einzelne Fraktionen verschiedenen Bindungsmechanismen zugeordnet werden. Die räumliche Verteilung der Fe- und As-Gehalte war vor allem an das Vorhandensein von Eisen(oxyhydr)oxiden gebunden, welche sich überall dort bilden konnten, wo Spuren von Sauerstoff verfügbar waren. Aluminium und Cr waren überwiegend in Form von Aluminosilikaten gebunden und zeigten kaum Mobilisierung. Die niedrigen Gehalte rund um das Entgasungszentrum waren hauptsächlich auf einen niedrigeren Gesamtmineralgehalt aufgrund der SOM-Anreicherung zurückzuführen. Die Bodengehalte von Co, Mn und Ni waren im gesamten CO₂-beeinflussten Bereich deutlich erniedrigt. Diese Metalle wurden vermutlich durch die CO₂-induzierte Bodenversauerung und die dadurch deutlich beschleunigte Silikatverwitterung freigesetzt und aus dem Bereich der Mofette ausgewaschen. Cadmium, Cu und Zn waren die einzigen Elemente, die im Entgasungszentrum angereichert wurden. Die effektive Festlegung dieser chalkophilen Elemente konnte auf die Bildung und (Mit-)Fällung von Sulfidmineralen zurückgeführt werden. Die höchsten Metall(oid)-Konzentrationen im Porenwasser wurden in unmittelbarer Nähe zum Entgasungszentrum für die Elemente Al, As, Cr, Cu, Fe und Zn beobachtet und korrelierten mit dem gelösten organischen Kohlenstoff. Aufgrund der anoxischen Bedingungen reichert sich nur gering zersetzte organische Substanz in den Mofetten an, welche leicht in die Flüssigphase mobilisiert werden kann. Eine

Komplexierung der genannten Metall(oid)e mit gelöster organischer Substanz (DOM) kann eine Adsorption verhindern und die Mobilität der Metall(oid)e erhöhen.

In einer zweiten Studie wurden Kurzzeit-Mobilisierungsprozesse für Fe, As, Mn und Cu untersucht, die unmittelbar nach einer CO₂-Freisetzung in einen bis dahin nicht CO₂-beeinflussten Boden auftreten können. Dafür wurden Batchversuche mit einem CO₂-unbeeinflussten Boden aus unmittelbarer Nähe zur Mofette durchgeführt. Zunächst war die schnelle, abiotische Mobilisierung von Metallkationen (gezeigt an Mn) durch eine fortschreitende Protonierung der Sorptionsoberflächen zu beobachten, jedoch war die Gesamtmobilisierung über diesen Prozess recht niedrig. Nach 1 bis 3 Tagen begann eine starke Fe-Mobilisierung durch die mikrobiell getriggerte, reduktive Auflösung von Eisen(oxyhydr)oxiden, durch die auch inkorporierte Metal(loid)e wie As freigesetzt wurden.

In einer dritten Studie wurde der CO₂-Einfluss auf die Mobilität von Cu untersucht. Dafür wurden Boden- und Porenwasserproben von einem Transekt über die Mofette analysiert und Cu-Spike-Experimente mit natürlichem, SOM-reichem Oberboden dieses Transekts durchgeführt, um Sorptionsisothermen zu bestimmen. Des Weiteren wurde die Festphasenspezifizierung von Cu mittels Röntgenabsorptionsspektroskopie bestimmt. Die Cu-Mobilität war im Übergangsbereich zwischen oxidischen (Referenz) und anoxischen (Mofette) Bedingungen am höchsten, wohingegen im Entgasungszentrum eine starke Cu-Festlegung und sehr hohe Adsorptionskoeffizienten beobachtet wurden. Anhand der Cu-Festphasenspezifizierung konnte gezeigt werden, dass die starke Cu-Sequestrierung im permanent anoxischen Entgasungszentrum durch eine Cu-Reduktion und die anschließende Fällung von Sulfidmineralen verursacht wurde. Im Übergangsbereich und im Referenzboden war Cu überwiegend an SOM gebunden. Ein zunehmendes Verhältnis von gelöstem organischen Kohlenstoff zu Festphasen-Kohlenstoff mit zunehmendem CO₂-Einfluss zeigte, dass sich der geringere Zersetzungsgrad von SOM in Mofetten negativ auf die SOM-Stabilisierung auswirkt. Kupfer bindet sowohl an DOM als auch an Festphasen-SOM. Dies bewirkte die beobachtete Zunahme der Cu-Mobilität mit zunehmendem CO₂-Gehalt des Bodens. Die Cu-Mobilität war einige Meter vom Entgasungszentrum entfernt am höchsten, da hier das Vorhandensein geringer Sauerstoffmengen die Ausfällung von Cu-Sulfiden verhinderte.

Insgesamt konnte gezeigt werden, dass sowohl Metall(oid)-Mobilisierungs- als auch Immobilisierungsprozesse in CO₂-beeinflussten Böden stattfinden. Potenzielle Risiken hinsichtlich einer Grundwasserkontamination oder durch die Immobilisierung essenzieller Spurenelemente sollten an solchen Standorten berücksichtigt werden. Desorption und Mineralauflösung sind Hauptprozesse bezüglich der Metall(oid)-Mobilisierung in Mofettenböden, während die Fällung chalkophiler Metalle in Form von Sulfidmineralen einen Hauptimmobilisierungsprozess darstellt. Das CO₂ wirkt sich über die induzierte Bodenversauerung und die anoxischen Bodenbedingungen in erster Linie indirekt auf diese Prozesse aus. Bei kurzzeitigem CO₂-Einfluss ist mit einer schnellen Metall(oid)-Mobilisierung

durch Desorption und Eisen(oxyhydr)oxid-Auflösung zu rechnen. Eine kontinuierliche CO₂-Ausgasung kann durch verstärkte Silikatverwitterung weitere Metall(oid)-Freisetzung und -Auswaschung bewirken. Das größte langfristige Risiko für eine erhöhte Metall(oid)-Mobilität stellen die stark erhöhten DOM-Konzentrationen in der Nähe des Entgasungszentrums durch die mögliche Bildung von Metall(oid)-DOM-Komplexen dar.

TABLE OF CONTENTS

| | |
|--|------|
| Acknowledgements | V |
| Abstract | VII |
| Zusammenfassung | IX |
| Table of contents | XIII |
| List of Abbreviations | XV |
| List of Figures | XVII |
| Extended Summary | 1 |
| 1 Introduction | 1 |
| 1.1 Mofettes – special study sites and natural laboratories | 1 |
| 1.1.1 Geological background, surface appearance, fauna, and flora | 1 |
| 1.1.2 Mofettes as natural laboratories and analogies to leakage from GCS sites | 3 |
| 1.1.3 Study site in the Plesná valley (Czech Republic) | 4 |
| 1.1.4 Carbon dioxide as soil-forming factor | 8 |
| 1.2 Influence of carbon dioxide on metal(loid) mobility in soil | 10 |
| 1.2.1 Influence of carbon dioxide induced soil acidification | 10 |
| 1.2.2 Influence of carbon dioxide induced anoxic conditions | 10 |
| 1.2.3 Previous results on metal(loid) mobility at the mofette site studied in this thesis | 11 |
| 1.3 Objectives | 13 |
| 2 Methods | 15 |
| 2.1 General practices and analytical methods | 15 |
| 2.1.1 Sampling and laboratory practices | 15 |
| 2.1.2 Analytical methods with respect to metal(loid)s | 15 |
| 2.1.3 Methods used for soil and pore water characterization | 16 |
| 2.2 Spatial scale: determination of metal(loid) distribution patterns around a mofette (study 1) | 17 |
| 2.3 Temporal scale: time dependency of carbon dioxide induced metal(loid) mobilization in soil (study 2) | 17 |
| 2.4 Case study on copper: sorption behavior and solid-phase speciation of copper in mofettes (study 3) | 18 |

| | | |
|-----|---|-----|
| 3 | Results and Discussion..... | 19 |
| 3.1 | Spatial distribution of metal(loid)s around a mofette and implications on soil processes (study 1)..... | 19 |
| 3.2 | Time and temperature dependency of carbon dioxide induced metal(loid) mobilization in soil (study 2)..... | 21 |
| 3.3 | Copper mobilization and sequestration in mofettes – the role of redox conditions and soil organic matter (study 3) | 25 |
| 4 | Conclusion..... | 29 |
| | References | 33 |
| | Contribution to studies 1 to 3 | 41 |
| | Appendix: Studies 1 - 3..... | 43 |
| | STUDY 1: Spatial distribution of metal(loid) depletion and accumulation zones around a natural carbon dioxide degassing site..... | 45 |
| | STUDY 2: Time and temperature dependency of carbon dioxide triggered metal(loid) mobilization in soil. | 75 |
| | STUDY 3: Copper mobilization and immobilization along an organic matter and redox gradient – insights from a mofette site | 109 |
| | List of publications..... | 147 |
| | Supervised Bachelor theses | 149 |
| | (Eidesstattliche) Versicherungen und Erklärungen | 151 |

LIST OF ABBREVIATIONS

| | |
|------------------|---|
| CCS | carbon capture and storage |
| DOC | dissolved organic carbon |
| DOM | dissolved organic matter |
| EXAFS | extended X-ray absorption fine structure |
| FTIR | Fourier-transform infrared spectroscopy |
| GCS | geologic carbon storage |
| ICDP | International Continental Scientific Drilling Program |
| ICP-MS | inductively coupled plasma mass spectrometry |
| MLFZ | Mariánské Lázně Fault Zone |
| MPN | most probable number |
| NMR | nuclear magnetic resonance |
| $p(\text{CO}_2)$ | partial pressure of carbon dioxide |
| PPZ | Počátky-Plesná Zone |
| r_s | Spearman's rank correlation coefficient |
| SEM-EDS | scanning electron microscopy energy-dispersive X-ray spectroscopy |
| SOC | soil organic carbon |
| SOM | soil organic matter |
| SSR | soil-to-solution ratio |
| XANES | X-ray absorption near edge structure |
| XAS | X-ray absorption spectroscopy |
| XRD | X-ray powder diffraction |

LIST OF FIGURES

| | |
|---|----|
| Figure 1. Geological situation at the study site. (a) Geological map of the Ohře Rift (Eger Graben) System as presented by Bussert et al. (2017). The black cross marks the study site of this thesis. (b) Conceptual model of the geodynamic situation in northwest Bohemia as presented by Bräuer et al. (2008) with the three main degassing areas Bublák, Mariánské Lázně, and Karlovy Vary being supplied from different reservoirs at the crust-mantle boundary. Blue stars mark areas of high seismicity. Moho = Mohorovičić discontinuity, LAB = lithosphere-asthenosphere boundary, G1 - G4 = granite outcrops..... | 5 |
| Figure 2. (a) Aerial image of the study site with mofette sites A and B. (image source: https://maps.google.de , accessed on: 2 October 2018). (b) Photographs of Site A in summer with detail from degassing center. (c, d) Photographs of Site B in summer (c) and in late winter (d) with detail from degassing center..... | 6 |
| Figure 3. Processes and properties in mofette soils as presented by Rennert and Pfanz (2016). | 10 |
| Figure 4. Conceptual model of metal(loid) binding processes and mobility at a mofette and a non-CO ₂ -influenced reference site as presented by Mehlhorn et al. (2014)..... | 12 |
| Figure 5. Conceptual model comparing short-term (top graph) and long-term (bottom graph) CO ₂ -induced metal(loid) mobilization (red-framed arrows) and immobilization (blue-framed arrow) processes. The short-term processes correspond to a temporal change in CO ₂ , i.e., a sudden CO ₂ release into a hitherto non-CO ₂ -influenced soil as investigated in study 2. The long-term processes correspond to a change in spatial metal(loid) distribution at a mofette site, in which CO ₂ exhalation influenced pedogenesis for at least several decades, going from non-CO ₂ -influenced reference soil (left) towards the degassing center (right) as investigated in studies 1 and 3. | 29 |

EXTENDED SUMMARY

1 Introduction

1.1 Mofettes – special study sites and natural laboratories

1.1.1 Geological background, surface appearance, fauna, and flora

Mofettes are defined as natural exhalations of carbon dioxide (CO₂) from fissures in the Earth (Oxford English Dictionary online, 2018a). The word ‘mofette’ originates from the Italian word ‘mofeta’, which stems from the Latin ‘mefitis’ or ‘mephitis’, meaning ‘a noxious or pestilential emanation, especially from the Earth’ (Oxford English Dictionary online, 2018a, b). Mofettes occur in areas influenced by recent volcanic activity, close to tectonic plate boundaries, or at active fault systems (Irwin and Barnes, 1980). Thereby, the CO₂ can have various origins: besides CO₂ release from carbonate containing rocks during metamorphic processes, biogenic respiration and oxidation of hydrocarbons, large amounts of CO₂ can be released from mantle degassing (D’Alessandro, 2006). In this case, the CO₂ originates from magma that has ascended from the Earth’s mantle into the lower Earth’s crust. Such magma only contains up to 1.5 weight-% of CO₂ (D’Alessandro, 2006), however, due to the decreased pressure in the Earth’s crust and its low solubility, CO₂ as well as traces of other gasses, are released as fluid and can ascend via tectonic faults and fissures into sediments and soils and, finally, into the atmosphere.

The temperature of the CO₂ released in mofettes is lower than 100 °C. This ‘cold’ degassing distinguishes mofettes from fumaroles, which mainly emit hot water vapor besides volcanic gasses (Grotzinger and Jordan, 2014). Other forms of volcanic exhalations that can co-occur with mofettes are solfatara, which mainly emit sulfur gasses, and geysers, which are characterized by periodic eruptions of hot water (Grotzinger and Jordan, 2014).

Depending on whether the soil is water saturated or not, wet and dry mofettes are distinguished. While wet mofettes are relatively easily detectable by the gas bubbles ascending through the water, the degassing might remain unnoticed at dry mofettes. If the CO₂ already dissolves in the ground water at greater depths and then is released together with the water, gaseous mineral springs are formed (Grotzinger and Jordan, 2014, Pfanz, 2008). However, the difference between wet and dry mofettes is not consistently defined. Some authors also account degassing of undissolved CO₂ in water saturated soils as dry mofettes and only mineral springs with release of dissolved CO₂ as wet mofettes (Rennert and Pfanz, 2016).

Degassing rates of CO₂ can vary strongly with published rates ranging from 0.1 to 11,900 kg CO₂ (m² a)⁻¹; even a rate of 165,800 kg CO₂ (m² a)⁻¹ has been reported for a single spot of a Czech mofette field (Rennert and Pfan, 2016 and references therein).

If mofettes are located in small sinks or topographic depressions, CO₂ can accumulate under calm conditions and CO₂ lakes may form, which constitute a danger to animals and humans. Such CO₂ lakes can develop an own diurnal circle in meteorological conditions as has been shown for the mofette 'Il Bossoleto' in Central Italy (Kies et al., 2015). Various reports exist on tragedies that have been or might have been caused by CO₂ accumulation from mofettes, e.g., 142 persons were killed by CO₂ on the Dieng Plateau, Indonesia, in 1979 (Le Guern et al., 1982), approx. 1700 people died at Lake Nyos, Cameroon, in 1986 (Baxter et al., 1989), and also some mysterious deaths close to the Laacher See, Rhineland-Palatinate, Germany, in the 18th and 19th century might have been linked to the presence of mofettes (Pfan, 2008). Thereby, it is not only direct toxicity but rather the displacement of oxygen by the heavier CO₂ that makes inhalation dangerous. Already partial pressures ($p(\text{CO}_2)$) above 0.1 can be lethal to humans and animals and inhalation of $p(\text{CO}_2)$ above 0.3 leads to hypoxia, acidosis, and respiratory paralysis, followed by death within only a few breaths of air (Henderson and Haggard, 1943, Langford, 2005, Stupfel and Le Guern, 1989).

Quite often, dead insects, birds, and smaller mammals can be found around mofettes. Cotrufo et al. (1999) reported a very limited population of soil fauna in an Italian mofette. Decreased abundancies and lower diversity of nematode and collembolan fauna in mofettes have also been reported (Fernández-Montiel et al., 2016, Hohberg et al., 2015, Russell et al., 2011, Yeates et al., 1999). However, some collembolan and nematode species are able to tolerate extreme CO₂ concentrations in mofette soils, where they might profit from decreased competition or from alternative food resources (Rennert and Pfan, 2016, Russell et al., 2011). Even an up to then unknown collembolan species, *Folsomia mofettophil*, was discovered in a mofette soil in Czech Republic (Schulz and Potapov, 2010). Furthermore, an up to now unknown mofettophilic yeast species, *Occultifur mephitis* was recently detected in Slovenia (Šibanc et al., 2018), while arbuscular mycorrhizal fungi seem to be negatively influenced by increased $p(\text{CO}_2)$ (Maček et al., 2012).

The high CO₂ concentrations at mofette sites are not only a risk for animals and fungi but they are also a challenge for plants. Several studies could show that plant height, root depth, chlorophyll content, and nutrient supply of plants growing at mofette sites are decreased compared to plants growing at non-CO₂-influenced soils (e.g., Pfan et al., 2004, 2007, Vodnik et al., 2002). At sites that are not agriculturally used, a CO₂-induced zonation in vegetation develops around mofettes (Pfan, 2008). Degassing centers with $p(\text{CO}_2)$ of almost 1 are generally completely free of vegetation. Plants that can tolerate the highest CO₂ concentrations are species, which are known to grow in wetlands or marshes and are thus adopted to low oxygen availability in waterlogged soils. Some examples for plant genera,

which have been identified to tolerate $p(\text{CO}_2)$ above 0.5, i.e., mofettophilic genera, are *Cyperaceae* (sedges) and *Juncaceae* (rushes) (Pfan, 2008, Rennert and Pfan, 2016, Saßmannshausen, 2010). These species are able to transport oxygen from upper plant parts into their roots via different transport systems, e.g., via *aerenchyma* (Jackson and Armstrong, 1999, Vartapetian and Jackson, 1997). Vegetation changes induced by CO_2 facilitate the identification of mofettes in the field whereby the occurrence of medium tolerant (i.e., mofettovague) and non- CO_2 -tolerant (i.e., mofettophobic) species, e.g., *Filipendula ulmaria* (meadowsweet) and *Urtica dioica* (common nettle), clearly indicate the boundaries of CO_2 influence (Saßmannshausen, 2010).

1.1.2 Mofettes as natural laboratories and analogies to leakage from GCS sites

Mofettes are very suitable as natural laboratories since they allow to study gradients in soil air $p(\text{CO}_2)$ and thus in soil redox conditions within only some meters distance from the degassing center. Thus, investigation of mofettes can increase general knowledge on processes occurring in other redoximorphic soils, e.g., wetland and floodplain soils, or soils above landfills or organic contaminant spills.

Mofettes are also of particular interest regarding their analogy to potential leakages from geologic carbon storage (GCS) sites. GCS is one possibility that is discussed and practiced with regard to Carbon Capture and Storage (or Carbon Capture and Sequestration, CCS). The aim of CCS is to reduce CO_2 emissions into the atmosphere by capturing CO_2 from industrial production processes and transporting it to storage sites for final deposition. Different possibilities for carbon storage have been suggested and tested. Among the most important ones with regard to terrestrial systems are geological storage and mineral carbonation (IPCC, 2005, Oelkers and Cole, 2008).

For geological storage, CO_2 is injected into porous rock formations that are underlying an impermeable cap rock, e.g., depleted oil reservoirs or sedimentary basins (Benson and Cole, 2008). GCS projects are in operation in numerous countries, both on pilot-scale and on commercial scale, with the most well-known one being the Sleipner Project in Norway (Baklid et al., 1996). In Germany, GCS was studied in a pilot-scale project by the German Research Center for Geosciences (GeoForschungsZentrum Potsdam). From 2008 to 2013, more than 67,000 t of CO_2 were injected into porous sandstone formations close to Ketzin in Brandenburg (Martens et al., 2014).

Mineral carbonation is considered to be the safest way to sequester CO_2 since the gas will react with cations and form stable minerals such as calcite or magnesite (IPCC, 2005, Oelkers et al., 2008). This storage technique was and is currently successfully applied in the CarbFix project in Iceland where more than 95% of the CO_2 injected into basaltic rocks was mineralized in less than two years (Gislason et al., 2010, Matter et al., 2016). Mineral carbonation is thus the most desirable long-term storage mechanism for CO_2 at GCS sites. However, if geological conditions are not as superior as they

are for example in the basaltic rocks of Iceland, mineralization might take centuries to millennia (IPCC, 2005). For this long period, the integrity of the cap rock has to be guaranteed.

Under the high pressures present in deep storage reservoirs, the CO₂ forms acidic fluids, which might be able to corrode wellbores or the cap rock (Benson and Cole, 2008, Shukla et al., 2010). An additional risk arises from seismic events, which could increase the permeability of the cap rock (IPCC, 2005). If leakage occurs, the CO₂ will start to rise along fissures into overlying sediments, aquifers, the soil, and finally into the atmosphere. Besides the unintended gas emission, CO₂-induced processes can have large effects on groundwater and soil, e.g., the mobilization of potentially toxic trace metal(loid)s into aquifers used for drinking water supply. Numerous studies on risks arising from potential leakages of carbon storage sites have been conducted during the last years (Jun et al., 2012, 2013 and references therein). Several authors suggest studying natural CO₂ deposits as analogues for GCS in order to better understand the behavior of CO₂ in storage formations but also to investigate the risks and consequences of potential CO₂ leakage into overlying sediments and soils (Lewicki et al., 2007, Pearce, 2006, Schütze et al., 2012).

Regarding consideration of CCS in Germany, the pilot project near Ketzin officially finished in 2017 and no further projects are planned, yet. However, the Federal Ministry for the Environment, Nature Conservation and Nuclear Safety mentions CCS as potential possibility in their Climate Action Plan 2050 (BMUB, 2016) and the National Academy of Science and Engineering (acatech) recently presented a position paper demanding to restore the discussion on CCS potentials in Germany (acatech, 2018). Thus, the further, in-depth investigation of potential risks arising from CO₂ leakage into soils is still an urgent research need. The investigation of natural analogues like mofettes represents a relatively simple and low-cost way to explore the long-term influence of CO₂ on sediment, soil, and ground water, as well as on the potential mobilization or immobilization of metal(loid)s (Lübben and Leven, 2018, Paoletti et al., 2005, Schütze et al., 2012).

1.1.3 Study site in the Plesná valley (Czech Republic)

The mofette site studied for this thesis is located in the floodplain of the river Plesná in Czech Republic, about 8 km northeast of Františkovy Lázně. The whole area is part of the European Cenozoic Rift System (Ziegler, 1992) and belongs to the Ohře (or Eger) Rift System, which began to develop more than 50 million years ago during the Tertiary (Bankwitz et al., 2003, Peterek and Schunk, 2008). Important parts of the system are the northeast–southwest striking Ohře Rift (or Eger Graben) and the Cheb Basin, which is a sedimentary basin located at the southwestern end of the Rift (Figure 1a). The Neogene sediments of the Cheb Basin mainly consist of weathering products from the magmatic and metamorphic rocks (granites, gneisses, quartzes, mica schists, and phyllites) of the northwestern Bohemian Massif (Flechsigs et al., 2008). Located at the eastern boundary of the Cheb Basin is the north-northwest–south-southeast striking Mariánské Lázně Fault Zone (MLFZ). Along the

MLFZ, a vertical movement of up to 400 m was induced during the last 4 million years (Peterek and Schunk, 2008), which can still be seen in a 50 to 200 m high escarpment. Another active fault zone that was first described by Bankwitz et al. (2003) is the north–south trending Počátky-Plesná Zone (PPZ). The river Plesná follows the PPZ for approximately 10 km. Many mofettes can be found along the floodplain or in the river itself, where CO₂ can ascend from underground along the fault structures and fissures.

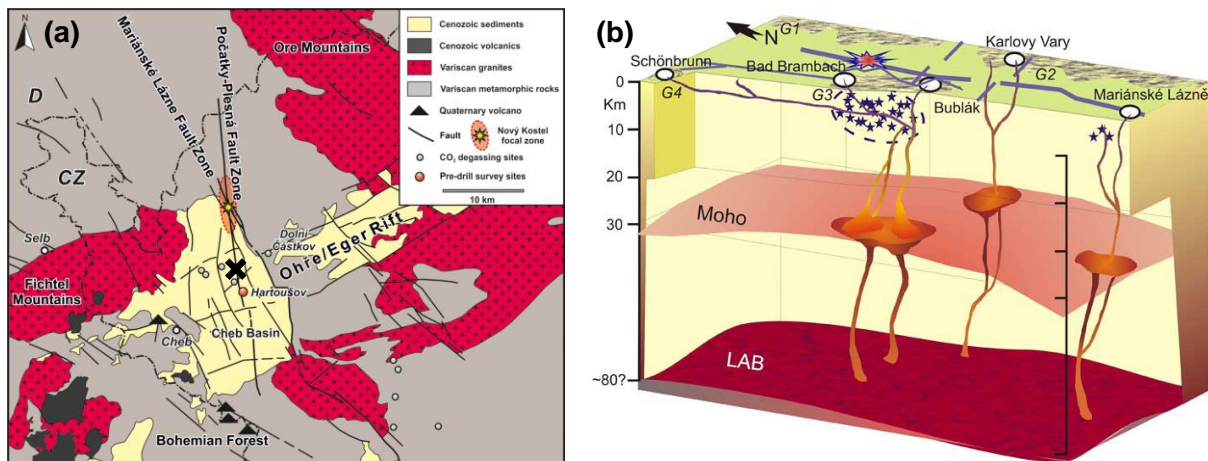


Figure 1. Geological situation at the study site. (a) Geological map of the Ohře Rift (Eger Graben) System as presented by Bussert et al. (2017). The black cross marks the study site of this thesis. (b) Conceptual model of the geodynamic situation in northwest Bohemia as presented by Bräuer et al. (2008) with the three main degassing areas Bublák, Mariánské Lázně, and Karlovy Vary being supplied from different reservoirs at the crust-mantle boundary. Blue stars mark areas of high seismicity. Moho = Mohorovičić discontinuity, LAB = lithosphere-asthenosphere boundary, G1 - G4 = granite outcrops.

The gas which is released by these mofettes has its origin in magma chambers located in the sub-crustal Earth's mantle in approximately 27 to 31 km depth, as indicated by helium ($^3\text{He}/^4\text{He}$) and carbon ($\delta^{13}\text{C}_{\text{CO}_2}$) isotope signatures (Bräuer et al., 2003, Weinlich et al., 1999). Besides the degassing area in which the studied mofettes are located (called 'Bublák' in most publications after the strongest degassing feature in this area), two more degassing areas exist in northwest Bohemia, one at Mariánské Lázně and one at Karlovy Vary. Using isotope signatures, Weinlich et al. (1999), later confirmed by Bräuer et al. (2008), found that these three main degassing sites are probably supplied by different magma reservoirs (Figure 1b). Besides numerous gas vents in eight mofette fields, more than 100 gaseous mineral springs can be found in these areas (Horálek and Fischer, 2008, Weinlich et al., 1999). These springs led to the development of the famous spa towns Františkovy Lázně, Mariánské Lázně, and Karlovy Vary, beginning already in the 14th century.

The two wetland mofettes, which were studied in detail for this thesis, are located close to the locality Vackovec, between Milhostov and Hartoušov (Figure 2a). All three studies, which were performed within the scope of this thesis, were conducted at Site A (50°8'43.9" N, 12°27'1.0" E), located in

approximately 20 m distance to the river Plesná. Site B ($50^{\circ}8'48.1''$ N, $12^{\circ}27'4.6''$ E) is located in approximately 80 m distance to the Plesná and was investigated only in study 3.

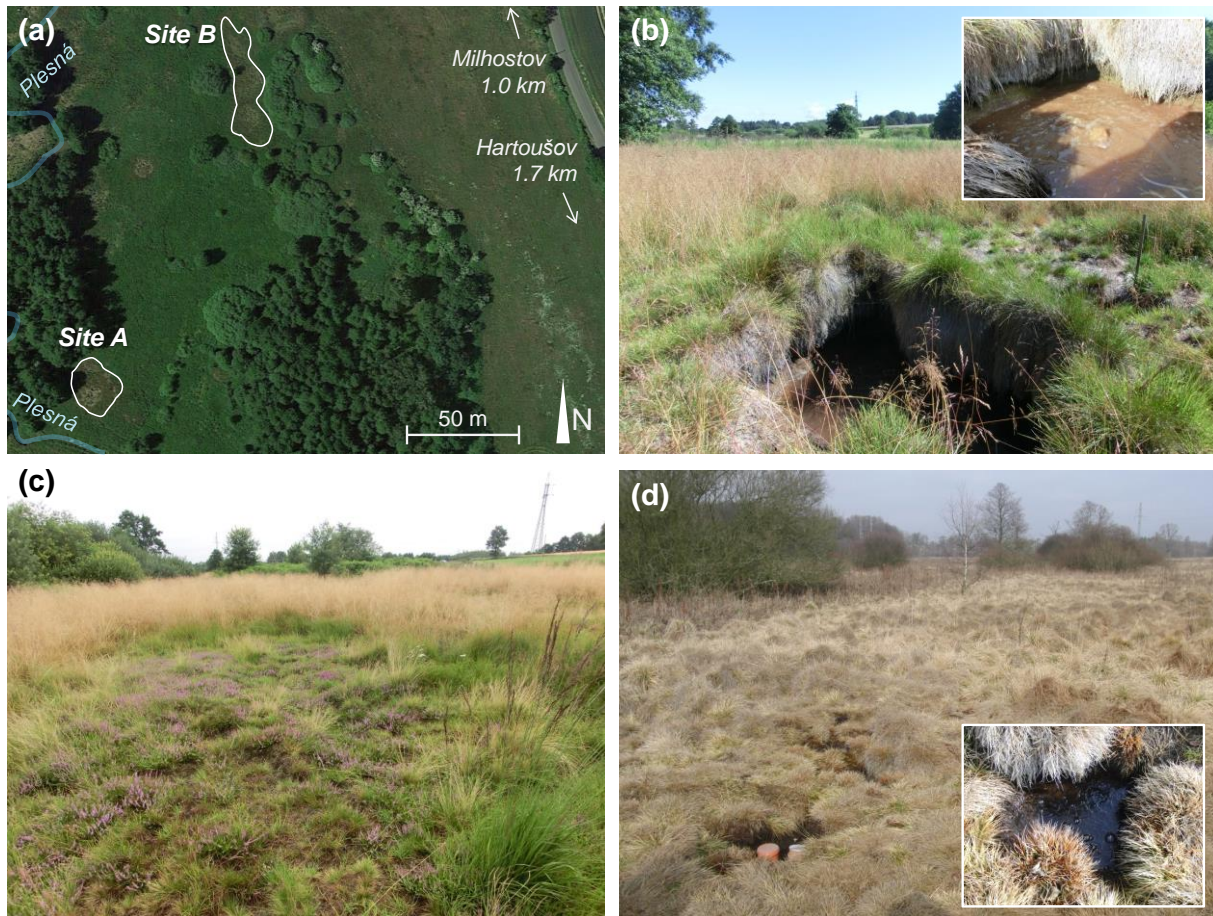


Figure 2. (a) Aerial image of the study site with mofette sites A and B. (image source: <https://maps.google.de>, accessed on: 2 October 2018). (b) Photographs of Site A in summer with detail from degassing center. (c, d) Photographs of Site B in summer (c) and in late winter (d) with detail from degassing center.

The studied mofettes are not agriculturally used and covered by mofettophilic meadow vegetation mainly consisting of *Eriophorum vaginatum* (cotton-grass), *Deschampsia cespitosa* (hair-grass), and *Calluna vulgaris* (heather) (Saßmannshausen, 2010) (Figure 2b-d). In the degassing centers, up to 1 m deep, flooded depressions are formed, in which the gas ascent can be observed visually by escaping gas bubbles (Figure 2b, d). The soils in this area of the Cheb Basin developed from fluvial Holocene and Pleistocene sediments (Flechsigt et al., 2008) and have been characterized by Beulig et al. (2016) as Gleyic Fluvisol for the non-CO₂-influenced soil, whereas the mofette soil has been characterized as Histosol with reductimorphic properties. Based on own observations, the qualifier Hemic could be added to the Histosol of the mofette site.

Flechsigt et al. (2008) studied a mofette field located approximately 1.5 km southeast ('Hartoušov mofette') and found that a small domal hummock of 0.5 m height and 5 m diameter formed above the degassing centers, which were small, vegetation-free, and sometimes water filled depressions. They

also observed an updoming of a sediment clay layer which might have been caused by a combination of strong gas pressure and swelling of smectite minerals. Other major minerals detected in soil and sediment were quartz, feldspars, micas, illite, kaolinite, and chlorite (Flechsig et al., 2008, Rennert et al., 2011). In greater depths, pyrite was detected, indicating permanently reducing conditions (Bussert et al., 2017, Flechsig et al., 2008). The observed accumulation of quartz pebbles close to the degassing center might indicate an upward transport with the gas flow (Flechsig et al., 2008). While similar domal hummock structures could also be observed at the mofette sites studied in this thesis (Figure 2b-d), an accumulation of quartz pebbles was not detected.

Rennert et al. (2011) determined soil air CO₂ in 10 to 60 cm depth for the Hartoušov mofette and found $p(\text{CO}_2)$ of up to 1 in the degassing center. Generally, degassing patterns at mofette sites were found to be very heterogeneous due to small scale variations in soil and sediment permeability (Rennert and Pfan, 2016 and references therein). Detailed gas flux analysis of the strongest degassing feature in this area, the mofette ‘Bublák’ located approximately 500 m south of the study site, showed that CO₂ made up 99.7% (Bräuer et al., 2008). Besides CO₂, the gas contained 0.2% nitrogen and traces of argon, helium, and methane. The exact timing of the onset of CO₂ exhalation at the study site and thus the age of the mofettes is unknown, but according to historic maps the gas exhalations have been known already in 1945 (Saßmannshausen, 2010).

The CO₂ ascent at the study site is not only related to the formation of mofettes and gaseous mineral springs but it is also supposed to provoke earthquake swarms. These are periodically occurring, intraplate earthquakes, which mostly have magnitudes below 3.5 and occur at focal depths between 4 and 22 km (Horálek and Fischer, 2008). The term ‘earthquake swarm’ was first used by Knett (1899) and by Credner (1900) and is considered a *locus typicus* for the West Bohemia/Vogtland region. The exact processes causing these earthquakes are still under debate but ascending, high pressure fluids (mixture of pressurized gas and groundwater) are thought to play a key role in triggering earthquake swarms by interacting with tectonic stress fields in subcritical fault zones (Fischer et al., 2014, Horálek and Fischer, 2008). Since 1986, earthquake activity is highest at the Nový Kostel focal zone, which is located at the intersection of the MLFZ and PPZ (Fischer et al., 2014), about 8 km north of the studied mofette site. Nickschick et al. (2015) recently proposed that the mofette fields in the Plesná valley are related to two pull-apart basin-like structures that have formed along the PPZ, facilitating the gas release through the Earth’s crust. Since no gas exhalations were found around Nový Kostel (Kämpf et al., 2013), it is assumed that less permeable rock units are blocking the ascending fluids, leading to buildup of overpressure and inducing seismicity (Bräuer et al., 2003, Nickschick et al., 2015).

According to recently published newspaper articles based on interviews with scientists from the German Research Center for Geosciences, the earthquake swarms seem to occur in shorter cycles and

with increased magnitudes (Jähn, 2018, MDR Wissen, 2018). Also, progressive changes in the isotopic composition of the upstreaming gas have been reported (Bräuer et al., 2008, 2018, Kämpf et al., 2013), which hints towards an ongoing magmatic process beneath the Cheb Basin.

1.1.4 Carbon dioxide as soil-forming factor

The extreme $p(\text{CO}_2)$ at mofette sites significantly influences soil conditions and soil development as recently reviewed by Rennert and Pfanzen (2016). In degassing centers, the soil is anoxic up to the surface and dissolution of CO_2 in pore water leads to formation of carbonic acid and thus causes soil acidification (e.g., Beaubien et al., 2008, Maček et al., 2009, Rennert et al., 2011). In a pre-study for this thesis, Mehlhorn et al. (2014) found that soil pH in the degassing centers of Sites A and B was 3.8 ± 0.2 compared to 4.1 ± 0.2 in the non- CO_2 -influenced surrounding soil and that pore water pH had a significant negative correlation with dissolved CO_2 concentrations ($r_s = -0.8$, $P < 0.01$).

Cation exchange capacity decreases with increasing $p(\text{CO}_2)$ (Rennert, 2018, Videmšek et al., 2009) and the weathering of silicate minerals is accelerated at mofette sites due to soil acidification (Rennert and Pfanzen, 2016, Stephens and Hering, 2002). Already more than 100 years ago, Gagel and Stremme (1909) described kaolinite formation from granite close to a CO_2 -rich mineral spring. Beaubien et al. (2008) observed increasing contents of K-feldspar with increasing $p(\text{CO}_2)$, which they attributed to weathering of albite, and Blume and Felix-Henningsen (2009) reported transformation of plagioclase to kaolinite or dickite at natural Reductosols. Around the Hartoušov mofette close to the study site of this thesis, Flechsig et al. (2008) found increased contents of smectite, probably formed by weathering of mica, chlorite, and illite. However, for a dry mofette close to Site B, Rennert (2018) could not detect any systematic CO_2 effect on clay mineral composition, which was attributed to the already acidic parent material and a superimposition of CO_2 effects over time.

Furthermore, the formation and maturation of pedogenic iron (Fe), manganese (Mn), and aluminum (Al) oxides and/or (oxy)hydroxides (hereafter summarized as (oxyhydr)oxides) is inhibited by the limited supply of oxygen (e.g., Beaubien et al., 2008, Mehlhorn et al., 2014, Rennert et al., 2011, 2012, 2015, 2018). For the Hartoušov mofette field, Rennert et al. (2011) found negative correlations of $p(\text{CO}_2)$ and Fe contents and the small amounts of Fe (oxyhydr)oxides detected at increased $p(\text{CO}_2)$ were generally of low crystallinity. Determination of Fe solid-phase speciation by X-ray absorption spectroscopy (XAS) on thin sections of soil samples from spots with a $p(\text{CO}_2)$ of 1 revealed that most Fe was present in different clay minerals (smectites, illites, and chlorites) and in form of Fe(II) and mixed Fe(II)/Fe(III) minerals, e.g., vivianite, siderite, green rust, and magnetite (Rennert et al., 2012). The Fe(III) (oxyhydr)oxides ferrihydrite and maghemite could only be detected close to a root channel, where micro-oxic conditions occurred.

Geogenic CO_2 does not only influence physical and chemical soil processes but also has a strong influence on soil fauna (compare section 1.1.1) and microorganisms. The microbial community shows

a lower diversity and is shifted towards anaerobic, acidophilic taxa, like sulfur-reducing and acetogenic bacteria or methanogenic archaea (e.g., Beulig et al., 2015, Frerichs et al., 2013, Krauze et al., 2017, Maček et al., 2009, Oppermann et al., 2010, Šibanc et al., 2014). Due to the anaerobic and acidic conditions, macro- and mesoscopic eukaryotes like earthworms or moles are absent in mofette soils, which leads to decreased bioturbation (Cotrufo et al., 1999, Rennert et al., 2011, 2016). Moreover, litter decomposition is decelerated under anaerobic conditions in mofettes, which causes an accumulation of soil organic matter (SOM) (e.g., Beaubien et al., 2008, Beulig et al., 2015, Olk et al., 2006, Rennert et al., 2011, Ross et al., 2000) and sometimes even the previously mentioned growth of hummocks (Flechsigt et al., 2008). Both plants and microbes are able to utilize the exhaled CO₂ for primary production, leading to up to 67% of geogenic carbon in SOM (Beulig et al., 2016, Nowak et al., 2015).

The composition of the SOM, which is accumulating in mofettes, differs from that of non-CO₂-influenced soils. Due to the decreased carbon turnover, the C/N ratio is increased (e.g., Rennert et al., 2011, Ross et al., 2000) and sometimes even unaltered plant residues, like roots or pieces of wood, are preserved within the soil (Flechsigt et al., 2008, Rennert and Pfanz, 2016). Further indications for the accumulation of sparsely degraded SOM are the decreased accumulation of aliphatic carbon and of SOM of microbial origin in the clay fraction, higher contents of phenolic compounds like lignin, and the accumulation of particulate organic matter (Rennert et al., 2011, 2015). A smaller extent of oxidative SOM transformation and a lower abundance of carboxylic groups was recently described by Rennert (2018), providing further evidence on the significant influence of geogenic CO₂ on SOM composition. In addition, the interaction of SOM with soil minerals seems to be negatively affected in mofettes leading to a decreased SOM stabilization by adsorption and inclusion processes (Rennert and Pfanz, 2015). A significant correlation of exchangeable Al contents and a value indicative for oxidation and transformation of SOM, determined by diffuse reflectance infrared Fourier transform spectroscopy, may indicate that Al bridging between SOM and minerals promotes SOM stabilization in the clay fraction (Rennert, 2018).

Rennert and Pfanz (2016) summarized the soil processes induced by geogenic CO₂ in mofettes in the conceptual model presented in Figure 3. Given the numerous effects on soil processes, they suggested introducing the qualifier ‘mofettic’ into the World Reference Base for Soil Resources (IUSS Working Group WRB, 2015) to account for geogenic CO₂ as soil-forming factor.

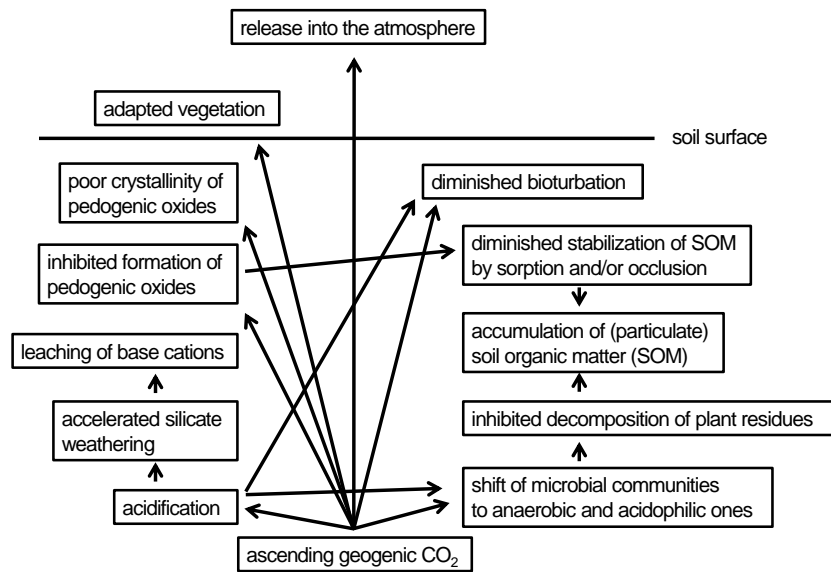


Figure 3. Processes and properties in mofette soils as presented by Rennert and Pfanz (2016).

1.2 Influence of carbon dioxide on metal(loid) mobility in soil

1.2.1 Influence of carbon dioxide induced soil acidification

The previously mentioned soil acidification, which is induced by CO_2 dissolution in soil pore water, can influence metal(loid) binding mechanisms and mobility in several ways. Weakly bound metal cations can be replaced by protons, which are formed from carbonic acid dissociation, resulting in mobilization of these metal(loid)s. Additionally, intensified weathering of minerals, which is induced by soil acidification, can release adsorbed or incorporated metal(loid)s into the liquid phase. These processes have been studied in detail with regard to risk assessment at GCS sites and many researcher groups could prove CO_2 -induced mobilization of several metal(loid), e.g., Al, arsenic (As), cadmium (Cd), cobalt (Co), copper (Cu), chromium (Cr), Fe, Mn, nickel (Ni), lead (Pb), and zinc (Zn), by desorption and mineral dissolution processes (e.g., Jones et al., 2015, Kirsch et al., 2014, Lawter et al., 2016, Little and Jackson, 2010, Lu et al., 2010, Smyth et al., 2009, Terzi et al., 2014). However, also re-adsorption of certain metal(loid)s, e.g., shown for As, Cd, Cu, and Zn, or precipitation of new minerals can occur (e.g., Lawter et al., 2015, Lu et al., 2010, Mickler et al., 2013, Montes-Hernandez et al., 2013, Shao et al., 2015).

1.2.2 Influence of carbon dioxide induced anoxic conditions

Due to the permanently anoxic conditions, the formation of pedogenic (oxyhydr)oxides is inhibited in mofette soils (compare section 1.1.4). This could not only increase the mobility of typical (oxyhydr)oxide forming metals like Fe, Al, and Mn, but also the mobility of metal(loid)s which are known to bind to or co-precipitate with these pedogenic minerals.

A further consequence of the permanently anoxic conditions in mofettes is the previously mentioned shift in microbial communities. Microbial processes could on the one hand contribute to metal(loid) mobilization, e.g., by the alteration of existing equilibria or microbially induced dissolution of certain minerals, like the reductive dissolution of Fe (oxyhydr)oxides (Kirk et al., 2013). On the other hand, microorganisms can promote mineral precipitation by increasing alkalinity or by direct biological formation of carbonates (Harvey et al., 2016, Kirk et al., 2013, Lions et al., 2014 and references therein) and thus contribute to metal(loid) immobilization. From other anoxic soils like wetlands or floodplain soils, it is known that under sulfur-reducing conditions chalcophilic metal(loid)s, e.g., Cu, Zn, As, or Fe, can react with microbially produced sulfide and (co-)precipitate in form of sulfidic minerals (Fulda et al., 2013a, 2013b, Hofacker et al., 2013, Morse and Luther, 1999, Weber et al., 2009b). This process may also play a role in mofette soils as suggested by Blume and Felix-Henningsen (2009) and as indicated by the presence of pyrite in deeper sediments of the Hartoušov mofette (Bussert et al., 2017, Flechsig et al., 2008).

Furthermore, SOM, which accumulates in mofettes due to anoxic conditions, can influence the binding mechanisms and the mobility of metal(loid)s. Increased contents of solid-phase SOM could provide potential new sorption sites for metal(loid)s with a high affinity for organic matter and thus contribute to their immobilization. However, dissolved organic matter (DOM) concentrations might also be increased in the pore water of mofettes and DOM can compete with metal(loid)s for sorption sites or mobilize organic matter-affine metal(loid)s by complexation (Kirk, 2004).

1.2.3 Previous results on metal(loid) mobility at the mofette site studied in this thesis

In a pre-study for this thesis, soil contents and pore water concentrations of As, Cu, Fe, Mn, and Ni of the two mofette sites were compared with nearby, non-CO₂-influenced soils (references) (Mehlhorn et al., 2014). It could be shown that the long-term CO₂ ascent in mofette soils influenced metal(loid) contents considerably (Figure 4). The mofette soils had significantly lower contents of Fe and As compared to the references and the mobility, i.e., the distribution coefficient between soil solid phase and pore water, of these elements was increased in the mofettes. This was attributed to the significantly lower content of poorly crystalline (content reduced by 75%) and well-crystalline Fe (oxyhydr)oxides (content reduced by 91%).

Besides the CO₂-induced increase in As mobility, also changes in As speciation were observed. In contrast to the references, up to 11% of methylated As and up to 9% of thiolated As could be detected in mofettes besides arsenite and arsenate. Thereby, the occurrence of methylated As species correlated with methane concentrations in the pore water. The formation of these As species was thus most probably related to microbial methane production by methanogenic archaea and to sulfide production by sulfur-reducing bacteria, which have been shown to predominate in these mofette soils (Beulig et al., 2015, 2016). Changes in speciation can also influence As mobility, since methylated As species

are known to be more mobile than arsenate (Bowell, 1994) and thiolated As species are even more mobile than arsenite (Suess and Planer-Friedrich, 2012).

While the mobilizing effect of geogenic CO_2 on Fe and As could clearly be shown in Mehlhorn et al. (2014), the results for Mn, Ni, and Cu were less clear. Soil Mn contents were slightly decreased in mofettes compared to reference soils, but also Mn pore water concentrations remained low. The soil contents of Cu and Ni were relatively equal in mofettes and references (Site A) or showed lower contents in the upper 60 cm depth and higher contents in deeper soil (Site B) in mofettes compared to references. Pore water concentrations of Ni and Cu were lower in the mofettes than in the references. The observed distribution patterns were attributed to a mixture of mobilization and re-adsorption processes under long-term CO_2 influence, with SOM being the main candidate for re-adsorption due to significantly increased SOM contents in the mofettes (Figure 4). This hypothesis was reinforced by strong accumulation of Ni, Cu, and also As in a peat lens, which was detected in approximately 2 m depth at Site A (named ‘site 1’ in Mehlhorn et al. (2014)).

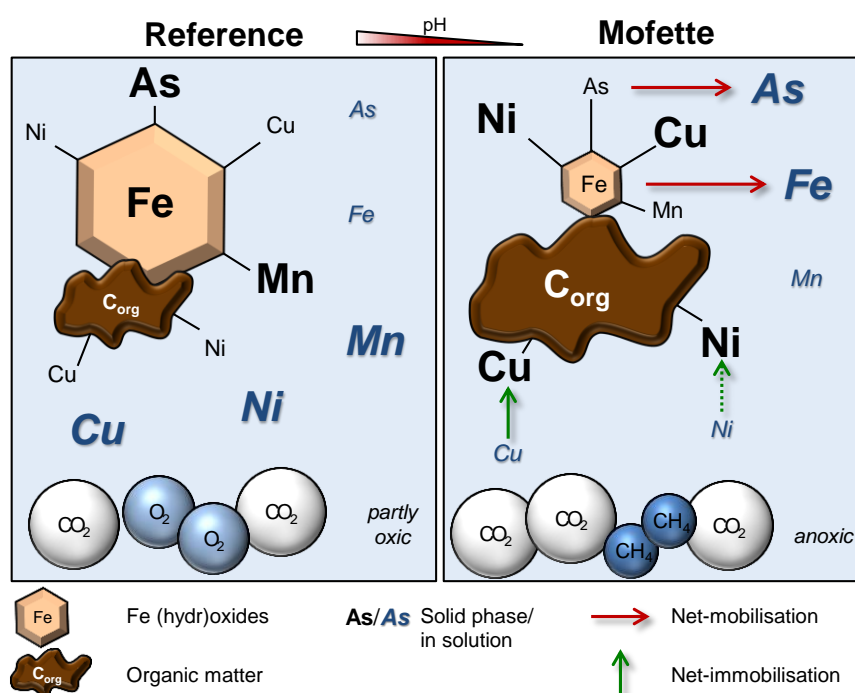


Figure 4. Conceptual model of metal(loid) binding processes and mobility at a mofette and a non- CO_2 -influenced reference site as presented by Mehlhorn et al. (2014).

However, the exact processes that caused the distribution patterns observed for Cu, Mn, and Ni could not be explained entirely. Comparing samples from the degassing center of the mofettes with a $p(\text{CO}_2)$ of 1 with non- CO_2 -influenced reference soils has not been sufficient to completely understand the mobilization and immobilization processes in mofettes. Therefore, a more detailed investigation of the transition between permanently anoxic and oxic soil conditions is necessary.

In Mehlhorn et al. (2014), also an *in situ* mobilization experiment was conducted, in which soil from the reference sites was exposed for approximately one month in the degassing centers of the mofettes. During this experiment, strong mobilization of all considered metal(loid)s could be observed, indicating that short-term and long-term processes in mofettes differ significantly and that a more detailed investigation of the distinct mobilization and immobilization processes is necessary.

1.3 Objectives

The aim of this thesis was to investigate CO₂-induced metal(loid) mobilization and sequestration processes in mofettes. Therefore, it was necessary to determine individual metal(loid) binding processes and the influence of CO₂-induced changes in soil conditions on these binding mechanisms. The first study focused on the spatial scale of metal(loid) mobilization and immobilization processes, which should help to understand interdependencies between CO₂-induced changes in soil conditions and metal(loid) distribution under long-term CO₂ influence. In the second study, the temporal scale of CO₂-induced, short-term (im)mobilization processes was investigated in more detail using batch incubations. The third study focused on the behavior of the metal Cu in mofettes, since this element showed distinct differences compared to the other metal(loid)s investigated in this thesis. A greater knowledge of the processes occurring in mofettes is not only helpful for a better risk assessment at GCS sites but it will also increase our understanding of metal(loid) mobilization and immobilization processes occurring in other redoximorphic soils, like wetlands, floodplains, or contamination sites.

The specific objectives of the three studies presented in this thesis were the following:

- (1) to investigate the spatial distribution of metal(loid)s in soil and pore water around a mofette in order to identify long-term effects of CO₂ on metal(loid) binding and mobility (study 1: Mehlhorn et al. (2019)),
- (2) to determine the temporal scale of metal(loid) (im)mobilization processes, which occur after an hitherto non-CO₂-influenced soil was exposed to CO₂ (study 2: Mehlhorn et al. (2016)),
- (3) to study the temperature dependency of CO₂-induced, short-term (im)mobilization processes and thus the importance of microbial processes (study 2), and
- (4) to investigate Cu binding mechanisms and mobility along a CO₂ gradient in relation to redox conditions and SOM composition (study 3: Mehlhorn et al. (2018)).

2 Methods

2.1 General practices and analytical methods

2.1.1 Sampling and laboratory practices

During the collection of soil and pore water samples, attention was paid to minimize both the disturbance of the natural site and the influence of atmospheric oxygen on the samples. Soil samples were usually collected with an auger or, if larger amounts were required, with a spade, packed into bags, and either flash-frozen on dry ice or stored under cooled conditions, depending on the planned analyses or experiments. Collection of pore water samples for studies 1 and 3 was done with pore water peepers type Hesslein (1976). Oxygen influence on the water samples was minimized by conducting transport and storage of the peepers in a nitrogen-filled box. In studies 1 and 3, soil air composition (CO₂ and oxygen) at the respective sampling sites was analyzed in approximately 10 to 20 cm depth using a portable gas analyzer (BIOGAS 5000, Geotech). For all experiments and sample preparations, ultrapure water and reagents of at least analytical degree were used. Oxygen-sensitive experiments (study 3) were conducted inside an anoxic chamber (Coy, 95%/5% nitrogen/hydrogen).

For most analyses, the soil samples were freeze-dried, ground, and sieved (nylon, 1 mm mesh size). If the soil samples were used for analyses of potentially oxygen-sensitive parameters, i.e., for Mössbauer spectroscopy (study 2), X-ray absorption spectroscopy (XAS), ¹³C nuclear magnetic resonance spectroscopy (NMR), scanning electron microscopy energy-dispersive X-ray spectroscopy (SEM-EDS; all study 3) or for sequential extraction (study 1), preparation and storage was done inside an anoxic chamber. In addition, samples were stored under dark conditions to reduce photooxidation effects.

2.1.2 Analytical methods with respect to metal(loid)s

For the determination of total metal(loid) and sulfur contents, soil samples were digested in aqua regia using microwave-assisted digestion at 160 °C (MARS Xpress, CEM). Pore water and other liquid phase samples were stabilized in 0.45% H₂O₂ and 0.65% HNO₃ directly after sampling. Analysis of total sulfur and metal(loid) concentrations (Al, As, Cd, Co, Cr, Cu, Fe, Mn, Ni, Zn) in soil digests and in pore water or any other liquid phase samples was conducted by inductively coupled plasma mass spectrometry (ICP-MS, X-Series 2, Thermo Scientific). All samples were filtered (0.2 µm, cellulose-acetate) and diluted at least 1:10 before ICP-MS analysis.

In study 1, a five-step sequential extraction procedure according to Fulda et al. (2013a) was conducted in order to gain information on operationally defined metal(loid) fractions in soil and thus on dominating binding mechanisms. This sequential extraction is a combination of the methods established by McGrath et al. (1988), Tessier et al. (1979), and Zeien and Brümmer (1989). The

procedure included the following operationally defined fractions: (1) mobile (soluble and exchangeable, soluble metal(loid)-SOM complexes), (2) easily mobilizable (specifically adsorbed, bound to minerals labile at pH 5, and weak metal(loid)-SOM complexes), (3) organically bound (low affinity), (4) reducible (bound to amorphous and crystalline Fe and Mn (oxyhydr)oxides), (5) oxidizable (metal sulfides and bound to high affinity sites of SOM). To exclude any reactions induced by atmospheric oxygen, extraction steps 1 to 3 were conducted inside an anoxic chamber. Total metal(loid) contents in filtered (0.2 μm , cellulose-acetate) and diluted extracts were determined by ICP-MS.

In study 3, solid-phase speciation of Cu in natural and Cu-spiked soil samples was investigated using XAS at the Cu *K*-edge. Both X-ray absorption near edge structure (XANES) and extended X-ray absorption fine structure (EXAFS) spectra were collected at beamlines 4-1 and 4-3 of the Stanford Synchrotron Radiation Light Source (SSRL, Stanford, U.S.A.). Linear combination fitting was conducted both for normalized XANES and k^3 -weighted EXAFS sample spectra, using nine published spectra and one measured spectrum of Cu reference compounds. Details on spectra collection and data evaluation can be found in study 3. In addition, SEM-EDS data were collected in study 3 in order to detect any potential Cu-containing precipitates using a Leo Gemini 1530 (Carl Zeiss, Germany) with a Schottky emitter.

2.1.3 Methods used for soil and pore water characterization

Various other methods were used to characterize soil and pore water parameters, which are relevant for metal(loid) binding and mobility. The most important methods will briefly be mentioned in this chapter. Analytical details can be found in the individual studies.

Liquid samples were generally characterized by measuring pH and redox potential directly in solution or in soil suspensions. Methane and CO₂ concentrations were determined by calculating dissolved concentrations from head space concentrations in septum vials using Henry's law (Henry, 1803, Sander, 2015). Therefore, concentrations in the head space were measured with a gas chromatograph (SRI Instruments 8610C, U.S.) equipped with a methanizer and a flame ionization detector. In studies 1 and 3, additional photometrical analyses were conducted using a multiplate reader (Infinite 200 PRO, Tecan) and the ferrozine assay (Stookey, 1970) for determination of total Fe and ferrous Fe concentrations (absorbance measured at 570 nm), the methylene blue method (Cline, 1969) for determination of sulfide concentrations (absorbance measured at 650 nm), and the bathocuproine method (Maurer et al., 2013, Moffett et al., 1985) for determination of cuprous Cu (absorbance measured at 492 nm). Total dissolved organic carbon (DOC) and dissolved nitrogen concentrations were measured in filtered (0.45 μm , polyamide) liquid phase samples using thermo-catalytic oxidation with a TOC-VCPN Analyzer (Shimadzu). In study 3, DOM was characterized by Fourier-transform

infrared spectroscopy (FTIR) with a Vector 22 spectrometer (Bruker Optik) in transmission mode using freeze-dried water extracts of soil samples.

Soil samples were generally characterized by measuring soil pH in 0.01 M CaCl₂ solution at a soil-to-solution ratio (SSR) of 1:2.5. In addition, total soil organic carbon (SOC) and nitrogen contents were determined with a CHN elemental analyzer (Thermo Quest, Flash EA, 1112). In study 2, three soil samples were analyzed by Mössbauer spectroscopy in order to gain information on Fe mineralogy. Spectra were collected at 77 K and 5 K using a closed-cycle exchange gas cryostat (Janis cryogenics) and a constant acceleration drive system (WissEL) in transmission mode with a ⁵⁷Co/Rh source. In study 3, solid-phase SOM of soil samples was characterized by ¹³C NMR with an Avance III HD Spectrometer (Bruker) and soil mineralogy was characterized by X-ray powder diffraction (XRD) using a Philips X'Pert Pro diffractometer operating in reflection mode with Fe filtered CoK_{α1} radiation.

2.2 Spatial scale: determination of metal(loid) distribution patterns around a mofette (study 1)

In the first study of this thesis, the spatial distribution of the metal(loid)s Al, As, Cd, Co, Cr, Cu, Fe, Mn, Ni, and Zn in soil and pore water around the mofette Site A was determined. Soil samples were collected along a sampling grid with its center located in the degassing center and its margins in the non-CO₂-influenced area. The samples derived from three depths representing the SOM-rich topsoil (0 to 5 cm depth), the alternating oxic/anoxic zone (25 to 35 cm), and the hypothetically permanently water-saturated zone (55 to 65 cm) of the Gleyic Fluvisol in the non-CO₂-influenced area. To gain information on possible metal(loid) binding mechanisms, a five-step sequential extraction according to Fulda et al. (2013a) was conducted for the soil samples from the east transect. In addition, pore water samples from 10 to 60 cm depth were collected along the east transect of the sampling grid using pore water peepers type Hesslein (1976). Spatial distribution patterns of general soil and pore water parameters as well as total metal(loid) contents were plotted using universal Kriging interpolation. Calculation of Euclidian distances between normalized distribution patterns allowed to cluster the investigated metal(loid)s into groups of high similarity. By comparing general soil parameters with metal(loid) contents and fractionation derived from sequential extraction, conclusions on CO₂-induced long-term processes and on dominant binding mechanisms could be drawn for each individual metal(loid).

2.3 Temporal scale: time dependency of carbon dioxide induced metal(loid) mobilization in soil (study 2)

The second study of this thesis focused on the temporal scale of CO₂-induced metal(loid) mobilization processes. Therefore, hitherto non-CO₂-influenced soil from 20 to 30 cm depth of Site A (alternating oxic/anoxic zone) was incubated in triplicate with filtered (0.2 μm, cellulose-acetate) water from the

river Plesná (used as pore water equivalent) in batch reactors and purged with a gas flow of $28 \pm 5 \text{ mL CO}_2 \text{ min}^{-1}$ for up to 42 days. For the first experiment, incubation temperature was varied (16, 22 and 35 °C) while in the second experiment there was a variation in initial soil conditions (fresh spring soil, stored spring soil, and fresh summer soil). Over the course of the experiment, the liquid phase was sampled and analyzed for general parameters (pH and redox potential) and for total concentrations of As, Cu, Fe, and Mn. Metal(loid)-specific mobilization rates could be calculated from concentration changes observed over time. The amounts of cultivatable heterotrophic aerobic, Fe(III)-reducing, and sulfate-reducing microorganisms were determined by most probable numbers (MPN). Differences within the temperature treatments enabled the distinction between abiotic and biotic processes. Differences within the initial soil conditions helped to elucidate the influence of SOM content and Fe (oxyhydr)oxide crystallinity, determined by Mössbauer spectroscopy, on metal(loid) mobilization rates.

2.4 Case study on copper: sorption behavior and solid-phase speciation of copper in mofettes (study 3)

Study 3 of this thesis focused on Cu, since this element had shown some quite interesting behavior in Mehlhorn et al. (2014) and in study 2 of this thesis. Besides investigating Cu soil contents and Cu pore water concentrations with respect to dissolved CO₂ along the east transect of Site A, a Cu spike experiment was conducted. Therefore, SOM-rich topsoil (5 to 15 cm depth) from 4 spots along the transect of Site A ('Mofette A', 'Transition A1', 'Transition A2', and 'Reference A') as well as from 2 spots of Site B (degassing center 'Mofette B' and non-CO₂-influenced soil 'Reference B') were collected. The homogenized, fresh soil samples were incubated with 5 mM NaCl solution, pH 4.5, as background electrolyte at a SSR of 1:30 and spiked with up to 11.7 mmol kg⁻¹ CuCl₂ solution. Copper adsorption coefficients (Freundlich and linear coefficients) were calculated for the sorption isotherms, which could be obtained from this experiment. X-ray absorption spectra (XANES and EXAFS) were collected at the Cu K-edge for natural and Cu-spiked samples in order to elucidate the solid-phase speciation of Cu in these samples. In addition, a Cu-loaded soil sample was investigated by SEM-EDS in order to detect any potential Cu precipitates. The SOM and DOM composition of the respective soil samples were characterized by ¹³C NMR and FTIR, respectively.

3 Results and Discussion

3.1 Spatial distribution of metal(loid)s around a mofette and implications on soil processes (study 1)

The sampling grid of study 1 (Mehlhorn et al., 2019) over Site A covered two degassing features, the previously studied feature with a $p(\text{CO}_2)$ of almost 1 in the center of the grid, and a less intense feature with $p(\text{CO}_2)$ up to 0.56 in approximately 12 m distance to the northeast. Both the previously mentioned effects on soil pH (decreasing with increasing $p(\text{CO}_2)$) and on SOM content (accumulation in degassing areas) could be confirmed in study 1.

The three-dimensional spatial distribution patterns of the metal(loid)s Al, As, Cd, Co, Cr, Cu, Fe, Mn, Ni, and Zn around a main CO_2 exhalation of Site A revealed some interesting processes, which were not detectable by comparing just two spots of the system as done in the pre-study for this thesis (Mehlhorn et al., 2014). The normalized distribution patterns derived for soil contents of individual metal(loid)s could be assigned to four clusters of high similarity, which will be considered individually in the following paragraphs.

The metals Mn, Co, Ni, and Zn showed depletion in almost the whole CO_2 -influenced area. The only exception was a slight Zn enrichment in the deepest soil sample from the degassing center. From sequential extraction and from the negative relationship with SOM contents could be concluded that these elements were primarily mineral-associated, most probably with clay minerals and other silicates. High affinity of these metals for soil minerals is in accordance with literature (e.g., Bradl, 2004, McBride, 1989). Long-term CO_2 degassing at the mofette site and ongoing soil acidification has caused mobilization and leaching of Mn, Co, Ni, and Zn by desorption and mineral dissolution processes. Similar processes have been reported in monitoring or geochemical modelling studies at GCS sites (e.g., Kharaka et al., 2006, 2010, Wang and Jaffe, 2004, Zheng et al., 2012) as well as in laboratory batch and column studies on effects of CO_2 intrusion into sediments (e.g., Lawter et al., 2015, 2016, Qafoku et al., 2014, Terzi et al., 2014). In addition, the accumulation of SOM in the degassing center may have contributed indirectly to the depletion of these elements by a decrease in total mineral content.

Soil contents of Al and Cr were only decreased directly in the degassing center and showed an inverse correlation with SOC contents. In addition, less than half of total Cr and less than 30% of total Al (determined in aqua regia digests) could be extracted during the five-step sequential extraction procedure indicating that Al and Cr were predominantly present in the residual fraction, i.e., incorporated into silicates. Thus, direct CO_2 -induced depletion by desorption and mineral dissolution processes must have been way lower for these elements in comparison to Mn, Co, Ni, and Zn.

However, the accumulation of SOM led to the development of zones of low mineral and thus low Al and Cr contents directly in the degassing center.

For Fe and As, observations made in Mehlhorn et al. (2014) could be confirmed. Under oxic conditions, Fe was predominantly present in form of Fe (oxyhydr)oxides and As, which is known to have a high affinity for Fe (oxyhydr)oxides (e.g., Livesey and Huang, 1981, Manning and Goldberg, 1997), was incorporated in or adsorbed to these pedogenic minerals. Soil contents of As and Fe were lowest in the degassing areas and in deeper soil, where permanently anoxic conditions largely inhibited the oxidation of Fe(II) and thus the formation of Fe(III) (oxyhydr)oxides. As soon as traces of oxygen were available, Fe and As could accumulate, which led to the development of an enrichment zone in the topsoil located directly between the two degassing areas.

Cadmium and Cu were the only elements that exhibited a strong enrichment directly in the main degassing feature, most pronounced in the deeper soil. Zinc soil contents were also increased in the sample originating from 55 to 65 cm depth of the main degassing center. In samples from the center, the majority of Cd and Cu was extracted in the oxidizable fraction, i.e., metal sulfides and metals bound to SOM at high affinity sites (Tessier et al., 1979). Both, SOC contents and total soil sulfur contents were strongly enriched in the degassing center. Thus, considering only the results gained from solid-phase samples, both sequestration processes could be possible explanations for the Cd, Cu, and Zn accumulation. Apart from the enrichment in the mofette center, soil contents of Cd and Cu were highest in the upper soil and their contents were generally increasing with decreasing CO₂ influence. The latter implies that outside of the degassing center leaching has also occurred for these elements.

From cluster analysis of the normalized pore water metal(loid) concentrations, three groups of high similarity could be distinguished. The first cluster included Mn, Co, Ni, and Cd. The pore water concentrations of these elements increased with increasing distance from the degassing center, i.e., with decreasing CO₂ influence. Since for Mn, Co, and Ni both soil contents and pore water concentrations were increasing with distance, the solid-to-liquid-phase ratio was left more or less unaltered and no CO₂-induced change in metal mobility could be detected. The influence of CO₂-induced changes on the mobility of Mn, Co, and Ni by soil acidification and mineral dissolution seems to have reached a steady state after decades of CO₂ degassing, leaving soil contents and pore water concentration in quasi-equilibrium. This would also explain the observations in Mehlhorn et al. (2014), where both pore water and soil were depleted in Mn and Ni in the mofettes compared to the reference sites.

A second cluster of high similarity in normalized pore water concentrations was formed by Al, Cr, Fe, and As. These metal(loid)s were especially enriched in 2 to 4 m distance from the main degassing feature, with concentration hotspots in 10 to 15 cm and in 40 to 60 cm depth. Their pore water

concentration showed a strong correlation with DOC concentrations, indicating that complexation with DOM was the main process triggering metal(loid) mobilization in this area. All of these metal(loid)s are well-known for their affinity towards DOM (e.g., Bauer and Blodau, 2006, Carrillo-González et al., 2006, Du Laing et al., 2007, Kalbitz and Wennrich, 1998, Pohlman and McColl, 1988).

Pore water concentrations of Cu and Zn were also increased in some meters distance from the degassing center, indicating complex formation with DOM, although, these two metals formed an own cluster of high similarity. The reason for the distinct behavior was most probably that their pore water concentrations, in contrast to Al, Cr, Fe, and As, were close to detection limit in the degassing center despite high DOC concentrations. The effective removal of Cu and Zn from solution despite increased DOM concentrations as well as the presence of up to 1.8 mg L^{-1} sulfide in the pore water of the degassing center confirmed the hypothesis of a precipitation of sulfide minerals as effective sequestration process under permanently anoxic conditions. Copper, Zn, and also Cd are known to precipitate in form of sulfidic minerals under reducing conditions (Fulda et al., 2013a, 2013b, Kirk, 2004, Weber et al., 2009b).

Concluding from the results of this study, increased metal(loid) mobility at mofette sites could mainly be observed for those elements with a high affinity to DOM, i.e., Al, As, Cr, Cu, Fe, and Zn. Due to the accumulation of poorly degraded SOM (compare section 1.1.4), also DOM concentrations are increased in mofettes. Besides preventing metal(loid) sorption to the soil solid phase by the formation of metal(loid)-DOM complexes, DOM could also indirectly contribute to increased metal(loid) mobility by competition for sorption sites (Grafe et al., 2001, 2002, Redman et al., 2002, Theis and Singer, 1974). The elements Mn, Co, and Ni showed no changes in net-mobility. Long-term, CO_2 -induced soil acidification has led to the depletion of these elements within more or less the whole CO_2 -influenced area.

Iron and As were the only elements for which a direct, CO_2 -triggered mobilizing effect could still be observed after the long-term CO_2 -influence at this mofette site. This observation was attributed to the fast kinetics of Fe(II) oxidation and Fe(III) reduction (Kirk, 2004). As soon as traces of oxygen are available, pedogenic Fe (oxyhydr)oxides can form, but they can also be reductively dissolved again, if conditions get more reducing. Together with metal(loid) complexation by DOM, this leads to significantly increased net-mobilities of Fe and As in the mofette center and arises the question on exact mechanisms and rates of CO_2 -triggered, short-term mobilization processes.

3.2 Time and temperature dependency of carbon dioxide induced metal(loid) mobilization in soil (study 2)

In the second study of this thesis (Mehlhorn et al., 2016), the short-term effects on As, Cu, Fe, and Mn mobility, which follow a sudden CO_2 release into a hitherto non- CO_2 -influenced soil, were studied in

laboratory experiments and compared to long-term effects at the natural site. Two main processes could be distinguished in these experiments. Within the first 1 hour to 1 day of incubation with a constant flow of CO₂, fast abiotic mobilization of metal cations, especially pronounced for Mn, was observed. The mobilization was strongest in the cooled treatments (16 °C), followed by room temperature (22 °C) treatments, and lowest for the heated treatments (35 °C). This liquid phase concentration increase must have been caused by abiotic desorption of Mn following sorption site protonation with protons derived from the dissolution of CO₂ and following dissociation of carbonic acid. Since, according to Henry's law (Henry, 1803), more CO₂ can dissolve at lower temperature, mobilization rates increased in the order heated < room temperature < cooled. After the initial mobilization, Mn concentrations remained relatively constant, except for the heated treatments, in which low amounts of Mn were continuously released until the end of the experiment after 42 days. The control batches, which were not incubated with CO₂, also showed slight Mn mobilization within 1 day, however, significantly lower than the CO₂ treatments. This was attributed to desorption reactions following the mixing of soil with river water.

After an initial lag phase of 1 to 3 days, a strong and continuous Fe mobilization started and liquid phase Fe concentrations increased almost linearly until the end of the experiment after 42 days. In contrast to Mn, no Fe mobilization was detected in the non-CO₂-incubated controls. The fact that Fe mobilization followed the order cooled < room temperature < heated treatments already implied that microbes might have triggered this process. This hypothesis was reinforced by the significant decrease in redox potential from values above 500 mV down to a minimum of 340 ± 20 mV, which was observed in the CO₂ treatments and which followed the same order as Fe mobilization with regard to temperature treatment. Additionally, determination of MPNs showed that $4.7 \cdot 10^4$ to $1.0 \cdot 10^6$ MPN mL⁻¹ of Fe(III)-reducing microorganisms were present in the initial soil. Thus, this second main mobilization process was attributed to the microbially triggered reductive dissolution of Fe (oxyhydr)oxides.

In the heated treatments, an up to 111 ± 24 fold increase in liquid phase Fe concentrations could be observed. This value is much higher than the abiotic mobilization of Mn which only resulted in 2.5 to 3.3 fold concentration increases. For As, significant mobilization was only observed in the heated treatments and attributed to co-release from Fe (oxyhydr)oxide dissolution. In the cooled and room temperature treatments, As re-adsorption might have counteracted with any co-release. Also for Mn, only the heated treatments showed a continuous further mobilization over the course of the experiment, reaching final concentrations comparable to those of the cooled treatments after 42 days. This indicated that also some adsorbed or incorporated Mn must have been mobilized during microbially triggered reductive dissolution of Fe (oxyhydr)oxides.

Experiment repetitions with sterilized batch incubations were conducted in order to quantify the microbial influence on metal(loid) mobilization, but unfortunately all tested sterilization methods led to unintended changes in soil conditions and mobilization reactions, which is a well-known problem in soil science (Trevors, 1996 and references therein).

To further verify the assumed microbially triggered mobilization process, the influence of SOM content and Fe mineral crystallinity on CO₂ induced metal(loid) mobilization was tested with different soils in a second experiment. Mössbauer spectroscopy revealed that the main Fe phases in the soil used for the first batch experiment (fresh spring soil) were goethite, a short range ordered Fe mineral such as ferrihydrite, and some non-crystalline Fe(II)/Fe(III) phases. Storage of the soil for 11 weeks under cooled and dark conditions (stored spring soil) significantly increased the crystallinity of the Fe phases. Another soil sample was taken in summer (fresh summer soil), i.e., during high soil microbial activity. According to the Mössbauer spectra of this sample, little to no goethite was present and the majority of the Fe phases were present in form of short range ordered minerals, which might have been associated with SOM. In comparison to the fresh spring soil, mobilization of all considered metal(loid)s was decreased in the stored spring soil. In the fresh summer soil, however, mobilization of Fe and As was both faster and stronger compared to the fresh spring soil. These observations support the hypothesis of a strong microbial influence on metal(loid) mobilization, whereby the microbially triggered reductive dissolution of Fe (oxyhydr)oxides was inhibited by the increased crystallinity of Fe(III) minerals in the stored spring soil. In fresh summer soil, reductive dissolution was intensified, since Fe(III)-reducing bacteria profited from large amounts of organic matter and easily available, low crystalline Fe(III) minerals as energy source (Melton et al., 2014).

Following these results of study 2, further test experiments on the effect of CO₂ on pure cultures of Fe(III)-reducing bacteria were conducted (Metz, 2016, unpublished). The acidophilic, facultative anaerobic bacterium *Acidiphilium* SJH (A. SJH) was incubated with 5 mM ferrihydrite under either an oxic headspace, a pure nitrogen headspace, or a pure CO₂ headspace. The aim of these experiments was to test, if any CO₂-induced effects other than acidification influenced the microbially triggered reductive dissolution of the ferrihydrite. As expected, only slight Fe mobilization occurred under oxic conditions as result of co-respiration. Without pH buffering, mobilization was higher in CO₂ than in nitrogen treatments. Dissolution of CO₂ in the medium lowered pH significantly (pH 4.2 compared to 5.5 in nitrogen and air treatments), which triggered the proton-consuming reaction of microbial Fe(III) reduction. When pH was kept constantly low at the optimum pH of A. SJH (pH 3.0), the mobilization in batches with pure nitrogen and pure CO₂ headspace showed no significant differences indicating that besides acidification no other direct influences of CO₂ on the Fe(III) reduction rate of A. SJH exist in this simplified system. In a natural soil system, however, other effects might play a role, e.g., an advantage of Fe(III)-reducing bacteria over sulfide reducers at elevated CO₂ levels due to the constant delivery of protons (Kirk et al., 2013).

Another test experiment, which was conducted following the observations of study 2, was an *in situ* mobilization study, similar to the one in Mehlhorn et al. (2014). However, instead of incubating natural soil, the synthetic Fe (oxyhydr)oxides goethite and ferrihydrite, partially loaded with As or Cu, were incubated in the degassing center and the non-CO₂-influenced reference soil of Site A. Furthermore, instead of using 0.2 µm membrane for covering the individual compartments, a polyamide mesh with a pore size of 50 x 50 µm was used to enable microbial colonization. *In situ* incubation of natural and As- or Cu-loaded goethite was done during summer for 6.5 weeks. No metal(loid) mobilization could be observed during this experiment, probably due to the extreme Fe excess, and the dense, sludge-like structure and high crystallinity of the goethite, making the Fe (oxyhydr)oxide less available for microbial processes. Therefore, the following *in situ* mobilization experiment was conducted with natural and As- or Cu-loaded ferrihydrite coated sand in order to increase the porosity and the availability for microbes. The *in situ* mobilization chambers were exposed at Site A for 2 weeks in spring and for 4 weeks in summer. Again, no mobilization of Fe could be determined, but some of the adsorbed As and Cu was mobilized, most pronounced in the summer experiment. However, As mobilization was the same for mofette and reference (approximately 25% of the initial 216 µg g⁻¹) and only Cu showed stronger mobilization within the mofette (62% vs. 12% in the reference of initially 20 µg g⁻¹), probably caused by stronger desorption in the low-pH mofette soil. Oppositely to the experiment with natural soil in Mehlhorn et al. (2014), the incubation of synthetic Fe minerals did neither include any natural soil microbial community nor any carbon source. Thus, even if some Fe(III)-reducing microbes colonized the ferrihydrite during incubation, they were lacking a carbon source to reductively dissolve larger amounts of the Fe mineral and only abiotic desorption of Cu and As could be observed. Same as in the incubations with A. SJH, the soil system was represented in a too simplified way and processes, which could be observed in the experiments with natural soil, were not reproducible. Therefore, no further *in situ* experiments or experiments with pure microbial cultures were conducted for this thesis; instead, emphasis was put on the natural mofette site again.

Concluding from the results of study 2 it can be said that on the short-term scale two main CO₂-triggered metal(loid) mobilization processes can be distinguished. Abiotic mobilization of metal cations (here Mn) due to desorption processes will start immediately upon CO₂ intrusion into soil. However, the overall mobilization by this process was relatively low but might be higher for other soils. A high risk for strong metal(loid) mobilization arises from mineral dissolution processes, especially when these reactions are microbially triggered. Large amounts of Fe (and incorporated metal(loid)s like As and Mn) can be mobilized by microbially triggered reductive dissolution of Fe (oxyhydr)oxides, as shown for the Fe-rich Gleyic Fluvisol of Site A. However, a direct transfer of these results to the mofette site is difficult since the incubation of hitherto non-CO₂-influenced soil with CO₂ for up to 42 days is hardly comparable with decades of CO₂ exhalation at the mofette site. At

the mofettes, formation of pedogenic Fe (oxyhydr)oxides is inhibited by anoxic conditions or limited to micro-oxic conditions along root channels (Rennert et al., 2011) or at small elevations (compare the hummock with elevated Fe and As between two degassing features mentioned in study 1, section 3.1). Strong metal(loid) mobilization due to CO₂-triggered reductive dissolution of Fe (oxyhydr)oxides might play a major role, if degassing structures are moving or new mofettes are forming and hitherto non-CO₂-influenced soil comes under the influence of CO₂. The results of study 2 are especially relevant with regard to risk assessment at GCS sites, where CO₂ leakage could cause metal(loid) mobilization from soils and sediments into aquifers.

An interesting observation in study 2 was that Cu as only element scarcely showed any CO₂-induced changes in mobility. Almost no differences between treatments and controls or between different temperature treatments could be observed. Following minor initial mobilization after mixing of soil and water, which was observed for all elements in all incubations, only the CO₂ treatments with fresh summer soil showed further changes in Cu concentration with continuous immobilization over the course of the experiment. Since the summer soil was strongly enriched in organic carbon and since Cu is known to have a high affinity for SOM (McBride et al., 1997, McLaren and Crawford, 1973, McLaren et al., 1983), this Cu immobilization was attributed to re-adsorption to SOM. However, the strong decrease in redox potential (from 540 ± 10 to 340 ± 20 mV) and the presence of $2.1 \cdot 10^3$ to $4.7 \cdot 10^4$ MPN mL⁻¹ sulfate-reducing microorganisms indicate that also Cu reduction and precipitation in form of sulfidic minerals could have contributed to the observed Cu sequestration. To further elucidate the behavior of Cu under increased $p(\text{CO}_2)$ in mofettes, it was decided to focus on this specific element for the third study of this thesis.

3.3 Copper mobilization and sequestration in mofettes – the role of redox conditions and soil organic matter (study 3)

Copper had shown some quite interesting spatial distribution in study 1: Regarding total contents in SOM-rich topsoil, Cu was both enriched directly in the degassing center and in the non-CO₂-influenced areas, while soil contents were lowest in the transition zones with medium $p(\text{CO}_2)$. Pore water concentrations of Cu were highest in the upper 10 to 15 cm of these transition zones, i.e., also Cu mobility was highest there, especially pronounced in 2 to 4 m distance from the degassing center. Interestingly, Cu mobility was lowest directly in the degassing center, with pore water concentrations being close to or even below the limit of detection. These observations indicate that two distinct Cu binding processes occurred inside and outside of the degassing center and that, in contrast to most other metal(loid)s considered in studies 1 and 2, CO₂ degassing did not simply trigger Cu mobilization and leaching by soil acidification as might have been expected from studies on pH dependent Cu sorption in soil (Degryse et al., 2009).

In order to clarify the distinct Cu binding mechanisms, sorption isotherms were determined in study 3 (Mehlhorn et al., 2018) for four SOM-rich topsoil samples of Site A with increasing soil $p(\text{CO}_2)$ (Reference A, Transition A2, Transition A1, and Mofette A) and two samples from Site B (Reference B and Mofette B).

Copper adsorption was lowest for Transition A1, followed by Transition A2, followed by the two References A and B, which showed almost similar adsorption isotherms. The isotherms of Mofette A and B, however, differed completely from the others: while references and transitions showed linear adsorption isotherms, the Cu adsorption to mofette soils could be fitted best using Freundlich isotherms. In addition, Cu adsorption was significantly higher for mofettes than for the other soils, with Mofette A showing the strongest Cu adsorption of all samples.

Since SOM is known to be the predominant binding partner for Cu in oxic soils (Karlsson et al., 2006, McBride et al., 1997, McLaren and Crawford, 1973, McLaren et al., 1983), both DOM and SOM were studied in more detail. The Cu sorption isotherms were replotted with respect to total DOC for Cu concentrations in liquid phase and with respect to total SOC for Cu adsorbed. Interestingly, the isotherms and linear adsorption coefficients determined for Transitions A1, A2, and Reference A were almost identical when referred to organic carbon. This indicates that SOM was the dominating binding partner for Cu in these soils. However, equal amounts of the spiked Cu complexed with DOM as with solid-phase SOM, resulting in different Cu mobilities in Transitions and References. As expected, SOC contents increased towards the mofette center with Reference A < Transition A2 < Transition A1 < Mofette A. However, also the amount of DOC, which was mobilized into the liquid phase during the course of the experiment, as well as the DOC:SOC ratio increased with increasing SOC. This indicates that the stability of SOM decreases with increasing $p(\text{CO}_2)$ as previously reported by Rennert and Pfanzer (2015).

Differences in SOM quality were also detected in this study. Same as observed in other studies (e.g., Rennert et al., 2011, Ross et al., 2000) and in study 1 of this thesis, the C/N ratio increased towards the degassing center, indicating a lower decomposition state of mofettic SOM. While transitions and references were relatively similar in DOM composition determined by FTIR and in SOM composition determined by ^{13}C NMR, both DOM and SOM of the mofette soils showed some distinct differences from the other soils. The relative fraction of aliphatic carbon in SOM was increased and bands indicative for aliphatic structures and polypeptides were more pronounced in DOM from mofettes. Together with longer chain lengths of the aliphatic structures in DOM, as indicated by the ratio of bands indicative for asymmetric stretching of R-CH₃ and R-CH₂ (Ibarra et al., 1996), these observations confirmed the lower degradation state of DOM and SOM in mofettes.

A negative influence of geogenic CO₂ on the interaction of SOM with soil minerals and thus on SOM stabilization due to accumulation of poorly degraded SOM has been first reported by Rennert and

Pfanz (2015). Sorption isotherms determined in study 3 showed that the decreasing SOM stabilization with increasing $p(\text{CO}_2)$ significantly influenced Cu mobility, and regarding results of study 1, also the mobility of other metal(loid)s with a high affinity for complex formation with DOM. With increasing $p(\text{CO}_2)$, the DOC:SOC ratio increased and thus, also Cu mobility increased by formation of Cu-DOM complexes.

Determination of Cu solid-phase speciation by XAS confirmed the predominance of Cu binding to SOM for transition and reference soils. Using linear combination fitting, best fits could be achieved using reference compounds of Cu(II) adsorbed to organic substances. Binding of Cu(II) to SOM (or DOM) occurs via closely spaced hydroxylic (or amine) and carboxylic groups leading to the formation of very stable five- to six-membered ring chelates (Karlsson et al., 2006, Manceau and Matynia, 2010). Solid-phase speciation showed that also the spiked Cu predominantly adsorbed to organic matter and no significant differences in solid-phase speciation could be observed between transitions and references. This implies that structural changes in SOM composition, e.g., a lower abundance of carboxylic groups at elevated $p(\text{CO}_2)$ as recently described by Rennert (2018), did not influence Cu binding to a detectable extent. Only the DOC:SOC ratio determined Cu mobility in the sorption experiment of study 3.

In soils from the degassing center, another binding mechanism must have caused the strong Cu sequestration. This was indicated already by the differing shape of the sorption isotherms and further confirmed by the fact that Cu adsorption was strong despite high DOC concentrations and a low SOM degradation state in soil from Mofettes A and B. Copper solid-phase speciation determined by XAS further confirmed this hypothesis: according to linear combination fitting, 72% of the Cu in Mofette A was present in form of Cu(I) coordinated via sulfur. Even if no statistically significant distinction between Cu(I) bound to thiol groups of organic matter and Cu sulfide minerals was possible, it could be concluded from the strong Cu sequestration despite high DOC concentrations that Cu sulfide minerals were the dominating Cu compound in Mofette A. Furthermore, one fourth of the spiked Cu(II) must have been reduced and precipitated in form of Cu sulfide, besides adsorption of Cu(II) to SOM.

Copper(II) reduction and subsequent precipitation in form of sulfidic minerals is a process that is known from other anoxic soils, e.g., floodplains, wetlands, or paddy soils (Borch et al., 2009, Fulda et al., 2013a, 2013b, Weber et al., 2009a). Reduction can appear abiotically, e.g., by reaction with reduced humic substances (Maurer et al., 2013, Pham et al., 2012) or be triggered by microorganisms (Hofacker et al., 2015, Sugio et al., 1990). The formed Cu(I) is very reactive, thus, if it is not stabilized by complexation, e.g., with sulfide, it may disproportionate and form metallic Cu(0) and Cu(II) (Fenwick, 1926, Sharma and Millero, 1988). With SEM-EDS a small particle of metallic Cu was detected in a Cu-spiked sample from Mofette A, indicating that precipitation of Cu(0) following Cu(II)

reduction and disproportionation might also occur in mofettes. However, Cu solid-phase speciation determined by XAS did not confirm the presence of Cu(0), thus, contributions must have been low. The detected sulfide concentrations of 1.8 mg L^{-1} , which could be measured in pore water from the mofette center, imply that Cu(II) in mofettes is reduced either by microbes or abiotically, complexes with sulfide, and precipitates in form of sulfidic minerals. This can explain the strong Cu sequestration observed both in natural soils and in Cu spike experiments. In Mehlhorn et al. (2014), strong Cu accumulation was observed in a peat lens, which is located in approximately 2 m depth beneath mofette Site A. Solid-phase speciation of a sample from this peat lens revealed that the majority of the Cu is present as CuS, i.e., as covellite, reinforcing the hypothesis of Cu sequestration by sulfide mineral precipitation in mofettes.

Overall, this study helped to clarify the complex processes of Cu mobilization and sequestration processes along the redox and SOM gradient of a mofette. It could be shown that mofettes serve as sink for Cu and other chalcophilic elements by formation of or co-precipitation with sulfidic minerals. The accumulation of Cu, Cd, Zn, and sulfur that was observed in the degassing center of Site A in study 1 was most probably also caused by metal sulfide precipitation. However, metal sequestration is only guaranteed under completely anoxic conditions, i.e., directly in the degassing center. In the surrounding transition area, with low amounts of oxygen available, increased mobility of Cu and other metal(loid)s due to complexation with DOM has to be expected.

4 Conclusion

The aim of this thesis was to investigate the influence of geogenic CO₂ exhalations at wetland mofette sites on the binding mechanisms and the mobility of metal(loid)s in soil. Metal(loid) mobilization and immobilization processes were explored both on the spatial and temporal scale, differentiating short-term and long-term processes, and results were put in context with CO₂-induced changes in soil conditions and pedogenesis.

Three main processes, which trigger metal(loid) mobilization and immobilization, could be distinguished: desorption following surface protonation, mineral dissolution, and precipitation of sulfidic minerals. The conceptual model developed in a pre-study to this thesis (Figure 4) could be refined, now separating short-term and long-term processes (Figure 5).

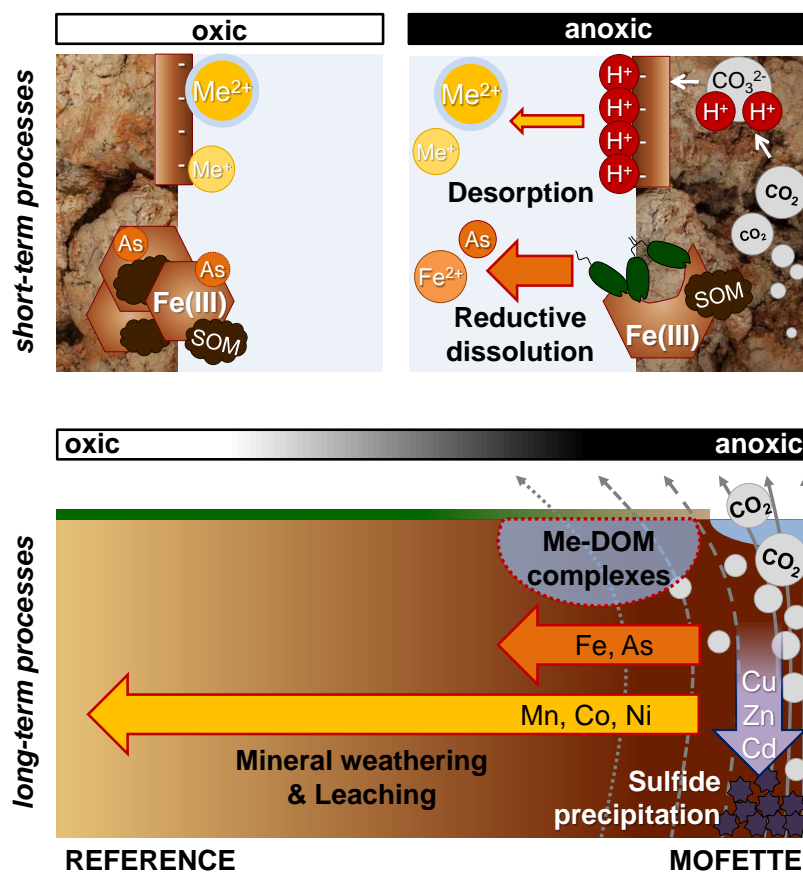


Figure 5. Conceptual model comparing short-term (top graph) and long-term (bottom graph) CO₂-induced metal(loid) mobilization (red-framed arrows) and immobilization (blue-framed arrow) processes. The short-term processes correspond to a temporal change in CO₂, i.e., a sudden CO₂ release into a hitherto non-CO₂-influenced soil as investigated in study 2. The long-term processes correspond to a change in spatial metal(loid) distribution at a mofette site, in which CO₂ exhalation influenced pedogenesis for at least several decades, going from non-CO₂-influenced reference soil (left) towards the degassing center (right) as investigated in studies 1 and 3.

Main mobilization processes following CO₂ intrusion into a hitherto non-CO₂-influenced soil are desorption of metal cations and the reductive dissolution of pedogenic Fe (oxyhydr)oxides (study 2; Figure 5, top graph). While desorption of metal cations occurs immediately and overall mobilization is

comparably low, reductive dissolution of Fe (oxyhydr)oxides as microbially triggered process only starts after depletion of more favorable electron acceptors, like oxygen or nitrate. However, significantly larger amounts of Fe and incorporated metal(loid)s are mobilized compared to mobilization via desorption. The dissolution of CO₂ in pore water further accelerates the reductive dissolution processes by constant supply of protons. Iron(II) oxidation and reductive dissolution of pedogenic Fe (oxyhydr)oxides are both reactions with fast kinetics due to the catalyzing effect of microbial activity (Kirk, 2004, Lovley, 1991). These fast kinetics and the small scale heterogeneity of soil conditions around mofettes lead to an increased As and Fe mobility in close vicinity to the degassing center of mofettes, which is still apparent after decades of CO₂ exhalation (study 1; Figure 5, bottom graph).

The above-mentioned, short-term mobilization processes can constitute a risk if large amounts of toxic trace elements, like As, are mobilized into aquifers. The extent of mobilization of course depends on further parameters like soil composition and climatic conditions. For example, dissolution of carbonate minerals would be a main process expected after CO₂ intrusion into limestone containing rocks and soils (e.g., at the Starzach mofette site in southern Germany (Lübben and Leven, 2018)), but could not be observed at the site studied for this thesis due to the absence of carbonates in the already relatively acidic parent material of the soil (sediments from magmatic and metamorphic rocks). Regarding climate, warmer temperatures would enhance microbially triggered reactions, while cold conditions would increase the net-mobilization via desorption since more CO₂ could dissolve in the pore water.

While reductive dissolution of pedogenic Fe (oxyhydr)oxides is a fast and reversible mineral dissolution process, weathering of silicates is a much slower, generally non-reversible process and could thus not be observed in study 2. Investigation of the spatial metal(loid) distribution around a main degassing feature of a mofette in study 1, however, suggests that mobilization of metal(loid)s (Mn, Ni, Co, Zn) due to mineral weathering occurred at this site. Increased weathering of silicates present in soil releases adsorbed and incorporated metal(loid)s into the pore water. In contrast to the dissolution of Fe (oxyhydr)oxides, silicate weathering is rather triggered by the CO₂-induced soil acidification than by anoxic conditions and microbial processes. Thus, depletion of metal(loid)s associated with silicates is not limited to the degassing center but occurs in the whole CO₂-influenced area. Moreover, depletion is not limited to the solid phase. The pore water of the mofette site was likewise depleted in these metals due to continuous leaching, indicating that quasi-equilibrium between soil and pore water has developed after long-term CO₂ influence (study 1).

Aluminum and partly also Cr seem to be less affected by metal(loid) mobilization following silicate weathering, which can be attributed to the fact that the aluminum octahedral and tetrahedral structures of aluminosilicates will stay intact for a long time and would only be dissolved in the final step of aluminosilicate hydrolysis. Furthermore, released Al might precipitate immediately with silicic acid,

forming kaolinite, or with water, forming gibbsite (Blume et al., 2016). Most likely, depletion in Al and Cr around CO₂ exhalations is primarily indirectly caused by accumulation of SOM and thus a decreased soil mineral content while actual mobilization due to silicate weathering remains low.

Accumulation of SOM is also responsible for the increased mobility of numerous metal(loid)s following long-term CO₂-influence in mofettes. Due to the poor decomposition state of the accumulating SOM, DOM concentrations are strongly increased around CO₂ exhalations. Metal(loid)s with a high affinity for DOM (Al, As, Cr, Cu, Fe, Zn) are complexed by DOM in these zones, which prevents adsorption or precipitation and thus increases metal(loid) mobility (study 1, study 3).

No evidence for net-immobilization of metal(loid)s by re-adsorption to solid-phase SOM, as postulated in Mehlhorn et al. (2014), was retrieved in the studies conducted for this thesis, however, the process might play a role at mofettes on the long-term scale. The net-immobilization in mofettes observed for Cu in the pre-study was more likely caused by precipitation of sulfidic minerals. Due to the permanently anoxic conditions in the degassing center of mofettes, Cu(II) is reduced to Cu(I), complexes with microbially produced sulfide, and precipitates in form of Cu sulfide minerals (study 3). This process leads to strong Cu accumulation in the degassing center and effectively sequesters Cu from pore water despite high DOM concentrations. Accumulation of Cd and Zn in the degassing center suggests that these chalcophilic metals are also sequestered by sulfide formation or co-precipitation (study 1). Immobilization of these metals may constitute a risk for soil organisms and plants by limitation of essential trace elements. However, regarding mofettes, the extreme $p(\text{CO}_2)$, especially in the degassing center, probably represents the more important limitation for plant growth and soil organisms.

With the studies conducted for this thesis, main processes causing mobilization and immobilization of metal(loid)s in soils affected by high $p(\text{CO}_2)$ in mofettes could be elucidated. The influence of CO₂ on sorption, dissolution, and precipitation processes mainly occurs via CO₂-induced soil acidification and/or (permanently) anoxic soil conditions. Thus, mobilization and immobilization processes are similar to processes known to occur in other anoxic soils (e.g., wetland or floodplain soils) or during soil acidification. However, the combination of several influencing factors, e.g., the increased SOM content and changed SOM composition, the spatial changes in redox conditions, soil and pore water pH, and microbial community changes, is unique for mofettes, as well as the variety of soil conditions that can be found within a relatively small area at these sites. Especially, the gradient in redox conditions from permanently anoxic conditions in the degassing center to oxic conditions within only several meters distance makes mofette sites a suitable natural laboratory to study metal(loid) mobilization and immobilization processes.

Regarding risk assessment for GCS sites, it could be shown that on a short-term scale metal(loid) mobilization via desorption and microbially triggered reductive dissolution of Fe (oxyhydr)oxides and

other minerals has to be expected. While these short-term effects can be easily tested for different types of soil and sediment in laboratory experiments, studies at mofettes, as done for this thesis, help to estimate the long-term influences of CO₂ on soil and metal(loid) mobility, which will be relevant if a leakage at a GCS site is not detected or cannot be sealed.

References

- acatech (Ed.), 2018. CCU und CCS – Bausteine für den Klimaschutz in der Industrie; Analyse, Handlungsoptionen und Empfehlungen. Herbert Utz Verlag, München.
- Baklid, A., Korbol, R., Owren, G., 1996. Sleipner Vest CO₂ disposal, CO₂ injection into a shallow underground aquifer, SPE Annual Technical Conference and Exhibition. Society of Petroleum Engineers.
- Bankwitz, P., Schneider, G., Kämpf, H., Bankwitz, E., 2003. Structural characteristics of epicentral areas in Central Europe: study case Cheb Basin (Czech Republic). *J. Geodyn.*, 35(1-2), 5-32.
- Bauer, M., Blodau, C., 2006. Mobilization of arsenic by dissolved organic matter from iron oxides, soils and sediments. *Sci. Total Environ.*, 354(2), 179-190.
- Baxter, P.J., Kapila, M., Mfonfu, D., 1989. Lake Nyos disaster, Cameroon, 1986: the medical effects of large scale emission of carbon dioxide? *BMJ*, 298(6685), 1437-1441.
- Beaubien, S., Ciotoli, G., Coombs, P., Dictor, M.C., Krüger, M., Lombardi, S., Pearce, J., West, J., 2008. The impact of a naturally occurring CO₂ gas vent on the shallow ecosystem and soil chemistry of a Mediterranean pasture (Latera, Italy). *Int. J. Greenh. Gas Control*, 2(3), 373-387.
- Benson, S.M., Cole, D.R., 2008. CO₂ sequestration in deep sedimentary formations. *Elements*, 4(5), 325-331.
- Beulig, F., Heuer, V.B., Akob, D.M., Viehweger, B., Elvert, M., Herrmann, M., Hinrichs, K.-U., Küsel, K., 2015. Carbon flow from volcanic CO₂ into soil microbial communities of a wetland mofette. *ISME J.*, 9(3), 746-759.
- Beulig, F., Urich, T., Nowak, M., Trumbore, S.E., Gleixner, G., Gilfillan, G.D., Fjelland, K.E., Küsel, K., 2016. Altered carbon turnover processes and microbiomes in soils under long-term extremely high CO₂ exposure. *Nat. Microbiol.*, 1, 15025.
- Blume, H.-P., Felix-Henningsen, P., 2009. Reductosols: Natural soils and Technosols under reducing conditions without an aquic moisture regime. *J. Plant Nutr. Soil Sci.*, 172(6), 808-820.
- Blume, H.-P., Brümmer, G.W., Fleige, H., Horn, R., Kandeler, E., Kögel-Knabner, I., Kretzschmar, R., Stahr, K., Wilke, B.-M., 2016. Scheffer/Schachtschabel: Soil Science. Springer-Verlag, Berlin Heidelberg.
- BMUB, 2016. Klimaschutzplan 2050 – Klimapolitische Grundsätze und Ziele der Bundesregierung, Bundesministerium für Umwelt, Naturschutz, Bau und Reaktorsicherheit.
- Borch, T., Kretzschmar, R., Kappler, A., Cappellen, P.V., Ginder-Vogel, M., Voegelin, A., Campbell, K., 2009. Biogeochemical redox processes and their impact on contaminant dynamics. *Environ. Sci. Technol.*, 44(1), 15-23.
- Bowell, R.J., 1994. Sorption of arsenic by iron oxides and oxyhydroxides in soils. *Appl. Geochem.*, 9(3), 279-286.
- Bradl, H.B., 2004. Adsorption of heavy metal ions on soils and soils constituents. *J. Colloid Interface Sci.*, 277(1), 1-18.
- Bräuer, K., Kämpf, H., Strauch, G., Weise, S.M., 2003. Isotopic evidence (³He/⁴He, ¹³C_{CO2}) of fluid-triggered intraplate seismicity. *J. Geophys. Res. B: Solid Earth*, 108(B2).
- Bräuer, K., Kämpf, H., Niedermann, S., Strauch, G., Tesář, J., 2008. Natural laboratory NW Bohemia: Comprehensive fluid studies between 1992 and 2005 used to trace geodynamic processes. *Geochem. Geophys. Geosyst.*, 9(4).
- Bräuer, K., Kämpf, H., Niedermann, S., Strauch, G., 2018. Monitoring of helium and carbon isotopes in the western Eger Rift area (Czech Republic): Relationships with the 2014 seismic activity and indications for recent (2000–2016) magmatic unrest. *Chem. Geol.*, 482, 131-145.
- Bussert, R., Kämpf, H., Flehsig, C., Hesse, K., Nickschick, T., Liu, Q., Umlauf, J., Vylita, T., Wagner, D., Wonik, T., 2017. Drilling into an active mofette: pilot-hole study of the impact of CO₂-rich mantle-derived fluids on the geo-bio interaction in the western Eger Rift (Czech Republic). *Sci. Dril.*, 23, 13.
- Carrillo-González, R., Šimůnek, J., Sauve, S., Adriano, D., 2006. Mechanisms and pathways of trace element mobility in soils. *Adv. Agron.*, 91, 111-178.
- Cline, J.D., 1969. Spectrophotometric determination of hydrogen sulfide in natural waters. *Limnol. Oceanogr.*, 14(3), 454-458.

- Cotrufo, M.F., Raschi, A., Lanini, M., Ineson, P., 1999. Decomposition and nutrient dynamics of *Quercus pubescens* leaf litter in a naturally enriched CO₂ Mediterranean ecosystem. *Funct. Ecol.*, 13(3), 343-351.
- Credner, H., 1900. Die vogtländischen Erdbebenschwärme während der Zeit des Juli und August 1900. *Berichte über die Verhandlungen der Königlich-Sächsischen Gesellschaft der Wissenschaften zu Leipzig, Mathematisch-Physische Klasse*, 52, 153-177.
- D'Alessandro, W., 2006. Gas hazard: an often neglected natural risk in volcanic areas. In: Martin-Duque, J., Brebbia, C., Emmanouloudis, D., Mander, U. (Eds.), *Geo-environment and landscape evolution II: evolution, monitoring, simulation, management and remediation of the geological environment and landscape*. WIT Transactions on Ecology and the Environment, pp. 10.
- Degryse, F., Smolders, E., Parker, D., 2009. Partitioning of metals (Cd, Co, Cu, Ni, Pb, Zn) in soils: concepts, methodologies, prediction and applications – a review. *Eur. J. Soil Sci.*, 60(4), 590-612.
- Du Laing, G., Vanthuyne, D., Vandecasteele, B., Tack, F., Verloo, M., 2007. Influence of hydrological regime on pore water metal concentrations in a contaminated sediment-derived soil. *Environ. Pollut.*, 147(3), 615-625.
- Fenwick, F., 1926. The equilibrium between cupric ion, cuprous ion and metallic copper. *J. Am. Chem. Soc.*, 48(4), 860-870.
- Fernández-Montiel, I., Sidrach-Cardona, R., Gabilondo, R., Pedescoll, A., Scheu, S., Bécares, E., 2016. Soil communities are affected by CO₂ belowground emissions at a natural vent in Spain. *Soil Biol. Biochem.*, 97, 92-98.
- Fischer, T., Horálek, J., Hrubcová, P., Vavryčuk, V., Bräuer, K., Kämpf, H., 2014. Intra-continental earthquake swarms in West-Bohemia and Vogtland: a review. *Tectonophysics*, 611, 1-27.
- Flechsig, C., Bussert, R., Rechner, J., Schütze, C., Kämpf, H., 2008. The Hartoušov mofette field in the Cheb Basin, western Eger Rift (Czech Republic): a comparative geoelectric, sedimentologic and soil gas study of a magmatic diffuse CO₂-degassing structure. *Z. Geol. Wiss.*, 36(3), 177-193.
- Frerichs, J., Oppermann, B.I., Gwosdz, S., Möller, I., Herrmann, M., Krüger, M., 2013. Microbial community changes at a terrestrial volcanic CO₂ vent induced by soil acidification and anaerobic microhabitats within the soil column. *FEMS Microbiol. Ecol.*, 84(1), 60-74.
- Fulda, B., Voegelin, A., Ehlert, K., Kretzschmar, R., 2013a. Redox transformation, solid phase speciation and solution dynamics of copper during soil reduction and reoxidation as affected by sulfate availability. *Geochim. Cosmochim. Acta*, 123, 385-402.
- Fulda, B., Voegelin, A., Kretzschmar, R., 2013b. Redox-controlled changes in cadmium solubility and solid-phase speciation in a paddy soil as affected by reducible sulfate and copper. *Environ. Sci. Technol.*, 47(22), 12775-12783.
- Gagel, C., Stremme, H., 1909. Ueber einen Fall von Kaolinbildung im Granit durch einen kalten Säuerling. *Centralblatt f. Mineralogie, Abt. A*, 427-437.
- Gislason, S.R., Wolff-Boenisch, D., Stefansson, A., Oelkers, E.H., Gunnlaugsson, E., Sigurdardottir, H., Sigfusson, B., Broecker, W.S., Matter, J.M., Stute, M., 2010. Mineral sequestration of carbon dioxide in basalt: A pre-injection overview of the CarbFix project. *Int. J. Greenh. Gas Control*, 4(3), 537-545.
- Grafe, M., Eick, M., Grossl, P., 2001. Adsorption of arsenate (V) and arsenite (III) on goethite in the presence and absence of dissolved organic carbon. *Soil Sci. Soc. Am. J.*, 65(6), 1680-1687.
- Grafe, M., Eick, M.J., Grossl, P.R., Saunders, A.M., 2002. Adsorption of arsenate and arsenite on ferrihydrite in the presence and absence of dissolved organic carbon. *J. Environ. Qual.*, 31(4), 1115-1123.
- Grotzinger, J., Jordan, T.H., 2014. *Understanding Earth*. W. H. Freeman, USA, 3rd edition.
- Harvey, O.R., Qafoku, N.P., Cantrell, K.J., Wilkins, M.J., Brown, C.F., 2016. Methanogenesis-induced pH–Eh shifts drives aqueous metal(loid) mobility in sulfide mineral systems under CO₂ enriched conditions. *Geochim. Cosmochim. Acta*, 173, 232-245.
- Henderson, Y., Haggard, H.W., 1943. *Noxious gases*. Reinhold Publishing Corporation.

- Henry, W., 1803. III. Experiments on the quantity of gases absorbed by water, at different temperatures, and under different pressures. *Philosophical Transactions of the Royal Society of London*, 93, 29-42 and 274-276.
- Hesslein, R.H., 1976. An in situ sampler for close interval pore water studies. *Limnol. Oceanogr.*, 21(6).
- Hofacker, A.F., Voegelin, A., Kaegi, R., Weber, F.-A., Kretzschmar, R., 2013. Temperature-dependent formation of metallic copper and metal sulfide nanoparticles during flooding of a contaminated soil. *Geochim. Cosmochim. Acta*, 103, 316-332.
- Hofacker, A.F., Behrens, S., Voegelin, A., Kaegi, R., Lösekann-Behrens, T., Kappler, A., Kretzschmar, R., 2015. *Clostridium* species as metallic copper-forming bacteria in soil under reducing conditions. *Geomicrobiol. J.*, 32(2), 130-139.
- Hohberg, K., Schulz, H.-J., Balkenhol, B., Pilz, M., Thomalla, A., Russell, D.J., Pfanzer, H., 2015. Soil faunal communities from mofette fields: effects of high geogenic carbon dioxide concentration. *Soil Biol. Biochem.*, 88, 420-429.
- Horálek, J., Fischer, T., 2008. Role of crustal fluids in triggering the West Bohemia/Vogtland earthquake swarms: just what we know (a review). *StGG*, 52(4), 455.
- Ibarra, J., Munoz, E., Moliner, R., 1996. FTIR study of the evolution of coal structure during the coalification process. *Org. Geochem.*, 24(6), 725-735.
- IPCC, 2005. IPCC special report on carbon dioxide capture and storage. Prepared by Working Group III of the Intergovernmental Panel on Climate Change. Cambridge University Press, United Kingdom and New York, NY, USA, 442 pp.
- Irwin, W.P., Barnes, I., 1980. Tectonic relations of carbon dioxide discharges and earthquakes. *J. Geophys. Res. B: Solid Earth*, 85(B6), 3115-3121.
- IUSS Working Group WRB, 2015. World Reference Base for Soil Resources 2014, Update 2015, International soil classification system for naming soils and creating legends for soil maps. World Soil Resources Reports No. 106. Food and Agriculture Organization of the United Nations, Rome, Italy, 192 pp.
- Jackson, M., Armstrong, W., 1999. Formation of aerenchyma and the processes of plant ventilation in relation to soil flooding and submergence. *Plant Biol.*, 1(3), 274-287.
- Jähn, N., 2018. Erdbeben: Erwacht hier ein Vulkan? , Freie Presse, https://www.freiepresse.de/vogtland/oberes-vogtland/erdbeben-erwacht-hier-ein-vulkan-artikel10255812?utm_campaign=Echobox&utm_medium=Social&utm_source=Facebook#Ec_hobox=1531202051. Accessed 4 October 2018.
- Jones, D., Beaubien, S., Blackford, J., Foekema, E., Lions, J., De Vittor, C., West, J., Widdicombe, S., Hauton, C., Queirós, A., 2015. Developments since 2005 in understanding potential environmental impacts of CO₂ leakage from geological storage. *Int. J. Greenh. Gas Control*, 40, 350-377.
- Jun, Y.-S., Giammar, D.E., Werth, C.J., 2012. Impacts of geochemical reactions on geologic carbon sequestration. *Environ. Sci. Technol.*, 47(1), 3-8.
- Jun, Y.-S., Giammar, D.E., Werth, C.J., Dzombak, D.A., 2013. Environmental and geochemical aspects of geologic carbon sequestration: a special issue. *Environ. Sci. Technol.*, 47(1), 1-2.
- Kalbitz, K., Wennrich, R., 1998. Mobilization of heavy metals and arsenic in polluted wetland soils and its dependence on dissolved organic matter. *Sci. Total Environ.*, 209(1), 27-39.
- Kämpf, H., Bräuer, K., Schumann, J., Hahne, K., Strauch, G., 2013. CO₂ discharge in an active, non-volcanic continental rift area (Czech Republic): Characterisation ($\delta^{13}\text{C}$, $^3\text{He}/^4\text{He}$) and quantification of diffuse and vent CO₂ emissions. *Chem. Geol.*, 339(0), 71-83.
- Karlsson, T., Persson, P., Skyllberg, U., 2006. Complexation of copper(II) in organic soils and in dissolved organic matter – EXAFS evidence for chelate ring structures. *Environ. Sci. Technol.*, 40(8), 2623-2628.
- Kharaka, Y.K., Cole, D.R., Hovorka, S.D., Gunter, W.D., Knauss, K.G., Freifeld, B.M., 2006. Gas-water-rock interactions in Frio Formation following CO₂ injection: implications for the storage of greenhouse gases in sedimentary basins. *Geology*, 34(7), 577-580.
- Kharaka, Y.K., Thordsen, J.J., Kakouros, E., Ambats, G., Herkelrath, W.N., Beers, S.R., Birkholzer, J.T., Apps, J.A., Spycher, N.F., Zheng, L., Trautz, R.C., Rauch, H.W., Gullickson, K.S., 2010.

- Changes in the chemistry of shallow groundwater related to the 2008 injection of CO₂ at the ZERT field site, Bozeman, Montana. *Environ. Earth Sci.*, 60(2), 273-284.
- Kies, A., Hengesbach, O., Tosheva, Z., Raschi, A., Pfanzer, H., 2015. Diurnal CO₂-cycles and temperature regimes in a natural CO₂ gas lake. *Int. J. Greenh. Gas Control*, 37, 142-145.
- Kirk, G., 2004. *The biogeochemistry of submerged soils*. John Wiley & Sons, England.
- Kirk, M.F., Santillan, E.F., Sanford, R.A., Altman, S.J., 2013. CO₂-induced shift in microbial activity affects carbon trapping and water quality in anoxic bioreactors. *Geochim. Cosmochim. Acta*, 122, 198-208.
- Kirsch, K., Navarre-Sitchler, A.K., Wunsch, A., McCray, J.E., 2014. Metal release from sandstones under experimentally and numerically simulated CO₂ leakage conditions. *Environ. Sci. Technol.*, 48(3), 1436-1442.
- Knett, J., 1899. Das erzgebirgische Schwarmbeben zu Hartenberg vom 1. Jänner bis 5. Feber 1824. *Sitzungsber. Dtsch. Naturwiss. Med. Ver. Böhmen Lotos Prague*(19), 167-191.
- Krauze, P., Kämpf, H., Horn, F., Liu, Q., Voropaev, A., Wagner, D., Alawi, M., 2017. Microbiological and geochemical survey of CO₂-dominated mofette and mineral waters of the Cheb Basin, Czech Republic. *Front. Microbiol.*, 8, 2446.
- Langford, N.J., 2005. Carbon dioxide poisoning. *Toxicol. Rev.*, 24(4), 229-235.
- Lawter, A., Qafoku, N., Shao, H., Bacon, D., Brown, C., 2015. Evaluating impacts of CO₂ and CH₄ gas intrusion into an unconsolidated aquifer: fate of As and Cd. *Front. Environ. Sci.*, 3, 49.
- Lawter, A., Qafoku, N.P., Wang, G., Shao, H., Brown, C.F., 2016. Evaluating impacts of CO₂ intrusion into an unconsolidated aquifer: I. Experimental data. *Int. J. Greenh. Gas Control*, 44, 323-333.
- Le Guern, F., Tazieff, H., Pierret, R.F., 1982. An example of health hazard: people killed by gas during a phreatic eruption: Dieng Plateau (Java, Indonesia), February 20th 1979. *Bulletin Volcanologique*, 45(2), 153-156.
- Lewicki, J.L., Birkholzer, J., Tsang, C.-F., 2007. Natural and industrial analogues for leakage of CO₂ from storage reservoirs: identification of features, events, and processes and lessons learned. *Environ. Geol.*, 52(3), 457-467.
- Lions, J., Devau, N., De Lary, L., Dupraz, S., Parmentier, M., Gombert, P., Dictor, M.-C., 2014. Potential impacts of leakage from CO₂ geological storage on geochemical processes controlling fresh groundwater quality: a review. *Int. J. Greenh. Gas Control*, 22, 165-175.
- Little, M.G., Jackson, R.B., 2010. Potential impacts of leakage from deep CO₂ geosequestration on overlying freshwater aquifers. *Environ. Sci. Technol.*, 44(23), 9225-9232.
- Livesey, N., Huang, P., 1981. Adsorption of arsenate by soils and its relation to selected chemical properties and anions. *Soil Sci.*, 131(2), 88-94.
- Lovley, D.R., 1991. Dissimilatory Fe(III) and Mn(IV) reduction. *Microbiol. Rev.*, 55(2), 259-287.
- Lu, J., Partin, J.W., Hovorka, S.D., Wong, C., 2010. Potential risks to freshwater resources as a result of leakage from CO₂ geological storage: a batch-reaction experiment. *Environ. Earth Sci.*, 60(2), 335-348.
- Lübben, A., Leven, C., 2018. The Starzach site in Southern Germany: a site with naturally occurring CO₂ emissions recovering from century-long gas mining as a natural analog for a leaking CCS reservoir. *Environ. Earth Sci.*, 77(8), 316.
- Maček, I., Videmšek, U., Kastelec, D., Stopar, D., Vodnik, D., 2009. Geological CO₂ affects microbial respiration rates in Stavešinci mofette soils. *Acta Biol. Slov.*, 52(2), 41-48.
- Maček, I., Kastelec, D., Vodnik, D., 2012. Root colonization with arbuscular mycorrhizal fungi and glomalin-related soil protein (GRSP) concentration in hypoxic soils in natural CO₂ springs. *Agr. Food. Sci.*, 21(1), 62-71.
- Manceau, A., Matynia, A., 2010. The nature of Cu bonding to natural organic matter. *Geochim. Cosmochim. Acta*, 74(9), 2556-2580.
- Manning, B.A., Goldberg, S., 1997. Arsenic (III) and arsenic (V) adsorption on three California soils. *Soil Sci.*, 162(12), 886-895.
- Martens, S., Möller, F., Streibel, M., Liebscher, A., Group, T.K., 2014. Completion of five years of safe CO₂ injection and transition to the post-closure phase at the Ketzin pilot site. *Energy Procedia*, 59, 190-197.

- Matter, J.M., Stute, M., Snæbjörnsdóttir, S.Ó., Oelkers, E.H., Gislason, S.R., Aradóttir, E.S., Sigfusson, B., Gunnarsson, I., Sigurdardóttir, H., Gunnlaugsson, E., 2016. Rapid carbon mineralization for permanent disposal of anthropogenic carbon dioxide emissions. *Sci.*, 352(6291), 1312-1314.
- Maurer, F., Christl, I., Fulda, B., Voegelin, A., Kretzschmar, R., 2013. Copper redox transformation and complexation by reduced and oxidized soil humic acid. 2. Potentiometric titrations and dialysis cell experiments. *Environ. Sci. Technol.*, 47(19), 10912-10921.
- McBride, M., 1989. Reactions controlling heavy metal solubility in soils. *Adv. Soil Sci.*, 1-56.
- McBride, M., Sauve, S., Hendershot, W., 1997. Solubility control of Cu, Zn, Cd and Pb in contaminated soils. *Eur. J. Soil Sci.*, 48(2), 337-346.
- McGrath, S.P., Sanders, J.R., Shalaby, M.H., 1988. The effects of soil organic matter levels on soil solution concentrations and extractabilities of manganese, zinc and copper. *Geoderma*, 42(2), 177-188.
- McLaren, R., Williams, J., Swift, R., 1983. Some observations on the desorption and distribution behaviour of copper with soil components. *Eur. J. Soil Sci.*, 34(2), 325-331.
- McLaren, R.G., Crawford, D.V., 1973. Studies on soil copper II. The specific adsorption of copper by soils. *J. Soil Sci.*, 24(4), 443-452.
- MDR Wissen, 2018. Hinweise auf "Magma-Reservoir" – Vogtland "demnächst" Vulkangebiet MDR AKTUELL RADIO, 16 July 2018, 07:49 <https://www.mdr.de/wissen/umwelt/vogtland-vulkan-beben-gfz-100.html>. Accessed 30 October 2018.
- Mehlhorn, J., Beulig, F., Küsel, K., Planer-Friedrich, B., 2014. Carbon dioxide triggered metal(loid) mobilisation in a mofette. *Chem. Geol.*, 382, 54-66.
- Mehlhorn, J., Byrne, J.M., Kappler, A., Planer-Friedrich, B., 2016. Time and temperature dependency of carbon dioxide triggered metal(loid) mobilization in soil. *Appl. Geochem.*, 74, 122-137.
- Mehlhorn, J., Besold, J., Lezama-Pacheco, J.S., Gustafsson, J.P., Kretzschmar, R., Planer-Friedrich, B., 2018. Copper mobilization and immobilization along an organic matter and redox gradient – insights from a mofette site. *Environ. Sci. Technol.*, 52(23), 13698-13707.
- Mehlhorn, J., Gerber, L.A., Planer-Friedrich, B., 2019. Spatial distribution of metal(loid) depletion and accumulation zones around a natural carbon dioxide degassing site. *Chem. Geol.*, 509, 64-76.
- Melton, E.D., Swanner, E.D., Behrens, S., Schmidt, C., Kappler, A., 2014. The interplay of microbially mediated and abiotic reactions in the biogeochemical Fe cycle. *Nat. Rev. Microbiol.*, 12(12), 797-808.
- Metz, R., 2016, unpublished. Influence of CO₂ on mobilization of Fe and As by abiotic and microbially triggered dissolution of ferrihydrite, Bachelor Thesis, University of Bayreuth, Environmental Geochemistry.
- Mickler, P.J., Yang, C., Scanlon, B.R., Reedy, R., Lu, J., 2013. Potential impacts of CO₂ leakage on groundwater chemistry from laboratory batch experiments and field push-pull tests. *Environ. Sci. Technol.*, 47(18), 10694-10702.
- Moffett, J.W., Zika, R.G., Petasne, R.G., 1985. Evaluation of bathocuproine for the spectrophotometric determination of copper(I) in copper redox studies with applications in studies of natural waters. *Anal. Chim. Acta*, 175, 171-179.
- Montes-Hernandez, G., Renard, F., Lafay, R., 2013. Experimental assessment of CO₂-mineral-toxic ion interactions in a simplified freshwater aquifer: Implications for CO₂ leakage from deep geological storage. *Environ. Sci. Technol.*, 47(12), 6247-6253.
- Morse, J., Luther, G., 1999. Chemical influences on trace metal-sulfide interactions in anoxic sediments. *Geochim. Cosmochim. Acta*, 63(19), 3373-3378.
- Nickschick, T., Kämpf, H., Flechsig, C., Mrlina, J., Heinicke, J., 2015. CO₂ degassing in the Hartoušov mofette area, western Eger Rift, imaged by CO₂ mapping and geoelectrical and gravity surveys. *IJEaS*, 104(8), 2107-2129.
- Nowak, M., Beulig, F., von Fischer, J., Muhr, J., Küsel, K., Trumbore, S.E., 2015. Autotrophic fixation of geogenic CO₂ by microorganisms contributes to soil organic matter formation and alters isotope signatures in a wetland mofette. *Biogeosciences*, 12, 7169-7183.
- Oelkers, E.H., Cole, D.R., 2008. Carbon dioxide sequestration a solution to a global problem. *Elements*, 4(5), 305-310.

- Oelkers, E.H., Gislason, S.R., Matter, J., 2008. Mineral carbonation of CO₂. *Elements*, 4(5), 333-337.
- Olk, D.C., Cassman, K.G., Schmidt-Rohr, K., Anders, M.M., Mao, J.-D., Deenik, J.L., 2006. Chemical stabilization of soil organic nitrogen by phenolic lignin residues in anaerobic agroecosystems. *Soil Biol. Biochem.*, 38(11), 3303-3312.
- Oppermann, B.I., Michaelis, W., Blumenberg, M., Frerichs, J., Schulz, H.M., Schippers, A., Beaubien, S.E., Krueger, M., 2010. Soil microbial community changes as a result of long-term exposure to a natural CO₂ vent. *Geochim. Cosmochim. Acta*, 74(9), 2697-2716.
- Oxford English Dictionary online, 2018a. "mofette, *n.*", Oxford University Press, July 2018, <http://www.oed.com/view/Entry/120708?redirectedFrom=mofette&>. Accessed 5 September 2018.
- Oxford English Dictionary online, 2018b. "mephitis, *n.*", Oxford University Press, July 2018, <http://www.oed.com/view/Entry/116592?redirectedFrom=mephitis>. Accessed 6 September 2018.
- Paoletti, E., Pfan, H., Raschi, A., 2005. Pros and cons of CO₂ springs as experimental sites, Plant responses to air pollution and global change. Springer, pp. 195-202.
- Pearce, J.M., 2006. What can we learn from natural analogues? In: Lombardi, S., Altunina, L.K., Beaubien, S.E. (Eds.), *Advances in the Geological Storage of Carbon Dioxide*. Springer Netherlands, pp. 127-139.
- Peterek, A., Schunk, R., 2008. Zitternde Erde – Die Schwarmbeben in Nordwestböhmen. Sonderveröffentlichung Bayerisch-Böhmischer Geopark 1/2008.
- Pfan, H., Vodnik, D., Wittmann, C., Aschan, G., Raschi, A., 2004. Plants and Geothermal CO₂ Exhalations – Survival in and Adaptation to a High CO₂ Environment. *Prog. Bot.*, 65, 499-538.
- Pfan, H., Vodnik, D., Wittmann, C., Aschan, G., Batic, F., Turk, B., Macek, I., 2007. Photosynthetic performance (CO₂-compensation point, carboxylation efficiency, and net photosynthesis) of timothy grass (*Phleum pratense* L.) is affected by elevated carbon dioxide in post-volcanic mofette areas. *Environ. Exp. Bot.*, 61(1), 41-48.
- Pfan, H., 2008. Mofetten: Kalter Atem schlafender Vulkane. Deutsche Vulkanologische Gesellschaft e. V., Rheinischer Ver. f. Denkmalpflege u. Landschaftsschutz, Köln.
- Pham, A.N., Rose, A.L., Waite, T.D., 2012. Kinetics of Cu(II) reduction by natural organic matter. *J. Phys. Chem. A*, 116(25), 6590-6599.
- Pohlman, A.A., McColl, J.G., 1988. Soluble organics from forest litter and their role in metal dissolution. *Soil Sci. Soc. Am. J.*, 52(1), 265-271.
- Qafoku, N.P., Lawter, A.R., Shao, H., Wang, G., Brown, C.F., 2014. Evaluating Impacts of CO₂ Gas Intrusion Into a Confined Sandstone aquifer: Experimental Results. *Energy Procedia*, 63, 3275-3284.
- Redman, A.D., Macalady, D.L., Ahmann, D., 2002. Natural organic matter affects arsenic speciation and sorption onto hematite. *Environ. Sci. Technol.*, 36(13), 2889-2896.
- Rennert, T., Eusterhues, K., Pfan, H., Totsche, K.U., 2011. Influence of geogenic CO₂ on mineral and organic soil constituents on a mofette site in the NW Czech Republic. *Eur. J. Soil Sci.*, 62(4), 572-580.
- Rennert, T., Eusterhues, K., Andrade, V.D., Totsche, K.U., 2012. Iron species in soils on a mofette site studied by Fe K-edge X-ray absorption near-edge spectroscopy. *Chem. Geol.*, 332-333, 116-123.
- Rennert, T., Pfan, H., 2015. Geogenic CO₂ affects stabilization of soil organic matter. *Eur. J. Soil Sci.*, 66(5), 838-846.
- Rennert, T., Pfan, H., 2016. Hypoxic and acidic—Soils on mofette fields. *Geoderma*, 280, 73-81.
- Rennert, T., 2018. Geogenic CO₂ affects inorganic soil properties and the composition of soil organic matter in physical fractions. *Soil Res.*, 56(4), 396-403.
- Ross, D.J., Tate, K.R., Newton, P.C.D., Wilde, R.H., Clark, H., 2000. Carbon and nitrogen pools and mineralization in a grassland gley soil under elevated carbon dioxide at a natural CO₂ spring. *Global Change Biol.*, 6(7), 779-790.
- Russell, D.J., Schulz, H.-J., Hohberg, K., Pfan, H., 2011. Occurrence of collembolan fauna in mofette fields (natural carbon-dioxide springs) of the Czech Republic. *Soil Org.*, 83(3), 489-505.
- Sander, R., 2015. Compilation of Henry's law constants (version 4.0) for water as solvent. *ACP*, 15(8).

- Saßmannshausen, F., 2010. Vegetationsökologische Charakterisierung terrestrischer Mofettenstandorte am Beispiel des west-tschechischen Plesná-Tals (Doctoral Thesis), University of Duisburg-Essen.
- Schulz, H.-J., Potapov, M.B., 2010. A new species of *Folsomia* from mofette fields of the Northwest Czechia (Collembola, Isotomidae). *Zootaxa*, 2553(1), 60-64.
- Schütze, C., Sauer, U., Beyer, K., Lamert, H., Bräuer, K., Strauch, G., Flechsig, C., Kämpf, H., Dietrich, P., 2012. Natural analogues: a potential approach for developing reliable monitoring methods to understand subsurface CO₂ migration processes. *Environ. Earth Sci.*, 67(2), 411-423.
- Shao, H., Qafoku, N.P., Lawter, A.R., Bowden, M.E., Brown, C.F., 2015. Coupled geochemical impacts of leaking CO₂ and contaminants from subsurface storage reservoirs on groundwater quality. *Environ. Sci. Technol.*, 49(13), 8202-8209.
- Sharma, V.K., Millero, F.J., 1988. Oxidation of copper(I) in seawater. *Environ. Sci. Technol.*, 22(7), 768-771.
- Shukla, R., Ranjith, P., Haque, A., Choi, X., 2010. A review of studies on CO₂ sequestration and caprock integrity. *Fuel*, 89(10), 2651-2664.
- Šibanc, N., Dumbrell, A.J., Mandić-Mulec, I., Maček, I., 2014. Impacts of naturally elevated soil CO₂ concentrations on communities of soil archaea and bacteria. *Soil Biol. Biochem.*, 68, 348-356.
- Šibanc, N., Zalar, P., Schroers, H.-J., Zajc, J., Pontes, A., Sampaio, J.P., Macek, I., 2018. *Occultifur mephitis* f.a., sp. nov. and other yeast species from hypoxic and elevated CO₂ mofette environments. *Int. J. Syst. Evol. Microbiol.*, 1-14.
- Smyth, R.C., Hovorka, S.D., Lu, J., Romanak, K.D., Partin, J.W., Wong, C., Yang, C., 2009. Assessing risk to fresh water resources from long term CO₂ injection – laboratory and field studies. *Energy Procedia*, 1(1), 1957-1964.
- Stephens, J.C., Hering, J.G., 2002. Comparative characterization of volcanic ash soils exposed to decade-long elevated carbon dioxide concentrations at Mammoth Mountain, California. *Chem. Geol.*, 186(3-4), 301-313.
- Stookey, L.L., 1970. Ferrozine – a new spectrophotometric reagent for iron. *Anal. Chem.*, 42(7), 779-781.
- Stupfel, M., Le Guern, F., 1989. Are there biomedical criteria to assess an acute carbon dioxide intoxication by a volcanic emission? *JVGR*, 39(2-3), 247-264.
- Suess, E., Planer-Friedrich, B., 2012. Thioarsenate formation upon dissolution of orpiment and arsenopyrite. *Chemosphere*, 89(11), 1390-1398.
- Sugio, T., Tsujita, Y., Inagaki, K., Tano, T., 1990. Reduction of cupric ions with elemental sulfur by *Thiobacillus ferrooxidans*. *Appl. Environ. Microbiol.*, 56(3), 693-696.
- Terzi, K., Aggelopoulos, C.A., Bountas, I., Tsakiroglou, C.D., 2014. Effects of carbon dioxide on the mobilization of metals from aquifers. *Environ. Sci. Technol.*, 48(8), 4386-4394.
- Tessier, A., Campbell, P.G., Bisson, M., 1979. Sequential extraction procedure for the speciation of particulate trace metals. *Anal. Chem.*, 51(7), 844-851.
- Theis, T.L., Singer, P.C., 1974. Complexation of iron (II) by organic matter and its effect on iron (II) oxygenation. *Environ. Sci. Technol.*, 8(6), 569-573.
- Trevors, J., 1996. Sterilization and inhibition of microbial activity in soil. *J. Microbiol. Methods*, 26(1), 53-59.
- Vartapetian, B.B., Jackson, M.B., 1997. Plant adaptations to anaerobic stress. *Ann. Bot.*, 79(suppl_1), 3-20.
- Videmšek, U., Hagn, A., Suhadolc, M., Radl, V., Knicker, H., Schloter, M., Vodnik, D., 2009. Abundance and diversity of CO₂-fixing bacteria in grassland soils close to natural carbon dioxide springs. *Microb. Ecol.*, 58(1), 1-9.
- Vodnik, D., Pfanz, H., Wittmann, C., Macek, I., Kastelec, D., Turk, B., Batic, F., 2002. Photosynthetic acclimation in plants growing near a carbon dioxide spring. *Phyton*, 42(3), 239-244.
- Wang, S., Jaffe, P.R., 2004. Dissolution of a mineral phase in potable aquifers due to CO₂ releases from deep formations; effect of dissolution kinetics. *Energy Convers. Manage.*, 45(18-19), 2833-2848.
- Weber, F.-A., Voegelin, A., Kaegi, R., Kretzschmar, R., 2009a. Contaminant mobilization by metallic copper and metal sulphide colloids in flooded soil. *Nat. Geosci.*, 2(4), 267-271.

- Weber, F.-A., Voegelin, A., Kretzschmar, R., 2009b. Multi-metal contaminant dynamics in temporarily flooded soil under sulfate limitation. *Geochim. Cosmochim. Acta*, 73(19), 5513-5527.
- Weinlich, F., Bräuer, K., Kämpf, H., Strauch, G., Tesář, J., Weise, S., 1999. An active subcontinental mantle volatile system in the western Eger rift, Central Europe: Gas flux, isotopic (He, C, and N) and compositional fingerprints. *Geochim. Cosmochim. Acta*, 63(21), 3653-3671.
- Yeates, G.W., Newton, P.C., Ross, D.J., 1999. Response of soil nematode fauna to naturally elevated CO₂ levels influenced by soil pattern. *Nematology*, 1(3), 285-293.
- Zeien, H., Brümmer, G.W., 1989. Chemische Extraktion zur Bestimmung von Schwermetallbindungsformen in Boden. *Mitteilungen der Deutschen Bodenkundlichen Gesellschaft*, 59(1), 505-510.
- Zheng, L., Apps, J.A., Spycher, N., Birkholzer, J.T., Kharaka, Y.K., Thordsen, J., Beers, S.R., Herkelrath, W.N., Kakouros, E., Trautz, R.C., 2012. Geochemical modeling of changes in shallow groundwater chemistry observed during the MSU-ZERT CO₂ injection experiment. *Int. J. Greenh. Gas Control*, 7(0), 202-217.
- Ziegler, P.A., 1992. European Cenozoic rift system. *Tectonophysics*, 208(1-3), 91-111.

CONTRIBUTION TO STUDIES 1 TO 3

STUDY 1: Spatial distribution of metal(loid) depletion and accumulation zones around a natural carbon dioxide degassing site

| | | |
|-------------------------|-----|---|
| Judith Mehlhorn | 80% | development of research concept, field and laboratory work, analyses and data interpretation, preparation of manuscript |
| Lukas A. Gerber | 10% | assistance with laboratory experiments, comments on manuscript |
| Britta Planer-Friedrich | 10% | development of research concept, discussion of results, comments on manuscript |

STUDY 2: Time and temperature dependency of carbon dioxide triggered metal(loid) mobilization in soil

| | | |
|-------------------------|-----|---|
| Judith Mehlhorn | 80% | development of research concept, field and laboratory work, analyses and data interpretation, preparation of manuscript |
| James M. Byrne | 5% | Mössbauer analyses and data interpretation, comments on manuscript |
| Andreas Kappler | 5% | comments on manuscript |
| Britta Planer-Friedrich | 10% | development of research concept, discussion of results, comments on manuscript |

STUDY 3: Copper mobilization and immobilization along an organic matter and redox gradient – insights from a mofette site

| | | |
|-------------------------|------|---|
| Judith Mehlhorn | 75% | development of research concept, field and laboratory work, analyses and data interpretation, preparation of manuscript |
| Johannes Besold | 5% | assistance with XAS analyses and data interpretation, comments on manuscript |
| Juan S. Lezama Pacheco | 2.5% | assistance with XAS analyses, comments on manuscript |
| Jon Petter Gustafsson | 2.5% | assistance with XAS analyses, comments on manuscript |
| Ruben Kretzschmar | 5% | assistance with XAS and XRD data interpretation, comments on manuscript |
| Britta Planer-Friedrich | 10% | development of research concept, discussion of results, comments on manuscript |

APPENDIX: STUDIES 1 - 3

STUDY 1

Mehlhorn, J., Gerber, L.A., Planer-Friedrich, B. (2018): Spatial distribution of metal(loid) depletion and accumulation zones around a natural carbon dioxide degassing site. *Chemical Geology*, 509: 64-76, DOI: 10.1016/j.chemgeo.2019.01.010.

STUDY 2

Mehlhorn, J., Byrne, J.M., Kappler, A., Planer-Friedrich, B. (2016): Time and temperature dependency of carbon dioxide triggered metal(loid) mobilization in soil. *Applied Geochemistry*, 74: 122-137, DOI: 10.1016/j.apgeochem.2016.09.007.

STUDY 3

Mehlhorn, J., Besold, J., Lezama-Pacheco, J.S., Gustafsson, J.P., Kretzschmar, R., Planer-Friedrich, B. (2018): Copper mobilization and immobilization along an organic matter and redox gradient – insights from a mofette site. *Environmental Science & Technology*, 52(23): 13698-13707, DOI: 10.1021/acs.est.8b02668.

**STUDY 1: Spatial distribution of metal(loid) depletion and accumulation zones
around a natural carbon dioxide degassing site**

Judith Mehlhorn, Lukas A. Gerber, Britta Planer-Friedrich

Reprinted with permission from

Chemical Geology 509 (pp. 64 - 76)

Copyright 2019 Elsevier



Spatial distribution of metal(loid) depletion and accumulation zones around a natural carbon dioxide degassing site



Judith Mehlhorn, Lukas A. Gerber, Britta Planer-Friedrich*

Environmental Geochemistry, Bayreuth Center for Ecology and Environmental Research (BayCEER), University of Bayreuth, Universitaetsstrasse 30, D-95440 Bayreuth, Germany

ARTICLE INFO

Editor: Michael E. Böttcher

Keywords:

Mofette

Iron (oxyhydr)oxides

Sulfidic mineral

Soil organic matter (SOM)

ABSTRACT

Long-term influence of geogenic CO₂ affects soil conditions and pedogenesis. Mobilization of metals and metalloids from soil to solution has been reported to occur in natural CO₂ degassing sites, so-called mofettes. We determined metal(loid)-specific spatial distribution patterns in soil around a mofette as well as metal(loid) pore water concentrations along a CO₂ gradient (0–98% CO₂ in soil air). Depletion of Mn, Co, and Ni in soil in the mofette center was caused by leaching due to the long-term soil acidification leading to correspondingly low pore water concentrations and thus indicating no recent influence of CO₂ on metal(loid) mobility. Iron and As were also depleted in soil within the mofette center where pedogenic Fe (oxyhydr)oxides could not form due to absence of oxygen. Small-scale variations in redox conditions lead to ongoing Fe cycling and the repeated reduction of Fe (oxyhydr)oxides resulted in increased Fe and As pore water concentrations at high CO₂. Precipitation in form of sulfide minerals caused immobilization and accumulation of Cd, Cu, and Zn directly in the degassing center. The highest mobilization risk occurred within 2–4 m distance from the degassing center, where complexation with dissolved organic matter (DOM) increased the mobility of Al, As, Cr, Cu, Fe, and Zn. Our results show that CO₂ as soil-forming factor influences the spatial distribution of metal(loid)s. The highest metal(loid) mobilization risk after long-term CO₂ influence arises from accumulation of scarcely degraded organic matter, which can easily dissolve and form mobile metal(loid)-DOM complexes.

1. Introduction

Research interest in mofettes has strongly increased within the last years, among others due to their analogy to leakages from geologic carbon storage (GCS) sites (Lewicki et al., 2007; Pearce, 2006; Schütze et al., 2012). Mofettes are characterized by diffuse degassing of mainly carbon dioxide (CO₂) as well as traces of other gases like nitrogen or noble gases (Bräuer et al., 2004). They occur as (post-)volcanic features in areas where magma ascends and gases like CO₂ are released due to the decrease in pressure and ascend via tectonic faults to the surface (Irwin and Barnes, 1980). Long-term effects of ascending CO₂ on soil properties and pedogenesis are manifold and have been recently reviewed by Rennert and Pfanz (2016). They suggest introducing the qualifier “mofettic” into WRB soil classification, since the CO₂ acts as soil-forming factor. Dissolution of CO₂ in pore water causes soil acidification at mofette sites (e.g., Beaubien et al., 2008; Maček et al., 2009; Mehlhorn et al., 2014; Rennert et al., 2011), which affects both abiotic and biotic soil processes. Weathering of silicates is accelerated, as reported e.g., by Beaubien et al. (2008), Blume and Felix-Henningsen

(2009), and Flechsig et al. (2008). Formation of pedogenic Fe, Mn, and Al (oxyhydr)oxides is decreased in mofettes due to the limited availability of oxygen (Beaubien et al., 2008; Rennert et al., 2011, 2012; Rennert and Pfanz, 2015).

The vegetation on mofettes is dominated by acidophilic and nitrophobic species (Rennert and Pfanz, 2016; Saßmannshausen, 2010) and microbial communities are shifted towards acidophilic and anaerobic organisms, like sulfur-reducing and acetogenic bacteria or methanogenic archaea (Beulig et al., 2015; Frerichs et al., 2013; Oppermann et al., 2010). Both plants and microbes have been reported to assimilate the geogenic CO₂ leading to up to 67% mantle-derived carbon in soil organic matter (SOM) of mofettes (Beulig et al., 2016; Nowak et al., 2015). The degradation of SOM is decreased in mofettes due to anaerobic conditions, absence of macro- and mesoscopic eukaryotes and the mentioned shifts in microbial community, resulting in significant SOM accumulation (e.g., Beaubien et al., 2008; Beulig et al., 2015; Olk et al., 2006; Rennert et al., 2011; Ross et al., 2000).

Also, major cations and trace elements in soil are affected by geogenic CO₂. Decreases in cation exchange capacity, exchangeable Ca and

* Corresponding author.

E-mail address: b.planer-friedrich@uni-bayreuth.de (B. Planer-Friedrich).

<https://doi.org/10.1016/j.chemgeo.2019.01.010>

Received 3 September 2018; Received in revised form 11 January 2019; Accepted 19 January 2019

Available online 25 January 2019

0009-2541/ © 2019 Elsevier B.V. All rights reserved.

Mg, and total contents of Al, Mg, and Mn have been recently reported by Rennert (2018). In a previous study, we compared total soil and pore water contents of several metal(loid)s from a mofette with a non-CO₂-influenced reference soil nearby (Mehlhorn et al., 2014). We could show that the mobility of Fe and As is increased in mofettes due to decreased Fe (oxyhydr)oxide contents while, e.g., Cu seems to be immobilized in CO₂ degassing centers. In a recent study, we identified Cu reduction and precipitation in form of sulfide minerals as the main mechanism for Cu sequestration in mofettes, besides adsorption to SOM (Mehlhorn et al., 2018). For other elements, e.g., Mn and Ni, the net effect of long-term CO₂ influence on mobility remained unclear.

Results from prior studies imply that metal(loid)-specific accumulation and depletion zones develop around mofette sites. Most studies on natural CO₂ springs or projects on GCS risk assessment either compare CO₂-influenced and non-CO₂-influenced soil or study a linear transect along a CO₂-gradient. To our knowledge, up to now no studies on two- or three-dimensional spatial distribution of (trace) elements around natural or anthropogenically caused CO₂ degassing sites exist. Determination of metal(loid) distribution patterns can help both to understand CO₂ influence on metal(loid) binding processes in soil and to evaluate risks arising from CO₂-triggered mobilization and immobilization.

The aim of this study was to determine spatial distribution of the metal(oids) Al, As, Cd, Co, Cr, Cu, Fe, Mn, Ni, and Zn in a mofette soil and to identify element-specific areas of depletion and accumulation. We used sequential extractions to assign metal(oid)s to different soil fractions and determine the influence of geogenic CO₂ on metal(loid) adsorption and binding. By comparing soil and pore water concentrations we evaluated the effect of increased CO₂ in soil air on net metal(loid) mobility. We hypothesized that long-term CO₂ influence will lead to the depletion of metal(loid)s due to surface protonation and mineral dissolution following soil acidification, while metal(loid)s with a high affinity to SOM or sulfide may accumulate in mofettes.

2. Material and methods

2.1. Site description and sampling

The investigated mofette site is located in Czech Republic, about 10 km east of Františkovy Lázně. A detailed site description can be found in Mehlhorn et al. (2014). Soil samples were collected in September 2017 at a mofette located in close vicinity to the river Plesná (50°8'43.9" N, 12°27'1.0" E) along a sampling grid with its center in the main degassing feature of this mofette. Starting from the center, sampling points were located in 2, 4, 8, and 12 m distance to the cardinal directions, and in 6 and 12 m distance to the intercardinal directions. Due to the irregular extension of the mofette (determined optically by a change in vegetation from mofette-specific species towards a typical floodplain vegetation, see Rennert and Pfanz (2016) and Saßmannshausen (2010)), additional sampling points were located at 20 m N, NE, and E and at 22 m N (sampling grid shown in Fig. 1a). The grid design was chosen in order to increase the number of samples around the degassing center where we expected to observe the most interesting processes. The soils at this site have been characterized as (Hemic) Histosol with reductimorphic properties (reduced Y horizons) for mofette and as Gleyic Fluvisol for non-CO₂-influenced surrounding soil by Beulig et al. (2016). Soil samples were collected with an auger from approx. 0–5, 25–35, and 55–65 cm depth and immediately frozen on dry ice. Sampling depths were chosen in order to compare organic-rich topsoil, the alternating oxic-anoxic zone, and the permanently anoxic (water saturated) zone with respect to the Fluvisol. Due to relatively dry weather conditions in the weeks before sampling, groundwater level was below 1 m depth at most sampling points. Only in the Eastern part of the sampling grid, soil samples were completely water saturated at 55–65 cm depth. However, visible signs of oxic conditions (orange color of Fe (oxyhydr)oxides) occurred only scarcely below

50 cm depth for all samples. Soil air CO₂ was determined with a portable gas analyzer (BIOGAS 5000, Geotech) in the auger holes in approx. 15–25 cm depth. Only in the degassing center, soil air CO₂ had to be determined in 0–5 cm depth of the auger hole due to water saturation.

Pore water samples were collected along the East transect only, using 60 cm long pore water peepers type Hesslein (1976). The peepers had separate compartments from 10 to 60 cm with a 1 cm depth resolution. Preparation of the peepers followed a previously described procedure (Mehlhorn et al., 2014). The peepers were installed next to the soil sampling points and left to equilibrate for 9 weeks.

2.2. Laboratory analysis

Soil samples were freeze-dried, grinded, and (if larger stones or plant debris were present) sieved (nylon, 1 mm mesh size). Samples from the East transect were treated and stored in an anoxic chamber (Coy, 95%/5% nitrogen/hydrogen) for later sequential extraction. Soil pH was determined in 0.01 M CaCl₂ at a soil-to-solution ratio of 1:2.5 (pH meter HQ40d equipped with a PHC101 electrode, Hach). Total C and N contents were determined with a CHN elemental analyzer (Thermo Quest, Flash EA, 1112). Soil samples were digested in aqua regia at a soil-to-solution ratio of 1:100 (microwave assisted digestion using a MARS Xpress, CEM). Total concentrations of Al, S, Cr, Mn, Fe, Co, Ni, Cu, Zn, As, and Cd were determined in filtered (0.2 µm, cellulose-acetate, CHROMAFIL® Xtra) and 1:10 to 1:5000 diluted extracts using a quadrupole inductively coupled plasma mass spectrometer (ICP-MS, X-Series2, Thermo Scientific) with matrix-matched calibrations and Rh as internal standard.

Carbon dioxide induced changes in metal(loid) binding were investigated by conducting a sequential extraction procedure (SEP) for all soil samples from the East transect. We used the 5-step SEP described in Fulda et al. (2013a) in order to extract the following operationally defined fractions: F1: mobile (soluble and exchangeable, soluble metal(loid)-SOM complexes), F2: easily mobilizable (specifically adsorbed, bound to minerals labile at pH 5, and weak metal(loid)-SOM complexes), F3: organically bound (low affinity), F4: reducible (bound to amorphous and crystalline Fe and Mn (oxyhydr)oxides), and F5: oxidizable (metal sulfides and bound to SOM (high affinity)). Details on exact extraction steps can be found in Supporting information (SI), A.1. For extraction, approx. 0.2 g of dried and ground soil were weighed into centrifuge tubes and the respective amount of extractant was added. Extraction of fractions 1 to 3 was done inside the anoxic chamber with nitrogen purged solutions. The soil samples were washed between the individual extraction steps to reduce carry-over of residual solution (Fulda et al., 2013a). After extraction, the vials were centrifuged (outside anoxic chamber, 5 min at 4500 g) and the supernatant was filtered (0.2 µm, cellulose-acetate, CHROMAFIL® Xtra) and stabilized in 0.45% H₂O₂ and 0.65% HNO₃ for total metal(loid) analysis by ICP-MS.

Sampling of pore water peepers was done under atmospheric conditions. To reduce oxygen influence on the pore water, the peepers were stored in a nitrogen-filled box and sampled one after the other. Pore water from 5 chambers each was mixed in order to gain sufficient sample volume. Pore water redox potential and pH were determined (pH meter HQ40d equipped with electrodes MTC301 and PHC101, Hach) and the remaining sample was stabilized for the following analyses: 2 mL of unfiltered sample were injected into nitrogen-filled septum vials and stored at 8 °C overnight for analysis of dissolved CO₂ and methane, 8 mL were filtered (0.45 µm, polyamide, CHROMAFIL® Xtra) and stored at 8 °C overnight for analysis of total dissolved organic carbon (DOC) and total dissolved nitrogen (TN), the remaining sample was filtered (0.2 µm, cellulose-acetate, CHROMAFIL® Xtra) and stabilized in 0.45% H₂O₂ and 0.65% HNO₃ for total metal(loid) analysis by ICP-MS, in 0.5 M HCl for photometric determination of Fe(II) and total Fe, and with 2% (w/v) Zn acetate for photometric sulfide determination.

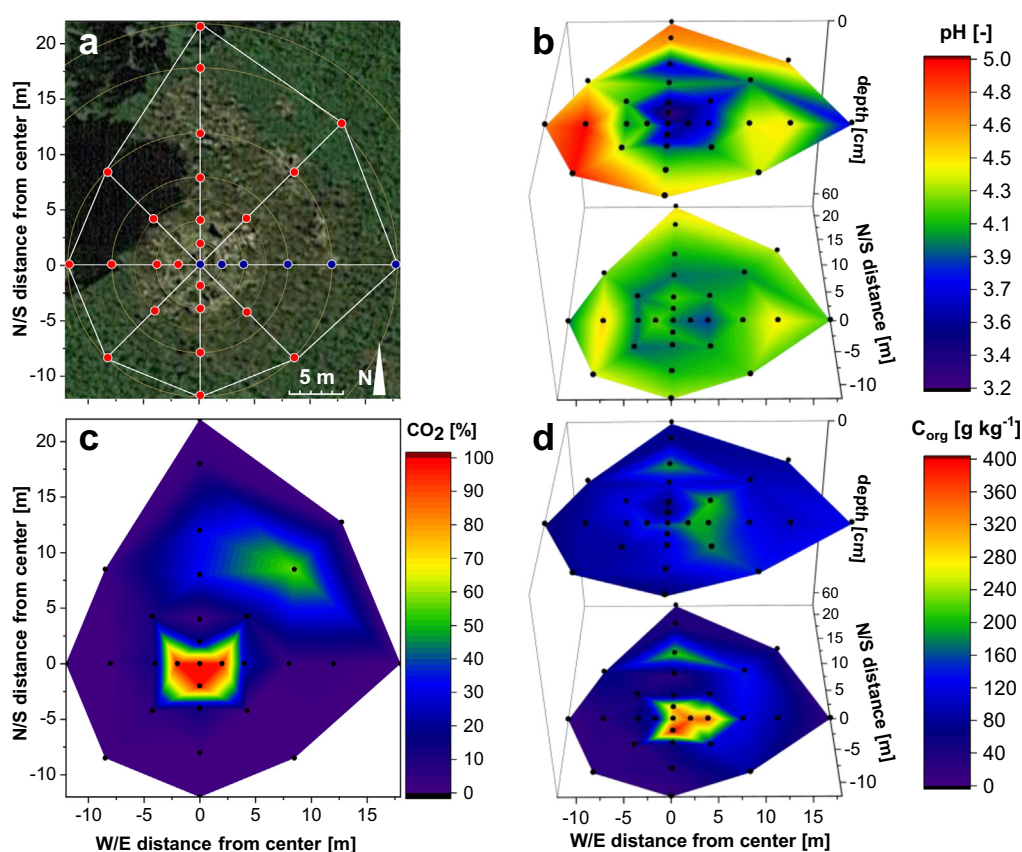


Fig. 1. (a) Aerial image of the mofette site with sampling grid (red circles: soil sampling only, blue circles: soil and pore water sampling), image source: <https://maps.google.de>. (b) CO₂ in soil air sampled in approx. 15–25 cm depth. (c) Soil pH determined in 0.01 M CaCl₂ at a soil-to-solution ratio of 1:2.5 for samples from 0 to 5 cm depth (top graph) and from 55 to 65 cm depth (bottom graph). (d) Total organic carbon (C_{org}) content in samples from 0 to 5 cm depth (top graph) and from 55 to 65 cm depth (bottom graph). Black dots mark sampling points, pH and contents were extrapolated between these points from measured values using universal kriging interpolation. Graphs (a, c) are two-dimensional, (b, d) are three-dimensional. (For interpretation of the references to color in this figure legend, the reader is referred to the web version of this article.)

Gaseous CO₂ and methane concentrations in the head space of the septum vials were measured by gas chromatography (SRI Instruments 8610C, U.S.) using a methanizer and a flame ionization detector. Dissolved concentrations were calculated from head space contents using Henry's law ($k_{H,CO_2} = 0.03344 \text{ mol L}^{-1} \text{ atm}^{-1}$, $k_{H,CH_4} = 0.001419 \text{ mol L}^{-1} \text{ atm}^{-1}$ from Sander (2015)). Dissolved CO₂ as well as total Cu pore water concentrations from three depths from this sampling have been previously published with respect to Cu sequestration along a SOM and redox gradient in Mehlhorn et al. (2018). Total DOC and TN were determined by thermo-catalytic oxidation with a TOC-VCPN Analyzer (Shimadzu). The ferrozine assay (Stookey, 1970) was used for photometric determination of dissolved Fe(II) and total Fe concentrations and the methylene blue method (Cline, 1969) for determination of sulfide concentrations. Absorbance was measured at 570 nm for Fe and at 650 nm for sulfide using a multi-plate reader (Infinite 200 PRO, Tecan). Total metal(loid) concentrations (except Fe) were determined in 1:10 or 1:100 diluted pore water samples by ICP-MS. Values below detection limit (LOD) were treated as 0.3·LOD.

2.3. Calculations and statistics

A cluster analysis was conducted on total metal(loid) and S soil contents as well as on total metal(loid) pore water concentrations in order to identify similarities between elements. Total soil contents and pore water concentrations were normalized to mean values of 0 and a standard deviation of 1. Clustering was done by calculating the Euclidean distances between element distribution patterns using the software R (R Development Core Team, 2008).

Total metal(loid) and organic carbon (C_{org}) contents, soil pH, and CO₂ distribution patterns were plotted by extrapolating the values between the sampling points from measured values using universal kriging interpolation. Spearman's rank correlation was used to calculate correlation coefficients (r_s) and their significance level (P -value) since

data were not normally distributed. Numbers of variables were $n = 87$ for soil data, $n = 60$ for pore water data and $n = 18$ for combined soil and pore water data (East transect only).

3. Results and discussion

3.1. Carbon dioxide, soil pH, and soil organic matter

Soil air CO₂ content revealed two main degassing centers, one with almost 100% CO₂ in the center and one with up to 56% CO₂ in soil air in approx. 12 m distance NE (Fig. 1b). Despite the high number of sampling points, we could not completely cover the heterogeneity of this mofette site. Some smaller degassing centers in approx. 3 m SW and 4 m NNE were optically visible but were not covered by our sampling grid. However, the 87 soil samples collected from 29 sampling points demonstrated well the influence of CO₂ degassing on metal(loid) distribution in soil even if some small scale heterogeneity could not be represented completely.

Soil pH was strongly decreased around CO₂ degassing centers (Fig. 1c), most pronounced in the topsoil where soil pH was 3.2–3.7 close to the degassing center compared to values up to 5.0 in the non-CO₂-influenced soil. A significant negative correlation between $\log(p(\text{CO}_2))$ (with $p(\text{CO}_2)$: CO₂ partial pressure) and soil pH ($r_s = -0.55$, $P < 0.01$) could be detected illustrating the acidifying effect of CO₂ dissolution that has been observed at this and other mofette sites before (e.g., Beaubien et al., 2008; Maček et al., 2009; Mehlhorn et al., 2014; Rennert et al., 2011).

The frequently reported accumulation of SOM in mofettes (e.g., Beaubien et al., 2008; Beulig et al., 2015; Mehlhorn et al., 2014; Nowak et al., 2015; Rennert et al., 2011) could also be observed in this study with C_{org} contents of 190 g kg⁻¹ in the upper soil and up to 400 g kg⁻¹ in 55–65 cm depth in the degassing center compared to values around 20–120 g kg⁻¹ in the non-CO₂-influenced surrounding soil (Fig. 1d).

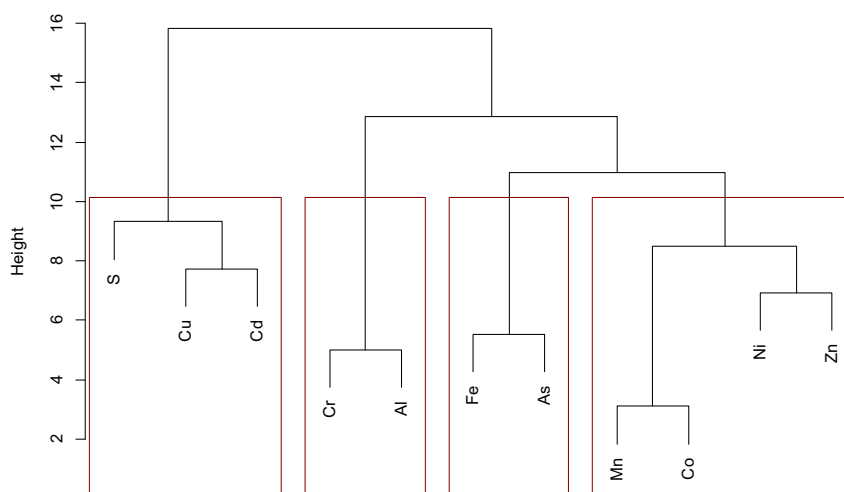


Fig. 2. Cluster dendrogram of total metal(loid) and S contents in soil samples. Contents were normalized for each element prior to calculation of Euclidean distances for clustering. Similarity coefficients can be found in Table A.2, SI.

While the accumulation pattern in the upper soil was irregular with the main accumulation occurring in some meters distance from the degassing center, the strong SOM accumulation in 55–65 cm depth was clearly confined to the main degassing channel. Patterns of carbon-to-nitrogen ratios were relatively similar to those of total C_{org} (SI, Fig. A.1) indicating the poorly decomposed nature of the accumulated SOM. The influence of geogenic CO_2 on SOM was studied in detail by Rennert and Pfanz (2015) and Rennert (2018). Less degraded SOM accumulates, which is reflected e.g., by higher carbon-to-nitrogen ratios (Rennert et al., 2011; Ross et al., 2000), decreased accumulation of aliphatic carbon or microbial SOM in the clay fraction (Rennert et al., 2011), accumulation of particulate organic matter (Rennert and Pfanz, 2015), as well as changes in SOM functional group abundancies and a lower degree of oxidation (Rennert, 2018).

3.2. Distribution patterns of metal(loid) soil contents

3.2.1. Metal(loid) clustering

Cluster analysis of normalized soil metal(loid) and sulfur contents revealed that the elements could be sorted into 4 to 5 groups of similar spatial distribution patterns (Fig. 2). The metals Co and Mn showed the highest similarity (similarity coefficient $s = 3.1$). Similarity between these elements and Ni and Zn was also high ($s < 8.5$), thus, we assigned these four elements into one group. The other three groups consisted of Fe and As ($s = 5.5$), Cr and Al ($s = 5.0$), as well as Cu, Cd, and S ($s < 9.3$). Metal(loid) distribution patterns will be discussed within these groups. When discussing metal(loid) depletion or enrichment zones, we generally refer to the non- CO_2 -influenced samples, i.e., most distanced from the degassing center, as background contents and interpret higher contents as accumulation and lower contents as depletion. For the sake of clarity, we only present the metal(loid) distribution patterns determined in samples from the upper (0–5 cm) and the lower (55–65 cm) soil depths in the main text. Metal(loid) distribution patterns from 25 to 35 cm depth can be found in SI (Figs. A.3–A.6).

3.2.2. Manganese, cobalt, nickel, and zinc

The elements Mn, Co, Ni, and Zn showed a strong depletion in soil within the whole CO_2 -influenced area as could be seen by a negative correlation with CO_2 in soil air ($r_s = -0.62, -0.78, -0.57, -0.6$ for Mn, Co, Ni, and Zn, respectively, $P < 0.01$) and a positive correlation with distance from degassing center ($r_s = 0.54, 0.67, 0.54, 0.41$ for Mn, Co, Ni, and Zn, respectively, $P < 0.01$). Soil contents only increased towards the most distanced, non- CO_2 -influenced areas (Fig. 3).

Minimum values for 0–5 cm depth in the CO_2 -influenced area were 38 mg kg^{-1} Mn, 2 mg kg^{-1} Co, 13 mg kg^{-1} Ni, and 33 mg kg^{-1} Zn compared to values around 600 mg kg^{-1} Mn, 20 mg kg^{-1} Co, 35 mg kg^{-1} Ni, and 150 mg kg^{-1} Zn in the non- CO_2 -influenced soil. The high metal(loid) contents, especially pronounced for Mn ($1881 \pm 21 \text{ mg kg}^{-1}$, high content confirmed by triplicate digestion and analysis), in 8 m distance W (Fig. 3) will be discussed below. In deeper soil, total contents of these metals were even lower. Only Zn showed an enrichment directly in the degassing center with soil contents reaching 158 mg kg^{-1} (Fig. 3d, bottom graph).

Sequential extraction of Mn, Co, Ni, and Zn showed that in non- CO_2 -influenced soil the majority of these elements was extracted in Fractions 4 and 5 (Fig. 4a for Mn, other elements in Fig. A.7, SI). These fractions can be assigned to metals bound to or present in form of Fe (oxyhydr)oxides (Zeien and Brümmer, 1989) and high-affinity sites of SOM and metal sulfides (Tessier et al., 1979), respectively. The amount of metals bound to these fractions in non- CO_2 -influenced soil showed the strongest decrease compared to samples from 55 to 65 cm depth of the mofette center (except for Ni, Fig. A.7c, SI), where the largest amounts of metals were extracted in Fraction 1 (mobile fraction (McGrath et al., 1988)). All four metals are known to bind to Fe (oxyhydr)oxides (Dzombak, 1990; Fischer et al., 2007) and decreased contents in the CO_2 -influenced mofette center fit to the previously observed decreased content of pedogenic Fe (oxyhydr)oxides in mofette soils (Rennert et al., 2011, 2012). Also, all these metals are known to adsorb to SOM (McBride, 1989; Uren, 1993). However, the fact that their contents decrease towards the center (Fig. 3) while SOM contents strongly increase (Fig. 1d) makes SOM an unlikely binding candidate for these metals. Tessier et al. (1979) reported a co-release of silicates like smectites, chlorites, and mica during extraction of Fraction 5. Thus, it is possible that Mn, Co, Ni, and Zn released during extraction of Fraction 5 were associated with clay minerals and other phyllosilicates which are also known to serve as binding partners for these metals (Bradl, 2004; McBride, 1989). The total mineral content in the degassing center must have been decreased due to the accumulation of SOM, thus, also the content of mineral-associated Mn, Co, Ni, and Zn should be decreased. However, this cannot be the only explanation since SOM accumulation zones and metal depletion zones differed in their extents. Assuming silicates to be the main binding partners for Mn, Co, Ni, and Zn, we evaluated the extent of mobilization by calculating the molar ratios of these elements with Al. Aluminum was shown to be more or less immobile (cf. Section 3.2.4) and therefore used as a reference for silicate content. Except for a relative enrichment of Zn and Ni in the degassing center in 55–65 cm depth (which will be discussed in Section 3.2.5), the

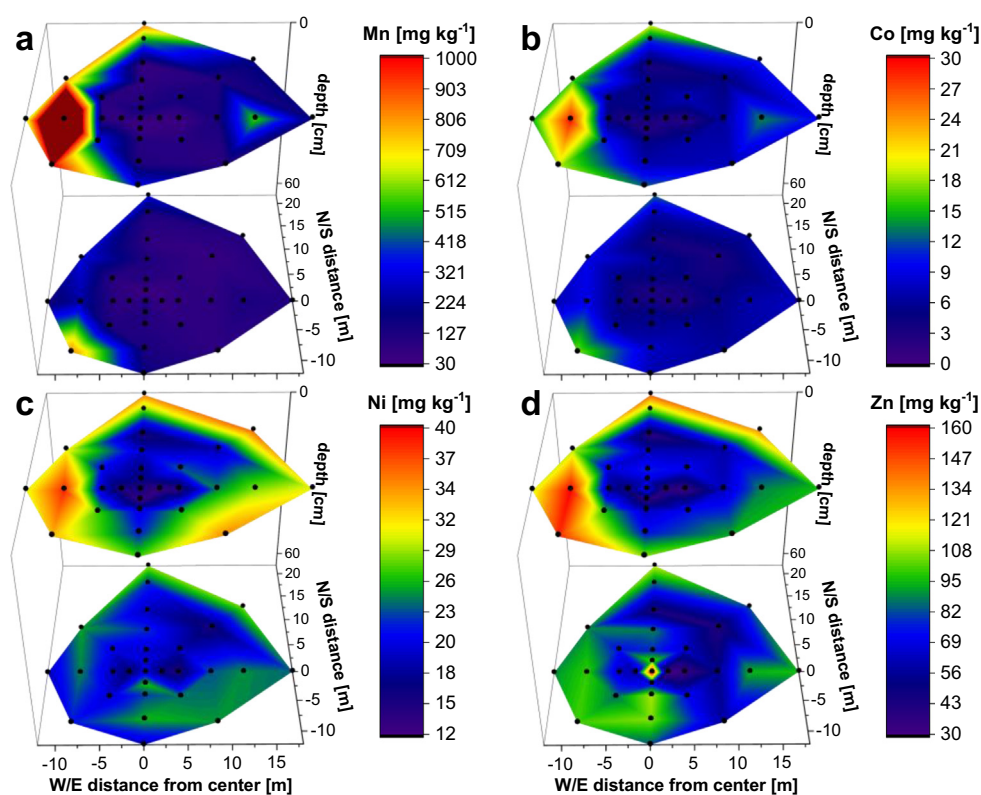


Fig. 3. Total contents of Mn (a), Co (b), Ni (c), and Zn (d) determined in aqua regia digests of soil samples from 0 to 5 (top graphs) and 55–65 cm depth (bottom graphs). Maximum Mn content at 8 m East and 0–5 cm depth is $1881 \pm 21 \text{ mg kg}^{-1}$ ($n = 3$). Black dots mark sampling points, contents were extrapolated between these points from measured concentrations using universal kriging interpolation.

distribution patterns of these metal(loid)/Al ratios (Fig. A.10, SI) were relatively similar to the total contents presented in Fig. 3, indicating that leaching of these elements must have occurred. Numerous studies have shown the mobilization and leaching of cations following soil acidification by CO_2 . Mobilization can be caused directly by protonation of potential cation binding sites or indirectly by increased weathering of silicates. A decreased cation exchange capacity in mofette soil compared to surrounding non- CO_2 -influenced soil was e.g., reported by Videmšek et al. (2009) and Beaubien et al. (2008). The predominant clay mineral in mofettes close to the one investigated in this study is kaolinite (Bussert et al., 2017; Flechsig et al., 2008; Rennert et al., 2011). However, no direct influence of CO_2 on clay mineralogy was detected at this mofette site and the kaolinite is assumed to be eroded and transported as debris to this site (Flechsig et al., 2008; Rennert, 2018; Rennert et al., 2011). In a prior study, we incubated non- CO_2 -influenced reference soil, which has been collected close to the mofette investigated in the present study, with CO_2 and monitored metal(loid) concentrations in liquid phase over time. We detected fast, abiotic mobilization of Mn which we attributed to surface protonation (Mehlhorn et al., 2016). Also several field, laboratory, and chemical modelling studies dealing with risk assessment of geologic carbon storage (GCS) have demonstrated the mobilization of metal(loid)s due to desorption and mineral dissolution processes (e.g., Kharaka et al., 2006, 2010; Kirsch et al., 2014; Lawter et al., 2016; Qafoku et al., 2014; Wang and Jaffe, 2004; Zheng et al., 2012). The soil contents of these four metals showed a significant negative correlation with proton activity $\{\text{H}^+\}$ ($r_s = -0.59, -0.69, -0.66, -0.57$ for Mn, Co, Ni, and Zn, respectively, $P < 0.01$), i.e., a positive relationship with soil pH. Besides the decreased total contents, also the relative increase of Mn extracted in the mobile fraction (Fraction 1, Fig. 4b) for samples from the CO_2 -influenced area indicates that increased mineral weathering and desorption processes induced by soil acidification and following leaching must have contributed to depletion of Mn, Co, Ni, and Zn in this mofette.

Another parameter influencing the distribution patterns of these

metals could be the occurrence of Mn oxides, which are known to adsorb Co, Ni, Zn, and other metals (Post, 1999). In the degassing center, pedogenic Mn oxides cannot form due to the absence of oxygen. A decreasing content in Mn oxides with increasing CO_2 has also been observed by Beaubien et al. (2008) and Rennert and Pfanz (2015) found that oxalate-extractable Mn contents showed a negative correlation with CO_2 partial pressure. Manganese bound in form of Mn oxides would have been extracted in Fraction 4 of the SEP used in this study (Fulda et al., 2013a). However, an increase in Mn extracted in Fraction 4 with distance was only observed for the deepest sampling depth (Fig. 4a) and did not correspond to trends observed for total Mn content but was rather comparable to the patterns observed for Fe (Fig. 4b). Thus, the contribution of pure Mn oxides to total Mn extracted in this fraction must have been low in comparison to Mn associated with Fe (oxyhydr)oxides. This is in agreement with our prior study, where only low contents of Mn oxides were detected by SEP (Mehlhorn et al., 2014).

It remains unclear, whether accumulation of Mn, Co, Ni, and Zn leached from the center of the mofette caused the aforementioned enrichment in the eastern, non- CO_2 -influenced part of the mofette (Fig. 3) or if the high soil contents in this area were caused by natural variation or contamination. Currently, there is no information on the transport regime in this mofette available. Regarding the strong CO_2 degassing and the elevated water table in the mofette center, it is quite likely that groundwater is transported vertically upwards in areas close to degassing channels, while in the non- CO_2 -influenced area infiltration of meteoric water might be the prevailing vertical transport process. Additionally, a radial lateral transport of the groundwater transported upwards in the degassing areas might also play a role, distributing the leached elements on a horizontal scale. Due to its location in the floodplain of river Plesná, a lateral groundwater transport from the valley slopes towards the river, which would be from (north-)east to (south-)west, could be plausible as well and would support the hypothesis of an accumulation of leached Mn, Co, Ni, and Zn in the western part of the mofette. Also leaching beyond the studied sampling

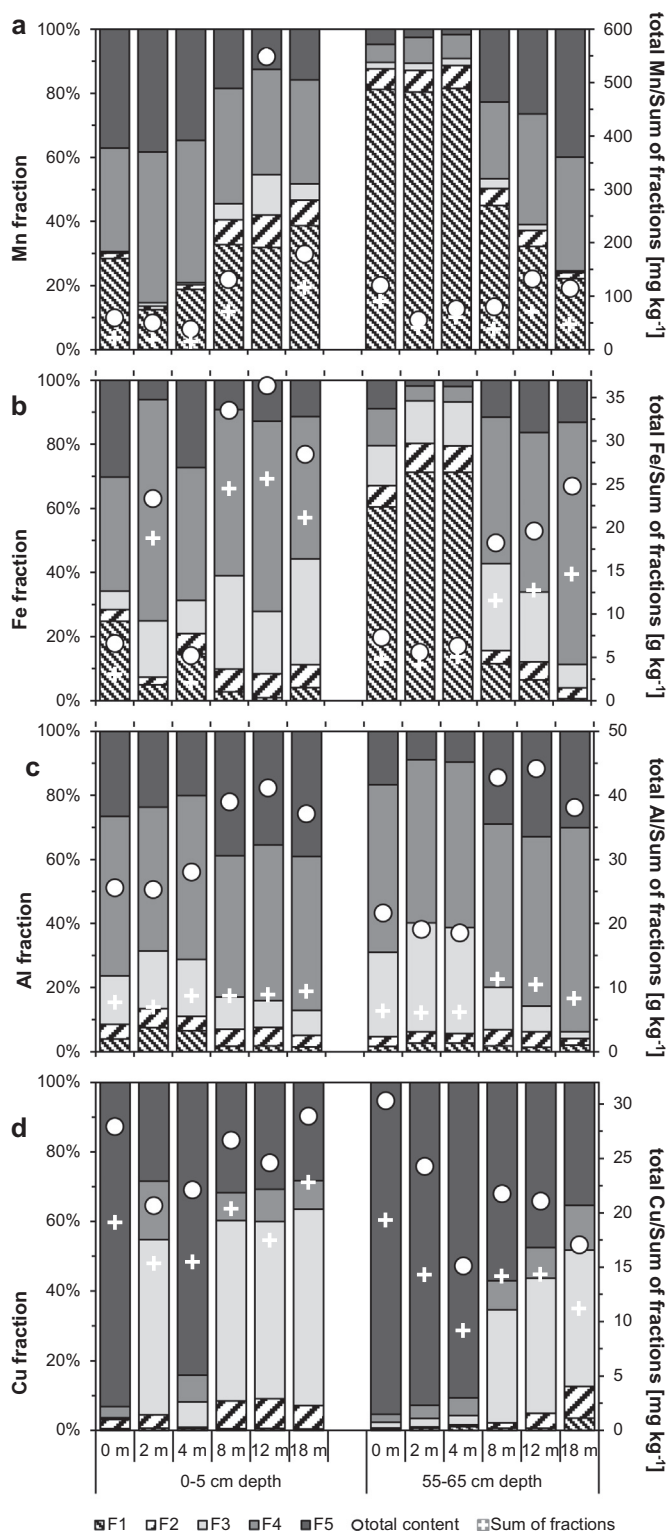


Fig. 4. Mn (a), Fe (b), Al (c), and Cu (d) content distribution in different chemical fractions according to the procedure described in Fulda et al. (2013a) for soil samples from the East transect. Circles mark total contents determined in aqua regia digests, crosses mark sum of fractions. Sampling depth and distance from degassing center are indicated on the x-axis. Data for other elements can be found in Figs. A.7–A.9, SI.

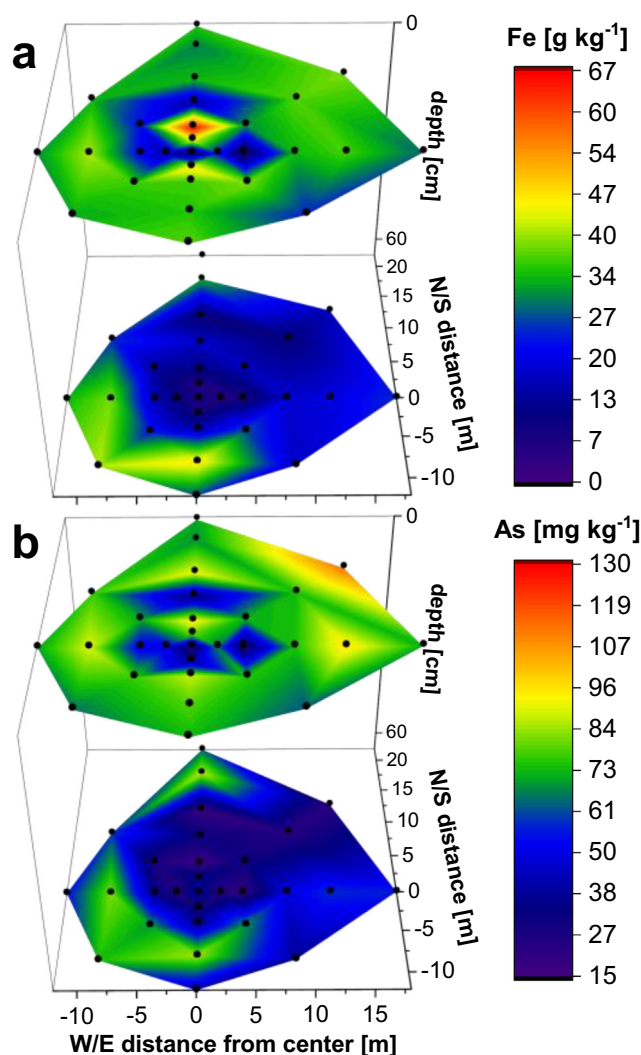


Fig. 5. Total contents of Fe (a) and As (b) determined in aqua regia digests of soil samples from 0 to 5 cm (top graphs) and 55–65 cm depth (bottom graphs). Black dots mark sampling points, contents were extrapolated between these points from measured concentrations using universal kriging interpolation.

grid, into the river or deeper groundwater cannot be excluded.

3.2.3. Iron and arsenic

Iron and As were also depleted within the mofette (significant negative correlation with CO₂, $r_s = -0.58$ and -0.50 for Fe and As, respectively, $P < 0.01$), however, their distribution patterns looked different to those of Mn, Co, Ni, and Zn (Fig. 5). In the upper soil, contents were lowest around the degassing center with 5–7 g kg⁻¹ Fe and 25–30 mg kg⁻¹ As, but increased to values of 35–40 g kg⁻¹ Fe and 70–110 mg kg⁻¹ As within only some meters distance. Interestingly, the highest Fe soil content was detected in a sample from 4 m N of the main degassing center (67 g kg⁻¹), directly between the two degassing areas. Arsenic was also enriched in this sample in comparison to the surrounding soil (93 mg kg⁻¹). In deeper soil, Fe and As contents decreased further and also the area of depletion around the degassing center increased. Higher contents were only present in > 6 m distance to N, W, and S.

Sequential extraction revealed that most of the Fe and As was extracted in Fraction 4, i.e. in form of or bound to Fe (oxyhydr)oxides (Fig. 4b for Fe, As in Fig. A.8b, SI). This is in line with SEP results from our previous study (Mehlhorn et al., 2014). Binding in form of Fe (oxyhydr)oxides would also explain the observed Fe and As distribution

patterns: typical pedogenic soil Fe (oxyhydr)oxides like goethite or lepidocrocite cannot form in mofettes due to the absence of oxygen (Rennert et al., 2012). Thus, total soil contents of Fe and also As, which is known to have a high affinity for Fe (oxyhydr)oxides (e.g., Livesey and Huang, 1981; Manning and Goldberg, 1997), and also the amount of Fe and As extracted in Fraction 4 (Figs. 4b and A.8b, SI) are decreased. According to a study from a nearby mofette site by Rennert et al. (2012), the majority of Fe in mofettes was present in different clay minerals and in form of Fe(II) and mixed Fe(II)/Fe(III) minerals, e.g., vivianite, siderite, green rust, and magnetite. Ferrihydrite was only detected close to a root channel, where micro-oxic conditions occurred. The fast precipitation of Fe (oxyhydr)oxides as soon as oxygen is available (Kirk, 2004) can explain the observed distribution patterns of Fe and As in the upper soil: within only some meters distance from the main degassing channels CO₂ partial pressure in soil air decreases immediately and oxygen becomes available. In only 4 m distance, oxygen in soil air already reached 14–17% (data not shown), enabling Fe (oxyhydr)oxide formation. The Fe enriched sample taken from 4 m N was located directly between the two degassing areas and additionally on a small hummock. Iron (and As) that is mobilized elsewhere (e.g., by weathering processes in the deeper sediment) and cannot precipitate in form of Fe (oxyhydr)oxides close to the degassing centers might accumulate in this spot due to local oxic conditions. It remains unclear, why other metals with a high affinity for Fe (oxyhydr)oxides, e.g., Mn, did not accumulate in this spot as well.

In deeper soil, (micro-)oxic conditions, e.g., along root channels, are scarce. Additionally, groundwater can cause anoxic conditions also in areas of less or no CO₂ influence. Thus, the overall contents of Fe and As were lower in 55–65 cm depth and higher contents were only found in non-CO₂-influenced areas to the N, W, and S, where groundwater level was assumingly below 65 cm depth.

3.2.4. Aluminum and chromium

Aluminum and Cr were more homogeneously distributed around the mofette area, especially in the upper soil (0–5 cm depth, Fig. 6) where mean contents were $35 \pm 7 \text{ g kg}^{-1}$ for Al and $38 \pm 5 \text{ mg kg}^{-1}$ for Cr. Minimum contents of 24–25 g kg⁻¹ Al and 29–32 mg kg⁻¹ Cr were detected in the degassing center and in 2–6 m distance to NE and E. In the deeper soil (55–65 cm depth) the mean concentrations remained relatively similar to the upper soil ($35 \pm 9 \text{ g kg}^{-1}$ for Al and $36 \pm 8 \text{ mg kg}^{-1}$ for Cr), however, a strong depletion directly in the degassing center became obvious with contents of 19–22 g kg⁻¹ Al and 18–24 mg kg⁻¹ Cr. A negative relationship of CO₂ partial pressure and Al contents indicating Al depletion in mofettes was also observed by Rennert (2018).

Sequential extraction of Al was incomplete, removing only $27 \pm 3\%$ of the total Al content determined in aqua regia digests (Fig. 4c). Most Al must have been present in the residual fraction, i.e., most probably in form of aluminosilicates, in which Al(OH)₆ octahedral sheets are essential components. Thus, the Al distribution pattern represents primarily the phyllosilicate content in the mofette soil, justifying the calculation of molar metal(loid)/Al ratios for determination of leaching and accumulation zones (cf. Sections 3.2.2 and A.2, SI). We did not determine the exact mineral content of the soil samples, however, this parameter should have a negative relationship with C_{org} content. In the areas, where SOM was accumulated (compare Fig. 1d), i.e. in the degassing center, especially in 55–65 cm depth, the mineral content and, thus, Al contents were decreased compared to the surrounding soil (Fig. 6). This interdependency is also shown by a significant negative correlation of Al with C_{org} ($r_s = -0.21$, $P = 0.05$). The reason for the local Al maximum in 0–5 cm depth and 2 m distance S (61 mg kg^{-1} , Fig. 6a, top graph) remains unclear. Since no other parameter showed an anomaly here, measurement error cannot be excluded.

Due to its chemical similarity, Cr often shows a comparable behavior to Al in soils (Bartlett and James, 1988). This is confirmed by the

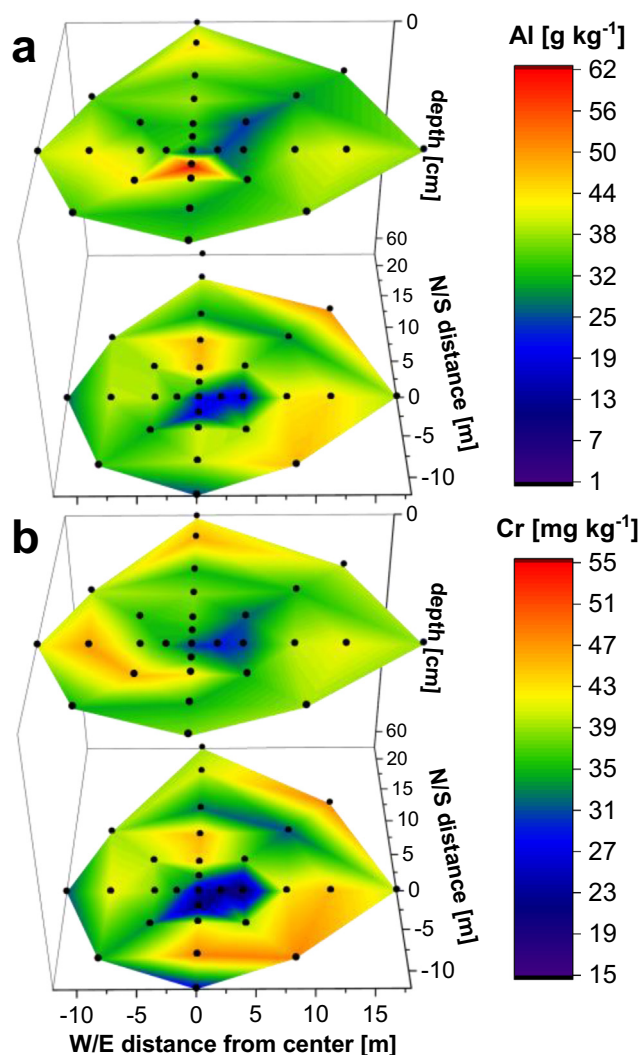


Fig. 6. Total contents of Al (a) and Cr (b) determined in aqua regia digests of soil samples from 0 to 5 cm (top graphs) and 55–65 cm depth (bottom graphs). Black dots mark sampling points, contents were extrapolated between these points from measured concentrations using universal kriging interpolation.

present study, in which total soil contents of Al and Cr showed a highly significant correlation ($r_s = 0.91$, $P = 0$) and molar Cr/Al ratios did not show large variations (Fig. A.11, SI). For Cr, extraction efficiency was better with $45 \pm 4\%$ of total Cr being extracted in Fractions 1–5, which probably results from the fact that, compared to Al, a larger fraction of the Cr was present in the hypothetically Fe (oxyhydr)oxide bound fraction (Fraction 4, $24 \pm 5\%$ of total Cr content compared to $17 \pm 5\%$ of total Al, Fig. A.8d, SI).

3.2.5. Copper and cadmium

The distribution patterns of Cu and Cd differed completely from those of the other elements. Both metals showed accumulation directly in the degassing center (Fig. 7a, b). In the upper soil, highest contents were still located in $\geq 12 \text{ m}$ distance from the degassing center ($29\text{--}39$ and $0.5\text{--}1 \text{ mg kg}^{-1}$ versus $14\text{--}22$ and $0.1\text{--}0.4 \text{ mg kg}^{-1}$ close to the degassing centers for Cu and Cd, respectively). However, an accumulation in the sampling point located directly in the main degassing center was detectable with concentrations reaching 28 mg kg^{-1} Cu and 0.6 mg kg^{-1} Cd. In deeper soil (55–65 cm), the overall concentrations were lower (approx. $13\text{--}22 \text{ mg kg}^{-1}$ Cu and $0.1\text{--}0.4 \text{ mg kg}^{-1}$ Cd) but a strong accumulation in the main degassing center was detected with soil contents reaching maxima of 33 mg kg^{-1} Cu and 1.9 mg kg^{-1} Cd.

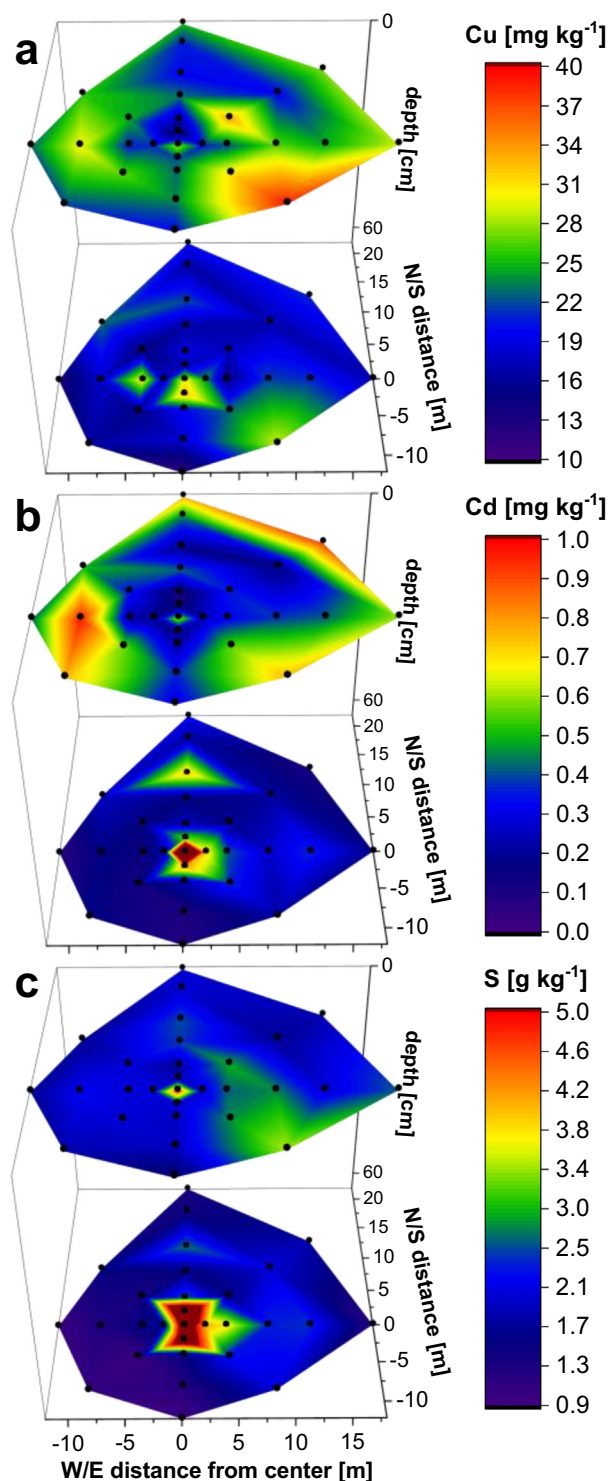


Fig. 7. Total contents of Cu (a), Cd (b), and S (c), determined in aqua regia digests of soil samples from 0 to 5 cm (top graphs) and 55–65 cm depth (bottom graphs). Maximum contents in the degassing center in 55–65 cm depth are 1.9 mg kg^{-1} for Cd and 7.4 g kg^{-1} for S. Black dots mark sampling points, contents were extrapolated between these points from measured concentrations using universal kriging interpolation.

Sequential extraction revealed that two different binding processes occurred in the mofette center and the surrounding soil: while for samples from $\geq 8 \text{ m}$ distance from the center Cu was mainly present in Fraction 3 (interpreted as organically bound fraction), for samples originating directly from the mofette center the majority of Cu

(93–95%) was extracted in Fraction 5. For Cd, similarly a high share of total concentrations (58–79%) was extracted in Fraction 5 for samples from the mofette center while in the surrounding soil most Cd (up to 76%) was present in the mobile fraction (Fraction 1, compare SI, Fig. A.9b).

Fraction 5 can be interpreted as metal sulfides or metals bound to SOM at high affinity sites (Tessier et al., 1979). Both sulfur (Fig. 7c) and SOM (Fig. 1d) were enriched in the degassing center, especially pronounced in 55–65 cm depth. Thus, both interpretations are possible. In a recent study, focused on the behavior of Cu along a redox and SOM gradient, we could show by X-ray absorption spectroscopy that most of the Cu in the mofette center is present in form of Cu(I) coordinated via sulfur (Mehlhorn et al., 2018). From this and additional results from a sorption study, we concluded that Cu is reduced and precipitates in form of Cu sulfides in the degassing center. Same as Cu, Cd is known to form sulfide minerals under sulfur-reducing conditions, e.g., in paddy soils (Fulda et al., 2013b; Weber et al., 2009). Besides precipitation of metal sulfides, binding of Cu and Cd to SOM via thiol groups, as previously described in Fulda et al. (2013b,c), could additionally contribute to metal accumulation, especially regarding the high SOM content and the significant correlation between C_{org} and total S contents ($r_S = 0.92$, $P = 0$).

Besides Cu and Cd, Zn showed an enrichment directly in the degassing center with concentrations reaching 158 mg kg^{-1} in 55–65 cm depth (Fig. 3d). This enrichment was even more obvious when considering the molar Zn/Al ratio and also Ni showed a relative enrichment in this sample when referred to Al (Fig. A.10a, b, SI). The relative accumulation of Ni could have been caused by an increased adsorption to SOM to which Ni has a high affinity (Uren, 1993), but also a contribution of (co-)precipitation of or adsorption to sulfidic minerals cannot be excluded (Di Toro et al., 1992). Zinc is also known to readily precipitate in form of sulfide minerals under reducing conditions (Kirk, 2004) and according to SEP results up to 49% of Zn were extracted in Fraction 5 (metal sulfides and metals bound to SOM at high affinity sites, compare SI, Fig. A.7d). However, the accumulation of Ni and Zn was not as pronounced as for Cu and Cd, which is in line with observations from Weber et al. (2009) who reported a decreasing tendency for metal sulfide formation with increasing solubility products ($\text{Ni} < \text{Cu} < \text{Cd} < \text{Zn}$ according to Allison et al. (1991)). Flechsig et al. (2008) and Bussert et al. (2017) detected significant amounts of pyrite in samples from $> 4 \text{ m}$ depth in a nearby mofette. In this study, no Fe enrichment was detected in the degassing center, which can be explained by the even higher solubility products of Fe sulfide minerals compared to Ni, Cu, Cd, and Zn (Allison et al., 1991).

3.3. Carbon dioxide influence on pore water and metal(loid) mobility

3.3.1. Pore water conditions and microbial influence

Pore water data were collected along the East transect for 10–60 cm depth. Dissolved CO_2 concentrations were highest directly in the degassing center (17–22 mM) and decreased to $5 \pm 2 \text{ mM}$ in the non- CO_2 -influenced reference soil in 18 m distance (Fig. 8a). Except for the degassing center, CO_2 concentration also increased with depth. Assuming a saturation or even oversaturation of the pore water with regard to CO_2 in the degassing center, the expected concentrations would have been even higher (approx. 33 mM using the Henry constant from Sander (2015): $k_{\text{H},\text{CO}_2} = 0.03344 \text{ mol L}^{-1} \text{ atm}^{-1}$). A detailed discussion on potential measurement problems can be found in Mehlhorn et al. (2018), where CO_2 concentrations from three depths have been previously reported with respect to their correlation with Cu concentrations.

Interestingly, dissolution of CO_2 had no significant influence on pore water pH. While for soil pH the acidifying effect of permanent CO_2 degassing was clearly visible (Fig. 1c), pore water pH was relatively similar over the whole transect with 4.9 ± 0.2 (Fig. 8b). Exceptions are the pore water samples from 8 m distance and 10–35 cm depth which

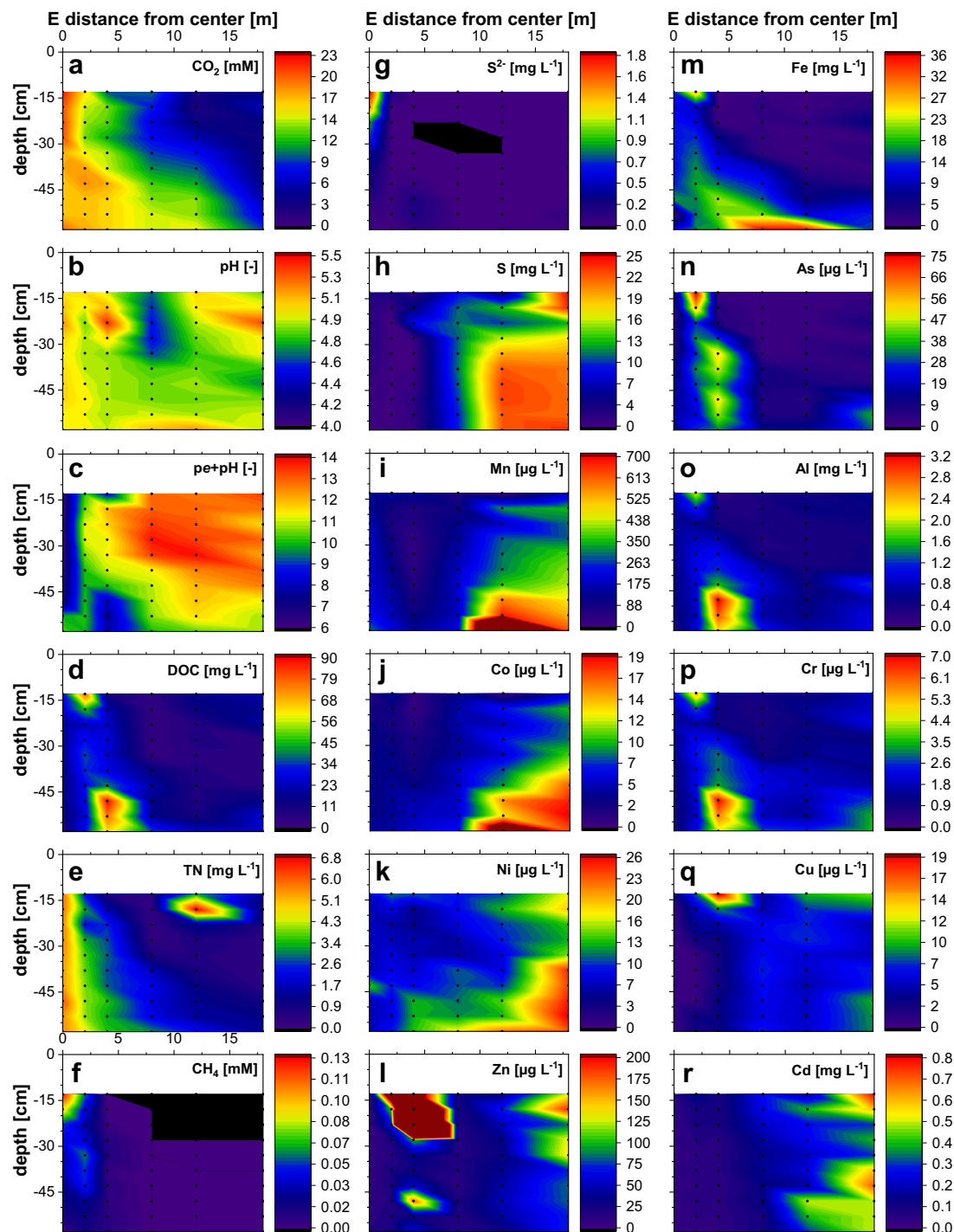


Fig. 8. Chemical data from pore water samples collected with dialysis chambers along the East transect of the mofette site. (a) Dissolved CO_2 concentrations, (b) pore water pH, (c) $pe + pH$, (d) total dissolved organic carbon (DOC), (e) total dissolved nitrogen (TN), (f) dissolved methane concentration, (g) sulfide, (h) total S, (i) total Mn, (j) Co, (k) Ni, (l) Zn, (m) Fe, (n) As, (o) Al, (p) Cr, (q) Cu, and (r) Cd concentrations. Maximum concentrations are $1540 \mu\text{g L}^{-1}$ for Mn (i, in 12 m distance and 56–60 cm depth), $24 \mu\text{g L}^{-1}$ for Co (j, in 12 m distance and 56–60 cm depth), and $1060 \mu\text{g L}^{-1}$ for Zn (l, in 4 m distance and 21–25 cm depth). Black dots mark sampling points, concentrations were extrapolated between these points from measured concentrations using universal kriging interpolation. Black colored areas result from missing data.

showed a lower pH of 4.5–4.6. The reasons for this pH minimum are unclear, especially since no anomalies of other parameters were observed within these samples. Pore water pH in the mofette center is comparable with observations from our previous study from 2014 (4.9 ± 0.1), but it is slightly lower for the non- CO_2 -influenced reference (5.2 ± 0.2 in 2014 study vs. 4.9 ± 0.2 in the present study) (Mehlhorn et al., 2014). While the pore water pH in the degassing

center, thus, seems to be rather stable, it might be influenced by seasonal variations in microbial activity in the surrounding non- CO_2 -influenced soil.

Oppositely to pore water pH, redox potential was strongly influenced by CO_2 degassing and showed a significant negative correlation with CO_2 concentrations ($r_s = -0.84$, $P = 0$). To facilitate the interpretation of redox conditions, $pe + pH$ is presented in Fig. 8c with

values < 9 indicating anoxic conditions and $9 < pe + pH < 14$ indicating suboxic conditions (redox potential (E_H) can be found in Fig. A.12, SI). Values in the degassing center reached minima of $pe + pH$ 6.0, indicating permanently anoxic conditions. They increased fast with distance from the center and already reached values > 9 in 2 m distance. Oxidic conditions indicated by $pe + pH$ around 14 were only detected in > 8 m distance and up to 40 cm depth. As expected, $pe + pH$ decreased with depth, except for the degassing center where values of $pe + pH$ 10 were detected below 50 cm depth. The reason for these relatively high values is unclear since permanently anoxic conditions would be expected in this depth.

Interestingly, total DOC concentrations showed no homogeneous increase or decrease but two hotspots: In 10–20 cm depth in 2 m distance from the degassing center as well as in 45–60 cm depth in 4 m distance, DOC concentrations reached $46\text{--}89\text{ mg L}^{-1}$ compared to $18 \pm 9\text{ mg L}^{-1}$ in other pore water samples (Fig. 8d). Rennert and Pfanz (2015) could show that the amount of K_2SO_4 -extractable SOM is higher in mofettes compared to non- CO_2 -influenced soils. They also could show that the interaction of SOM and soil minerals is negatively affected by high soil CO_2 partial pressures. Thus, particulate organic matter (POM) accumulates in mofettes, but is not stabilized (Rennert and Pfanz, 2015, 2016). We could also observe that the amount of DOC mobilized in soil batch experiments decreased with distance from the degassing center (Mehlhorn et al., 2018). A general increase in DOC with increasing dissolved CO_2 concentrations ($r_s = 0.54$, $P < 0.01$) could be observed in this study as well. Formation of these two hotspots (one in the upper soil and one in > 45 cm depth) was probably caused by the comparably high soil C_{org} contents in these spots, shown by a correlation of DOC and C_{org} along the East transect ($r_s = 0.49$, $P = 0.04$). The reason for slightly lower concentrations directly in the degassing center ($17 \pm 6\text{ mg L}^{-1}$) compared to 2 and 4 m distance was probably the permanent upwelling of groundwater that transferred DOM towards the surrounding soil.

Dissolved nitrogen concentrations (TN) increased with depth and decreased with distance from the center with values of $5.4\text{--}6\text{ mg L}^{-1}$ in the center and $0.4\text{--}1.5\text{ mg L}^{-1}$ in 18 m distance (Fig. 8e). Zones of high DOC concentrations did not correspond with high TN concentrations indicating that the majority of TN, especially in the degassing center, must have been present as inorganic dissolved species. We did not determine N species at the time, but assume that due to the reducing conditions the dominant inorganic N species will be ammonia. This assumption is supported by recent observations of Krauze et al. (2017) that nitrite and nitrate concentrations in nearby mofettes were $\leq 0.1\text{ mg L}^{-1}$. However, further speciation analyses are required to

confirm the postulated high ammonia concentrations.

In the degassing center, we could detect dissolved methane concentrations of up to 0.13 mM (for 10–15 cm depth, Fig. 8f). The methane originated from methanogenic archaea which have been shown to dominate in mofettes besides acetogenic and sulfur-reducing bacteria (Beaubien et al., 2008; Beulig et al., 2015; Krauze et al., 2017; Oppermann et al., 2010). Outside of the main degassing center, methane concentrations decreased to values close to or below LOD. The concentrations detected in this study are about 10 times higher than the methane concentrations detected in a previous study (up to 0.014 mM in Mehlhorn et al. (2014)), which might result from a longer equilibration time of the pore water peepers (9 compared to 2 weeks) or could also indicate a higher microbial activity in fall (September–November 2017) compared to spring (March 2013).

Sulfide concentrations in 10–50 cm depth of the degassing center were strongly elevated (up to 1.8 mg L^{-1}) compared to the surrounding pore water where concentrations were mostly $\leq LOD$ (Fig. 8g). The sulfide originates from sulfur-reducing bacteria, which have been shown to have an increased activity in mofettes compared to non- CO_2 -influenced soil (Beulig et al., 2016; Frerichs et al., 2013; Oppermann et al., 2010). The presence of sulfide and microbial sulfur-reduction in the degassing center lends further support to the hypothesized precipitation of Cd, Cu, and Zn sulfides (compare Section 3.2.5).

Total sulfur concentrations in pore water were, oppositely to sulfide, highest in the non- CO_2 -influenced soil ($21 \pm 3\text{ mg L}^{-1}$) and decreased towards the degassing center ($< 3\text{ mg L}^{-1}$) (Fig. 8h). Interestingly, there is a very clear transition between low and high sulfur concentration in approx. 8 m distance. Since DOC and pore water sulfur concentrations were negatively correlated ($r_s = -0.51$, $P < 0.01$), the majority of the sulfur must have been present as inorganic species, in > 8 m distance most likely as sulfate. Several processes could contribute to the observed sudden decrease in sulfur concentrations at < 8 m distance. The upwelling groundwater from deeper aquifers might contain lower total sulfur concentrations than the surrounding groundwater, which might be more strongly influenced by agriculture. Additionally, sulfate and also sulfide might bind to SOM, leading to the observed sulfur accumulation in soil from the mofette center. Also, the continuous sulfur reduction and following precipitation of sulfide minerals, as described for Cu in Mehlhorn et al. (2018) and postulated for Cd and Zn in this study, might lead to sulfur sequestration and removal from the liquid phase in the degassing center.

3.3.2. Metal(loid) pore water concentrations and implications on mobility

Clustering of normalized metal(loid) pore water concentrations

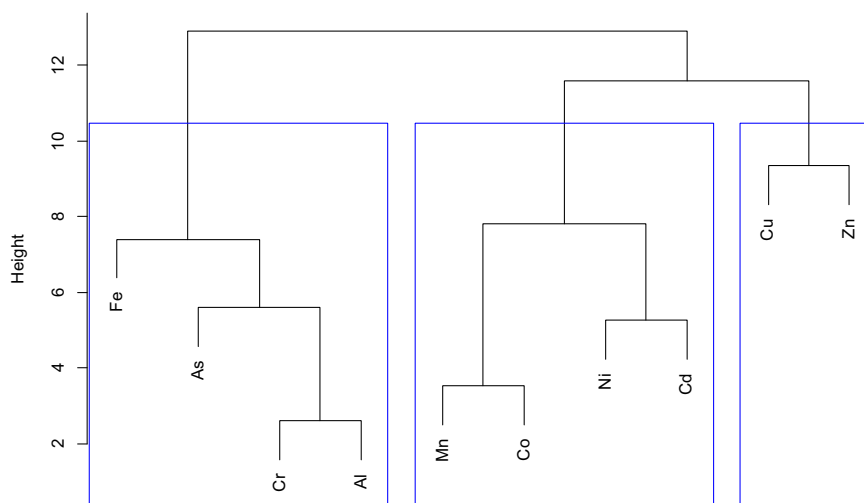


Fig. 9. Cluster dendrogram of total metal(loid) concentrations in pore water samples. Concentrations were normalized for each element prior to calculation of Euclidean distances for clustering. Similarity coefficients can be found in Table A.3, SI.

revealed that the elements could be considered in three groups of high similarity: Fe, As, Cr, and Al with similarity coefficients $s < 7.4$, Mn, Co, Ni, and Cd with $s < 7.8$, and Cu and Zn with $s = 9.3$ (Fig. 9, similarity coefficients s in SI, Table A.3).

The metal(loid)s Fe, As, Cr, and Al correlated significantly with DOC concentrations ($r_s = 0.71, 0.76, 0.8, \text{ and } 0.81$ for Fe, As, Cr, and Al, respectively, $P < 0.01$) as could be seen from strongly increased concentrations in approx. the same two spots (in 10–20 cm depth in 2 m distance and 45–60 cm depth in 4 m distance) as DOC concentrations (Fig. 8m–p). All of these elements are known to form complexes with DOM and it has been shown that their mobility in natural soils is largely determined by complexation with DOM (e.g., Carrillo-González et al., 2006; Du Laing et al., 2007; Kalbitz and Wennrich, 1998; Pohlman and McColl, 1988). Recently, Rennert (2018) proposed that exchangeable Al might preferentially interact with SOM in mofettes and, thus, contribute to SOM stabilization in mofettes.

Arsenic and especially Fe had the lowest similarity coefficients within this group and also their pore water distribution patterns imply that other processes influenced their mobility as well. The two elements were mainly enriched in 2 and 4 m distance from the degassing center and especially Fe also in 50–60 cm depth over the whole transect which indicates that also some free, i.e., not DOM-complexed ions must have been present in the pore water. The observed zones of high mobility fit well to our assumptions from soil content distribution patterns and they confirm the observations of our prior study (Mehlhorn et al., 2014): the mobility of Fe and As is increased in mofettes where no Fe (oxyhydr) oxides could form due to absence of oxygen. This could also be seen by increased dissolved-to-solid-phase ratios of Fe and As in the mofette compared to the non-CO₂-influenced soil (Fig. 10a–c). In greater depth (> 50 cm), also the non-CO₂-influenced soil was anoxic due to groundwater saturation, thus, Fe and As concentrations increased with depth. The high DOC concentrations close to the degassing center additionally increased metal(loid) mobility since complex formation with DOM can hinder adsorption and oxidation or compete for sorption sites (Grafe et al., 2001, 2002; Redman et al., 2002; Theis and Singer, 1974).

The highest pore water concentrations of Mn, Co, Ni, and Cd were found in deeper samples of the non-CO₂-influenced soil and

concentrations decreased towards the degassing center (Fig. 8i–k, r). Decreased pore water concentrations in mofette center compared to the non-CO₂-influenced reference soil were already observed for Mn and Ni in our prior study (Mehlhorn et al., 2014). In the case of Mn, Co, and Ni (and also for Cd, excluding the degassing center) pore water concentrations were highest in areas, where soil contents were highest and dissolved-to-solid-phase ratios did not vary much along the East transect (Fig. 10a–c). The relatively constant ratios imply that the mobility of Mn, Co, and Ni was kinetically controlled and only depended on total soil contents. A CO₂-triggered increase in mobility, i.e. pore water concentrations, of these elements could, thus, not be detected. The frequently observed mobilizing effect of CO₂ on metal cations due to surface protonation (e.g., Apps et al., 2010; Kharaka et al., 2010; Qafoku et al., 2014; Zheng et al., 2012), which we also observed for Mn in non-CO₂-influenced soil incubated at 100% CO₂ in a prior study (Mehlhorn et al., 2016), does not seem to play a major role at this mofette site anymore. One reason probably is that surface protonation and related mobilization of cations is an abiotic and fast process that can be observed within hours to days (e.g., Mehlhorn et al., 2016; Qafoku et al., 2014). The natural mofette site has been influenced by CO₂ over decades and pedogenesis occurred concurrently (Rennert and Pfanz, 2016). CO₂-induced, intensified mineral weathering probably led to an initial mobilization of cations into the pore water. When all mobilizable fractions were removed by leaching, only the more inert fractions (e.g., incorporated into silicates) remained. Under long-term constant CO₂-influence, desorption, dissolution, and leaching processes have thus led to both decreased soil contents and pore water concentrations of these metals in mofettes.

Equal to Mn, Co, Ni, and Cd, also Zn and Cu had relatively high pore water concentrations in the non-CO₂-influenced soil and concentrations generally decreased towards the mofette center (Fig. 8l, q). However, these metals had their highest concentration close to the DOM enriched zones in 10–20 cm depth in 2 and 4 m distance and for Zn also in 45–50 cm depth in 4 m distance. The pore water concentrations in these spots reached maxima of 20 µg L⁻¹ for Cu and even 1060 µg L⁻¹ for Zn. This indicates that the pore water concentrations of these two metals were both influenced by higher total soil contents in the non-CO₂-

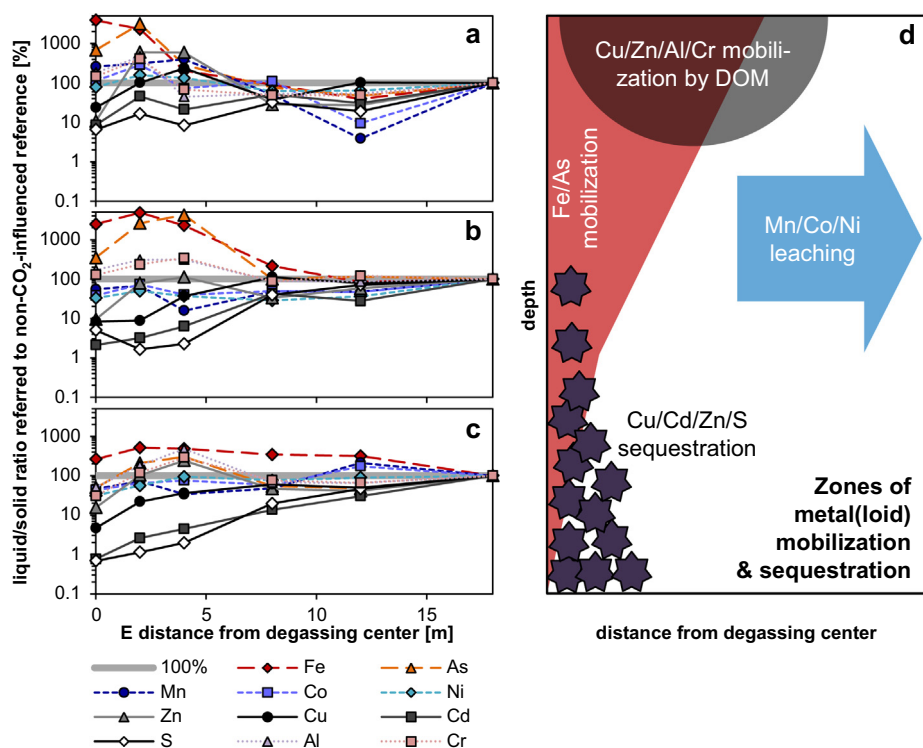


Fig. 10. (a–c) Percentage ratio of metal(loid) and sulfur pore water concentration vs. soil content along the East transect referred to non-CO₂-influenced reference soil in 18 m distance (100%) for 3 depths: (a) soil sample from 0 to 5 cm depth, respective pore water sample from 10 to 20 cm depth (no pore water sample above 10 cm depth available), (b) soil sample from 25 to 35 cm depth, respective pore water sample from 25 to 30 cm or 30–35 cm depth (depending on the exact soil sampling depth), (c) soil sample from 55 to 65 cm depth, respective pore water sample from 55 to 60 cm depth. Values > 100% mean increased net-mobility, values < 100% mean decreased net-mobility. Note the logarithmic scale of y-axis. (d) Conceptual model showing expected zones of increased metal(loid) mobility and metal(loid) sequestration along a transect through a mofette.

influenced soil (like Mn, Co, Ni, and Cd) and by complexation with DOM close to the degassing center (like Al, Cr, Fe, and As). The high affinity of Zn and Cu to organic matter has been reported in numerous previous studies (e.g., Flogeac et al., 2004; Hering and Morel, 1988; McBride et al., 1997; McLaren et al., 1983; McLaren and Crawford, 1973; Tipping, 2002). It remains unclear what caused the extremely high Zn concentration in 4 m distance and 21–25 cm depth (Fig. 8l). Since a reanalysis of this sample was not possible due to limited sample volume, an analytical error cannot be excluded.

One special observation regarding Cd, Zn, and Cu is that their pore water concentrations directly in the degassing center were decreased to values close to or below LOD (Fig. 8l, q, r). These low concentrations indicate that the precipitation of metal sulfide minerals effectively sequestered Zn, Cu, and Cd from pore water into the solid phase, as could be seen by a strong decrease in dissolved-to-solid-phase ratios, especially in the deeper soil (Fig. 10a–c).

4. Conclusions

Pedogenesis under long-term CO₂ influence at the studied mofette site has led to the development of element-specific distribution patterns with some metal(loid)s showing depletion and some showing accumulation within the mofette. The results of the present study are of specific interest regarding risk assessment of CO₂ leakage on potential metal(loid) mobilization and contamination of shallow aquifers or, with regard to immobilization, trace metal limitations for microbes or plants. Calculation of dissolved-to-solid ratios for the individual elements allowed to identify zones of metal(loid) mobilization and sequestration (Fig. 10a–c) which are summarized in a conceptual model in Fig. 10d.

The only elements, for which a direct CO₂-triggered mobilization in mofettes could be identified, are Fe and As. Fe (oxyhydr)oxides cannot form under permanently anoxic conditions or can be rapidly dissolved if soil conditions become more reducing, leading to an increased mobility of Fe and associated As. Soil distribution patterns of these elements are thus primarily determined by oxygen availability. Both Fe oxidation and precipitation of (oxyhydr)oxides under oxic conditions and Fe reduction and (re-)dissolution of (oxyhydr)oxides under anoxic conditions are relatively fast processes (Kirk, 2004). Small-scale and/or temporal variations of redox conditions as well as the rapidity of Fe oxidation/reduction are, besides complexation with DOM, probably main reasons why an increased Fe and As mobility is still detectable in the studied mofette even after decades of CO₂-influence.

For Mn, Co, and Ni, no change in net-mobility could be identified along the studied CO₂-gradient. Their pore water concentrations correspond to the total soil contents, which showed depletion within more or less the whole CO₂-influenced area. Mobilization and leaching of these elements by CO₂-induced, intensified weathering of silicates is – oppositely to Fe oxidation/reduction – generally a non-reversible process, which led to the removal of all mobilizable fractions and thus to both decreased metal soil contents and pore water concentrations. Enrichment zones in the west of the mofette site indicate that the leached metals might accumulate again in the non-CO₂-influenced soil, however, the exact transport and sequestration processes remain to be investigated.

Distribution patterns of the metals Al and Cr are in large parts only indirectly influenced by CO₂ degassing. The mineral content around the degassing center is decreased due to the accumulation of SOM, leading to overall decreased soil contents of these primary mineral-associated metals.

Sulfide mineral precipitation leads to strong immobilization, i.e., low pore water concentrations and accumulation in the solid phase, for the chalcophilic elements Zn, Cu, and Cd. However, immobilization only occurs under permanently anoxic conditions directly in the degassing center, where plant growth is rather limited by high CO₂ concentrations than by trace element limitation. Trace element limitation by sulfide mineral precipitation might, however, play a role for

microorganisms, e.g., Zn is an essential trace element for methanogens (Glass and Orphan, 2012).

The overall highest risk for increased metal(loid) mobility arises from increased DOM pore water concentrations in the mofette, which are caused by the accumulation of scarcely degraded SOM. Metal(loid)s with high tendency for complex formation, in our study Al, Cr, Fe, As, Zn, and Cu, can thus exhibit strongly increased mobilities in mofettes. Other than expected, the highest DOM concentrations are not located directly in the degassing center where upwelling groundwater flushes DOM to the surrounding soil, but in its direct vicinity (2–4 m distance).

The results of our study show that geogenic CO₂ as soil-forming factor influences both the mobility and spatial distribution of metal (loids) in soil. Especially the mobilization of potential contaminants by increased DOM concentrations under moderate CO₂ influence can be a problem at contaminated sites. The transferability of our results to other mofettes or to other sites exhibiting a gradient in redox conditions (e.g., leakages from GCS, organic contaminant spills, or wetlands) remains to be tested and should be addressed in future studies.

Acknowledgements

We acknowledge financial support for a PhD stipend to Judith Mehlhorn from the German Academic Scholarship Foundation. From Bayreuth University, we thank Ruth Freitag and Nicolas Weithmann (Process Biotechnology) for borrowing the portable gas analyzer, Manfred Fischer (Geomorphology) for borrowing soil auger equipment; from the Hydrology Department we thank Jutta Eckert and Martina Rohr for DOC analysis as well as Benjamin Gilfedder and Silke Hammer for providing access to GC. For field and lab assistance we are grateful to Esther Breuninger and Kai Jansen.

Appendix A. Supplementary data

Supplementary data to this article can be found online at <https://doi.org/10.1016/j.chemgeo.2019.01.010>.

References

- Allison, J.D., Brown, D.S., Novo-Gradac, K.J., 1991. MINTEQA2/PRODEFA2, A Geochemical Assessment Model for Environmental Systems: Version 3.0 User's Manual. Environmental Research Laboratory, Office of Research and Development, US Environmental Protection Agency.
- Apps, J., Zheng, L., Zhang, Y., Xu, T., Birkholzer, J., 2010. Evaluation of potential changes in groundwater quality in response to CO₂ leakage from deep geologic storage. *Transp. Porous Media* 82 (1), 215–246.
- Bartlett, R.J., James, B., 1988. Mobility and bioavailability of chromium in soils. In: *Chromium in the Natural and Human Environments*. vol. 20. pp. 571.
- Beaubien, S., Ciotoli, G., Coombs, P., Dictor, M.C., Krüger, M., Lombardi, S., Pearce, J., West, J., 2008. The impact of a naturally occurring CO₂ gas vent on the shallow ecosystem and soil chemistry of a Mediterranean pasture (Latera, Italy). *Int. J. Greenhouse Gas Control* 2 (3), 373–387.
- Beulig, F., Heuer, V.B., Akob, D.M., Viehweger, B., Elvert, M., Herrmann, M., Hinrichs, K.-U., Küsel, K., 2015. Carbon flow from volcanic CO₂ into soil microbial communities of a wetland mofette. *ISME J.* 9 (3), 746–759.
- Beulig, F., Urich, T., Nowak, M., Trumbore, S.E., Gleixner, G., Gilfillan, G.D., Fjelland, K.E., Küsel, K., 2016. Altered carbon turnover processes and microbiomes in soils under long-term extremely high CO₂ exposure. *Nat. Microbiol.* 1, 15025.
- Blume, H.-P., Felix-Henningsen, P., 2009. Reductosols: natural soils and Technosols under reducing conditions without an aquic moisture regime. *J. Plant Nutr. Soil Sci.* 172 (6), 808–820.
- Bradl, H.B., 2004. Adsorption of heavy metal ions on soils and soils constituents. *J. Colloid Interface Sci.* 277 (1), 1–18.
- Bräuer, K., Kämpf, H., Niedermann, S., Strauch, G., Weise, S.M., 2004. Evidence for a nitrogen flux directly derived from the European subcontinental mantle in the Western Eger Rift, central Europe. *Geochim. Cosmochim. Acta* 68 (23), 4935–4947.
- Bussert, R., Kämpf, H., Flechsig, C., Hesse, K., Nickschick, T., Liu, Q., Umlauf, J., Vylita, T., Wagner, D., Wonik, T., 2017. Drilling into an active mofette: pilot-hole study of the impact of CO₂-rich mantle-derived fluids on the geo-bio interaction in the western Eger Rift (Czech Republic). *Sci. Drill.* 23, 13.
- Carrillo-González, R., Šimůnek, J., Saue, S., Adriano, D., 2006. Mechanisms and pathways of trace element mobility in soils. *Adv. Agron.* 91, 111–178.
- Cline, J.D., 1969. Spectrophotometric determination of hydrogen sulfide in natural waters. *Limnol. Oceanogr.* 14 (3), 454–458.
- Di Toro, D.M., Mahony, J.D., Hansen, D.J., Scott, K.J., Carlson, A.R., Ankley, G.T., 1992.

- Acid volatile sulfide predicts the acute toxicity of cadmium and nickel in sediments. *Environ. Sci. Technol.* 26 (1), 96–101.
- Du Laing, G., Vanthuyne, D., Vandecasteele, B., Tack, F., Verloo, M., 2007. Influence of hydrological regime on pore water metal concentrations in a contaminated sediment-derived soil. *Environ. Pollut.* 147 (3), 615–625.
- Dzombak, D.A., 1990. *Surface Complexation Modeling: Hydrous Ferric Oxide*. John Wiley & Sons.
- Fischer, L., Brümmer, G.W., Barrow, N.J., 2007. Observations and modelling of the reactions of 10 metals with goethite: adsorption and diffusion processes. *Eur. J. Soil Sci.* 58 (6), 1304–1315.
- Flechsig, C., Bussert, R., Rechner, J., Schütze, C., Kämpf, H., 2008. The Hartoušov mofette field in the Cheb Basin, western Eger Rift (Czech Republic): a comparative geo-electric, sedimentologic and soil gas study of a magmatic diffuse CO₂-degassing structure. *Z. Geol. Wiss.* 36 (3), 177–193.
- Flogeac, K., Guillon, E., Aplincourt, M., 2004. Surface complexation of copper (II) on soil particles: EPR and XAFS studies. *Environ. Sci. Technol.* 38 (11), 3098–3103.
- Frerichs, J., Oppermann, B.I., Gwosdz, S., Möller, I., Herrmann, M., Krüger, M., 2013. Microbial community changes at a terrestrial volcanic CO₂ vent induced by soil acidification and anaerobic microhabitats within the soil column. *FEMS Microbiol. Ecol.* 84 (1), 60–74.
- Fulda, B., Voegelin, A., Ehlert, K., Kretzschmar, R., 2013a. Redox transformation, solid phase speciation and solution dynamics of copper during soil reduction and re-oxidation as affected by sulfate availability. *Geochim. Cosmochim. Acta* 123, 385–402.
- Fulda, B., Voegelin, A., Kretzschmar, R., 2013b. Redox-controlled changes in cadmium solubility and solid-phase speciation in a paddy soil as affected by reducible sulfate and copper. *Environ. Sci. Technol.* 47 (22), 12775–12783.
- Fulda, B., Voegelin, A., Maurer, F., Christl, I., Kretzschmar, R., 2013c. Copper redox transformation and complexation by reduced and oxidized soil humic acid. 1. X-ray absorption spectroscopy study. *Environ. Sci. Technol.* 47 (19), 10903–10911.
- Glass, J., Orphan, V., 2012. Trace metal requirements for microbial enzymes involved in the production and consumption of methane and nitrous oxide. *Front. Microbiol.* 3 (61).
- Grafe, M., Eick, M., Grossl, P., 2001. Adsorption of arsenate (V) and arsenite (III) on goethite in the presence and absence of dissolved organic carbon. *Soil Sci. Soc. Am. J.* 65 (6), 1680–1687.
- Grafe, M., Eick, M.J., Grossl, P.R., Saunders, A.M., 2002. Adsorption of arsenate and arsenite on ferrihydrite in the presence and absence of dissolved organic carbon. *J. Environ. Qual.* 31 (4), 1115–1123.
- Hering, J.G., Morel, F.M., 1988. Humic acid complexation of calcium and copper. *Environ. Sci. Technol.* 22 (10), 1234–1237.
- Hesslein, R.H., 1976. An in situ sampler for close interval pore water studies. *Limnol. Oceanogr.* 21 (6).
- Irwin, W.P., Barnes, I., 1980. Tectonic relations of carbon dioxide discharges and earthquakes. *J. Geophys. Res. B: Solid Earth* 85 (B6), 3115–3121.
- Kalbitz, K., Wennrich, R., 1998. Mobilization of heavy metals and arsenic in polluted wetland soils and its dependence on dissolved organic matter. *Sci. Total Environ.* 209 (1), 27–39.
- Kharaka, Y.K., Cole, D.R., Hovorka, S.D., Gunter, W.D., Knauss, K.G., Freifeld, B.M., 2006. Gas-water-rock interactions in Frio Formation following CO₂ injection: implications for the storage of greenhouse gases in sedimentary basins. *Geology* 34 (7), 577–580.
- Kharaka, Y.K., Thordsen, J.J., Kakouros, E., Ambats, G., Herkelrath, W.N., Beers, S.R., Birkholzer, J.T., Apps, J.A., Spycher, N.F., Zheng, L., Trautz, R.C., Rauch, H.W., Gullickson, K.S., 2010. Changes in the chemistry of shallow groundwater related to the 2008 injection of CO₂ at the ZERT field site, Bozeman, Montana. *Environ. Earth Sci.* 60 (2), 273–284.
- Kirk, G., 2004. *The Biogeochemistry of Submerged Soils*. John Wiley & Sons, England.
- Kirsch, K., Navarre-Sitchler, A.K., Wunsch, A., McCray, J.E., 2014. Metal release from sandstones under experimentally and numerically simulated CO₂ leakage conditions. *Environ. Sci. Technol.* 48 (3), 1436–1442.
- Krauze, P., Kämpf, H., Horn, F., Liu, Q., Voropaev, A., Wagner, D., Alawi, M., 2017. Microbiological and geochemical survey of CO₂-dominated mofette and mineral waters of the Cheb Basin, Czech Republic. *Front. Microbiol.* 8, 2446.
- Lawter, A., Qafoku, N.P., Wang, G., Shao, H., Brown, C.F., 2016. Evaluating impacts of CO₂ intrusion into an unconsolidated aquifer: I. Experimental data. *Int. J. Greenhouse Gas Control* 44, 323–333.
- Lewicki, J.L., Birkholzer, J., Tsang, C.-F., 2007. Natural and industrial analogues for leakage of CO₂ from storage reservoirs: identification of features, events, and processes and lessons learned. *Environ. Geol.* 52 (3), 457–467.
- Livesey, N., Huang, P., 1981. Adsorption of arsenate by soils and its relation to selected chemical properties and anions. *Soil Sci.* 131 (2), 88–94.
- Maček, I., Videmšek, U., Kastelec, D., Stopar, D., Vodnik, D., 2009. Geological CO₂ affects microbial respiration rates in Stavešinci mofette soils. *Acta Biol. Slov.* 52 (2), 41–48.
- Manning, B.A., Goldberg, S., 1997. Arsenic (III) and arsenic (V) adsorption on three California soils. *Soil Sci.* 162 (12), 886–895.
- McBride, M., 1989. Reactions controlling heavy metal solubility in soils. *Adv. Soil Sci.* 1–56.
- McBride, M., Sauve, S., Hendershot, W., 1997. Solubility control of Cu, Zn, Cd and Pb in contaminated soils. *Eur. J. Soil Sci.* 48 (2), 337–346.
- McGrath, S.P., Sanders, J.R., Shalaby, M.H., 1988. The effects of soil organic matter levels on soil solution concentrations and extractabilities of manganese, zinc and copper. *Geoderma* 42 (2), 177–188.
- McLaren, R.G., Crawford, D.V., 1973. Studies on soil copper II. The specific adsorption of copper by soils. *J. Soil Sci.* 24 (4), 443–452.
- McLaren, R., Williams, J., Swift, R., 1983. Some observations on the desorption and distribution behaviour of copper with soil components. *Eur. J. Soil Sci.* 34 (2), 325–331.
- Mehlhorn, J., Beulig, F., Küsel, K., Planer-Friedrich, B., 2014. Carbon dioxide triggered metal(loid) mobilisation in a mofette. *Chem. Geol.* 382, 54–66.
- Mehlhorn, J., Byrne, J.M., Kappler, A., Planer-Friedrich, B., 2016. Time and temperature dependency of carbon dioxide triggered metal(loid) mobilization in soil. *Appl. Geochem.* 74, 122–137.
- Mehlhorn, J., Besold, J., Lezama-Pacheco, J.S., Gustafsson, J.P., Kretzschmar, R., Planer-Friedrich, B., 2018. Copper mobilization and immobilization along an organic matter and redox gradient – insights from a mofette site. *Environ. Sci. Technol.* 52 (23), 13698–13707.
- Nowak, M., Beulig, F., von Fischer, J., Muhr, J., Küsel, K., Trumbore, S.E., 2015. Autotrophic fixation of geogenic CO₂ by microorganisms contributes to soil organic matter formation and alters isotope signatures in a wetland mofette. *Biogeosciences* 12, 7169–7183.
- Olk, D.C., Cassman, K.G., Schmidt-Rohr, K., Anders, M.M., Mao, J.-D., Deenik, J.L., 2006. Chemical stabilization of soil organic nitrogen by phenolic lignin residues in anaerobic agroecosystems. *Soil Biol. Biochem.* 38 (11), 3303–3312.
- Oppermann, B.I., Michaelis, W., Blumenberg, M., Frerichs, J., Schulz, H.M., Schippers, A., Beaubien, S.E., Krueger, M., 2010. Soil microbial community changes as a result of long-term exposure to a natural CO₂ vent. *Geochim. Cosmochim. Acta* 74 (9), 2697–2716.
- Pearce, J.M., 2006. What can we learn from natural analogues? In: Lombardi, S., Altunina, L.K., Beaubien, S.E. (Eds.), *Advances in the Geological Storage of Carbon Dioxide*. Springer, Netherlands, pp. 127–139.
- Pohlman, A.A., McColl, J.G., 1988. Soluble organics from forest litter and their role in metal dissolution. *Soil Sci. Soc. Am. J.* 52 (1), 265–271.
- Post, J.E., 1999. Manganese oxide minerals: Crystal structures and economic and environmental significance. *Proc. Natl. Acad. Sci. U. S. A.* 96 (7), 3447–3454.
- Qafoku, N.P., Lawter, A.R., Shao, H., Wang, G., Brown, C.F., 2014. Evaluating impacts of CO₂ gas intrusion into a confined sandstone aquifer: experimental results. *Energy Procedia* 63, 3275–3284.
- R Development Core Team, 2008. *R: A Language and Environment for Statistical Computing*. R Foundation for Statistical Computing, Vienna, Austria.
- Redman, A.D., Macalady, D.L., Ahmann, D., 2002. Natural organic matter affects arsenic speciation and sorption onto hematite. *Environ. Sci. Technol.* 36 (13), 2889–2896.
- Rennert, T., 2018. Geogenic CO₂ affects inorganic soil properties and the composition of soil organic matter in physical fractions. *Soil Res.* 56 (4), 396–403.
- Rennert, T., Pfanz, H., 2015. Geogenic CO₂ affects stabilization of soil organic matter. *Eur. J. Soil Sci.* 66 (5), 838–846.
- Rennert, T., Pfanz, H., 2016. Hypoxic and acidic—soils on mofette fields. *Geoderma* 280, 73–81.
- Rennert, T., Eusterhues, K., Pfanz, H., Totsche, K.U., 2011. Influence of geogenic CO₂ on mineral and organic soil constituents on a mofette site in the NW Czech Republic. *Eur. J. Soil Sci.* 62 (4), 572–580.
- Rennert, T., Eusterhues, K., Andrade, V.D., Totsche, K.U., 2012. Iron species in soils on a mofette site studied by Fe K-edge X-ray absorption near-edge spectroscopy. *Chem. Geol.* 332–333, 116–123.
- Ross, D.J., Tate, K.R., Newton, P.C.D., Wilde, R.H., Clark, H., 2000. Carbon and nitrogen pools and mineralization in a grassland gley soil under elevated carbon dioxide at a natural CO₂ spring. *Glob. Chang. Biol.* 6 (7), 779–790.
- Sander, R., 2015. *Compilation of Henry's law constants (version 4.0) for water as solvent*. *Atmos. Chem. Phys.* 15 (8).
- Saßmannshausen, F., 2010. *Vegetationsökologische Charakterisierung terrestrischer Mofettenstandorte am Beispiel des west-tschechischen Plesná-Tals* (Doctoral Thesis). University of Duisburg-Essen.
- Schütze, C., Sauer, U., Beyer, K., Lamert, H., Bräuer, K., Strauch, G., Flechsig, C., Kämpf, H., Dietrich, P., 2012. Natural analogues: a potential approach for developing reliable monitoring methods to understand subsurface CO₂ migration processes. *Environ. Earth Sci.* 67 (2), 411–423.
- Stookey, L.L., 1970. Ferrozine – a new spectrophotometric reagent for iron. *Anal. Chem.* 42 (7), 779–781.
- Tessier, A., Campbell, P.G., Bisson, M., 1979. Sequential extraction procedure for the speciation of particulate trace metals. *Anal. Chem.* 51 (7), 844–851.
- Theis, T.L., Singer, P.C., 1974. Complexation of iron (II) by organic matter and its effect on iron (III) oxygenation. *Environ. Sci. Technol.* 8 (6), 569–573.
- Tippling, E., 2002. *Cation Binding by Humic Substances*. Cambridge University Press, pp. 12.
- Uren, N.C., 1993. Forms, reactions and availability of nickel in soils. *Adv. Agron.* 48, 141–203.
- Videmšek, U., Hagn, A., Suhadolc, M., Radl, V., Knicker, H., Schloter, M., Vodnik, D., 2009. Abundance and diversity of CO₂-fixing bacteria in grassland soils close to natural carbon dioxide springs. *Microb. Ecol.* 58 (1), 1–9.
- Wang, S., Jaffe, P.R., 2004. Dissolution of a mineral phase in potable aquifers due to CO₂ releases from deep formations; effect of dissolution kinetics. *Energy Convers. Manag.* 45 (18–19), 2833–2848.
- Weber, F.-A., Voegelin, A., Kretzschmar, R., 2009. Multi-metal contaminant dynamics in temporarily flooded soil under sulfate limitation. *Geochim. Cosmochim. Acta* 73 (19), 5513–5527.
- Zeien, H., Brümmer, G.W., 1989. *Chemische Extraktion zur Bestimmung von Schwermetallbindungsformen in Boden*. Mitteilungen der Deutschen Bodenkundlichen Gesellschaft 59 (1), 505–510.
- Zheng, L., Apps, J.A., Spycher, N., Birkholzer, J.T., Kharaka, Y.K., Thordsen, J., Beers, S.R., Herkelrath, W.N., Kakouros, E., Trautz, R.C., 2012. Geochemical modeling of changes in shallow groundwater chemistry observed during the MSU-ZERT CO₂ injection experiment. *Int. J. Greenhouse Gas Control* 7 (0), 202–217.

A. Supporting Information

Chemical Geology

Spatial distribution of metal(loid) depletion and accumulation zones around a natural carbon dioxide degassing site

Judith Mehlhorn^a, Lukas A. Gerber^a, Britta Planer-Friedrich^{a}*

^a Environmental Geochemistry, Bayreuth Center for Ecology and Environmental Research (BayCEER), University of Bayreuth, Universitaetsstrasse 30, D-95440 Bayreuth, Germany

* Corresponding author: Tel.: +49 921 55 3999; E-mail address: b.planer-friedrich@uni-bayreuth.de

(14 pages, 12 figures, 3 tables)

CONTENTS

| | | |
|-----|---|----|
| A.1 | Sequential extraction procedure | 2 |
| A.2 | Additional data from soil samples | 3 |
| | pH, C _{org} contents, and C/N ratios | 3 |
| | Metal(loid) and S contents in 25-35 cm depth | 4 |
| | Metal(loid) distribution in different chemical fractions | 7 |
| | Molar metal(loid)/aluminum ratios for Mn, Co, Ni, Zn, and Cr | 10 |
| A.3 | Similarity coefficients for metal(loid) soil contents and pore water concentrations | 12 |
| A.4 | Pore water redox potential | 13 |
| | References | 14 |

A.1 Sequential extraction procedure

Table A.1

Summary of the 5-step sequential extraction procedure and the operationally defined fractions according to Fulda et al. (2013). SSR = soil-to-solution ratio in [g mL⁻¹]. Steps F1 to F3 were conducted in an anoxic chamber (Coy, 95%/5% nitrogen/hydrogen).

| Step | Extracting solution | Extraction conditions | Wash step | Hypothetical interpretation |
|-----------------|---|---|---------------------------|---|
| F1 ^a | 0.1 M CaCl ₂ | 24 h shaking; 23 °C; SSR 1:25 | MQ; 10 min; SSR 1:12.5 | mobile fraction (soluble and exchangeable, soluble metal-organic complexes) |
| F2 ^b | 1 M NaOAc (pH 5, adjusted with HOAc) | 24 h shaking; 23 °C; SSR 1:25 | MQ; 10 min; SSR 1:12.5 | easily mobilizable fraction (specifically adsorbed, bound to CaCO ₃ and other minerals labile at pH 5, weak metal-organic complexes) |
| F3 ^c | 0.025 M NH ₄ -EDTA (pH 4.6) 1 M NH ₄ OAc (pH 4.6) | 90 min shaking; 23 °C; SSR 1:25 10 min shaking; 23 °C; SSR 1:12.5 | MQ; 10 min; SSR 1:25 | organically bound fraction (low affinity sites) |
| F4 ^c | 0.1 M ascorbic acid + 0.2 M NH ₄ Ox/HOx (pH 3.25) 0.2 M NH ₄ Ox/HOx (pH 3.25) | 2 h; 96 °C (heat block); SSR 1:25; dark 10 min shaking; 23 °C; SSR 1:12.5; dark | MQ; 10 min; SSR 1:12.5 | reducible fraction (bound to amorphous and crystalline Fe- and Mn (oxyhydr)oxides) |
| F5 ^b | 30% H ₂ O ₂ (pH 2) + 2 M HNO ₃ 3.2 M NH ₄ OAc (in 20% v/v HNO ₃) | 5 mL H ₂ O ₂ + 3 mL HNO ₃ ; 2 h; 85 °C (heat block) 3 mL H ₂ O ₂ ; 3 h; 85 °C (heat block) 5 mL NH ₄ OAc; 30 min; 23 °C | | oxidizable fraction (metal sulfides and organically bound fraction (high affinity sites)) |

^a McGrath et al. (1988)

^b Tessier et al. (1979)

^c Zeien and Brümmer (1989)

A.2 Additional data from soil samples

pH, C_{org} contents, and C/N ratios

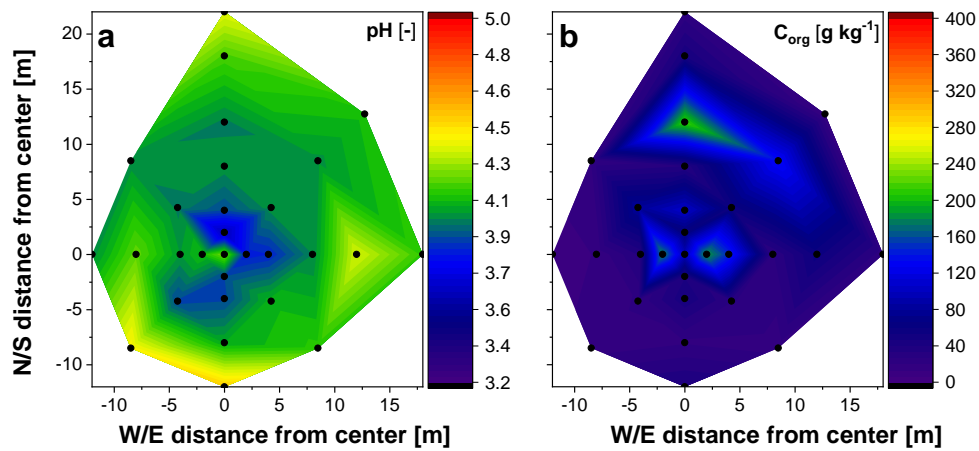


Fig. A.1. (a) Soil pH determined in 0.01 M CaCl₂ at a soil-to-solution ratio of 1:2.5 and (b) total organic carbon (C_{org}) content in samples from 25-35 cm depth. Black dots mark sampling points, pH and C_{org} contents were extrapolated between these points from measured values using universal kriging interpolation.

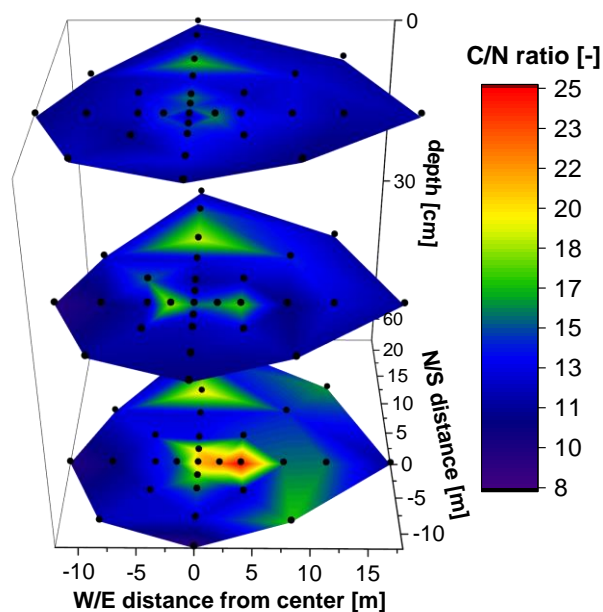


Fig. A.2. C/N ratios in soil samples from 0-5 cm (top graph), 25-35 cm (middle graph), and 55-65 cm depth (bottom graph). Black dots mark sampling points, contents were extrapolated between these points from measured concentrations using universal kriging interpolation.

Metal(loid) and S contents in 25-35 cm depth

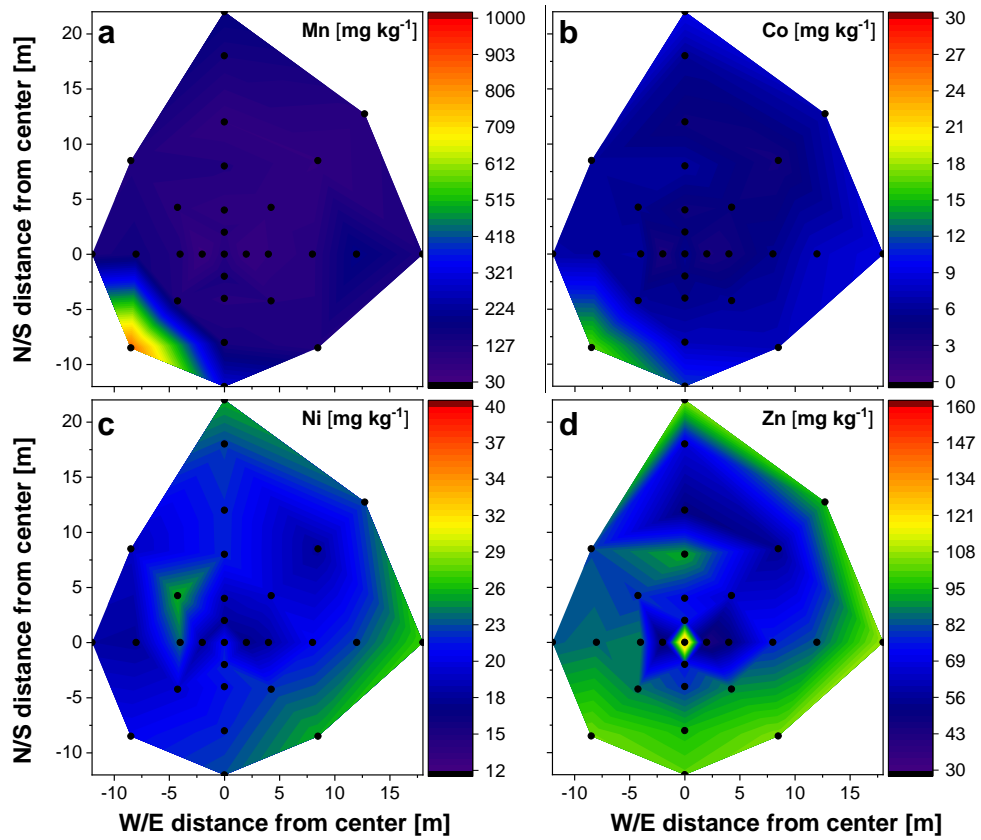


Fig. A.3. Total contents of Mn (a), Co (b), Ni (c), and Zn (d) determined in aqua regia digests of soil samples from 25-35 cm depth. Black dots mark sampling points, contents were extrapolated between these points from measured concentrations using universal kriging interpolation.

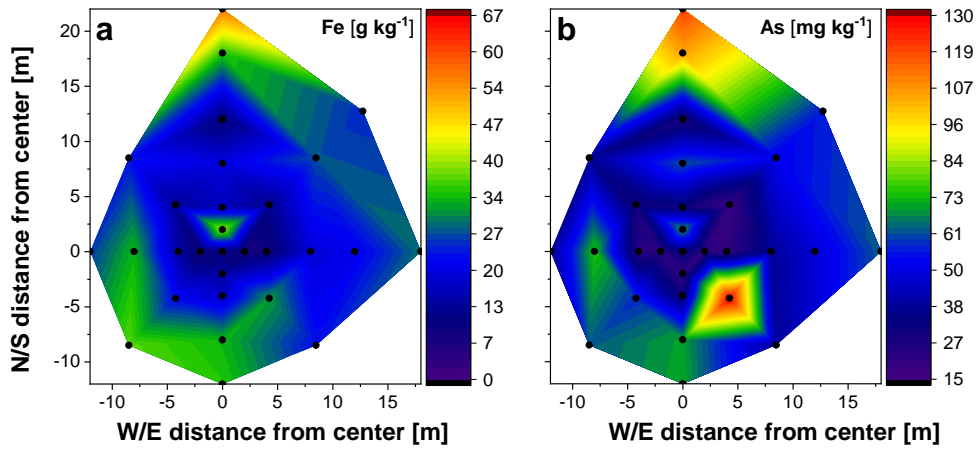


Fig. A.4. Total contents of Fe (a) and As (b) determined in aqua regia digests of soil samples from 25-35 cm depth. Black dots mark sampling points, contents were extrapolated between these points from measured concentrations using universal kriging interpolation.

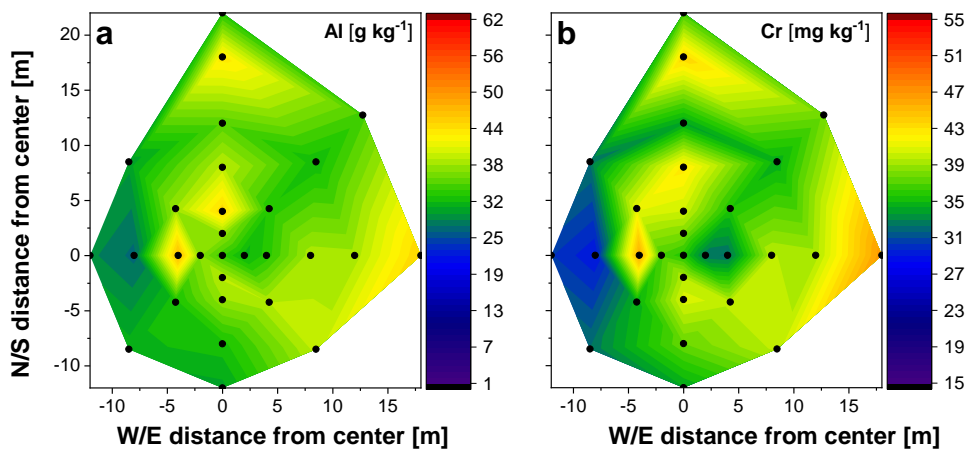


Fig. A.5. Total contents of Al (a) and Cr (b) determined in aqua regia digests of soil samples from 25-35 cm depth. Black dots mark sampling points, contents were extrapolated between these points from measured concentrations using universal kriging interpolation.

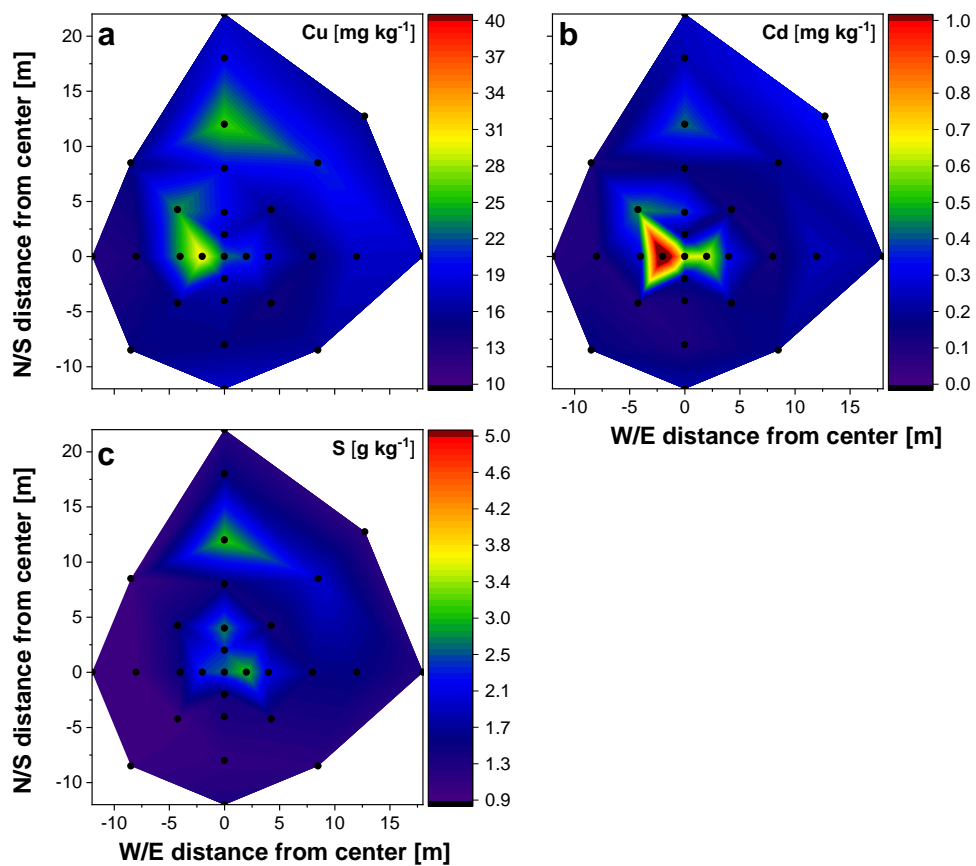


Fig. A.6. Total contents of Cu (a), Cd (b), and S (c) determined in aqua regia digests of soil samples from 25-35 cm depth. Maximum Cd content is 1.3 mg kg^{-1} at 2 m W from degassing center. Black dots mark sampling points, contents were extrapolated between these points from measured concentrations using universal kriging interpolation.

Metal(loid) distribution in different chemical fractions

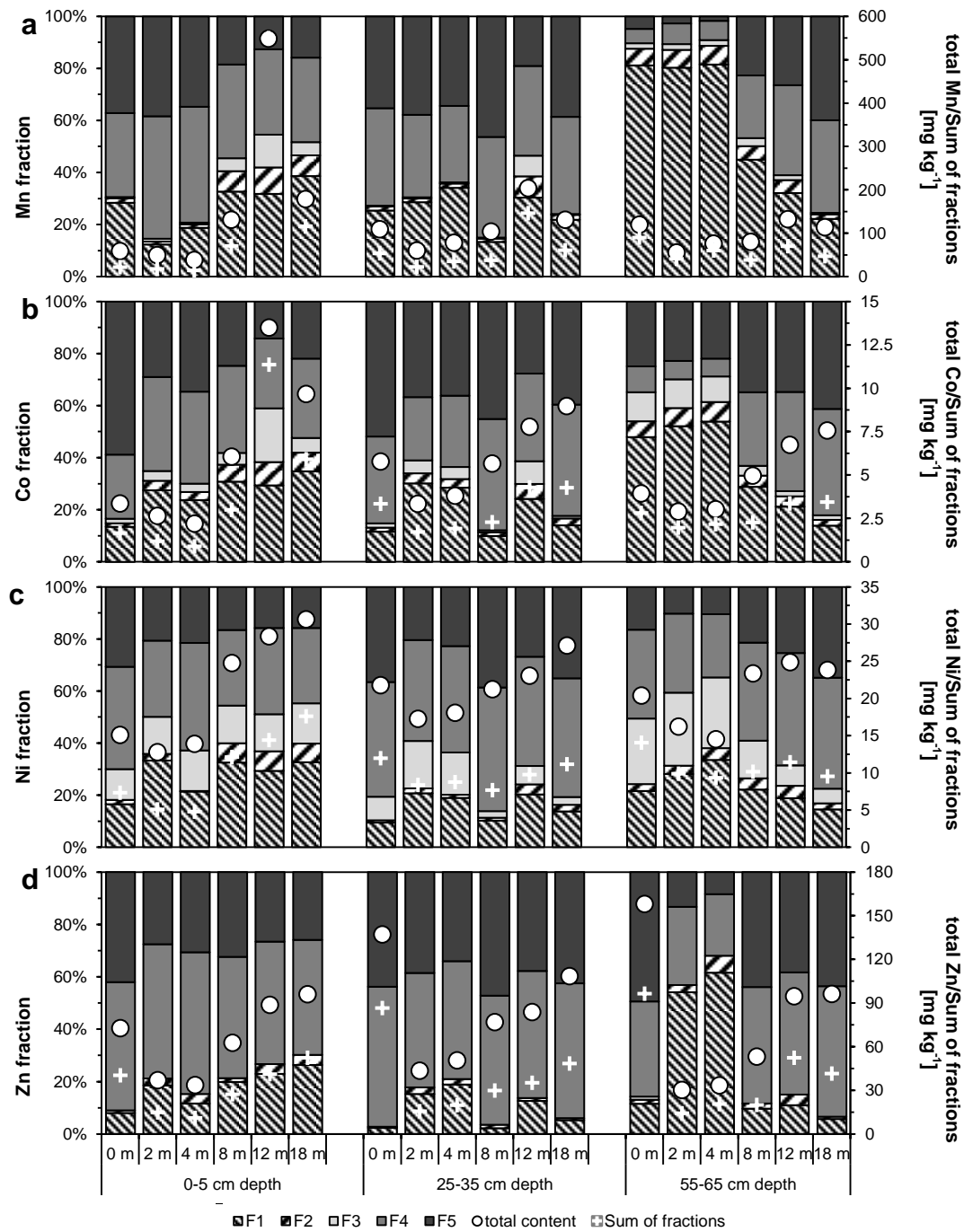


Fig. A.7. Mn (a), Co (b), Ni (c), and Zn (d) content distribution in different chemical fractions according the procedure described in Fulda et al. (2013) for soil samples from the East transect. Circles mark total contents determined in aqua regia digests, crosses mark sum of fractions. Sampling depth and distance from degassing center is given on x-axis.

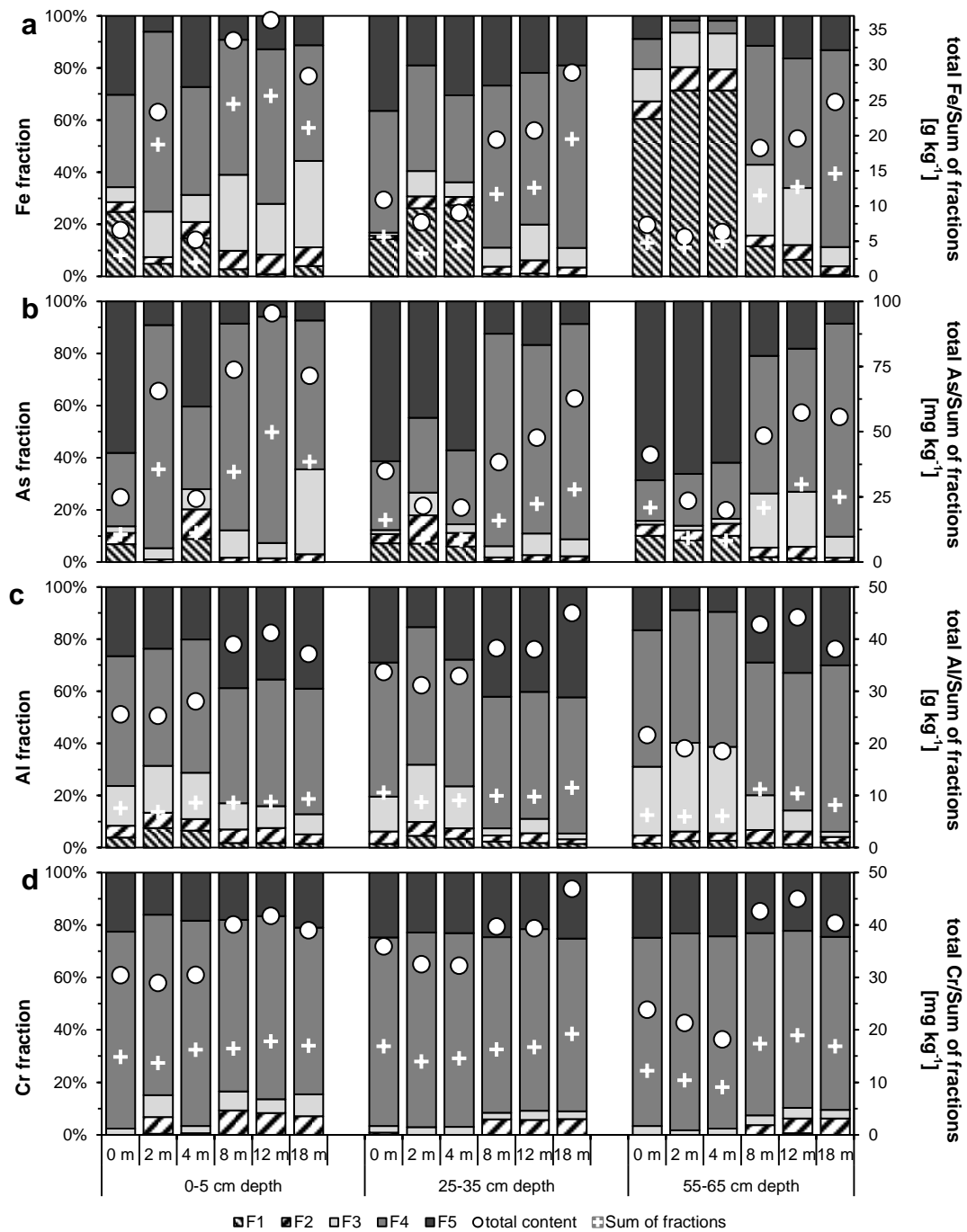


Fig. A.8. Fe (a), As (b), Al (c), and Cr (d) content distribution in different chemical fractions according the procedure described in Fulda et al. (2013) for soil samples from the East transect. Circles mark total contents determined in aqua regia digests, crosses mark sum of fractions. Sampling depth and distance from degassing center is given on x-axis.

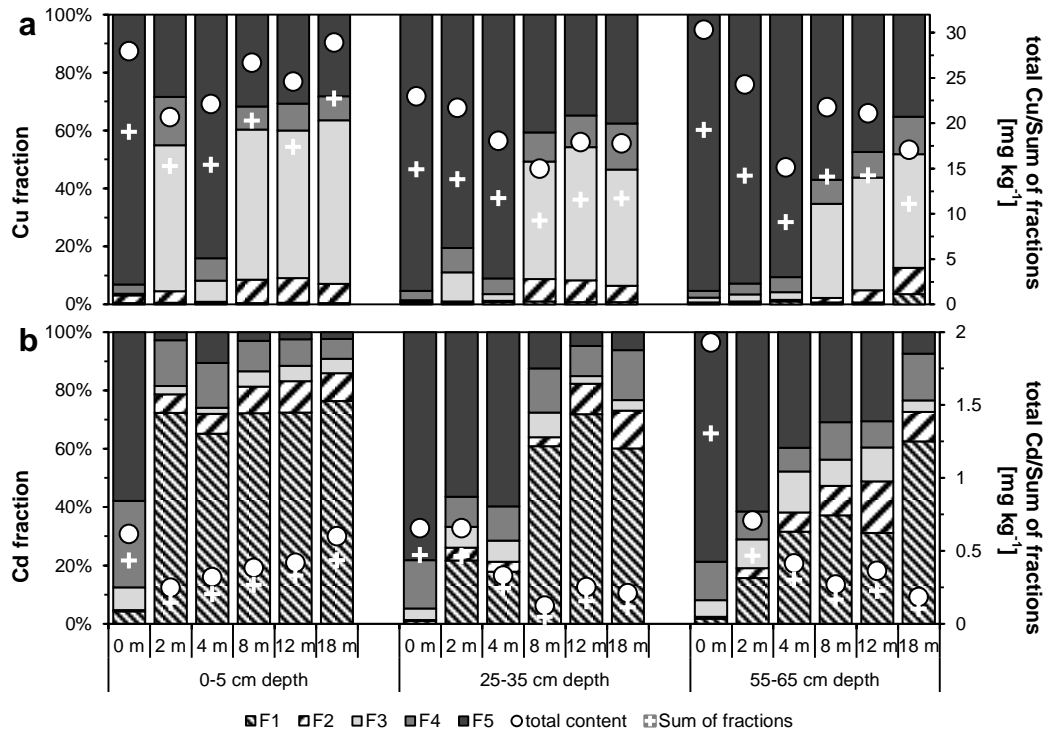


Fig. A.9. Cu (a) and Cd (b) content distribution in different chemical fractions according to the procedure described in Fulda et al. (2013) for soil samples from the East transect. Circles mark total contents determined in aqua regia digests, crosses mark sum of fractions. Sampling depth and distance from degassing center is given on x-axis.

Molar metal(loid)/aluminum ratios for Mn, Co, Ni, Zn, and Cr

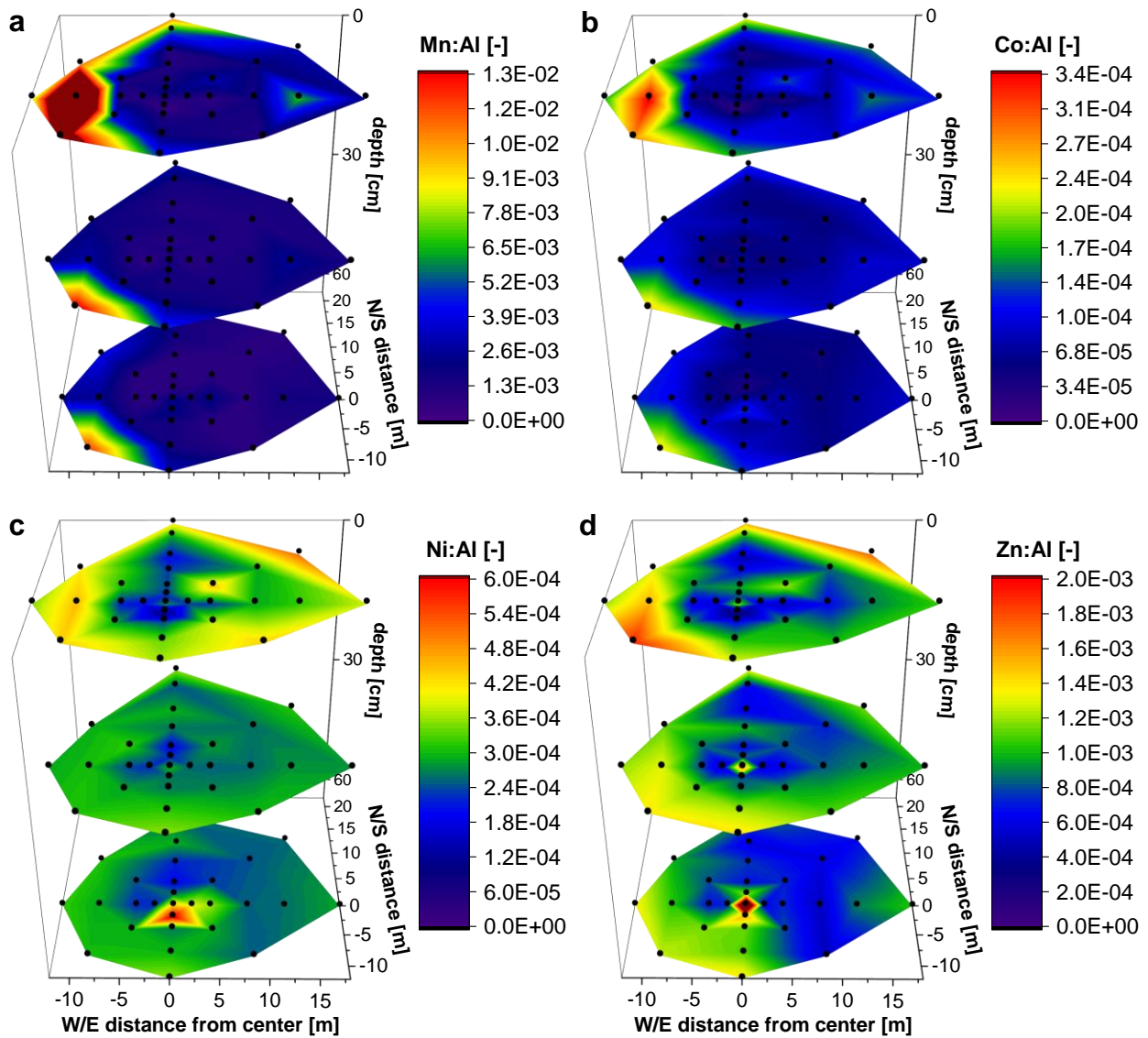


Fig. A.10. Molar ratio of soil contents for Mn/Al (a), Co/Al (b), Ni/Al (c), and Zn/Al (d) determined in aqua regia digests of soil samples from 0-5 cm (top graph), 25-35 cm (middle graph), and 55-65 cm depth (bottom graph). Maximum Zn/Al ratio is 0.003 in the degassing center. Black dots mark sampling points, molar ratios were extrapolated between these points using universal kriging interpolation.

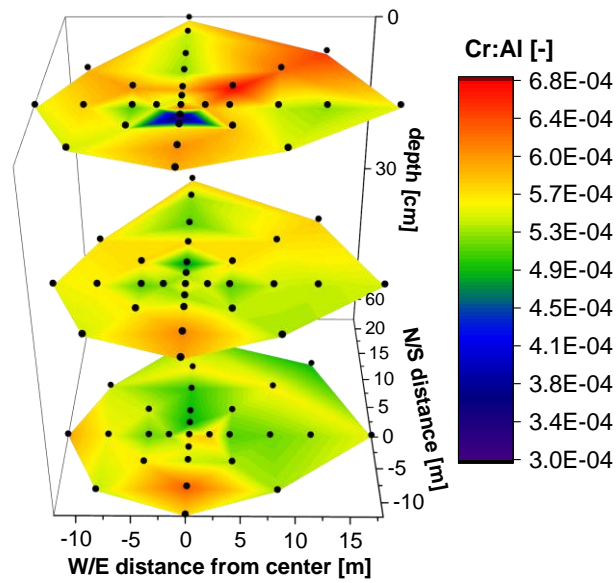


Fig. A.11. Molar ratio of Cr/Al soil contents determined in aqua regia digests of soil samples from 0-5 cm (top graph), 25-35 cm (middle graph), and 55-65 cm depth (bottom graph). Black dots mark sampling points, molar ratios were extrapolated between these points using universal kriging interpolation.

A.3 Similarity coefficients for metal(loid) soil contents and pore water concentrations

Table A.2

Similarity matrix for the cluster analysis of normalized soil metal(loid) and S contents.

| | Fe | S | Cr | Mn | Co | Ni | Cu | Zn | As | Cd | Al |
|----|----|------|------|------|------|------|------|------|------|------|------|
| Fe | 0 | 15.8 | 11.2 | 10.6 | 9.6 | 11.0 | 14.0 | 10.8 | 5.5 | 14.8 | 12.0 |
| S | | 0 | 15.7 | 14.0 | 14.8 | 13.7 | 9.3 | 13.8 | 14.9 | 8.0 | 15.0 |
| Cr | | | 0 | 11.8 | 10.9 | 9.1 | 12.7 | 10.9 | 11.3 | 14.5 | 5.0 |
| Mn | | | | 0 | 3.1 | 8.2 | 12.2 | 8.5 | 10.9 | 11.5 | 12.6 |
| Co | | | | | 0 | 6.4 | 12.3 | 7.0 | 9.9 | 11.9 | 12.2 |
| Ni | | | | | | 0 | 10.1 | 6.9 | 10.2 | 10.9 | 11.0 |
| Cu | | | | | | | 0 | 12.8 | 13.1 | 7.7 | 13.0 |
| Zn | | | | | | | | 0 | 10.4 | 10.9 | 12.3 |
| As | | | | | | | | | 0 | 13.6 | 12.9 |
| Cd | | | | | | | | | | 0 | 14.6 |
| Al | | | | | | | | | | | 0 |

Table A.3

Similarity matrix for the cluster analysis of normalized pore water metal(loid) concentrations.

| | Fe | Cr | Mn | Co | Ni | Cu | Zn | As | Cd | Al |
|----|----|-----|------|------|------|------|------|------|------|------|
| Fe | 0 | 7.1 | 9.7 | 10.2 | 10.3 | 12.6 | 12.1 | 7.4 | 12.9 | 7.2 |
| Cr | | 0 | 11.0 | 10.2 | 9.3 | 11.1 | 11.0 | 4.9 | 11.4 | 2.6 |
| Mn | | | 0 | 3.5 | 6.8 | 10.0 | 11.6 | 11.8 | 7.8 | 11.7 |
| Co | | | | 0 | 4.5 | 9.4 | 11.6 | 11.3 | 6.0 | 11.0 |
| Ni | | | | | 0 | 8.1 | 11.3 | 10.9 | 5.3 | 10.0 |
| Cu | | | | | | 0 | 9.3 | 12.0 | 7.6 | 11.8 |
| Zn | | | | | | | 0 | 10.9 | 10.8 | 11.1 |
| As | | | | | | | | 0 | 12.4 | 5.6 |
| Cd | | | | | | | | | 0 | 11.9 |
| Al | | | | | | | | | | 0 |

A.4 Pore water redox potential

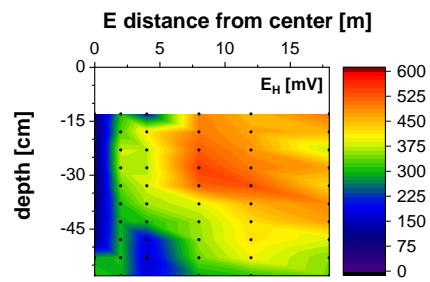


Fig. A.12. Redox potential (E_H) from pore water samples collected with dialysis chambers along the East transect of the mofette site. Black dots mark sampling points, values were extrapolated between these points from measured values using universal kriging interpolation.

References

- Fulda, B., Voegelin, A., Ehlert, K., Kretzschmar, R., 2013. Redox transformation, solid phase speciation and solution dynamics of copper during soil reduction and reoxidation as affected by sulfate availability. *Geochim. Cosmochim. Acta*, 123, 385-402.
- McGrath, S.P., Sanders, J.R., Shalaby, M.H., 1988. The effects of soil organic matter levels on soil solution concentrations and extractabilities of manganese, zinc and copper. *Geoderma*, 42(2), 177-188.
- Tessier, A., Campbell, P.G., Bisson, M., 1979. Sequential extraction procedure for the speciation of particulate trace metals. *Anal. Chem.*, 51(7), 844-851.
- Zeien, H., Brümmer, G.W., 1989. Chemische Extraktion zur Bestimmung von Schwermetallbindungsformen in Boden. *Mitteilungen der Deutschen Bodenkundlichen Gesellschaft*, 59(1), 505-510.

STUDY 2: Time and temperature dependency of carbon dioxide triggered metal(loid) mobilization in soil.

Judith Mehlhorn, James M. Byrne, Andreas Kappler, Britta Planer-Friedrich

Reprinted with permission from

Applied Geochemistry 74 (pp. 122 - 137)

Copyright 2016 Elsevier



Time and temperature dependency of carbon dioxide triggered metal(loid) mobilization in soil



Judith Mehlhorn ^a, James M. Byrne ^b, Andreas Kappler ^b, Britta Planer-Friedrich ^{a,*}

^a University of Bayreuth, Environmental Geochemistry, Bayreuth Center for Ecology and Environmental Research (BayCEER), Universitaetsstrasse 30, D-95440 Bayreuth, Germany

^b University of Tuebingen, Geomicrobiology, Center for Applied Geosciences, Sigwartstrasse 10, D-72076 Tuebingen, Germany

ARTICLE INFO

Article history:

Received 21 June 2016

Received in revised form

13 September 2016

Accepted 16 September 2016

Available online 17 September 2016

Keywords:

Mofette

Fluvisol

Carbon Capture and Storage (CCS)

Microbial iron reduction

Czech Republic

ABSTRACT

Assessing the influence of CO₂ on soil and aquifer geochemistry is a task of increasing interest when considering risk assessment for geologic carbon sequestration. Leakage and CO₂ ascent can lead to soil acidification and mobilization of potentially toxic metals and metalloids due to desorption or dissolution reactions. We studied the CO₂ influence on an Fe(III) (oxyhydr)oxide rich, gleyic Fluvisol sampled in close vicinity to a Czech mofette site and compared the short-term CO₂ influence in laboratory experiments with observations on long-term influence at the natural site. Six week batch experiments with/without CO₂ gas flow at 3 different temperatures and monitoring of liquid phase metal(loid) concentrations revealed two main short-term mobilization processes. Within 1 h to 1 d after CO₂ addition, mobilization of weakly adsorbed metal cations occurred due to surface protonation, most pronounced for Mn (2.5–3.3 fold concentration increase, mobilization rates up to $278 \pm 18 \mu\text{g Mn kg}_{\text{soil}}^{-1} \text{d}^{-1}$) and strongest at low temperatures. However, total metal(loid) mobilization by abiotic desorption was low. After 1–3 d significant Fe mobilization due to microbially-triggered Fe(III) (oxyhydr)oxide dissolution began and continued throughout the experiment (up to 111 ± 24 fold increase or up to $1.9 \pm 0.6 \text{ mg Fe kg}_{\text{soil}}^{-1} \text{d}^{-1}$). Rates increased at higher temperature and with a higher content of organic matter. The Fe(III) mineral dissolution was coupled to co-release of incorporated metal(loid)s, shown for As (up to 16 ± 7 fold, $11 \pm 8 \mu\text{g As kg}_{\text{soil}}^{-1} \text{d}^{-1}$). At high organic matter content, re-immobilization due to resorption reactions could be observed for Cu. The already low pH (4.5–5.0) did not change significantly during Fe(III) reduction due to buffering from sorption and dissolution reactions, but a drop in redox potential (from > +500 mV to minimum $+340 \pm 20$ mV) occurred due to oxygen depletion. We conclude that microbial processes following CO₂ induction into a soil can contribute significantly to metal(loid) mobilization, especially at optimal microbial growth conditions (moderate temperature, high organic carbon content) and should be considered for carbon sequestration monitoring and risk assessment.

© 2016 Elsevier Ltd. All rights reserved.

1. Introduction

The storage of carbon dioxide (CO₂) in geological structures (geologic carbon storage, GCS) is a promising option for the reduction of industrial greenhouse gas emissions and currently tested and practiced in numerous projects all over the world. Even though GCS sites are carefully selected in order to guarantee safe storage over centuries, leakage of CO₂ can never be completely ruled out and risks for overlying aquifers and soils have to be assessed (IPCC, 2005; Jun et al., 2012, 2013).

* Corresponding author.

E-mail address: b.planer-friedrich@uni-bayreuth.de (B. Planer-Friedrich).

One possibility to study long-term influence of CO₂ on soils and aquifers is using natural analogues (Lewicki et al., 2007; Pearce, 2006; Schütze et al., 2012). Cold, volcanic CO₂ exhalation sites, called mofettes, can have CO₂ partial pressures ($p(\text{CO}_2)$) of up to 1 (Bräuer et al., 2004; Kämpf et al., 2007) and thus represent excellent sites to study effects on soil and pore water conditions. Dissolution of CO₂ in pore water and dissociation of carbonic acid causes soil acidification and can lead to mobilization of trace elements due to mineral dissolution reactions (Blume and Felix-Henningsen, 2009; Kharaka et al., 2006, 2010; Mehlhorn et al., 2014; Wang and Jaffe, 2004; Zheng et al., 2009, 2012). The influence of high CO₂ partial pressures on iron (Fe) oxides and oxyhydroxides (hereafter summarized as Fe(III) (oxyhydr)oxides) was studied in

detail for a Czech grassland mofette site in Rennert et al. (2011, 2012). They found that Fe minerals in the mofette were of weak crystallinity and extractable pedogenic Fe(III) (oxyhydr)oxide content showed a negative correlation with $p(\text{CO}_2)$. Solid Fe phases were dominated by Fe(III) incorporated in silicates and fine grained Fe(II) as well as mixed Fe(II)/Fe(III) mineral phases, while pedogenic Fe(III) (oxyhydr)oxides could only be detected along old root channels. They concluded that Fe release by weathering of parent material is decreased in the mofettes and the small amount of Fe(II) released from weathering is not re-oxidized to Fe(III) (oxyhydr)oxides due to the absence of oxygen.

The organic matter content in mofettes can be significantly increased compared to surrounding sites which are unaffected by CO_2 . This increase is attributed to decreased decomposition rates under anoxic conditions in mofettes (Flechsigt et al., 2008; Maček et al., 2009; Rennert et al., 2011; Videmšek et al., 2009) and an additional organic matter input from autotrophic microbial carbon fixation of geogenic CO_2 (Beulig et al., 2015; Nowak et al., 2015). Furthermore, a shift in microbial community towards anaerobic, acidophilic microorganisms, a lowered microbial diversity as well as the exclusion of meso- and macroscopic eukaryotes have been observed in mofettes, which contributes to organic matter accumulation (Beulig et al., 2016; Fernández-Montiel et al., 2016; Frerichs et al., 2013; Nowak et al., 2015; Oppermann et al., 2010; Šibanc et al., 2014). Solid organic matter quality analyzed by ^{13}C NMR did not seem to be affected by geogenic CO_2 in a mofette with moderate $p(\text{CO}_2)$ (Rennert and Pfanz, 2015) while Fourier-transform infrared spectroscopy on a transect with $p(\text{CO}_2)$ up to 1 revealed detectable changes in organic matter quality with increased lignin concentrations at higher $p(\text{CO}_2)$ (Rennert et al., 2011).

Investigations on natural soil and pore water samples from a Czech mofette site conducted by our working group in 2013 confirmed the negative correlation of total Fe content in soil and $p(\text{CO}_2)$ as well as the increased organic matter content in mofettes compared to an adjacent CO_2 unaffected reference soil (Mehlhorn et al., 2014). We also showed that the reduced content of Fe(III) (oxyhydr)oxides led to an increased mobility of arsenic (As) in the mofettes while other elements, especially copper (Cu), showed a decreased net-mobility due to adsorption to organic matter in the mofettes.

However, as useful as natural analogues are for assessing the long-term effects of CO_2 on soil and aquifers, they cannot provide any information on time dependencies of the observed (im)mobilization processes. Also, other influences on metal(loid) mobilization, like microbial activity or seasonal effects can hardly be studied in a quantitative way at natural sites, since the current state of most mofettes represents the effects of CO_2 influence over decades or centuries. To further assess the pathway that leads to conditions found in mofettes, laboratory batch experiments with controlled CO_2 gas purging can help to increase the current knowledge by distinguishing between different (im)mobilization pathways and be used to determine mobilization rates. Numerous batch studies on the influence of CO_2 on different sediment materials exist indicating that mobilization reactions due to desorption or mineral dissolution are the dominating short-term processes following a CO_2 intrusion into an aquifer (e.g. Kirsch et al., 2014; Lawter et al., 2016; Little and Jackson, 2010; Smyth et al., 2009). However, also re-adsorption or formation of secondary minerals can occur and lead to net-immobilization of certain metal(loid)s (e.g. Lawter et al., 2015; Lu et al., 2010; Mickler et al., 2013; Shao et al., 2015). Significant knowledge gaps still exist on the influence of other relevant geochemical factors, like redox condition, microbial activity, or mineral composition (Harvey et al., 2012). The microbial influence in particular is not yet completely understood since the effects of

microbial activity on metal(loid) mobility largely depend on the community present in the sediment or soil, which will differ significantly between different sites. Microbes can either enhance mobilization rates by altering existing equilibria and triggering the dissolution of certain minerals, e.g., the dissolution of Fe(III) (oxyhydr)oxides (Kirk et al., 2013), or promote mineral precipitation by increasing alkalinity or direct biological carbonate formation (Harvey et al., 2016; Kirk et al., 2013; Lions et al., 2014 and references therein).

To further investigate the short-term effects of CO_2 intrusion on metal(loid) mobility, we conducted batch experiments with hitherto CO_2 unaffected soil suspensions from a gleyic Fluvisol in close vicinity to mofettes already studied in Mehlhorn et al. (2014). The aim of this study was (i) to distinguish between different mobilization and immobilization processes by detailed monitoring of metal(loid) concentrations during CO_2 incubation, (ii) to get qualitative information about the microbial influence on the (im) mobilization reactions by variation of incubation temperature, and (iii) to determine mobilization rates for certain metal(loid)s under the conditions prevailing in mofettes, hence, helping to increase our understanding of the risks arising from potential GCS leakage into soil and aquifers. Based on the results gained from our study at the natural mofette site, we hypothesized that mobilization of metal cations due to desorption will be the dominating short-term effect, combined with low total liquid phase concentration increases. Further, we expected mobilization of Fe and other metal(loid)s due to the reductive dissolution of Fe(III) (oxyhydr)oxides, a potentially microbially-triggered process that should be accelerated by increased incubation temperatures. The main advantage of using soil material from close vicinity of mofettes for the batch experiments is the possibility of direct comparison between experimental results on short-term CO_2 influence with results from field studies on long-term effects.

2. Material and methods

2.1. Site description and sampling

Soil and water samples for batch experiments were collected in a mofette area in northwestern Czech Republic. The mofettes are located in the flood plain of the river Plesná, which follows the north-south striking Počátky-Plesná Zone where CO_2 -rich mantle gasses ascend from a magma chamber in the lower earth crust (Bankwitz et al., 2003). We selected a mofette, already studied in Mehlhorn et al. (2014), that is located in direct vicinity of the river Plesná and thus is water saturated all year. Soil samples were not taken directly from the mofette, but from a "reference site" some meters away which was selected based on vegetation changes (N 50°08'43.7" E 12°27'1.4", for a more detailed description see Mehlhorn et al. (2014)). Thus, the soil selected for batch experiments is similar to the mofette soils but not CO_2 influenced. The first sampling took place on March 2nd, 2015. The vegetation and root zone were removed before 1 kg of soil, previously classified as gleyic Fluvisol (Beulig et al., 2016), was taken from a depth between 20 and 30 cm and packed in airtight closed plastic bags. The selected sampling depth was chosen based on results from 2013, where the most pronounced metal(loid) concentration differences between mofette and reference soils were found at approximately 25 cm depth. For the batch experiments, we chose river water as groundwater analogue, since groundwater was not available in the amounts needed. Metal(loid) concentrations in the river water were similar to or lower than in natural pore water (see Section 3.1) which justified the usage of river water as analogue for an uncontaminated aquifer. Two liters of river water were sampled as close as possible to the soil sampling site (distance approx. 15 m), a few

cm below the surface in 1 L-polypropylene bottles without gaseous headspace. The samples were kept cool during transport to the laboratory, where the river water was filtered (0.2 μm , cellulose-acetate filter, CHROMAFIL[®] Xtra) to remove particles and microorganisms. Before storage at 8 °C, the head space of the water bottles was filled with nitrogen and sealed airtight. The soil bags were opened and closed again in an anoxic COY-glovebox (95% N₂, 5% H₂) in order to remove oxygen from the gas phase. Afterwards, the bags were sealed and stored at 8 °C.

The second sampling took place on August 21st, 2015, and was conducted analogous to the first sampling. Due to the relatively hot and dry summer (average temperature of 19.5 °C in August 2015 and 231 mm precipitation between May and August 2015, compared to a 1961–1990 average of 15.7 °C and 272 mm precipitation in the same time span for the Karlovy Vary region, CHMI (2015)) the soil was exceptionally dry and had a relatively high root content. We therefore took the soil from a depth of 30–40 cm, where there were less roots and the humidity was slightly higher. Sample preparation in the laboratory was the same as for the first sampling.

2.2. Batch experiments

We conducted two batch experiments, one with temperature variation and one with variation of initial soil conditions. The first experiment (Batch Experiment I) started 1 d after the first sampling and lasted 42 d. Three different temperatures were applied to the batches in order to lower (16 °C) or stimulate (35 °C) microbial activity compared to room temperature (22 °C) and imitate different seasons. While 16 and 22 °C are typical average soil temperatures for spring, summer, and fall season in Central Europe (PIK, 2016), the relatively warm 35 °C were chosen to simulate maximum microbial activity when soil is exposed to direct sunlight on a warm summer day. Each differently treated set consisted of 7 batch reactors: a triplicate of batches with soil and water phase that were not treated with CO₂ (controls), a triplicate of batches with soil and water phase that were treated with CO₂ gas flow (treatments), and one batch that contained only water and was treated with CO₂ gas flow (water blank). The batches were prepared in 250 mL glass bottles, that were filled with 50 g of fresh soil and 75 mL of filtered river water (soil:water ratio 1:1.5) or with 75 mL of filtered river water only for the water blanks, and stoppered with a chlorobutyl septum each. Since the soil appeared to be relatively homogenous, there was no further treatment before the beginning of the experiment except for the removal of bigger roots and plant debris. The batches with CO₂ treatment were connected to the CO₂ gas flow (28 \pm 5 mL min⁻¹) with one long needle as gas inlet and one short needle as gas outlet. The batches without CO₂ treatment only received a short needle to guarantee gas exchange with the atmosphere. One set of samples was placed at room temperature ("RT" 22 \pm 1 °C), one set was placed in a thermoelectric cool box (MOBICOOL V26) for cooling ("C" 16 \pm 1 °C), and one set was placed in a heated water bath ("H" 35 \pm 0.1 °C). All batches were covered with aluminum foil to exclude light radiation. After 10 min of gas flow, all batches were shaken softly to mix liquid and solid phase. The mixing was repeated daily during the whole experiment. Gas flow was controlled daily with a bubble counter at the outlet needle and needles were exchanged in case of blockage. Sampling of the liquid phase of all batches was conducted 1 h, 1, 3, 7, 14, 28, and 42 d after the start of the experiment. The gas flow was turned off 10 min before sampling in order to let bigger particles settle from the liquid phase. Between 1.5 and 5 mL of the liquid phase were removed from the batch with needle and syringe and filtered (0.2 μm , cellulose-acetate filter, CHROMAFIL[®] Xtra). Redox potential and pH (WTW pH meter Multi340i equipped with a SenTix pH

electrode and a SenTix ORP redox electrode) were measured immediately after sampling to minimize oxygen influence, and 1.5 mL of the remaining sample were stabilized with 15 μL of 8 M HNO₃ to prevent precipitation and stored at 8 °C until determination of total Fe, Mn, As, and Cu concentrations by inductively coupled plasma mass spectrometry (ICP-MS). For the last time step (42 d), an additional 2 mL of sample was stabilized in N₂-purged septum vials and stored at 8 °C for analysis of dissolved CO₂ and CH₄ by gas chromatography (GC). Each batch was weighed before and after the experiment for calculation of evaporation loss. For analysis of the solid phase, the remaining supernatant was removed, samples were freeze-dried and ground into a powder. Soil pH was measured in 0.01 M CaCl₂ solution (w/v ratio 1:2.5, WTW pH meter Multi340i equipped with a SenTix pH electrode). Total Fe, As, Mn, and Cu concentrations were determined with ICP-MS, after microwave digestion (MARS Xpress, CEM) with 10 mL aqua regia per 100 mg soil sample (program: 20 min heating to 160 °C, 15 min holding, 20 min cooling) in filtered (0.2 μm , cellulose-acetate filter, CHROMAFIL[®] Xtra) and diluted extracts.

Since the heated batches ("H") showed the most interesting mobilization processes, this part of the experiment was repeated a second time (Batch Experiment II). This time, the initial soil conditions were varied in order to get more information on the influence of season and microbial activity on mobilization processes. For one set of batches ("H2"), the soil used was the same as for Batch Experiment I ("fresh spring soil"), but this time the soil had been stored under anoxic and dark conditions at 8 °C for 11 weeks ("stored spring soil"). This long storage increased the crystallinity of the Fe(III) (oxyhydr)oxides and thus should have made them less easily accessible for microorganisms (see Section 3.2). Experimental conditions and sampling were the same as in Batch Experiment I, except that no samples for dissolved CO₂ and CH₄ analysis were taken and that the experiment was finished after 41 d. For the other set of batches ("H3"), fresh soil and water samples were collected from the Czech site in August 2015, 4 d before starting the experiment ("fresh summer soil"). Due to the relatively hot summer and the high organic carbon content (especially fine root material that was hardly removable), the microbial activity was expected to be high compared to the other batches. Experimental setup and sampling were equal to H2. However, due to the extremely low soil moisture, this part of the experiment lasted only 28 d, since a big part of the added water was absorbed immediately by soil and less supernatant water for liquid sampling remained.

2.3. Quantification of microbial activity

We determined most probable numbers (MPN) for three samples of the stored spring soil from Batch Experiment II (one initial, one treatment, and one control sample) to quantify the amount of cultivatable heterotrophic aerobic, Fe(III)-reducing, and sulfate-reducing microorganisms. A detailed description of MPN methods and results can be found in the Supplementary data, Section S.1.

We also tried to quantify the microbial influence on the observed processes by conducting additional batch experiments with sterilized soil. Unfortunately, both sterilization methods used (addition of formaldehyde and steam sterilization) induced massive changes in soil properties and already led to abiotic mobilization reactions, which made direct comparison with non-sterilized batches impossible. A detailed method description and results from sterile experiments can be found in Supplementary data, Section S.2.

Thus, we conducted an additional incubation experiment aiming at delivering a proof of principle for the correlation between microbial activity and Fe release in the soils used for this study. In

this additional incubation experiment, microbial activity was quantified by CO₂ production, a method that could not be used directly in the batch experiments which required specifically CO₂ addition. Both spring and summer soil were incubated with filtered river water in 50 mL septum vials at the same ratio as in the batch experiments but at a smaller scale (10 g soil + 15 mL water) and purged with N₂ for 1 h to generate anoxic conditions. Afterwards, the bottles were incubated in the dark at 12 °C (thermoelectric cool box), 21 °C (room temperature), and 35 °C (water bath) for 7 d. As in the batch experiments, the bottles were shaken daily. At the end of the incubation period, 4 mL were removed from the liquid phase with needle and syringe in an anoxic glovebox, 2 mL were stabilized in N₂-purged septum vials and stored overnight at 8 °C for analysis of dissolved CO₂, the remaining 2 mL were filtered (0.2 µm cellulose-acetate filter, CHROMAFIL® Xtra), and 1 mL was stabilized with 10 µL 8 M HNO₃ for total Fe analysis by ICP-MS.

2.4. Laboratory analysis

Total concentrations of Fe, Mn, As, and Cu were measured with a quadrupole ICP-MS (X-Series2, Thermo Scientific). Samples from the liquid phase were diluted with 0.16 M HNO₃, aqua regia digests from soil samples were diluted to a 1:10 dilution deionized water:aqua regia. Dilution factors were 1:10 for Mn, As, and Cu analysis, and between 1:10 and 1:10,000 for Fe analysis. Copper was measured in standard mode, As was measured in O₂ mode as AsO⁺, Fe and Mn were measured in KED mode (kinetic energy discrimination, –2 V for Mn, –3 V for Fe, with a mixture of 93% He and 7% H₂ as collision gas) to avoid polyatomic interferences. Rhodium was added as internal standard and internal drift correction was conducted by measuring a mid-range standard every 10 to 25 samples. We used TMDA-54.4 (National Water Research Institute, Environment Canada) as external reference material for quality control. A blank correction was conducted for the aqua regia digests. Calculated limits of detection (LOD) were 2.2 ± 4.4 µg L⁻¹ for Fe, 0.03 ± 0.06 µg L⁻¹ for Mn, 0.2 ± 0.1 µg L⁻¹ for As, and 0.16 ± 0.12 µg L⁻¹ for Cu.

Diluted CO₂ and CH₄ concentrations were calculated from head space concentrations in the septum vials using Henry's law. Gaseous head space concentrations were measured with a gas chromatograph (SRI Instruments 8610C, U.S.) equipped with a methanizer and a flame ionization detector.

Since a monitoring of nitrate and dissolved organic carbon (DOC) concentrations over the course of the experiment was not possible due to limited sample amount, these parameters were only determined for the initial river water as well as for the liquid phase directly after mixing with spring and summer soil in order to determine the amount of nitrate and DOC released from soil. Analysis of DOC was conducted by thermo-catalytic oxidation with a TOC-V_{CPN} Analyzer (Shimadzu) in undiluted, filtered (0.45 µm, nylon, CHROMAFIL® Xtra) samples, which had been stored at 8 °C for 5 days. Nitrate was determined with a Spectroquant® quick test (Nitrate Test Photometric, Merck) and a photometer (DR 2800, Hach-Lange), in undiluted, filtered (0.45 µm, nylon, CHROMAFIL® Xtra) samples, which had been stored frozen until analysis.

Three freeze-dried soil samples were investigated using Mössbauer spectroscopy including fresh spring soil, stored spring soil, and fresh summer soil, each before incubation. Within an anoxic glovebox (100% N₂), samples were prepared for Mössbauer spectroscopy by loading as dry, ground powders into Plexiglas holders (area 1 cm²). Samples were then transported to the Mössbauer instrument within airtight bottles which were only opened immediately prior to loading into a closed-cycle exchange gas cryostat (Janis cryogenics) to minimize exposure to air. Spectra were collected at 77 K and 5 K using a constant acceleration drive

system (WissEL) in transmission mode with a ⁵⁷Co/Rh source. All spectra were calibrated against a 7 µm thick α-⁵⁷Fe foil that was measured at room temperature. Analysis was carried out using Recoil (University of Ottawa) and the Voigt Based Fitting (VBF) routine (Rancourt and Ping, 1991). The half width at half maximum (HWHM) was constrained to 0.131 mm/s during fitting. The same soil samples were used for determination of oxalate- and dithionite-citrate-extractable pedogenic Fe(III) (oxyhydr)oxides, following the methods according to Schwertmann (1964) and Mehra and Jackson (1960), respectively. Total Fe and Aluminium (Al) concentrations in extracts were determined by ICP-MS in –2 V KED mode as described above. Two freeze-dried and ground samples from the initial spring and summer soil were analyzed in triplicate on total carbon and nitrogen content with a CHN elemental analyzer (Thermo Quest, Flash EA, 1112).

2.5. Calculations and statistics

In the differently treated batches (with/without CO₂, different temperatures) the loss of liquid due to evaporation varied strongly and measured dissolved concentrations had to be corrected according to the respective fluid loss. Evaporation was assumed to be constant over the course of the experiment, so the amount of liquid, remaining in the batches at a certain time step, could be calculated from weight difference before and after the experiment with a linear function, deducting fluid loss due to sampling.

Since data were not normally distributed, the Mann-Whitney-U-test was used to test for significance in differences between treatments, Kruskal-Wallis-test was used to test for significant trends over time, and Spearman's rank correlation was used to calculate correlation coefficients (*r_s*) and their significance level (*P*-value) between parameters (*α* = 0.05). All statistical analyses were done with R (R Development Core Team, 2008).

3. Results

3.1. Initial soil and water conditions

The physicochemical properties of the river water indicated that it could be used quite well as an analogue for an uncontaminated aquifer (Table 1). A comparison with the pore water of the reference site analyzed in Mehlhorn et al. (2014) showed that redox potential and Cu concentration were almost exactly the same (+390 mV and 3.3 µg Cu L⁻¹ for 30 cm depth in natural pore water) and Fe, Mn, and As concentrations were even considerably lower (2366 µg Fe L⁻¹, 179 µg Mn L⁻¹ and 22 µg As L⁻¹ in natural pore water). Only the pH of 8.6 in the river water was clearly higher compared to natural pore water (pH of 5.0 in pore water). This, however, did not affect the experiment, since pH in the batch reactors was mainly determined by soil pH (see Section 3.3). The properties of the water sampled in spring and in summer differed slightly. While redox potential and Fe concentration were slightly increased in summer, pH, Mn, and As concentrations were decreased.

Total element contents and pH of the soil used for batch experiments (Table 1) were similar to the soil samples from the reference site sampled and analyzed in 2013 (Mehlhorn et al., 2014). Differences between the soil sampled in spring and the one sampled in summer were already optically visible. The organic matter content, especially pronounced in fine root content, was clearly increased in the summer soil (total C content of 45 mg g⁻¹ compared to 20 mg g⁻¹ in spring soil) due to the course of vegetation period. Additionally, the soil was more porous and less moist. It is noteworthy that the total soil contents of Fe and As were lower by 39% and 45%, respectively, in summer soil compared to spring soil. The reduced Fe(III) (oxyhydr)oxide content was already

Table 1
Initial pH, redox potential, total element concentrations, C, N, DOC and nitrate (NO₃⁻) content in soils and/or river water. Soil pH was measured in 0.01 M CaCl₂ solution.

| | pH | E _h [mV] | Fe [μg L ⁻¹] | Mn [μg L ⁻¹] | As [μg L ⁻¹] | Cu [μg L ⁻¹] | DOC [mg L ⁻¹] | C | NO ₃ ⁻ [mg L ⁻¹] | N |
|---------------|-----|------------------------|-----------------------------|-----------------------------|-----------------------------|-----------------------------|------------------------------|-----------------------|---|-----------------------|
| river, spring | 8.6 | 380 | 167 | 91.8 | 4.2 | 3.3 | 3.4 | | 14.6 ± 0.3 | |
| river, summer | 7.5 | 420 | 260 | 49.6 | 3.5 | 3.7 | NA | | NA | |
| | | | [mg g ⁻¹] | [μg g ⁻¹] | [μg g ⁻¹] | [μg g ⁻¹] | | [mg g ⁻¹] | | [mg g ⁻¹] |
| soil, spring | 4.1 | | 31.1 | 115 | 66.4 | 12.9 | | 20 | | 2 |
| soil, summer | 3.9 | | 18.8 | 119 | 36.2 | 13.7 | | 45 | | 3 |

optically visible with less orange colored areas in summer compared to spring soil. Both oxalate- (Fe_o) and dithionite-citrate-extractable Fe (Fe_d) were significantly reduced in summer soil (Table 2) and an Fe_o/Fe_d ratio of 1.1 ± 0.2 compared to 0.7 ± 0.1 in fresh and 0.6 ± 0.0 in stored spring soil already indicated the absence of well-crystalline Fe phases. This difference seemed to be too high to be explained by soil heterogeneity alone. We therefore attributed these content decreases to a natural mobilization process due to higher microbial activity in summer soil, triggering reductive mineral dissolution processes. The content of oxalate-extractable Al ranged from 1.4 mg g⁻¹ in fresh spring soil to 2.0 mg g⁻¹ in fresh summer soil.

3.2. Iron phases identified by Mössbauer spectroscopy

3.2.1. Fresh spring soil

The spectrum collected at 77 K indicated that there was more than one Fe phase in the sample (Fig. 1a). The fitting parameters of the two sextets (denoted S1 and S2 in Supplementary data, Table S2) closely agreed to the values expected of goethite (Murad, 2010). The hyperfine field (B_{hf}), however, was different for each sextet which potentially suggests that there were two distinct types of goethite present with different particle sizes, i.e. the site with B_{hf} = 46 T was likely to have a smaller particle size than the site with B_{hf} = 49 T. Combined, these two crystalline sextets contributed to 24% of the total spectral area at 77 K. The three doublets which were also required for accurate fitting of the data had hyperfine parameters which corresponded to Fe(II) and Fe(III) phases. The doublet denoted D3 in Supplementary data, Table S2 was within an intermediate region which could not accurately be defined as either Fe(II) or Fe(III). The calculated amount of Fe(II) in the system was thus between 19 and 26%.

As the temperature was lowered to 5 K, the total area of the crystalline Fe component (sextet) increased as the sample underwent magnetic ordering. Again two sextets were used to fit this region, however, now the quadrupole splitting (ΔE_Q) was different between the two suggesting that we could no longer ascribe both sextets to goethite. A potential explanation is that as the temperature decreased, the hyperfine field of S1 increased and at 5 K could no longer be distinguished from S2. Now, only one sextet corresponded to goethite which was a combination of S1 and S2 from the 77 K spectrum. The new sextet, denoted S3 (Supplementary data, Table S2) accounts for 49% of the total spectral area, corresponds to

Table 2
Oxalate-extractable Fe (Fe_o) and Al (Al_o), dithionite-citrate-extractable Fe (Fe_d) and ratio Fe_o/Fe_d for the 3 different start soils given as mean ± standard deviation (triplicates).

| | Fe _o [mg g ⁻¹] | Fe _d [mg g ⁻¹] | Fe _o /Fe _d | Al _o [mg g ⁻¹] |
|---------------------|---------------------------------------|---------------------------------------|----------------------------------|---------------------------------------|
| Spring soil, fresh | 10.8 ± 0.5 | 16.6 ± 2.0 | 0.7 ± 0.1 | 1.4 ± 0.0 |
| Spring soil, stored | 14.2 ± 0.6 | 22.3 ± 1.3 | 0.6 ± 0.0 | 1.5 ± 0.1 |
| Summer soil, fresh | 7.6 ± 1.4 | 6.7 ± 0.3 | 1.1 ± 0.2 | 2.0 ± 0.0 |

a mineral phase which was not magnetically ordered at 77 K and is perhaps more likely to correspond to a short range ordered mineral such as ferrihydrite (Murad, 2010). Three doublets were still required to fit the data at 5 K which suggests they were either too small to undergo magnetic ordering, or more likely corresponded to sulfide minerals or perhaps phyllosilicates.

3.2.2. Stored spring soil

As expected, the main components for the stored spring soil were almost identical to fresh spring soil (Fig. 1b). There were some small differences in the relative abundances of the sextets, specifically an increase in the crystalline components such as goethite. This indicates that the samples underwent some crystallization during the 11 week storage period. If we combine the relative abundances for S1+S2 and S3 for both fresh and stored spring soils at 5 K, we see the total spectral areas were in fact identical. However, the stored spring soil showed a higher proportion of goethite, likely due to crystallization during storage.

3.2.3. Fresh summer soil

The Mössbauer spectra for the fresh summer soil showed some clear differences compared to both fresh and stored spring soil (Fig. 1c). This was especially true at 77 K where no sextets could be detected. This suggests there was little to no goethite present when the soil was collected during the summer. The three doublets used during the fitting of this spectrum shared very similar characteristics to the three doublets observed in fresh and stored spring soil indicating that all three samples shared the same parent material.

Two crystalline sextets were required during the fitting of the fresh summer soil at 5 K (S2 and S3). An additional poorly defined sextet (S1) was also required indicating that part of the sample was still not fully magnetically ordered at this temperature. Such behavior is indicative of small particle size, substitution of additional elements into the mineral (Chadwick et al., 1986; Murad and Cashion, 2004), or a strong association to organic matter (Chen et al., 2015). Based on the hyperfine parameters it was difficult to accurately determine the mineral phases corresponding to these sextets. It is possible that these sextets were also present for fresh and stored spring soils however, due to the presence of more dominant phases such as ferrihydrite and goethite, they could not be clearly distinguished. It should also be noted that it was not possible to determine the mineral identities of several of the Fe phases present in the samples and in some cases these unknown phases accounted for more than 50% of the relative spectral area of the Mössbauer spectra (Supplementary data, Table S2). Nevertheless, it appears that based on the 77 K and 5 K data major Fe components in the soils were short range ordered minerals (e.g. ferrihydrite or goethite).

3.3. Batch Experiment I: variation of temperature

While the dissolved CO₂ concentration in the control batches increased only slightly (to 0.6 ± 0.1 mmol L⁻¹ for C,

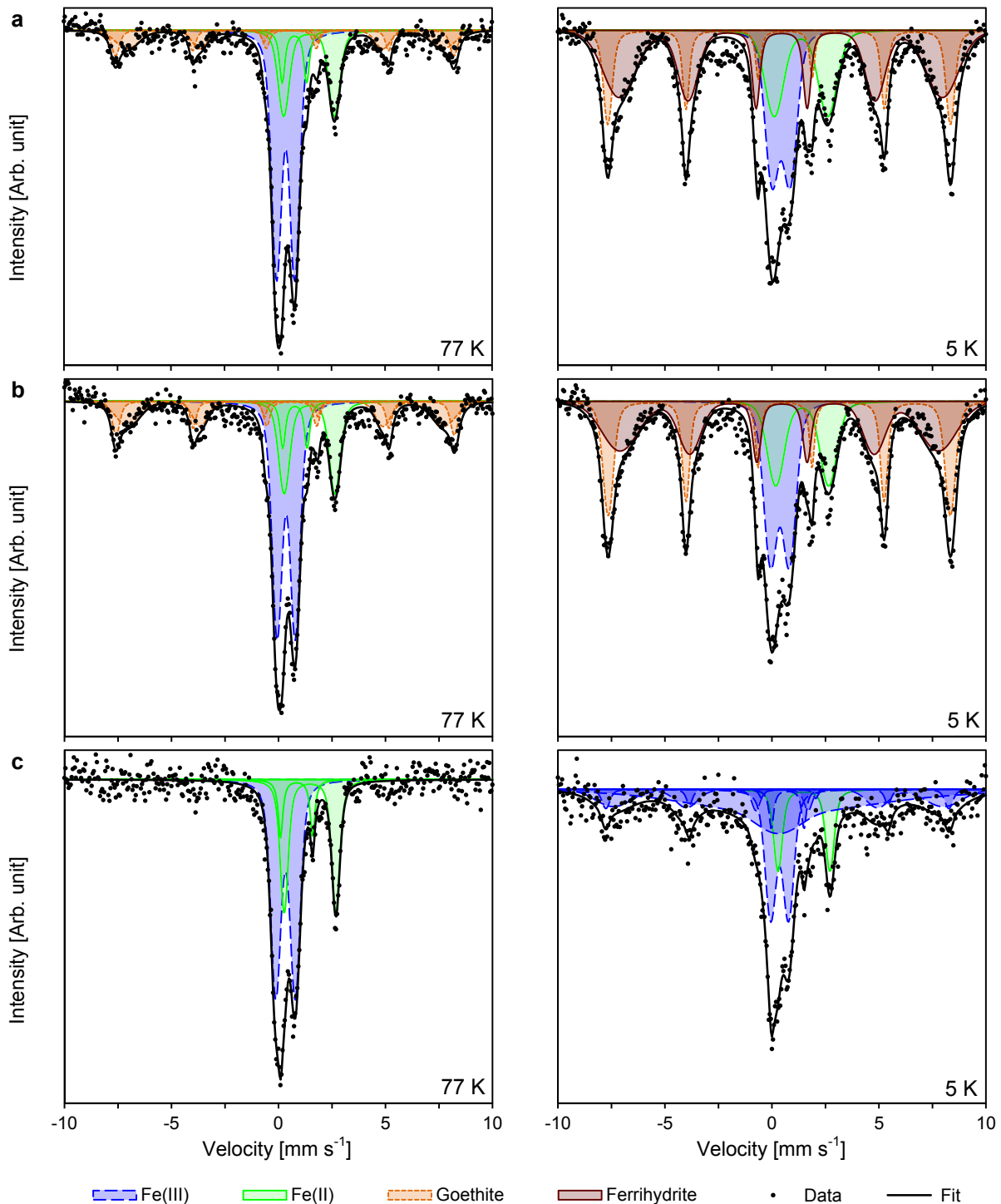


Fig. 1. Mössbauer spectra of fresh spring soil (a), stored spring soil (b), and fresh summer soil (c) each measured at 77 K (left) and 5 K (right).

$0.8 \pm 0.0 \text{ mmol L}^{-1}$ for RT, and $0.4 \pm 0.3 \text{ mmol L}^{-1}$ for H) compared to the initial river water (0.1 mmol L^{-1}), the batches with CO_2 treatment showed a strong increase (Supplementary data, Fig. S3). For the blank batches which only contained river water the dissolved CO_2 concentration increased in the order heated (H) < room temperature (RT) < cooled (C) ($17 < 23 < 29 \text{ mmol L}^{-1}$), as expected from the temperature dependency of the Henry's law constant, that predicts higher CO_2 solubility in colder water. For the batches with soil and CO_2 treatment, the cooled samples (C) showed again the

highest dissolved CO_2 concentration ($25 \pm 0.5 \text{ mmol L}^{-1}$), but batches RT and H were relatively similar (12 ± 1 , and $14 \pm 6 \text{ mmol L}^{-1}$, respectively), taking into account the high standard deviation for batches H. As expected, methane was not detected in any of the samples, since methanogenesis is thermodynamically very unlikely as long as high Fe(III) (oxyhydr)oxide concentrations are present.

The soil pH showed only a slight decrease during the course of the experiment, from initially 4.1 to 3.9 ± 0.1 . Since no difference

between different temperature treatments or between control and treatment could be observed, the decrease is probably caused by the mixing of soil and river water following desorption and dissolution reactions. The pH of the liquid phase showed a strong initial decrease both in batches with and without CO₂ treatment from 8.6 in river water to values between 4.4 and 5.2 within the first 1 h (Fig. 2a) that was caused by mixing with the already acidic soil. After this initial decrease, both controls and treatments remained at relatively constant pH for batches RT (controls: 4.9 ± 0.1 , treatments: 4.8 ± 0.1) and C (control: 5.0 ± 0.2 , treatments: 4.7 ± 0.1), but heated batches (H) showed a significant decrease ($P = 0.007$) in controls (from 5.0 ± 0.1 at 1 h to 4.3 ± 0.1 at 42 d) and increase ($P = 0.018$) in treatments (from 4.5 ± 0.1 at 1 d to 4.8 ± 0.1 at 42 d) over the course of the experiment. Comparison between different temperature treatments showed that pH in batches H was significantly lower than in batches RT ($P = 0.0003$) and C ($P = 0.011$), which contradicted the assumption, that higher CO₂ dissolution in batches C would cause a lower pH due to carbonic acid formation. Further processes like redox reactions seemed to buffer pH and prevent a further pH decrease.

After addition of river water to the soil, redox potential in the batches increased strongly within 1 h, both in controls (from +380 mV to +500 ± 10 mV in RT, +560 ± 10 mV in C, and +620 ± 0 mV in H) and treatments (to +560 ± 0 mV in RT, +570 ± 0 mV in C, and +610 ± 10 mV in H), probably caused by oxidizing soil constituents (Fig. 2b). During the course of the experiment, the controls stayed relatively constant at +570 ± 40 mV for RT, +590 ± 30 mV for C, and +570 ± 40 mV for H, while treatments showed a significant decrease, most pronounced for batches H (to +370 ± 10 mV, $P = 0.0037$), followed by RT (to +420 ± 10 mV, $P = 0.0062$) and C (to +480 ± 20 mV, $P = 0.016$), leading the soil towards more anoxic conditions. The decrease in redox potential hinted towards redox reactions that released reduced species into the pore water, thereby consumed protons and thus buffered pH, e.g., nitrate reduction and reductive dissolution of Fe(III) (oxyhydr)oxides. The order in redox potential decrease with H>RT>C might already be a hint towards stronger microbial activity at higher temperatures.

Mixing of river water with soil led to an initial concentration increase of nitrate (from 14.6 ± 0.3 to 32.8 ± 0.2 mg L⁻¹), DOC (from 3.4 to 4.0 mg L⁻¹), and all considered elements in the liquid phase within 1 h for both controls and treatments (except Fe treatments, data for As 1 h to 3 d (H) or 7 d (RT, C) are missing due to measurement problems) due to mixing with pore water and fast desorption of weakly bound ions (Fig. 2c–f). Calculated concentration increase factors X (Table 3) show that an increase in liquid phase concentration (end of experiment vs. river water blank) over the whole time of the experiment occurred for all elements both in controls and treatments, except for Fe controls and for As controls and treatments at batches RT and C. Observations for each individual element are described in detail as follows.

The highest increases in liquid phase concentrations were observed for Fe in CO₂ treatments (Table 3, Fig. 2c). After an initial “lag phase” of 1–3 d, in which concentrations changed only slightly, the concentration in the treatments increased almost linear from initially 0.2 mg Fe L⁻¹ to 3.2 ± 1.4 mg L⁻¹ in batches C (19 ± 9 fold increase), to 5.0 ± 1.6 mg L⁻¹ in RT (30 ± 9 fold increase), and 18.4 ± 4.0 mg L⁻¹ in H (111 ± 24 fold increase), while the controls showed no significant change of Fe over time and stayed relatively constant at 0.2 ± 0.1 mg L⁻¹ for C, 0.1 ± 0.1 mg L⁻¹ for RT, and 0.2 ± 0.1 mg L⁻¹ for H.

The mobilization behavior of Mn differed completely from that of Fe (Fig. 2d). Following the mixing of water and soil, all batches showed an increase in dissolved Mn concentration, slightly lower in controls (from 92 μg L⁻¹ in initial river water to 166 ± 15 μg L⁻¹ in C,

149 ± 12 μg L⁻¹ in RT, and 139 ± 6 μg L⁻¹ in H) compared to treatments (to 213 ± 6 μg L⁻¹ in C, 228 ± 6 μg L⁻¹ in RT, and 185 ± 2 μg L⁻¹ in H after 1 h). After this initial mobilization, the controls showed only a slight further increase of Mn in liquid phase concentration to 203 ± 12 μg L⁻¹ in batches C, 211 ± 15 μg L⁻¹ in RT, and 204 ± 20 μg L⁻¹ in H after 42 d. For the treatments, the strong Mn mobilization continued until 1 d with highest initial Mn mobilization for batches C (to 277 ± 12 μg L⁻¹), followed by RT (to 262 ± 14 μg L⁻¹), followed by H (to 218 ± 4 μg L⁻¹). For the rest of the experiment, the concentration of Mn in C treatments stayed relatively constant at 292 ± 28 μg L⁻¹, while RT treatments even showed a slight Mn re-immobilization to a final concentration only slightly above the respective controls (229 ± 27 μg L⁻¹). Only Mn in the H treatments continuously increased to 262 ± 40 μg L⁻¹ at d 42, but with a very low rate of 1.6 ± 1.3 μg kg_{soil}⁻¹ d⁻¹ and no significance ($P = 0.0868$).

Dissolved As concentration decreased in all control batches (from 4.2 μg L⁻¹ in initial river water to 2.5 ± 0.1 μg L⁻¹ in C, 2.6 ± 0.1 μg L⁻¹ in RT, and 2.5 ± 0.1 μg L⁻¹ in H) and also in the treatments for batches C (to 2.6 ± 0.7 μg L⁻¹) and RT (to 2.2 ± 0.4 μg L⁻¹) after 42 d (Fig. 2e). However, since a slight As concentration decrease at d 28 (to 3.8 ± 0.2 μg L⁻¹) and d 42 (3.4 ± 0.2 μg L⁻¹) was also observed in the water blanks (Supplementary data, Table S3), part of this As immobilization might be attributed to sensitivity changes during analysis (analysis of d 28 and d 42 samples in a separate run). Only the As concentrations in the heated batches with CO₂ exposure differed significantly from the related control ($P = 0.0007$) by showing a 1.5 ± 0.3 fold increase in As concentration up to 28 d (to 6.8 ± 1.6 μg L⁻¹) that was, however, not deemed as significant due to high standard variations ($P = 0.074$).

Copper is the only element where almost no differences between controls and treatments and between different temperature treatments could be detected (Fig. 2f). After an initial, immediate (1 h) Cu mobilization in both controls (from 3.3 μg L⁻¹ in initial river water to 11.1 ± 1.8 μg L⁻¹ in C, 7.9 ± 4.6 μg L⁻¹ in RT, and 6.5 ± 1.3 μg L⁻¹ in H) and treatments (to 5.9 ± 0.6 μg L⁻¹ in C, 5.7 ± 0.6 μg L⁻¹ in RT, and 6.6 ± 0.7 μg L⁻¹ in H), dissolved Cu concentrations in the different batches stayed relatively constant at values around 5.0–9.0 μg L⁻¹. Only the H treatment differed ($P = 0.0369$) from the respective control and showed a significant ($P = 0.0096$) change in Cu over time, with a continuous increase up to 10.9 ± 1.6 μg L⁻¹ until d 14 and a following decrease to 7.4 ± 1.0 μg L⁻¹ after 42 d.

Total solid phase contents did not show any change during the course of the experiment that was significantly higher than the natural variation in the soil (Supplementary data, Tables S4 and S5) which is probably due to the high pool of the considered elements in the soil compared to the small amounts mobilized into liquid phase.

3.4. Batch Experiment II: variation of start soil conditions

Both the batches with stored spring soil (H2) and the ones with fresh summer soil (H3) showed remarkable differences to the batches with fresh spring soil from Batch Experiment I (for better distinction hereafter referred to as H1) despite the similar temperature treatment (incubation at 35 °C).

As in Batch Experiment I, mixing of the filtered river water with soil caused a strong decrease in liquid phase pH for both controls and treatments (from 8.6 to values between 4.4 and 5.1 after 1 h–7 d, Fig. 3a). This initial pH decrease was followed by a slow increase in the treatments, with the fastest increase in the fresh summer soil H3 (to 4.8 ± 0.1 after 21 d, $P = 0.015$), followed by the fresh spring soil H1 (to 4.8 ± 0.1 after 42 d, $P = 0.018$) and slowest for the stored

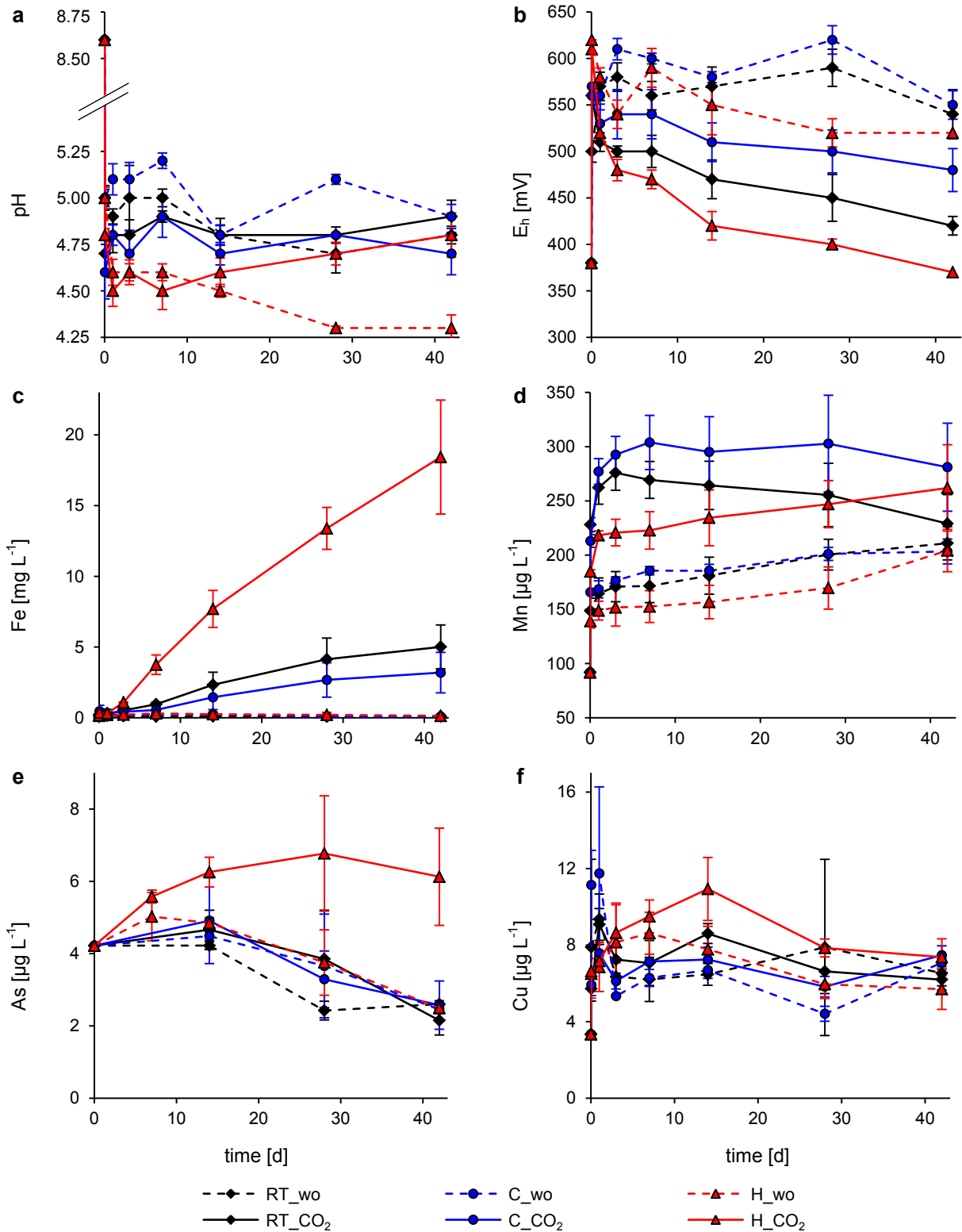


Fig. 2. Changes in liquid phase pH (a), redox potential (b), and total dissolved concentration (evaporation corrected) of Fe (c), Mn (d), As (e), and Cu (f) during Batch Experiment I with (solid line) and without (abbreviation “wo”, dashed line) CO₂ at room temperature (RT, 22 °C, black squares), cooled (C, 16 °C, blue circles), and heated (H, 35 °C, red triangles) in liquid phase. Data for As for 1 h - 3 d (H) or 7 d (RT, C) are missing due to measurement problems. Single outliers from triplicates had to be removed for the following data points, resulting in duplicates: H_wo_1h for Fe, RT_wo_d28 and H_CO₂_d3 for Cu. (For interpretation of the references to colour in this figure legend, the reader is referred to the web version of this article.)

spring soil H2 (to 4.6 ± 0.1 after 41 d, $P = 0.008$). A further increase was also observed for H3 controls (to 4.7 ± 0.1 after 21 d, $P = 0.009$),

while pH in H2 controls stayed relatively constant (at 4.6 ± 0.1 from 7 to 41 d) and H1 controls showed a significant decrease (to

Table 3

Factor X of concentration increase in liquid phase compared to day 0 and average daily mobilization rate r_{avg} for Batch Experiment I (3 different temperatures: cooled (C), room temperature (RT), and heated (H)) given as *mean ± standard deviation* (triplicates).

| Element | Treatment | X-fold initial concentration [-] | | r_{avg} [$\mu\text{g kg}_{soil}^{-1} \text{d}^{-1}$] | |
|---------|-----------|----------------------------------|-----------------|--|-----------------|
| | | wo | CO ₂ | wo | CO ₂ |
| Fe | C | 0.5 ± 0.3 | 19 ± 9 | -2.9 ± 1.7 | 108 ± 51 |
| | RT | 0.6 ± 0.5 | 30 ± 9 | -2.2 ± 2.8 | 173 ± 56 |
| | H | 0.8 ± 0.5 | 111 ± 24 | -1.2 ± 2.8 | 652 ± 144 |
| Mn | C | 2.2 ± 0.1 | 3.1 ± 0.4 | 4.0 ± 0.4 | 6.8 ± 1.4 |
| | RT | 2.3 ± 0.2 | 2.5 ± 0.3 | 4.3 ± 0.5 | 4.9 ± 1.0 |
| | H | 2.2 ± 0.2 | 2.9 ± 0.4 | 4.0 ± 0.7 | 6.1 ± 1.4 |
| As | C | 0.58 ± 0.03 | 0.61 ± 0.16 | -0.06 ± 0.00 | -0.06 ± 0.02 |
| | RT | 0.62 ± 0.02 | 0.51 ± 0.10 | -0.06 ± 0.00 | -0.07 ± 0.01 |
| | H | 0.59 ± 0.03 | 1.45 ± 0.32 | -0.06 ± 0.00 | 0.07 ± 0.05 |
| Cu | C | 2.1 ± 0.1 | 2.2 ± 0.1 | 0.13 ± 0.01 | 0.15 ± 0.02 |
| | RT | 2.0 ± 0.2 | 1.9 ± 0.2 | 0.11 ± 0.02 | 0.10 ± 0.02 |
| | H | 1.7 ± 0.3 | 2.2 ± 0.3 | 0.08 ± 0.04 | 0.14 ± 0.03 |

4.3 ± 0.1 at 42 d, $P = 0.007$). However, pH differences between controls and treatments were not significant. Again, a strong increase of redox potential after mixing of soil and river water within 1 h was observed (from +380 mV in H1 and H2 and +420 mV in H3 to +620 ± 10 mV in H1, +550 ± 10 mV in H2, and +540 ± 10 mV in H3, Fig. 3b). The initial increase was followed by a decrease in CO₂ treatments, that was strongest for the organic-rich batches H3 (to +340 ± 20 mV after 21 d, $P = 0.0058$), followed by the fresh spring soil H1 (to +370 ± 10 mV after 42 d, $P = 0.0037$) followed by the stored soil H2 (to +410 ± 20 mV after 41 d, $P = 0.0052$). The controls remained at significantly higher redox potentials over the course of the experiment (between +460 and +600 mV, $P < 0.0005$). The concentration increases of nitrate (from 14.6 ± 0.3 to 49.5 ± 0.3 mg L⁻¹) and DOC (from 3.4 to 6.1 mg L⁻¹) following mixing of soil and river water were also clearly higher for the organic rich summer soil compared to spring soil (increase to 32.8 ± 0.2 mg L⁻¹ for nitrate and to 4.0 mg L⁻¹ for DOC).

Same as for Batch Experiment I, an initial liquid phase concentration increase within 1 h was also observed in this experiment for most of the considered elements (Fig. 3c–f). Exceptions were As and Fe, that showed a slight initial decrease in the batches with summer soil (H3). Calculated concentration increase factors (X , Table 4) indicated that over the full experiment time (end of experiment vs. river water blank) liquid phase concentrations of all elements increased, with Fe and As controls being the only exceptions.

Again, the highest increase rates were observed for Fe in CO₂ treatments, with an average daily mobilization rate (r_{avg} , Table 4) of 0.3 ± 0.2 mg kg_{soil}⁻¹ d⁻¹ for treatments with stored spring soil (H2), 0.7 ± 0.1 mg kg_{soil}⁻¹ d⁻¹ for treatments with fresh spring soil (H1), and 1.9 ± 0.6 mg kg_{soil}⁻¹ d⁻¹ for treatments with fresh summer soil (H3), while controls stayed relatively constant at 0.28 ± 0.32 mg L⁻¹ for batches H1, 0.32 ± 0.42 mg L⁻¹ for H2, and 0.24 ± 0.13 mg L⁻¹ for H3 (Fig. 3c). However, clear Fe mobilization only began after an initial lag phase of 3 d for batches H1 and H2 and 1 d for batches H3. Final dissolved Fe concentrations in the treatments were 7.95 ± 5.67 mg L⁻¹ after 41 d in batches H2, 18.43 ± 4.03 mg L⁻¹ after 42 d in H1, and 26.33 ± 7.80 mg L⁻¹ after 21 d in H3.

The Mn mobilization pattern was similar to Batch Experiment I with a shift in mobilization rate within the first 24 h (Fig. 3d). Following mixing of soil and river water, a fast increase in dissolved Mn concentration occurred, again slightly higher in treatments (from 92 μg L⁻¹ to 218 ± 4 μg L⁻¹ for H1, to 206 ± 6 μg L⁻¹ for H2, and from 50 μg L⁻¹ to 185 ± 9 μg L⁻¹ for H3) compared to controls

(to 149 ± 9 μg L⁻¹ for H1, to 153 ± 4 μg L⁻¹ for H2, and to 131 ± 3 μg L⁻¹ for H3). But while in the experiment with fresh spring soil (H1) the average liquid phase concentration of Mn in the treatments further increased over the remaining experiment time, even at a very low rate (to 262 ± 40 μg L⁻¹ after 42 d), the treatments of H2 and H3 showed a slight re-immobilization of Mn (final concentrations of 159 ± 28 μg L⁻¹ after 41 d in H2 and 164 ± 10 μg L⁻¹ after 21 d in H3). The Mn concentration of the controls stayed relatively constant for the rest of the experiment at 160 ± 24 μg L⁻¹ in batches H1, 157 ± 20 μg L⁻¹ in H2, and 134 ± 19 μg L⁻¹ in H3. Only the controls of H1 and H2 showed a Mn concentration increase at the last sampling day (to 204 ± 20 μg L⁻¹ in H1 and 193 ± 16 μg L⁻¹ in H2), leading even to a higher final dissolved Mn concentration in controls compared to treatments for H2.

Arsenic had shown a 1.5 ± 0.3 fold concentration increase in the liquid phase of the treatments with fresh spring soil (H1), however, after storage of the soil for 11 weeks (H2) the repetition of the batch experiment led to no As mobilization at all (liquid phase As concentration of 3.55 ± 0.90 μg L⁻¹ over the whole experiment, Fig. 3e). The same effect was observed for the controls of H1 and H2 which even showed a slight immobilization (from 4.2 μg L⁻¹ to 2.5 ± 0.1 μg L⁻¹ after 42 d for H1 and to 2.0 ± 0.03 μg L⁻¹ after 41 d for H2). The extreme As mobilization in treatments with fresh summer soil (H3) was particularly remarkable. Liquid phase As concentration increased significantly from 3.5 μg L⁻¹ to 55.9 ± 24.7 μg L⁻¹ after 21 d ($P = 0.0088$), despite the high variation between the triplicates. The mobilization seemed to occur within the first 7 d, while As concentration stayed relatively constant afterwards. However, this impression is biased by one of the triplicate samples, that showed an extremely high As mobilization to up to 97.6 μg L⁻¹ on day 7, followed by a further decrease to 81.3 μg L⁻¹ on day 21 (compare Supplementary data, Fig. S4). The other 2 treatment batches showed a continuous increase over the course of the experiment. Like Fe mobilization in treatments of H3, liquid phase concentration increase of As only started after >1 d and As and Fe concentrations correlated significantly ($r_S = 0.95$, $P = 0$).

Copper was again the element with the smallest differences between controls and treatments (Fig. 3f). An initial Cu mobilization within 1 h occurred in both controls and treatments, following the mixing of filtered river water and soil, that was highest for batches H3 (from 3.7 μg L⁻¹ to 9.0 ± 0.6 μg L⁻¹, compared to a Cu increase from 3.4 μg L⁻¹ to 6.6 ± 0.5 μg L⁻¹ in H1 and to 6.5 ± 1.6 μg L⁻¹ in H2). Batches with stored spring soil (H2) showed a Cu mobilization over the course of the experiment for both controls and treatments. However, the relatively high Cu concentrations on days 28 and 41 are probably caused by analysis problems, since the water blank sample without soil showed the same increase (Supplementary data, Table S3). Differences between H2 controls and treatments were not significant. The batches with fresh summer soil showed a completely different behavior than batches H1 and H2 with significant differences between controls and treatments ($P = 0.0304$): while the controls stayed relatively constant at 9.4 ± 2.2 μg L⁻¹ after initial mobilization, the treatments showed an increase to 10.9 ± 0.1 μg L⁻¹ at day 1, followed by a further decrease to 6.2 ± 1.1 μg L⁻¹ at day 21. An immobilization process for Cu seemed to have occurred in CO₂ treatments.

4. Discussion

4.1. Soil processes following exposure to CO₂

When a CO₂ outgassing builds up in a redoximorphic Fluvisol, due to the formation of a mofette or leakage from a GCS site, CO₂ will dissolve in the pore water and form carbonic acid. According to

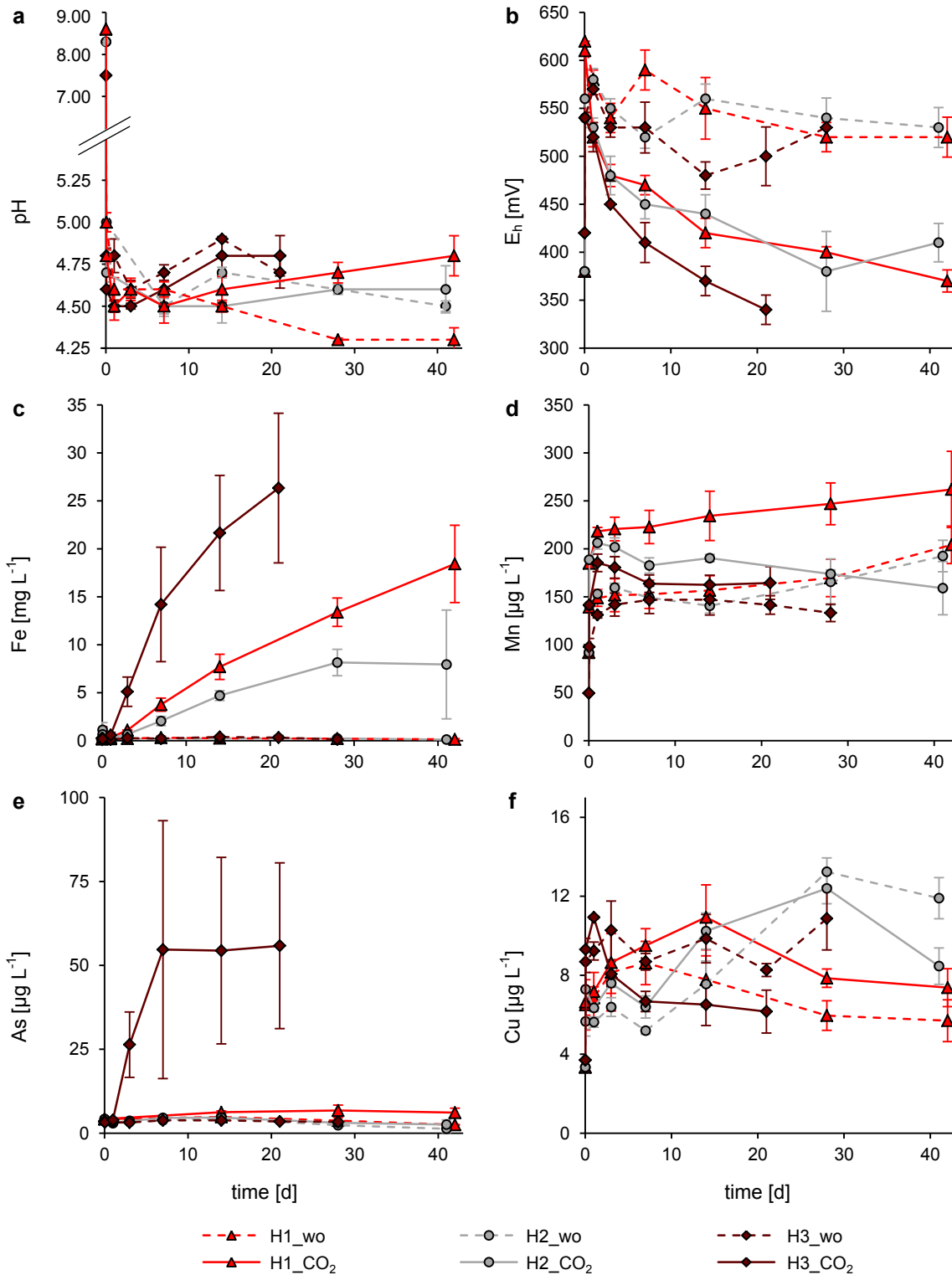


Fig. 3. Changes in liquid phase pH (a), redox potential (b), and total dissolved concentration (evaporation corrected) of Fe (c), Mn (d), As (e), and Cu (f) during Batch Experiment II with (solid line) and without (abbreviation “wo”, dashed line) CO₂ at 35 °C with 3 different start soil conditions (H1: fresh spring soil from Batch Experiment I, red triangles, H2: stored spring soil, grey circles, H3: fresh summer soil, dark red squares) in liquid phase. Note the change in scaling after y-axis break in (a); pH data for H2 are missing on 1 d and 3 d due to electrode calibration problems. Data for As 1 h – 3 d are missing for H1 due to measurement problems. Single outliers from triplicates had to be removed for the following data points, resulting in duplicates: H3_wo_d7 for Fe, Mn, and Cu, H2_wo_d41 and H3_wo_d3 for As, H1_CO₂_d3 for Cu. (For interpretation of the references to colour in this figure legend, the reader is referred to the web version of this article.)

Henry's Law, more CO₂ will dissolve in colder water, as could be verified in Batch Experiment I with different temperature

treatments. However, the dissolution of CO₂ did not cause a significant pH decrease in our experiments as has been observed in

Table 4

Factor X of concentration increase in liquid phase compared to day 0 and average daily mobilization rate r_{avg} for Batch Experiment II (3 different “start” soil conditions, ordered according to mobilization rates: stored spring soil (H2), fresh spring soil (H1), and fresh summer soil (H3)) given as *mean ± standard deviation* (triplicates).

| Element | Soil | X-fold initial concentration [–] | | r_{avg} [$\mu\text{g kg}_{\text{soil}}^{-1} \text{d}^{-1}$] | |
|---------|------|----------------------------------|-----------------|---|-----------------|
| | | wo | CO ₂ | wo | CO ₂ |
| Fe | H2 | 0.7 ± 0.3 | 48 ± 34 | –1.9 ± 1.7 | 285 ± 207 |
| | H1 | 0.8 ± 0.5 | 111 ± 24 | –1.2 ± 2.8 | 652 ± 144 |
| | H3 | 0.5 ± 0.0 | 101 ± 30 | –7.2 ± 0.4 | 1862 ± 557 |
| Mn | H2 | 2.1 ± 0.2 | 1.7 ± 0.3 | 3.7 ± 0.6 | 2.5 ± 1.0 |
| | H1 | 2.2 ± 0.2 | 2.9 ± 0.4 | 4.0 ± 0.7 | 6.1 ± 1.4 |
| | H3 | 2.7 ± 0.2 | 3.3 ± 0.3 | 4.5 ± 0.5 | 8.2 ± 1.2 |
| As | H2 | 0.31 ± 0.26 | 0.61 ± 0.33 | –0.08 ± 0.01 | –0.06 ± 0.05 |
| | H1 | 0.59 ± 0.03 | 1.45 ± 0.32 | –0.06 ± 0.00 | 0.07 ± 0.05 |
| | H3 | 0.96 ± 0.00 | 15.9 ± 7.0 | –0.01 ± 0.00 | 3.74 ± 1.76 |
| Cu | H2 | 3.6 ± 0.3 | 2.5 ± 0.3 | 0.31 ± 0.04 | 0.19 ± 0.03 |
| | H1 | 1.7 ± 0.3 | 2.2 ± 0.3 | 0.08 ± 0.04 | 0.14 ± 0.03 |
| | H3 | 2.9 ± 0.4 | 1.7 ± 0.3 | 0.38 ± 0.09 | 0.18 ± 0.08 |

numerous other batch studies (e.g. Kirsch et al., 2014; Lawter et al., 2015, 2016; Little and Jackson, 2010; Lu et al., 2010; Shao et al., 2015; Smyth et al., 2009). One reason for this is the already acidic Fluvisol used in this study. Mixing of river water and soil alone decreased the liquid phase pH to 4.5–5.0 in both controls and treatments. These pH values are in accordance with the pore water pH at the natural mofette site (Beulig et al., 2015; Mehlhorn et al., 2014). Since only slight changes in liquid phase pH occurred over the course of the experiment, despite the continuous supply of CO₂ in treatments and therefore a supply of protons, processes that buffer pH must have taken place. At a soil pH of 4.1 or 3.9, the buffer systems of silicates and cation exchange should be depleted and Aluminum and Fe(III) (oxyhydr)oxides are defined as the most important buffer systems at pH < 4.2 (Blume et al., 2016). Oxalate extraction indicated the presence of Al (hydr)oxides (1.4–2.0 mg g^{–1}) which might have contributed to buffer reactions. However, a screening of total dissolved Al concentration for 1 h vs. end-of-experiment samples revealed that no significant Al mobilization occurred in our experiments (data not shown), thus, Al (hydr)oxides were not dissolved. The initial fast drop in pH could have been caused by the rapid mobilization of dissolved organic matter (DOM) from soil by mixing with river water, indicated by increased DOC concentrations (increased by 19% after mixing with spring soil and by 81% after mixing with summer soil), initiating microbial processes, as observed in Porsch et al. (2014). Interestingly, the lowest liquid phase pH occurred in the heated batches H which contradicts the assumption of a lower CO₂ dissolution at higher temperatures. Since the heated, non-CO₂-treated control setups showed an even further pH decrease over the course of the experiment, the low pH might be caused by additional CO₂ release into the liquid phase from microbial respiration processes or production of fatty acids from microbial fermentation processes which should be highest in heated batches where temperature is within optimum range of many mesophilic bacteria. Unfortunately, no direct proof of fatty acid production was possible during this study due to limited sampling amount, but the presence of fermenting bacteria at the soil sampling site was recently demonstrated by Beulig et al. (2016). The pH increase in H treatments following the initial decrease might be caused by microbially enhanced proton consuming reactions like the reductive dissolution of Fe(III) (oxyhydr)oxides (Lions et al., 2014).

Relatively high redox potentials of +500 to +620 mV were measured in both controls and CO₂-treatments right after mixing of soil and river water. They were caused by the initially relatively

high oxygen content. The redox potential decrease during the course of the experiment, which could be observed in the CO₂ treatments, was most likely caused by microbial consumption of oxidizing compounds. The anoxic conditions caused by CO₂ purging forced heterotrophic microbes to use electron acceptors with less and less energy yield. While in the first 3 d, there was probably still oxygen available for aerobic respiration and the decrease in redox potential was relatively fast, the much slower decrease following day 3 indicates that heterotrophic microorganisms had switched to another respiration process. This process was most probably microbial Fe(III) reduction to Fe(II) coupled to Fe(III) (oxyhydr)oxide dissolution which is evidenced by the highly significant negative correlation between redox potential and dissolved total Fe concentration calculated with data from all experiments ($r_S = -0.74$, $P < 10^{-10}$). Additionally, fermentation has to be taken into account as possible microbial process under anoxic conditions that might both influence the pH by production of fatty acids and could also contribute indirectly to the reductive dissolution of Fe(III) (oxyhydr)oxide via electron shuttling (Benz et al., 1998; Kappler et al., 2004). The lowest final redox potentials were achieved in heated treatments with +370 ± 10 mV for batches H1 and +340 ± 20 mV for H3. However, these values were still higher than the redox potential measured in natural pore water of mofettes (+270 ± 50 mV and +310 ± 10 mV), but similar to those measured in pore water from references (+360 ± 40 mV and +390 ± 20 mV) (Mehlhorn et al., 2014). An influence of oxygen on the measured redox potential could not completely be ruled out, since the measurement had to be conducted under atmospheric conditions. However, the observed decrease in redox potential and the similarity between lab and field values indicated that artefact effects are probably negligible.

4.2. Mobility of Fe, Mn, As, and Cu following CO₂ exposure

Looking at the mobility of the metal(loid)s considered in this study, experiments with different temperature treatments allowed a clear distinction between two mobilization processes: at first the abiotic desorption of metal cations due to increasingly positively charged surfaces or competition with DOM released after mixing of soil and water phase and later the release of elements due to microbially-triggered dissolution of Fe(III) (oxyhydr)oxides and co-release of incorporated elements (Borch et al., 2009). The process of mobilization via desorption was relatively fast with main mobilization occurring within the first 3 d. Cooled treatments showed the highest mobilization rates, since more CO₂ was dissolved compared to warmer batches. The second, microbially-triggered mobilization process did not start until day 3 when all remaining oxygen was depleted and the microbes had to switch to the less favorable electron acceptor Fe(III). The generally higher mobilization rates for heated and organic-rich treatments provide evidence for a microbial nature of this process. Observations for the individual elements will be discussed in detail in the following section.

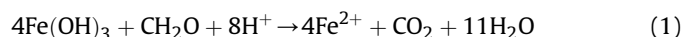
4.2.1. Iron

The results of our study suggest that the dissolution of Fe(III) (oxyhydr)oxides is the most pronounced mobilization process that occurs in an Fe-rich Fluvisol after a CO₂ outgassing event. The dominating Fe phases in the soils used for this study were identified to be goethite and ferrihydrite as well as some non-crystalline Fe(II) and Fe(III) phases (Section 3.2). Since we observed significantly increased Fe mobilization rates at higher incubation temperatures ($C < RT < H$) and an increased mobilization in the organic-rich summer soil (H2 < H1 < H3), we attributed this release to the microbially-triggered process of Fe(III) (oxyhydr)oxide reduction (Melton et al., 2014). The presence of Fe(III)-reducing bacteria was

proven by determination of most probable numbers (MPN) and revealed that $4.7 \cdot 10^4$ to $1.0 \cdot 10^6$ MPN mL⁻¹ of Fe(III)-reducing microorganisms were present in the spring soil (compare Supplementary data, Section S.1). However, no significant change in MPNs of heterotrophic aerobic, Fe(III)-, and sulfate-reducing bacteria could be detected in spring soil after incubation without/with CO₂ indicating that the relatively short experiment time of 6 weeks did not alter the microbial soil community, but only the activity of certain microbes, or that the changes were within the error of the MPN method. All attempts to quantify the microbial share on mobilization processes by comparison with data from sterilized batches were not successful: both sterilization with formaldehyde and via steam sterilization led to strongly increased mobilization rates for all considered elements (Supplementary data, Section S.2). Alteration of soil properties due to different sterilization methods is a well-known problem (Trevors, 1996 and references therein), especially in organic-rich soils (Berns et al., 2008). We thus concluded that sterilization of the natural soil used in this study was not suitable, since soil properties were influenced gravely and no comparability to the unaltered soil was given.

However, to further validate the activity of Fe(III)-reducing bacteria as main factor for Fe mobilization, we conducted an anoxic, 1 week-lasting post-study in which we quantified microbial activity by CO₂ production and correlated it with total Fe concentrations in the liquid phase, incubation temperature, and start soil (see Section 2.3 for detailed method description and Supplementary data, Section S.8 for detailed results). For both soils used (spring and summer soil), we found significant correlations between temperature treatment and CO₂ production (for both soils: $r_S = 0.96$, $P = 0.0028$) as well as between CO₂ production and Fe mobilization (spring soil: $r_S = 0.94$, $P = 0.0048$; summer soil: $r_S = 0.83$, $P = 0.0416$). The higher microbial activity in the organic-rich summer soil could also be verified with this experiment: CO₂ production in the summer soil was 2.4 ± 0.5 times higher compared to the spring soil and Fe mobilization was up to 9.7 ± 0.7 times higher (35 °C) leaving no doubt about the role of Fe(III)-reducing microbes on Fe mobilization. An additional factor for increased mobilization in summer soil was probably also the absence of crystalline Fe phases in summer soil and therefore a higher share of poorly-crystalline minerals (see Sections 3.1 and 3.2) that are more easily accessible for microbes (Cornell and Schwertmann, 2003; Porsch et al., 2014). The significantly decreased Fe mobilization in batches with stored spring soil (H2) can vice versa be explained by increased crystallinity of the Fe(III) (oxyhydr)oxides present in soil, as shown for goethite by Mössbauer spectroscopy and by increased Fe_d content.

This study provides evidence that a microbially-triggered, reductive dissolution of Fe(III) (oxyhydr)oxides can occur in CO₂ influenced soils, even if the redox potential is above the generally assumed threshold of +150 mV at neutral conditions (Blume et al., 2016). The reason for this is that the energy yield of microbial Fe(III) reduction increases with decreasing pH, since protons are consumed (Eq. (1)).



While the standard redox potential of Fe(II)/Fe(III) at pH 7 is -112 mV for a 1 mM Fe(II) solution, it is increased to +330 mV at pH 4.5 (Stumm et al., 1996). Kirk et al. (2013) observed that the activity of Fe(III)-reducing microorganisms surpassed that of sulfate-reducers at CO₂ partial pressures of 1 atm. They contributed this to increased proton concentrations (accompanied by a lowered pH) due to the dissociation of the carbonic acid formed and thus, a thermodynamic advantage of Fe(III)-reducers over sulfate-reducers. MPNs showed that sulfate-reducing bacteria were also

present in the soil used in this study (Supplementary data, Table S1). However, their activity must have been low, since most of the sulfur (S) mobilization in the treatments occurred within the first day and in the order C>RT>H (Supplementary data, Fig. S5). Thus, S mobilization was most likely caused by desorption reactions. Only the treatments of H1 (fresh spring soil) and H3 (fresh summer soil) showed a 2.2 ± 0.4 fold and 1.6 ± 0.1 fold concentration increase, respectively. However, since these were also the treatments with the highest Fe mobilization, the correlating S mobilization (H1: $r_S = 0.97$, $P = 0$; H3: $r_S = 0.93$, $P = 1.38 \cdot 10^{-9}$) might also be contributed to a co-release from Fe(III) (oxyhydr)oxide dissolution and not to direct microbial sulfate reduction.

4.2.2. Manganese

A sequential extraction procedure conducted with natural mofette and reference soil in 2013 detected most of the Mn in the non-specifically adsorbed fraction or bound to Fe(III) (oxyhydr)oxides, while Mn oxides were not detected (Mehlhorn et al., 2014). This is in good agreement with the mobilization processes we observed for Mn in the CO₂ treatments. Two different processes could be clearly distinguished: within the first 24 h, a fast and strong Mn mobilization occurred with initial mobilization rates r_{initial} increasing in the order H<RT<C (Table 5). This mobilization was caused by desorption of weakly bound Mn due to the increasing competition with protons, that was higher at lower temperatures, where more CO₂ could dissolve. The same pattern could be observed in the controls that were not treated with CO₂, but to a significantly lower extent. However, total differences between different temperature treatments were small, thus, an effect of soil heterogeneity cannot completely be ruled out. A further hint towards an abiotic desorption process was that in Batch Experiment II the heated batches showed quite similar initial mobilization rates (Table 5), despite the different start soil conditions. Similar patterns of Mn mobilization were also observed in other batch or field scale CO₂ studies (Lawter et al., 2016; Little and Jackson, 2010; Lu et al., 2010; Shao et al., 2015) and mainly attributed to co-release from calcite or dolomite dissolution. This process is unlikely in our study since these minerals are not stable under the acidic soil conditions and abiotic desorption must have been the dominating Mn mobilization process. The fast desorption stopped after at maximum 3 days when all weakly bound Mn was desorbed. Afterwards, the dissolved Mn concentration stayed relatively constant, or even decreased slightly (compare final mobilization rates r_{final} in Table 5; shift from r_{initial} to r_{final} is designated as “transition day”). One reason for the slight resorption of Mn could be the proton consumption by microbially-triggered Fe(III) (oxyhydr)oxide dissolution, decreasing competition for sorption sites. H1 treatments were the only batches, which showed a positive r_{final} of $1.6 \pm 1.3 \mu\text{g kg}_{\text{soil}}^{-1} \text{d}^{-1}$, however, with a very high standard variation. The Mn concentrations following day 3 correlated with Fe ($r_S = 0.71$, $P = 0.003$), which is a hint towards a Mn co-release from Fe(III) (oxyhydr)oxide dissolution that surpassed Mn resorption. Overall, the Mn mobilization in the CO₂ treatments was negligible when compared with the controls.

4.2.3. Arsenic

Sequential extraction in Mehlhorn et al. (2014) revealed that in reference soils from the Czech sampling site the biggest portion of As was adsorbed to or incorporated in poorly crystalline Fe(III) (oxyhydr)oxides. The reductive dissolution of Fe(III) (oxyhydr)oxides that we observed in the CO₂ treatments of the batch experiments should thus have led to an according As co-release. However, such an As co-release could only be observed in the heated treatments H1 and H3. In H1 treatments, an As mobilization up to 14 d could be observed ($r_{\text{initial}} = 0.22 \pm 0.04 \mu\text{g kg}_{\text{soil}}^{-1} \text{d}^{-1}$, Table 5), that

Table 5
Initial ($r_{initial}$) compared to final daily mobilization rates (r_{final}) for Batch Experiment I (3 different temperatures: cooled (C), room temperature (RT), heated (H)) and Batch Experiment II (3 different start soil conditions, ordered according to mobilization rates: stored spring soil (H2), fresh spring soil (H1), and fresh summer soil (H3)) given as *mean* \pm *standard deviation* (triplicates) for elements with a sharp shift in mobilization rate (Mn and As). The “transition day” between initial and final rate was determined optically from changes in element concentration in liquid phase over time.

| Element | Treatment | Transition day | $r_{initial}$ [$\mu\text{g kg}_{\text{soil}}^{-1} \text{d}^{-1}$] | | r_{final} [$\mu\text{g kg}_{\text{soil}}^{-1} \text{d}^{-1}$] | |
|---------|-----------|----------------|---|------------------|---|------------------|
| | | | wo | CO ₂ | wo | CO ₂ |
| Mn | C | 1 | 115 \pm 12 | 278 \pm 18 | 1.3 \pm 0.6 | 0.1 \pm 1.1 |
| | RT | 1 | 109 \pm 22 | 256 \pm 23 | 1.7 \pm 0.4 | -1.2 \pm 0.4 |
| | H | 1 | 86 \pm 13 | 190 \pm 6 | 2.0 \pm 0.4 | 1.6 \pm 1.3 |
| As | C | 14 | 0.03 \pm 0.01 | 0.07 \pm 0.13 | -0.11 \pm 0.01 | -0.13 \pm 0.03 |
| | RT | 14 | 0.00 \pm 0.01 | 0.05 \pm 0.06 | -0.09 \pm 0.01 | -0.13 \pm 0.02 |
| | H | 14 | 0.07 \pm 0.02 | 0.22 \pm 0.04 | -0.13 \pm 0.01 | -0.01 \pm 0.05 |
| Mn | H2 | 1 | 92 \pm 5 | 172 \pm 10 | 1.5 \pm 0.5 | -1.8 \pm 1.1 |
| | H1 | 1 | 86 \pm 13 | 190 \pm 6 | 2.0 \pm 0.4 | 1.6 \pm 1.3 |
| | H3 | 1 | 122 \pm 5 | 204 \pm 14 | 0.1 \pm 0.6 | -1.6 \pm 0.8 |
| As | H2 | 7 | -0.08 \pm 0.01 | 0.07 \pm 0.17 | -0.08 \pm 0.01 | -0.09 \pm 0.03 |
| | H1 | 14 | 0.07 \pm 0.02 | 0.22 \pm 0.04 | -0.13 \pm 0.01 | -0.01 \pm 0.05 |
| | H3 | 7 | 0.06 \pm 0.04 | 10.97 \pm 8.23 | -0.03 \pm 0.01 | 0.12 \pm 1.62 |

correlated significantly with Fe mobilization ($r_s = 0.78$, $P = 2.5 \cdot 10^{-7}$). In the fresh summer soil of H3 treatments, the As mobilization occurred mainly within the first 7 days and was significantly higher than in H1 ($r_{initial} = 11 \pm 8 \mu\text{g kg}_{\text{soil}}^{-1} \text{d}^{-1}$). Here, too, As and Fe concentrations correlated significantly ($r_s = 0.95$, $P = 0$), but while in batches H1 a 111 \pm 24 fold Fe concentration increase caused a 1.5 \pm 0.3 fold As concentration increase, it was 101 \pm 30 fold for Fe vs. 16 \pm 7 fold for As in batches H3. This almost 10 times higher As mobilization in H3 despite a similar total Fe mobilization could either be caused by a different As content of the Fe(III) (oxyhydr)oxides in the start soil or by a differing resorption behavior. We would rate differences in As content of Fe(III) (oxyhydr)oxides as unlikely since both total As and total Fe concentration in the summer soil were decreased in the same order of magnitude, by 45 and 39%, respectively, compared to the spring soil (Table 1). This indicates that abiotic resorption of released As to positively charged soil surfaces must have been higher in spring compared to summer soil. Arsenic speciation measurements in pore water from the mofette site in Mehlhorn et al. (2014) revealed that most of the dissolved As is present as arsenite followed by arsenate. In the study presented here, As speciation analyses were not successful due to low total As concentrations. However, we assume arsenite and arsenate to be the dominant dissolved As species, since methylation or thioarsenates seem unlikely because no CH₄ formation and no significant S mobilization were observed. At the pH values observed in this study, arsenate should be present as negatively charged H₂AsO₄⁻ and arsenite as uncharged H₃AsO₃ (Cullen and Reimer, 1989). Most soil constituents, especially Fe(III) (oxyhydr)oxides, have a net-positive surface charge at the pH values measured in this study (e.g. points of zero charge (pH_{PZC}) are around 7.8–7.9 for ferrihydrite and 7.5–9.5 for goethite (Cornell and Schwertmann, 2003)), thus, the negatively charged arsenate has a high tendency to adsorb to these positively charged surfaces. Also, arsenite is known to have a high affinity to Fe(III) (oxyhydr)oxides, even at relatively low pH (Dixit and Hering, 2003; Goldberg and Johnston, 2001; Raven et al., 1998). Therefore, resorption to remaining Fe(III) (oxyhydr)oxide surfaces is the most likely re-immobilization process for As in the conducted batch experiments. Total Fe(III) (oxyhydr)oxide content in the spring soil was significantly higher than in the summer soil, thus, more resorption sites were available for released As, which could be one factor for the observed discrepancy in As mobilization. Another reason for a decreased resorption in the fresh summer soil of H3 could be the increased organic content. Dissolved organic matter and As can be

competitors for soil sorption sites (e.g. Bauer and Blodau, 2006; Redman et al., 2002). It is thus very likely that less As was re-immobilized in H3 since DOM covered most of the positively charged surfaces and less free sorption sites were available, resulting in a higher As net-mobilization. Additionally, As might have formed colloids or dissolved complexes with DOM and Fe (Bauer and Blodau, 2009; Ritter et al., 2006; Sharma et al., 2010, 2011), increasing its mobility in the organic rich summer soil. Competition between As and phosphate or between As and carbonate should have been of minor importance since no significant phosphorous mobilization was observed (data not shown) and carbonate was shown to be a weak competitor towards As under increased $p(\text{CO}_2)$ by Brechbühl et al. (2012).

In the RT and C batches, no net As-mobilization was observed. Arsenic resorption surpassed the significantly lower release from Fe(III) (oxyhydr)oxide dissolution. The stored spring soil H2 also did not show any As mobilization in the CO₂ treatments. The significantly decreased dissolution of Fe(III) (oxyhydr)oxides must have released less As compared to the fresh spring soil, that could all immediately resorb to other surfaces, resulting in no net-mobilization.

4.2.4. Copper

The main reason for focusing our study on the element Cu was that it seemed to be less mobile in natural mofettes compared to the respective reference sites as shown in Mehlhorn et al. (2014). Within that study, sequential extraction of natural reference soil showed, that Cu was mainly adsorbed to solid-phase organic matter or bound to poorly crystalline Fe(III) (oxyhydr)oxides. A smaller portion was also characterized as non-specifically adsorbed. In batch experiments of this study, mixing of soil and river water caused an immediate Cu mobilization in both CO₂ treatments and controls, which can be contributed to the release of weakly bound Cu. However, no order in mobilization rate according to temperature could be observed as it was for Mn, although the mobilization mechanism (competition with protons) should be similar for these cations. Copper is well known to form dissolved complexes with DOM (Blume et al., 2016), thus, the mixing of liquid and solid phase at the beginning of the experiment mobilized DOM and thereby might have also mobilized Cu through formation of dissolved Cu-DOM complexes. Unfortunately, we could not proof the existence of such complexes due to limited sample amount. At the moment, we also cannot exclude mobilization of particulate metallic Cu associated with microorganisms, as observed by Hofacker et al. (2015). Following this initial mobilization, Cu

concentrations in both controls and treatments stayed relatively constant, indicating that almost no Cu was incorporated into Fe(III) (oxyhydr)oxides or, alternatively, that Cu that was released by Fe(III) (oxyhydr)oxide dissolution could resorb immediately to other soil constituents. All these observations gave no hint on the net-immobilization of Cu that was observed in natural soil in Mehlhorn et al. (2014), but the fresh summer soil showed some interesting differences to all other batch experiments: following the initial concentration increase due to mixing of soil and water, the treatments showed a fast concentration decrease between 1 and 7 d followed by a slower decrease until the end of the experiment while the controls stayed relatively constant at the higher concentration level. Since the most obvious difference between fresh summer soil and spring soil is the higher organic matter content, resorption of Cu to solid organic matter could be a likely explanation for this decrease. Numerous studies have demonstrated the high affinity of Cu for organic matter (e.g. Brown et al., 2000; Kumpiene et al., 2007; McLaren and Crawford, 1973), however, the effect of CO₂ on this process has been unattended. The results presented in this study showed that under higher CO₂ partial pressure, Cu re-adsorption, most probably to solid organic matter, increased which supports the theory of a Cu net-immobilization in mofettes due to their higher organic matter content described in Mehlhorn et al. (2014). One possible explanation might be the formation of negatively charged Cu carbonate complexes (Cu(CO₃)₂²⁻) under high CO₂ partial pressures that can adsorb to the positively charged surfaces. However, geochemical modelling (PHREEQC Version 2.18.00) revealed negatively charged dissolved Cu carbonate complexes as minor species under the conditions given (data not shown). The formation of solid Cu carbonate minerals is also unlikely under the given acidic conditions. Another possible explanation already mentioned in Mehlhorn et al. (2014) is that Cu might have profited from the desorption of other cations (e.g. Mn) and attached to sorption sites previously covered by other elements. To completely clarify the process of Cu immobilization under CO₂ influence, further studies are required.

4.3. Implications for natural mofettes

The strong Fe mobilization observed in the CO₂ treatments of this study continued until the end of the experiments and no hint for approaching equilibrium could be seen. Similar to studies on Fe mobilization following a flooding event (e.g. Fiedler and Sommer, 2004; Meek et al., 1968; Ponnampereuma, 1972), the amount of Fe mobilized during the course of the experiment was small compared to the pool of total Fe available in the soil. It can thus be assumed that in case of a continuous CO₂ release into natural soil the Fe mobilization would have continued until Fe(III) (oxyhydr)oxide depletion. Assuming a continuous Fe mobilization with the rates calculated in Tables 3 and 4 and a total Fe(III) (oxyhydr)oxide content of approximately 11 mg g⁻¹ (Table 2), total depletion of Fe(III) (oxyhydr)oxides would have been reached after 280, 170, 46, and 16 years for C, RT, H1, and H3 treatments, respectively. Transferability of the exact rates determined in laboratory studies to the field is of course limited, because the calculation does not take into account any natural variations, like daily or seasonal changes in temperature or water regime. Nevertheless, they deliver a first estimate of minimum temperature-dependent time scales. Fe(III) (oxyhydr)oxides are almost completely absent in the center of the Czech mofette site, which is attributed to oxygen absence: Fe that is released during weathering cannot precipitate as (oxyhydr)oxides (Rennert et al., 2011, 2012). Since the mofettes in this area have formed at least decades or even centuries ago, this explanation is most likely, taking into account a continuous pedogenesis. However, data from our study give evidence that the formation of a new

CO₂ outgassing in a soil already rich in Fe(III) (oxyhydr)oxides can also lead to the microbially-triggered dissolution of Fe(III) (oxyhydr)oxides, despite the relatively high redox potential, which can be explained with the thermodynamic advantage of the proton consuming reduction process (Kirk et al., 2013). Toxic effects of high p(CO₂) on the microbial community were not observed in our study, as shown by constant MPNs. Beulig et al. (2016) also observed the ability of the microbial community from the reference soil to adapt to short-term (14 d) CO₂ exposure. However, CO₂ toxicity will probably be an issue considering long-term CO₂ influence on soils. Over longer time periods, a change in microbial community towards more CO₂ tolerant organisms and, after depletion of Fe(III) (oxyhydr)oxides, towards other functional groups (e.g. methanogens or acetogens, as detected in the center of the mofettes by Beulig et al. (2015)), could be expected.

The results of this study also confirmed the hypothesis from Mehlhorn et al. (2014) that the increased As mobility in natural mofettes is mainly caused by the absence of Fe(III) (oxyhydr)oxides, the most favored binding partner for As in the reference soil. They further provided some evidence for the hypothesis, that a net-immobilization of Cu occurs in the Czech mofettes, most probably due to increased resorption to solid organic matter under high p(CO₂). The results obtained for Mn did not necessarily help to answer the knowledge gaps on the Mn balance at the natural mofette site presented in Mehlhorn et al. (2014). There, both soil and liquid phase concentrations were decreased for Mn which contradicts the slight mobilization observed in this study. One important factor causing this discrepancy might be (reactive) transport of the liquid phase that cannot be taken into account in batch studies.

5. Conclusions

The results from this study increase our understanding regarding the kinetics and temperature dependency of soil processes following CO₂ intrusion into soil as it might occur during a CO₂ leakage from GCS sites or following the formation of a mofette. Within 1 h to 1 d the fast abiotic desorption of weakly bound cations due to competition with protons can be expected to cause a pore water concentration increase of some cationic elements. However, mobilization due to desorption was relatively small in the soil used in this study and resorption reactions could cause a complete re-immobilization over longer time periods. The risk for drinking water quality from a short-term CO₂ influence of <1 d on the considered soil is thus relatively low. Far more concerning are microbially-triggered mobilization processes, such as reductive dissolution of Fe(III) (oxyhydr)oxides in this study, since they tend to mobilize considerably larger amounts of certain elements (in this study especially Fe and As) than abiotic desorption. Higher temperatures as well as increased organic matter concentrations accelerated microbially-triggered Fe(III) (oxyhydr)oxide dissolution in our experiment. It can thus be assumed that biotically triggered mobilization processes will be enhanced in warm seasons and slowed down in cold seasons, while it will be the other way around for abiotic mobilization via desorption. This implies that GCS risk assessment should also take into account climatic factors. Our study also showed that pore water Fe concentrations could be a good additional short-term monitoring tool at sites with high Fe(III) (oxyhydr)oxide contents, where pH is no suitable monitoring parameter due to already low soil pH. However, distinguishing Fe mobilization caused by CO₂ intrusion from natural mobilization caused by changes in water regime in redoximorphic soils is difficult, but crucial for risk assessment, thus, the combined effects of water regime changes and temperature variations with CO₂ gas flow should be subject to further research.

Acknowledgements

We acknowledge financial support for a PhD stipend to Judith Mehlhorn from the German National Academic Foundation. We thank Kirsten Küsel (Aquatic Geomicrobiology, Friedrich Schiller University Jena) and Felix Beulig (Department of Bioscience, Aarhus University) for motivation to work on the mofettes, Stefan Will for help with ICP-MS analyses, Marcus Horn (Ecological Microbiology, University of Bayreuth) for help with MPN and interpretation of microbiological data, Ben Gilfedder and Silke Hammer (Hydrology, University of Bayreuth) for help with GC analysis and Martina Rohr (Hydrology, University of Bayreuth) for DOC analyses and help with nitrate analyses.

Appendix A. Supplementary data

Supplementary data related to this article can be found at <http://dx.doi.org/10.1016/j.apgeochem.2016.09.007>

References

- Bankwitz, P., Schneider, G., Kämpf, H., Bankwitz, E., 2003. Structural characteristics of epicentral areas in Central Europe: study case Cheb Basin (Czech Republic). *J. Geodyn.* 35, 5–32.
- Bauer, M., Blodau, C., 2006. Mobilization of arsenic by dissolved organic matter from iron oxides, soils and sediments. *Sci. Total Environ.* 354, 179–190.
- Bauer, M., Blodau, C., 2009. Arsenic distribution in the dissolved, colloidal and particulate size fraction of experimental solutions rich in dissolved organic matter and ferric iron. *Geochim. Cosmochim. Acta* 73, 529–542.
- Benz, M., Schink, B., Brune, A., 1998. Humic acid reduction by *Propionibacterium freudenreichii* and other fermenting bacteria. *Appl. Environ. Microbiol.* 64, 4507–4512.
- Berns, A., Philipp, H., Narres, H.-D., Burauel, P., Vereecken, H., Tappe, W., 2008. Effect of gamma-sterilization and autoclaving on soil organic matter structure as studied by solid state NMR, UV and fluorescence spectroscopy. *Eur. J. Soil Sci.* 59, 540–550.
- Beulig, F., Heuer, V.B., Akob, D.M., Viehweger, B., Elvert, M., Herrmann, M., Hinrichs, K.-U., Küsel, K., 2015. Carbon flow from volcanic CO₂ into soil microbial communities of a wetland mofette. *ISME J.* 9, 746–759.
- Beulig, F., Urich, T., Nowak, M., Trumbore, S.E., Gleixner, G., Gilfillan, G.D., Fjelland, K.E., Küsel, K., 2016. Altered carbon turnover processes and microbiomes in soils under long-term extremely high CO₂ exposure. *Nat. Microbiol.* 1, 15025.
- Blume, H.-P., Brümmer, G.W., Fleige, H., Horn, R., Kandeler, E., Kögel-Knabner, I., Kretzschmar, R., Stahr, K., Wilke, B.-M., 2016. Scheffer/Schachtschabel: Soil Science. Springer-Verlag, Berlin Heidelberg.
- Blume, H.-P., Felix-Henningsen, P., 2009. Reductosols: natural soils and technosols under reducing conditions without an aquatic moisture regime. *J. Plant Nutr. Soil Sci.* 172, 808–820.
- Borch, T., Kretzschmar, R., Kappler, A., Cappellen, P.V., Ginder-Vogel, M., Voegelin, A., Campbell, K., 2009. Biogeochemical redox processes and their impact on contaminant dynamics. *Environ. Sci. Technol.* 44, 15–23.
- Bräuer, K., Kämpf, H., Niedermann, S., Strauch, G., Weise, S.M., 2004. Evidence for a nitrogen flux directly derived from the European subcontinental mantle in the Western Eger Rift, central Europe. *Geochim. Cosmochim. Acta* 68, 4935–4947.
- Brechbühl, Y., Christl, I., Elzinga, E.J., Kretzschmar, R., 2012. Competitive sorption of carbonate and arsenic to hematite: combined ATR-FTIR and batch experiments. *J. Colloid Interface Sci.* 377, 313–321.
- Brown, P.A., Gill, S.A., Allen, S.J., 2000. Metal removal from wastewater using peat. *Water Res.* 34, 3907–3916.
- Chadwick, J., Jones, D., Thomas, M., Tatlock, G., Devenish, R., 1986. A Mössbauer study of ferrihydrite and aluminium substituted ferrihydrites. *J. Magn. Magn. Mater.* 61, 88–100.
- Chen, C., Kukkadapu, R., Sparks, D.L., 2015. Influence of coprecipitated organic matter on Fe²⁺_(aq)-catalyzed transformation of ferrihydrite: implications for carbon dynamics. *Environ. Sci. Technol.* 49, 10927–10936.
- CHMI, 2015. Czech Hydrometeorological Institute: Monthly Temperature and Precipitation Data for the Karlovy Vary Region retrieved from: <http://portal.chmi.cz>
- Cornell, R.M., Schwertmann, U., 2003. In: *The Iron Oxides: Structure, Properties, Reactions, Occurrences and Uses*, second ed. John Wiley & Sons, Weinheim.
- Cullen, W.R., Reimer, K.J., 1989. Arsenic speciation in the environment. *Chem. Rev.* 89, 713–764.
- Dixit, S., Hering, J.G., 2003. Comparison of arsenic(V) and arsenic(III) sorption onto iron oxide minerals: implications for arsenic mobility. *Environ. Sci. Technol.* 37, 4182–4189.
- Fernández-Montiel, I., Sidrach-Cardona, R., Gabilondo, R., Pedescoll, A., Scheu, S., Bécares, E., 2016. Soil communities are affected by CO₂ belowground emissions at a natural vent in Spain. *Soil Biol. Biochem.* 97, 92–98.
- Fiedler, S., Sommer, M., 2004. Water and redox conditions in wetland soils - their influence on pedogenic oxides and morphology. *Soil Sci. Soc. Am. J.* 68, 326–335.
- Flechsig, C., Bussert, R., Rechner, J., Schütze, C., Kämpf, H., 2008. The Hartoušov mofette field in the Cheb Basin, western Eger Rift (Czech Republic): a comparative geoelectric, sedimentologic and soil gas study of a magmatic diffuse CO₂-degassing structure. *Z. Geol. Wiss.* 36, 177–193.
- Frerichs, J., Oppermann, B.L., Gwosdz, S., Möller, I., Herrmann, M., Krüger, M., 2013. Microbial community changes at a terrestrial volcanic CO₂ vent induced by soil acidification and anaerobic microhabitats within the soil column. *FEMS Microbiol. Ecol.* 84, 60–74.
- Goldberg, S., Johnston, C.T., 2001. Mechanisms of arsenic adsorption on amorphous oxides evaluated using macroscopic measurements, vibrational spectroscopy, and surface complexation modeling. *J. Colloid Interface Sci.* 234, 204–216.
- Harvey, O.R., Qafoku, N.P., Cantrell, K.J., Lee, G., Amonette, J.E., Brown, C.F., 2012. Geochemical implications of gas leakage associated with geologic CO₂ storage - a qualitative review. *Environ. Sci. Technol.* 47, 23–36.
- Harvey, O.R., Qafoku, N.P., Cantrell, K.J., Wilkins, M.J., Brown, C.F., 2016. Methanogenesis-induced pH-Eh shifts drives aqueous metal(loid) mobility in sulfide mineral systems under CO₂ enriched conditions. *Geochim. Cosmochim. Acta* 173, 232–245.
- Hofacker, A.F., Behrens, S., Voegelin, A., Kaegi, R., Lösekann-Behrens, T., Kappler, A., Kretzschmar, R., 2015. *Clostridium* species as metallic copper-forming bacteria in soil under reducing conditions. *Geomicrobiol. J.* 32, 130–139.
- IPCC, 2005. In: Metz, B., Davidson, O., De Coninck, H., Loos, M., Meyer, L. (Eds.), *IPCC Special Report on Carbon Dioxide Capture and Storage*, p. 442. Prepared by Working Group III of the Intergovernmental Panel on Climate Change.
- Jun, Y.-S., Giammar, D.E., Werth, C.J., 2012. Impacts of geochemical reactions on geologic carbon sequestration. *Environ. Sci. Technol.* 47, 3–8.
- Jun, Y.-S., Giammar, D.E., Werth, C.J., Dzombak, D.A., 2013. Environmental and geochemical aspects of geologic carbon sequestration: a special issue. *Environ. Sci. Technol.* 47, 1–2.
- Kämpf, H., Geissler, W.H., Bräuer, K., 2007. Combined gas-geochemical and receiver function studies of the Vogtland/NW Bohemia intraplate mantle degassing field, central Europe. In: Ritter, J.R.R., Christensen, U.R. (Eds.), *Mantle Plumes*. Springer, Berlin Heidelberg, pp. 127–158.
- Kappler, A., Benz, M., Schink, B., Brune, A., 2004. Electron shuttling via humic acids in microbial iron(III) reduction in a freshwater sediment. *FEMS Microbiol. Ecol.* 47, 85–92.
- Kharaka, Y.K., Cole, D.R., Hovorka, S.D., Gunter, W.D., Knauss, K.G., Freifeld, B.M., 2006. Gas-water-rock interactions in Frio Formation following CO₂ injection: implications for the storage of greenhouse gases in sedimentary basins. *Geology* 34, 577–580.
- Kharaka, Y.K., Thordsen, J.J., Kakouros, E., Ambats, G., Herkelrath, W.N., Beers, S.R., Birkholzer, J.T., Apps, J.A., Spycher, N.F., Zheng, L., Trautz, R.C., Rauch, H.W., Gullickson, K.S., 2010. Changes in the chemistry of shallow groundwater related to the 2008 injection of CO₂ at the ZERT field site, Bozeman, Montana. *Environ. Earth Sci.* 60, 273–284.
- Kirk, M.F., Santillan, E.F., Sanford, R.A., Altman, S.J., 2013. CO₂-induced shift in microbial activity affects carbon trapping and water quality in anoxic bioreactors. *Geochim. Cosmochim. Acta* 122, 198–208.
- Kirsch, K., Navarre-Sitchler, A.K., Wunsch, A., McCray, J.E., 2014. Metal release from sandstones under experimentally and numerically simulated CO₂ leakage conditions. *Environ. Sci. Technol.* 48, 1436–1442.
- Kumpiene, J., Lagerkvist, A., Maurice, C., 2007. Stabilization of Pb- and Cu-contaminated soil using coal fly ash and peat. *Environ. Pollut.* 145, 365–373.
- Lawter, A., Qafoku, N., Shao, H., Bacon, D., Brown, C., 2015. Evaluating impacts of CO₂ and CH₄ gas intrusion into an unconsolidated aquifer: fate of As and Cd. *Front. Environ. Sci.* 3, 49.
- Lawter, A., Qafoku, N.P., Wang, G., Shao, H., Brown, C.F., 2016. Evaluating impacts of CO₂ intrusion into an unconsolidated aquifer: I. Experimental data. *Int. J. Greenh. Gas Control* 44, 323–333.
- Lewicki, J.L., Birkholzer, J., Tsang, C.-F., 2007. Natural and industrial analogues for leakage of CO₂ from storage reservoirs: identification of features, events, and processes and lessons learned. *Environ. Geol.* 52, 457–467.
- Lions, J., Devau, N., De Lary, L., Dupraz, S., Parmentier, M., Gombert, P., Dictor, M.-C., 2014. Potential impacts of leakage from CO₂ geological storage on geochemical processes controlling fresh groundwater quality: a review. *Int. J. Greenh. Gas Control* 22, 165–175.
- Little, M.G., Jackson, R.B., 2010. Potential impacts of leakage from deep CO₂ sequestration on overlying freshwater aquifers. *Environ. Sci. Technol.* 44, 9225–9232.
- Lu, J., Partin, J.W., Hovorka, S.D., Wong, C., 2010. Potential risks to freshwater resources as a result of leakage from CO₂ geological storage: a batch-reaction experiment. *Environ. Earth Sci.* 60, 335–348.
- Maček, I., Videmšek, U., Kastelec, D., Stopar, D., Vodnik, D., 2009. Geological CO₂ affects microbial respiration rates in Stavesinci mofette soils. *Acta Biol. Slov.* 52, 41–48.
- McLaren, R.G., Crawford, D.V., 1973. Studies on soil copper II. The specific adsorption of copper by soils. *J. Soil Sci.* 24, 443–452.
- Meek, B.D., MacKenzie, A., Grass, L., 1968. Effects of organic matter, flooding time, and temperature on the dissolution of iron and manganese from soil in situ. *Soil Sci. Soc. Am. J.* 32, 634–638.
- Mehlhorn, J., Beulig, F., Küsel, K., Planer-Friedrich, B., 2014. Carbon dioxide triggered metal(loid) mobilisation in a mofette. *Chem. Geol.* 382, 54–66.

- Mehra, O., Jackson, M., 1960. Iron oxide removal from soils and clays by a dithionite-citrate system buffered with sodium bicarbonate. In: National Conference on Clays and Clays Minerals, pp. 317–327.
- Melton, E.D., Swanner, E.D., Behrens, S., Schmidt, C., Kappler, A., 2014. The interplay of microbially mediated and abiotic reactions in the biogeochemical Fe cycle. *Nat. Rev. Microbiol.* 12, 797–808.
- Mickler, P.J., Yang, C., Scanlon, B.R., Reedy, R., Lu, J., 2013. Potential impacts of CO₂ leakage on groundwater chemistry from laboratory batch experiments and field push-pull tests. *Environ. Sci. Technol.* 47, 10694–10702.
- Murad, E., 2010. Mössbauer spectroscopy of clays, soils and their mineral constituents. *Clay Miner.* 45, 413–430.
- Murad, E., Cashion, J., 2004. Mössbauer Spectroscopy of Environmental Materials and Their Industrial Utilization. Kluwer Academic Publishers, Dordrecht, the Netherlands.
- Nowak, M., Beulig, F., von Fischer, J., Muhr, J., Küsel, K., Trumbore, S.E., 2015. Autotrophic fixation of geogenic CO₂ by microorganisms contributes to soil organic matter formation and alters isotope signatures in a wetland mofette. *Biogeosciences* 12, 7169–7183.
- Oppermann, B.I., Michaelis, W., Blumenberg, M., Frerichs, J., Schulz, H.M., Schippers, A., Beaubien, S.E., Krueger, M., 2010. Soil microbial community changes as a result of long-term exposure to a natural CO₂ vent. *Geochim. Cosmochim. Acta* 74, 2697–2716.
- Pearce, J.M., 2006. What can we learn from natural analogues? In: Lombardi, S., Altunina, L.K., Beaubien, S.E. (Eds.), *Advances in the Geological Storage of Carbon Dioxide*. Springer, Netherlands, pp. 127–139.
- PIK, 2016. Potsdam Institute for Climate Impact Research: Ground Temperature - Mean Annual Variability retrieved from: <https://www.pik-potsdam.de/services/klima-wetter-potsdam/klimazeitreihen/bodentemperatur/>.
- Ponnamperuma, F.N., 1972. The chemistry of submerged soils. *Adv. Agron.* 24, 29–96.
- Porsch, K., Rijal, M.L., Borch, T., Troyer, L.D., Behrens, S., Wehland, F., Appel, E., Kappler, A., 2014. Impact of organic carbon and iron bioavailability on the magnetic susceptibility of soils. *Geochim. Cosmochim. Acta* 128, 44–57.
- R Development Core Team, 2008. R: a Language and Environment for Statistical Computing. R Foundation for Statistical Computing, Vienna, Austria.
- Rancourt, D., Ping, J., 1991. Voigt-based methods for arbitrary-shape static hyperfine parameter distributions in Mössbauer spectroscopy. *Nucl. Instrum. Methods Phys. Res. Sec. B* 58, 85–97.
- Raven, K.P., Jain, A., Loeppert, R.H., 1998. Arsenite and arsenate adsorption on ferrihydrite: kinetics, equilibrium, and adsorption envelopes. *Environ. Sci. Technol.* 32, 344–349.
- Redman, A.D., Macalady, D.L., Ahmann, D., 2002. Natural organic matter affects arsenic speciation and sorption onto hematite. *Environ. Sci. Technol.* 36, 2889–2896.
- Rennert, T., Eusterhues, K., Andrade, V.D., Totsche, K.U., 2012. Iron species in soils on a mofette site studied by Fe K-edge X-ray absorption near-edge spectroscopy. *Chem. Geol.* 332–333, 116–123.
- Rennert, T., Eusterhues, K., Pfanz, H., Totsche, K.U., 2011. Influence of geogenic CO₂ on mineral and organic soil constituents on a mofette site in the NW Czech Republic. *J. Soil Sci.* 62, 572–580.
- Rennert, T., Pfanz, H., 2015. Geogenic CO₂ affects stabilization of soil organic matter. *Eur. J. Soil Sci.* 66, 838–846.
- Ritter, K., Aiken, G.R., Ranville, J.F., Bauer, M., Macalady, D.L., 2006. Evidence for the aquatic binding of arsenate by natural organic matter-suspended Fe(III). *Environ. Sci. Technol.* 40, 5380–5387.
- Schütze, C., Sauer, U., Beyer, K., Lamert, H., Bräuer, K., Strauch, G., Flechsig, C., Kämpf, H., Dietrich, P., 2012. Natural analogues: a potential approach for developing reliable monitoring methods to understand subsurface CO₂ migration processes. *Environ. Earth Sci.* 67, 411–423.
- Schwertmann, U., 1964. Differenzierung der Eisenoxide des Bodens durch Extraktion mit Ammoniumoxalat-Lösung. *Z. Pflanzenernähr. Düngung Bodenkd.* 105, 194–202.
- Shao, H., Qafoku, N.P., Lawter, A.R., Bowden, M.E., Brown, C.F., 2015. Coupled geochemical impacts of leaking CO₂ and contaminants from subsurface storage reservoirs on groundwater quality. *Environ. Sci. Technol.* 49, 8202–8209.
- Sharma, P., Ofner, J., Kappler, A., 2010. Formation of binary and ternary colloids and dissolved complexes of organic matter, Fe and As. *Environ. Sci. Technol.* 44, 4479–4485.
- Sharma, P., Rolle, M., Kocar, B., Fendorf, S., Kappler, A., 2011. Influence of natural organic matter on As transport and retention. *Environ. Sci. Technol.* 45, 546–553.
- Šibanc, N., Dumbrell, A.J., Mandić-Mulec, I., Maček, I., 2014. Impacts of naturally elevated soil CO₂ concentrations on communities of soil archaea and bacteria. *Soil Biol. Biochem.* 68, 348–356.
- Smyth, R.C., Hovorka, S.D., Lu, J., Romanak, K.D., Partin, J.W., Wong, C., Yang, C., 2009. Assessing risk to fresh water resources from long term CO₂ injection – laboratory and field studies. *Energy Procedia* 1, 1957–1964.
- Stumm, W., Morgan, J.J., Drever, J.I., 1996. In: *Aquatic Chemistry: Chemical Equilibria and Rates in Natural Waters*, third ed. John Wiley & Sons, New York.
- Trevors, J., 1996. Sterilization and inhibition of microbial activity in soil. *J. Microbiol. Methods* 26, 53–59.
- Videmšek, U., Hagn, A., Suhadolc, M., Radl, V., Knicker, H., Schloter, M., Vodnik, D., 2009. Abundance and diversity of CO₂-fixing bacteria in grassland soils close to natural carbon dioxide springs. *Microb. Ecol.* 58, 1–9.
- Wang, S., Jaffe, P.R., 2004. Dissolution of a mineral phase in potable aquifers due to CO₂ releases from deep formations; effect of dissolution kinetics. *Energy Convers. Manage.* 45, 2833–2848.
- Zheng, L., Apps, J.A., Spycher, N., Birkholzer, J.T., Kharaka, Y.K., Thordsen, J., Beers, S.R., Herkelrath, W.N., Kakouros, E., Trautz, R.C., 2012. Geochemical modeling of changes in shallow groundwater chemistry observed during the MSU-ZERT CO₂ injection experiment. *Int. J. Greenh. Gas Control* 7, 202–217.
- Zheng, L., Apps, J.A., Zhang, Y., Xu, T., Birkholzer, J.T., 2009. On mobilization of lead and arsenic in groundwater in response to CO₂ leakage from deep geological storage. *Chem. Geol.* 268, 281–297.

Supplementary data

to “Time and temperature dependency of carbon dioxide triggered metal(loid) mobilization in soil”

Judith Mehlhorn¹, James M. Byrne², Andreas Kappler², Britta Planer-Friedrich^{1*}

¹ University of Bayreuth, Environmental Geochemistry, Bayreuth Center for Ecology and Environmental Research (BayCEER), Universitaetsstrasse 30, D-95440 Bayreuth, Germany

² University of Tuebingen, Geomicrobiology, Center for Applied Geosciences, Sigwartstrasse 10, D-72076 Tuebingen, Germany

* Corresponding author: Tel.: +49 921 55 3999; fax: +49 921 55 2334; E-mail address: b.planer-friedrich@uni-bayreuth.de

Content

| | |
|--|----|
| List of Tables..... | 2 |
| List of Figures | 3 |
| S.1 Determination of most probable numbers (MPN) for cultivatable heterotrophic aerobic, Fe(III)-reducing, and sulfate-reducing microorganisms | 4 |
| S.2 Batch experiments with sterile controls | 6 |
| S.3 Results from Mössbauer spectroscopy of three initial soil samples..... | 9 |
| S.4 Total dissolved CO ₂ in Batch Experiment I..... | 10 |
| S.5 Water blanks for Batch Experiment I and II | 11 |
| S.6 Total soil concentrations in Batch Experiment I and II | 12 |
| S.7 Arsenic results for Batch Experiment II with individual graphs..... | 13 |
| S.8 Results from additional incubation experiment | 14 |
| S.9 Sulfur results for Batch Experiment I and II..... | 15 |
| References | 16 |

List of Tables

| | |
|--|----|
| Table S1. Most probable number (MPN) values (95 % confidence interval) for cultivatable heterotrophic aerobes, Fe(III)-reducers, and sulfate-reducers determined for stored spring soil (H2) before and after Batch Experiment II (incubation at 35 °C for 41 d without (H2_wo) and with CO ₂ purging (H2_CO ₂)) and graph (right) with error bars showing 95 % confidence interval for better comparison. | 5 |
| Table S2. Hyperfine parameters of Mössbauer spectra from fresh spring soil, stored spring soil, and fresh summer soil. CS - Center shift, ΔE_Q - Quadrupole splitting, ϵ - quadrupole shift, B_{hf} - hyperfine field, Pop. - relative abundance. | 9 |
| Table S3. pH, redox potential (E_h), and total dissolved concentration (evaporation corrected) of Fe, Mn, As, and Cu for water blanks of all batch experiments (single measurements). Missing data are marked as NA. | 11 |
| Table S4. Total soil concentrations of Fe, Mn, As, and Cu before (“initial”) and after Batch Experiment I with incubation of fresh spring soil without (“wo_CO ₂ ”) and with CO ₂ (“CO ₂ ”) at 3 different temperatures. Initial concentrations were only measured once, thus the relatively high value for initial As might have been caused by soil heterogeneity. | 12 |
| Table S5. Total soil concentrations of Fe, Mn, As, and Cu before (“initial”) and after Batch Experiment II with incubation of stored spring soil (H2) and fresh summer soil (H3) without (“wo_CO ₂ ”) and with CO ₂ (“CO ₂ ”) at 35 °C. Initial concentrations were only measured once, thus the relatively high value for As in initial H2 might have been caused by soil heterogeneity. | 12 |
| Table S6. Total amount of CO ₂ formed and total dissolved Fe concentration after 7 d of incubation of spring and summer soil at 3 different temperatures from an additional incubation experiment for proof of microbial Fe(III) reduction. Values are given as range between two replicates. | 14 |
| Table S7. Correlation coefficients r_s between incubation temperature, total CO ₂ , and dissolved Fe concentration for the additional 7 d incubation experiment. Significance level is indicated by stars with * $P < 0.05$, ** $P < 0.01$ | 14 |
| Table S8. Total dissolved concentration (evaporation corrected) of S for water blanks of all batch experiments (single measurements). | 15 |
| Table S9. Total soil concentrations of S before (“initial”) and after Batch Experiment I with incubation of fresh spring soil without (“wo_CO ₂ ”) and with CO ₂ (“CO ₂ ”) at 3 different temperatures and after Batch Experiment II with incubation of stored spring soil (H2) and fresh summer soil (H3). | 15 |

List of Figures

- Fig. S1. Changes in liquid phase pH (a), redox potential (b), and total dissolved concentration (evaporation corrected) of Fe (c), Mn (d), As (e), and Cu (f) during Batch Experiment II with (solid line) and without (abbreviation “wo”, dashed line) CO₂ for formaldehyde sterilized (S1, non-filled symbols and black lines) and non-sterilized (H2, filled symbols and grey lines) stored spring soil in liquid phase. Data on pH are missing on 1 d and 3 d due to electrode calibration problems. Single outliers from triplicates had to be removed for the following data points, resulting in duplicates: H2_wo_d41 for As and S1_CO₂_d7 for Cu. 7
- Fig. S2. Changes in liquid phase pH (a), redox potential (b), and total dissolved concentration (evaporation corrected) of Fe (c), Mn (d), As (e), and Cu (f) during Batch Experiment II with (solid line) and without (abbreviation “wo”, dashed line) CO₂ for steam-sterilized (S2, non-filled symbols and black lines) and non-sterilized (H2, dark red symbols and lines) fresh summer soil in liquid phase. Single outliers from triplicates had to be removed for the following data points, resulting in duplicates: H3_wo_d3 for As and H3_wo_d7 for Fe, Mn, and Cu. 8
- Fig. S3. Total dissolved CO₂ concentration at the end of Batch Experiment I (fresh spring soil) after 42 d for controls (“wo_CO₂”), water blanks (“blank_CO₂”, water only), and treatments (“CO₂”) at 16 ± 1 °C (C, blue stripes), at 22 ± 1 °C (RT, unfilled), and 35 ± 0.1 °C (H, filled red). 10
- Fig. S4. Changes in total dissolved concentration of As (evaporation corrected) during Batch Experiment II with (solid line) and without (abbreviation “wo”, dashed line) CO₂ at 35 °C with 3 different start soil conditions (H1: fresh spring soil from Batch Experiment I, red triangles, H2: stored spring soil, grey circles, H3: fresh summer soil, dark red squares) in liquid phase with all triplicates displayed individually. Data for As 1 h - 3 d are missing for H1 due to measurement problems. One outlier has been removed in H3_wo_d3. 13
- Fig. S5. Changes in total dissolved concentration (evaporation corrected) of S with (solid line) and without (abbreviation “wo”, dashed line) CO₂ (a) during Batch Experiment I at room temperature (RT, 22 °C, black squares), cooled (C, 16 °C, blue circles), and heated (H, 35 °C, red triangles) and (b) during Batch Experiment II with different start soil conditions (H1: fresh spring soil, red triangles; H2: stored spring soil, grey circles; H3: fresh summer soil, dark red squares) in liquid phase. 15

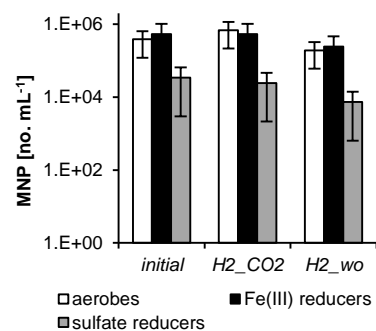
S.1 Determination of most probable numbers (MPN) for cultivatable heterotrophic aerobic, Fe(III)-reducing, and sulfate-reducing microorganisms

In order to quantify the amount of cultivatable aerobic, Fe(III)-reducing, and sulfate-reducing microorganisms we determined most probable numbers (MPN) for 3 samples of the stored spring soil: one initial sample, one treatment (H2_CO2), and one control sample (H2_wo) after Batch Experiment II. All MPNs were prepared under sterile conditions, using anoxic techniques (Drake et al., 1996).

The soil water suspensions of the respective batches were well-mixed and 1 mL each was removed with sterile needle and syringe and injected into a 20 mL glass incubation bottle closed with a butyl rubber stopper, containing 9 mL sterile saline (NaCl, 0.9 %) and anoxic N₂/CO₂ (80 %/20 %) headspace, resulting in a 10⁻¹ dilution. The bottles were left on an orbital shaker for 1 h to guaranty complete mixing and a further anoxic dilution series up to 10⁻⁹ was prepared by transferring 1 mL each to the next higher dilution. The medium used for MPN determination of heterotrophic aerobes consisted of 2.7 g L⁻¹ Tryptic Soy Broth (TSB) and 100 mg L⁻¹ Nystatin; pH was adjusted to 5.3 with HCl and the medium was steam-sterilized in an autoclave (FVS, Integra Biosciences, Germany) at 121 °C before Nystatin addition. Incubation for aerobic MPN was conducted in 96-well plates (Falcon, Becton Dickinson, Meylan Cedex, France) where 10 times 50 µL of each dilution were added to 150 µL TSB medium each. Well plates were incubated for 4 weeks at room temperature (22 ± 1 °C) in the dark. Microbial growth was visible from milky cloudiness of the otherwise clear medium. For MPN of Fe(III)-reducers, a FePPi medium (Caccavo et al., 1994) was used containing 3 g L⁻¹ Fe(III)-pyrophosphat (Fe₄(P₂O₇)₃), 2.5 g L⁻¹ NaHCO₃, 1.5 g L⁻¹ NH₄Cl, 0.05 g L⁻¹ yeast extract, 0.385 g L⁻¹ D(+)-glucose, 50 mL of a mineral solution (2 g L⁻¹ CaCl₂·2H₂O, 2 g L⁻¹ KCl, 12 g L⁻¹ NaH₂PO₄·H₂O, 2 g L⁻¹ NaCl, 2 g L⁻¹ MgCl₂·6H₂O, 2 g L⁻¹ MgSO₄·7H₂O, 0.1 g L⁻¹ MnCl₂·4H₂O, 0.02 g L⁻¹ NaMoO₄·2H₂O), 5 mL of a trace element solution (Drake, 1994), and 5 mL of a vitamin solution (Drake, 1994). The pH was adjusted to 5.5 with HCl. For MPN of sulfate-reducers, a modified Postgate medium B (Postgate, 1979) was used containing 0.5 g L⁻¹ KH₂PO₄, 1 g L⁻¹ NH₄Cl, 1 g L⁻¹ CaSO₄·2H₂O, 0.5 g L⁻¹ FeSO₄·7H₂O, 2 g L⁻¹ MgSO₄·7H₂O, 0.1 g L⁻¹ ascorbic acid, 1.2 g L⁻¹ Na-lactate, and 1 g L⁻¹ yeast extract, pH 5.2. Incubation for Fe(III)- and sulfate-reducer MPNs was conducted in triplicate in anoxic (80 % N₂/20 % CO₂) and rubber stoppered culture tubes and 1 mL from each dilution of the tenfold dilution series (10⁻¹-10⁻⁹) was added to 8 mL of steam-sterilized, anoxic medium, mixed, and incubated for 4 weeks in the dark at 22 ± 1 °C. Reduction of Fe(III) could be determined visually by color change of the FePPi medium from yellow to colorless and the formation of a white precipitate. Sulfate reduction could be determined visually by clouding of the usually clear SRP medium and formation of black FeS precipitates. Resulting MPN values were calculated following standard protocols (De Man, 1975). Results can be found in Table S1. Additional MPNs for formaldehyde sterilized samples showed no microbial growth and confirmed sterility of these samples (data not shown).

Table S1. Most probable number (MPN) values (95 % confidence interval) for cultivatable heterotrophic aerobes, Fe(III)-reducers, and sulfate-reducers determined for stored spring soil (H2) before and after Batch Experiment II (incubation at 35 °C for 41 d without (H2_wo) and with CO₂ purging (H2_CO₂)) and graph (right) with error bars showing 95 % confidence interval for better comparison.

| | MPN [no. mL ⁻¹] | | |
|---------------------|---|---|---|
| | <i>aerobes</i> | <i>Fe(III)-reducers</i> | <i>Sulfate-reducers</i> |
| <i>initial soil</i> | 1.2·10 ⁵ - 6.5·10 ⁵ | 4.7·10 ⁴ - 1.0·10 ⁶ | 3.0·10 ³ - 6.5·10 ⁴ |
| <i>H2_CO2</i> | 2.2·10 ⁵ - 1.2·10 ⁶ | 4.7·10 ⁴ - 1.0·10 ⁶ | 2.1·10 ³ - 4.7·10 ⁴ |
| <i>H2_wo</i> | 6.0·10 ⁴ - 3.2·10 ⁵ | 2.1·10 ⁴ - 4.7·10 ⁵ | 6.4·10 ² - 1.4·10 ⁴ |



S.2 Batch experiments with sterile controls

We attempted to quantify the influence of microbial activity on the observed mobilization processes by conducting additional batch experiments with sterilized controls. The first experiment with sterile batches (“S1”) was conducted parallel to H2 at room temperature (22 ± 1 °C), also with stored spring soil and water. The batch reactors were prepared the same way as for H2 (50 g soil + 75 mL filtered river water) and afterwards sterilized by adding 2 mL of a 5 % formaldehyde solution right before the start of the experiment (method modified after Weir et al., 1996). The second experiment with sterile batches (“S2”) was conducted parallel to H3, also at 35 °C with fresh summer soil and water. This time, the batch reactors were closed inside an anoxic COY-glovebox (95 % N₂, 5 % H₂) and steam-sterilized in an autoclave (FVS, Integra Biosciences, Germany) at 121 °C one day before the start of the experiment.

Both sterilization methods caused significant changes in pH and redox potential and led to an abiotic mobilization of almost all considered elements. Results are shown in comparison to the according non-sterilized H2 and H3 batches in Fig. S1 and Fig. S2. Formaldehyde as reducing agent caused an immediate drop in redox potential to values < 400 mV which led to significantly increased Fe and Mn mobilization over the course of the experiment. A direct comparison with non-sterile samples for the evaluation of the microbial influence on mobilization processes was thus not possible. However, the results give evidence that also an abiotic Fe mobilization from Fe(III) (oxyhydr)oxide dissolution can occur under CO₂ treatment. Steam sterilization of the soil led to an immediate mobilization of all considered elements and a clear drop in redox potential to < 400 mV. Autoclaving is known to cause changes in soil structure, especially affecting organic matter (Berns et al., 2008), causing collapsing and aggregation of clay minerals and thereby decreasing soil surface (Lotrario et al., 1995; Trevors, 1996), and inducing changes in solid phase speciation of Fe (Herbert et al., 2005; Wolf et al., 1989). Thus, also for S2 no comparison with non-sterilized batches in order to quantify microbial influence was possible.

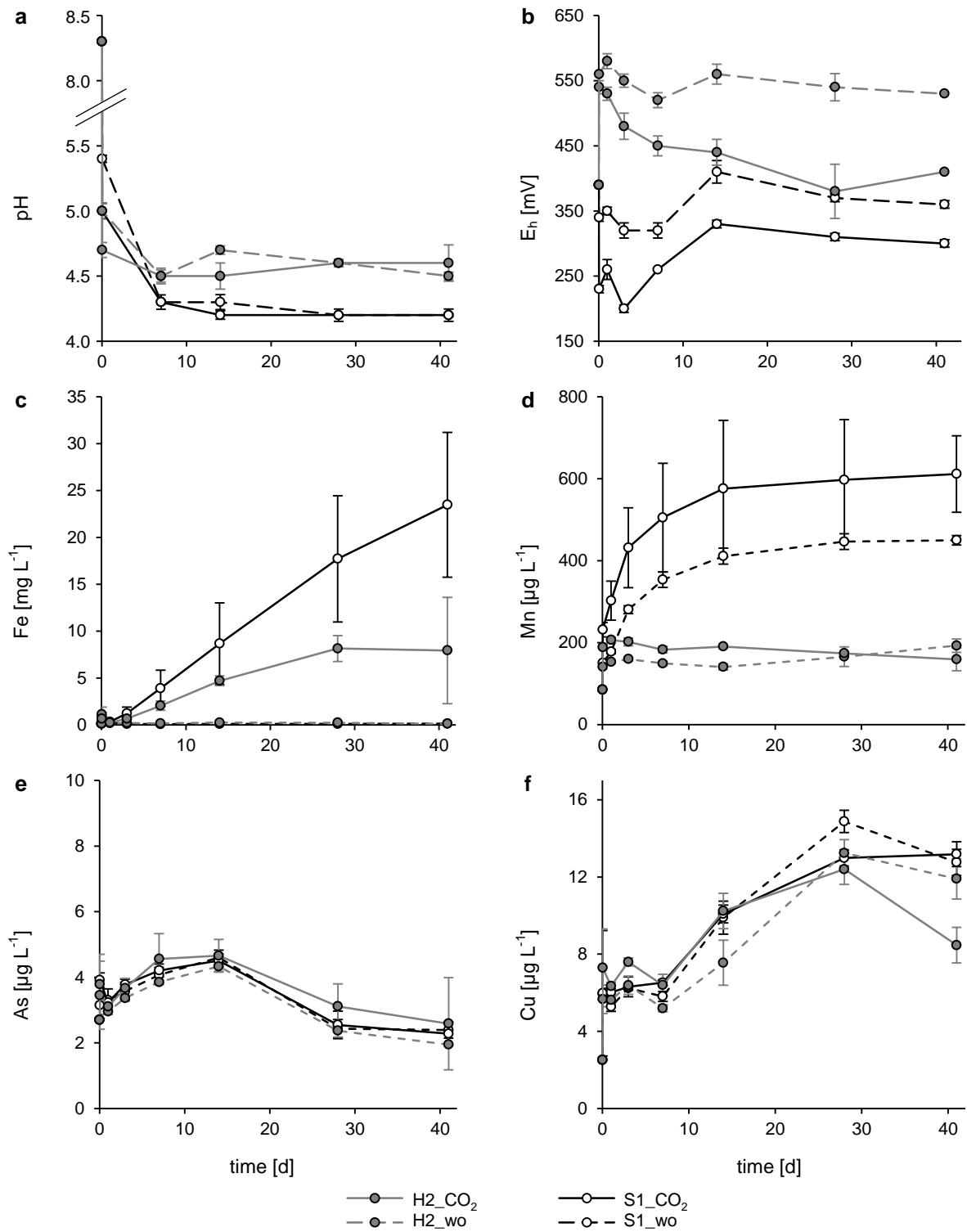


Fig. S1. Changes in liquid phase pH (a), redox potential (b), and total dissolved concentration (evaporation corrected) of Fe (c), Mn (d), As (e), and Cu (f) during Batch Experiment II with (solid line) and without (abbreviation “wo”, dashed line) CO₂ for formaldehyde sterilized (S1, non-filled symbols and black lines) and non-sterilized (H2, filled symbols and grey lines) stored spring soil in liquid phase. Data on pH are missing on 1 d and 3 d due to electrode calibration problems. Single outliers from triplicates had to be removed for the following data points, resulting in duplicates: H2_wo_d41 for As and S1_CO₂_d7 for Cu.

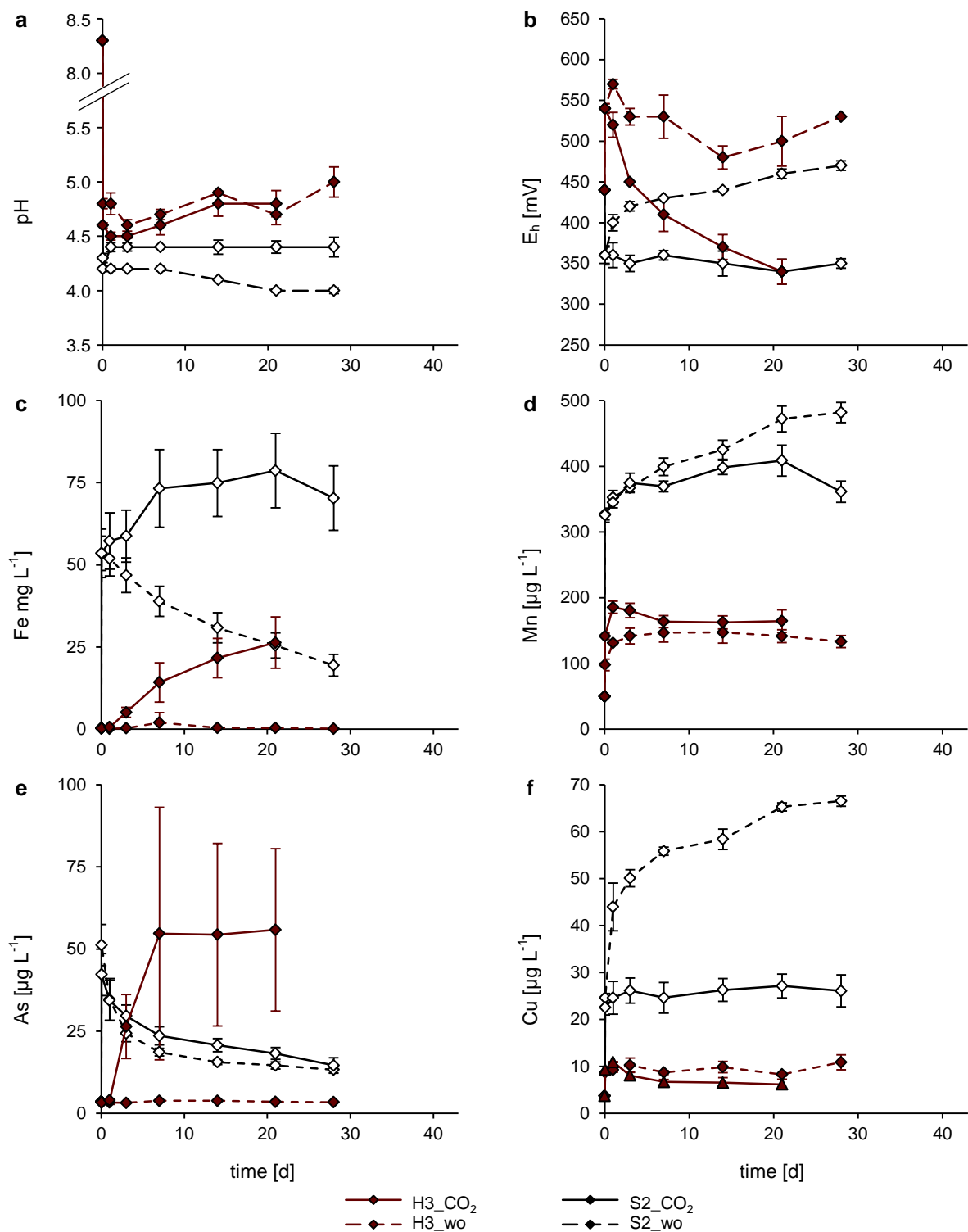


Fig. S2. Changes in liquid phase pH (a), redox potential (b), and total dissolved concentration (evaporation corrected) of Fe (c), Mn (d), As (e), and Cu (f) during Batch Experiment II with (solid line) and without (abbreviation “wo”, dashed line) CO₂ for steam-sterilized (S2, non-filled symbols and black lines) and non-sterilized (H2, dark red symbols and lines) fresh summer soil in liquid phase. Single outliers from triplicates had to be removed for the following data points, resulting in duplicates: H3_wo_d3 for As and H3_wo_d7 for Fe, Mn, and Cu.

S.3 Results from Mössbauer spectroscopy of three initial soil samples

Table S2. Hyperfine parameters of Mössbauer spectra from fresh spring soil, stored spring soil, and fresh summer soil. CS - Center shift, ΔE_Q - Quadrupole splitting, ϵ - quadrupole shift, B_{hf} - hyperfine field, Pop. - relative abundance.

| | Site | Phase | CS [mm/s] | ΔE_Q [mm/s] | ϵ [mm/s] | B_{hf} [T] | Pop. [%] | |
|-------------------|--------------------|-------------------|------------------------|------------------------|----------------------|-----------------|-------------|-------------|
| fresh spring soil | 77 | D1 | Fe(III) | 0.36 | 0.85 | | 49.3 ± 1.8 | |
| | | D2 | Fe(II) | 1.45 | 2.37 | | 19.3 ± 1.1 | |
| | | D3 | Fe(II)? | 0.77 | 1.14 | | 6.9 ± 0.9 | |
| | 5 | S1 | Goethite (Fe(III)) | 0.48 | | -0.14 | 45.9 | 16.0 ± 2.3 |
| | | S2 | Goethite (Fe(III)) | 0.45 | | -0.14 | 49.1 | 8.6 ± 1.6 |
| | 5 | D1 | Fe(III) | 0.43 | 0.88 | | | 21.8 ± 1.3 |
| | | D2 | Fe(II) | 1.36 | 2.51 | | | 16.4 ± 1.4 |
| | | S1+S2 | Goethite (Fe(III)) | 0.48 | | -0.14 | 49.7 | 19.4 ± 2.3 |
| | | S3 | Ferrihydrite (Fe(III)) | 0.44 | | -0.02 | 46.9 | 42.3 ± 2.6 |
| | stored spring soil | 77 | D1 | Fe(III) | 0.36 | 0.85 | | 44.0 ± 3.7 |
| D2 | | | Fe(II) | 1.45 | 2.37 | | 19.3 ± 1.9 | |
| D3 | | | Fe(II)? | 0.77 | 1.14 | | 5.7 ± 1.2 | |
| S1 | | | Goethite (Fe(III)) | 0.48 | | -0.14 | 45.9 | 20.4 ± 5.2 |
| S2 | | | Goethite (Fe(III)) | 0.45 | | -0.14 | 49.1 | 10.6 ± 4.5 |
| 5 | | D1 | Fe(III) | 0.38 | 0.91 | | | 23.0 ± 1.2 |
| | | D2 | Fe(II) | 1.42 | 2.48 | | | 14.8 ± 1.2 |
| | | S1+S2 | Goethite (Fe(III)) | 0.48 | | -0.13 | 49.7 | 26.9 ± 2.2 |
| | | S3 | Ferrihydrite (Fe(III)) | 0.41 | | -0.06 | 46.3 | 35.3 ± 2.4 |
| | | fresh summer soil | 77 | D1 | Fe(III) | 0.33 | 0.91 | |
| D2 | Fe(II) | | | 1.47 | 2.41 | | 31.3 ± 2.2 | |
| D3 | Fe(II)? | | | 0.85 | 1.50 | | 9.2 ± 2.2 | |
| 5 | D1 | | Fe(III) | 0.36 | 0.84 | | | 22.8 ± 7.4 |
| | D2 | | Fe(II) | 1.50 | 2.43 | | | 12.2 ± 4.4 |
| | D3 | | Fe(II)? | 0.74 | 1.53 | | | 3.8 ± 2.8 |
| | S1 | | Fe(III) | 0.82 | | 0.52 | 28.2 | 38.0 ± 18.0 |
| | S2 | | Fe(III) | 0.39 | | -0.08 | 47.9 | 18.0 ± 10.0 |
| | S3 | | Fe(III) | 0.52 | | -0.27 | 49.8 | 5.4 ± 4.4 |

S.4 Total dissolved CO₂ in Batch Experiment I

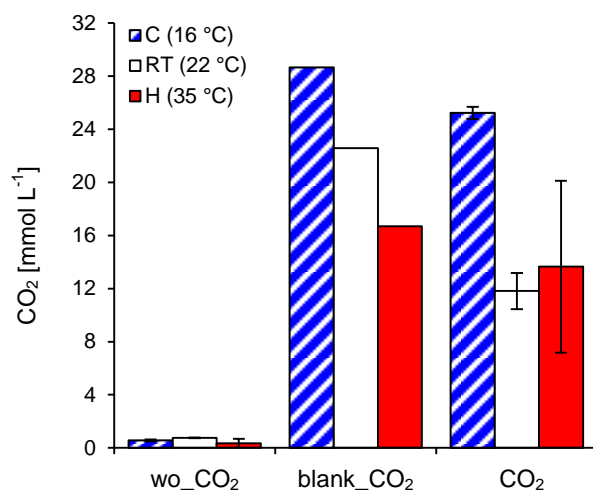


Fig. S3. Total dissolved CO₂ concentration at the end of Batch Experiment I (fresh spring soil) after 42 d for controls (“wo_CO₂”), water blanks (“blank_CO₂”, water only), and treatments (“CO₂”) at 16 ± 1 °C (C, blue stripes), at 22 ± 1 °C (RT, unfilled), and 35 ± 0.1 °C (H, filled red).

S.5 Water blanks for Batch Experiment I and II

Table S3. pH, redox potential (E_h), and total dissolved concentration (evaporation corrected) of Fe, Mn, As, and Cu for water blanks of all batch experiments (single measurements). Missing data are marked as *NA*.

| time [d] | 0 | 0.04 | 1 | 3 | 7 | 14 | 21 | 28 | 41 | 42 |
|-----------------|-------------------------------|------|------|------|------|------|------|------|------|------|
| | <i>pH [-]</i> | | | | | | | | | |
| <i>C_blank</i> | 8.6 | 4.8 | 4.8 | 4.6 | 4.5 | 4.6 | | 4.9 | | 4.8 |
| <i>RT_blank</i> | 8.6 | 4.6 | 5.0 | 4.9 | 5.0 | 5.0 | | 5.1 | | 5.3 |
| <i>H1_blank</i> | 8.6 | 5.2 | 5.0 | 5.0 | 4.9 | 5.2 | | 5.1 | | 5.2 |
| <i>H2_blank</i> | 8.6 | 5.3 | NA | NA | 4.9 | 4.8 | | 5.1 | 5.2 | |
| <i>H3_blank</i> | 7.5 | 5.1 | 5.1 | 5.1 | 5.1 | 5.1 | 5.1 | 5.2 | | |
| | <i>E_h [mV]</i> | | | | | | | | | |
| <i>C_blank</i> | 380 | 560 | 550 | 570 | 580 | 560 | | 560 | | 550 |
| <i>RT_blank</i> | 380 | 520 | 510 | 510 | 490 | 500 | | 500 | | 450 |
| <i>H1_blank</i> | 380 | 590 | 500 | 470 | 520 | 470 | | 470 | | 460 |
| <i>H2_blank</i> | 380 | 500 | 500 | 450 | 470 | 450 | | 470 | 460 | |
| <i>H3_blank</i> | 420 | 510 | 480 | 490 | 490 | 430 | 410 | 440 | | |
| | <i>Fe [mg L⁻¹]</i> | | | | | | | | | |
| <i>C_blank</i> | 0.17 | 0.16 | 0.15 | 0.14 | 0.14 | 0.15 | | 0.15 | | 0.13 |
| <i>RT_blank</i> | 0.17 | 0.17 | 0.16 | 0.15 | 0.14 | 0.16 | | 0.16 | | 0.15 |
| <i>H1_blank</i> | 0.17 | 0.16 | 0.15 | 0.14 | 0.16 | 0.13 | | 0.13 | | 0.13 |
| <i>H2_blank</i> | 0.17 | 0.12 | 0.10 | 0.11 | 0.13 | 0.15 | | 0.11 | 0.11 | |
| <i>H3_blank</i> | 0.26 | 0.24 | 0.20 | 0.18 | 0.19 | 0.21 | 0.22 | 0.19 | | |
| | <i>Mn [μg L⁻¹]</i> | | | | | | | | | |
| <i>C_blank</i> | 92 | 96 | 99 | 96 | 98 | 96 | | 102 | | 104 |
| <i>RT_blank</i> | 92 | 93 | 91 | 90 | 94 | 92 | | 96 | | 101 |
| <i>H1_blank</i> | 92 | 97 | 91 | 91 | 96 | 94 | | 102 | | 101 |
| <i>H2_blank</i> | 92 | 85 | 84 | 83 | 86 | 95 | | 95 | 94 | |
| <i>H3_blank</i> | 50 | 64 | 58 | 58 | 61 | 62 | 63 | 58 | | |
| | <i>As [μg L⁻¹]</i> | | | | | | | | | |
| <i>C_blank</i> | 4.2 | NA | NA | NA | NA | 5.4 | | 3.8 | | 3.6 |
| <i>RT_blank</i> | 4.2 | NA | NA | NA | NA | 5.2 | | 4.1 | | 3.6 |
| <i>H1_blank</i> | 4.2 | NA | NA | NA | 4.0 | 4.8 | | 3.6 | | 3.2 |
| <i>H2_blank</i> | 4.2 | 2.5 | 2.8 | NA | 3.7 | 3.9 | | 1.9 | 1.5 | |
| <i>H3_blank</i> | 3.5 | 3.4 | 3.3 | 3.5 | 3.5 | 3.5 | 3.1 | 2.8 | | |
| | <i>Cu [μg L⁻¹]</i> | | | | | | | | | |
| <i>C_blank</i> | 3.3 | 12.0 | 7.4 | 11.5 | 5.8 | 6.7 | | 4.8 | | 6.3 |
| <i>RT_blank</i> | 3.3 | 4.7 | 17.0 | 5.8 | 11.4 | 5.7 | | 4.0 | | 6.2 |
| <i>H1_blank</i> | 3.3 | 7.2 | 13.7 | 9.5 | 7.9 | 10.4 | | 6.7 | | 6.9 |
| <i>H2_blank</i> | 3.3 | 4.8 | 5.5 | 5.1 | 4.9 | 7.5 | | 10.4 | 7.4 | |
| <i>H3_blank</i> | 3.7 | 8.5 | 7.2 | 6.5 | 6.7 | 6.2 | 4.5 | 5.7 | | |

S.6 Total soil concentrations in Batch Experiment I and II

Table S4. Total soil concentrations of Fe, Mn, As, and Cu before (“initial”) and after Batch Experiment I with incubation of fresh spring soil without (“wo_CO₂”) and with CO₂ (“CO₂”) at 3 different temperatures. Initial concentrations were only measured once, thus the relatively high value for initial As might have been caused by soil heterogeneity.

| | | initial | C (16 °C) | RT (22 °C) | H (35 °C) |
|----------------------------------|--------------------------|----------------|------------------|-------------------|------------------|
| <i>Fe</i> [mg kg ⁻¹] | <i>wo_CO₂</i> | 31050 | 30139 ± 3118 | 26830 ± 1037 | 28106 ± 1599 |
| | <i>CO₂</i> | | 30636 ± 1563 | 33250 ± 1636 | 31086 ± 3124 |
| <i>Mn</i> [mg kg ⁻¹] | <i>wo_CO₂</i> | 115 | 132 ± 5 | 119 ± 6 | 123 ± 8 |
| | <i>CO₂</i> | | 122 ± 3 | 118 ± 6 | 116 ± 5 |
| <i>As</i> [mg kg ⁻¹] | <i>wo_CO₂</i> | 67 | 41 ± 9 | 32 ± 4 | 36 ± 6 |
| | <i>CO₂</i> | | 37 ± 4 | 43 ± 4 | 41 ± 6 |
| <i>Cu</i> [mg kg ⁻¹] | <i>wo_CO₂</i> | 13 | 14 ± 0 | 16 ± 1 | 15 ± 1 |
| | <i>CO₂</i> | | 15 ± 2 | 16 ± 1 | 16 ± 1 |

Table S5. Total soil concentrations of Fe, Mn, As, and Cu before (“initial”) and after Batch Experiment II with incubation of stored spring soil (H2) and fresh summer soil (H3) without (“wo_CO₂”) and with CO₂ (“CO₂”) at 35 °C. Initial concentrations were only measured once, thus the relatively high value for As in initial H2 might have been caused by soil heterogeneity.

| | | initial H2 | H2 (35 °C) | initial H3 | H3 (35 °C) |
|----------------------------------|--------------------------|-------------------|-------------------|-------------------|-------------------|
| <i>Fe</i> [mg kg ⁻¹] | <i>wo_CO₂</i> | 34992 | 29913 ± 3144 | 18817 | 18748 ± 540 |
| | <i>CO₂</i> | | 28532 ± 1932 | | 18273 ± 238 |
| <i>Mn</i> [mg kg ⁻¹] | <i>wo_CO₂</i> | 128 | 130 ± 8 | 119 | 114 ± 10 |
| | <i>CO₂</i> | | 123 ± 7 | | 115 ± 4 |
| <i>As</i> [mg kg ⁻¹] | <i>wo_CO₂</i> | 76 | 44 ± 3 | 36 | 30 ± 1 |
| | <i>CO₂</i> | | 44 ± 8 | | 31 ± 2 |
| <i>Cu</i> [mg kg ⁻¹] | <i>wo_CO₂</i> | 11 | 14 ± 0 | 14 | 16 ± 1 |
| | <i>CO₂</i> | | 14 ± 1 | | 15 ± 1 |

S.7 Arsenic results for Batch Experiment II with individual graphs

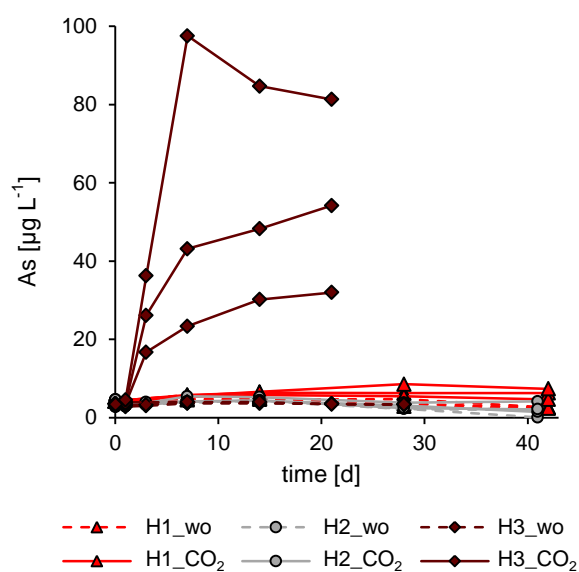


Fig. S4. Changes in total dissolved concentration of As (evaporation corrected) during Batch Experiment II with (solid line) and without (abbreviation “wo”, dashed line) CO₂ at 35 °C with 3 different start soil conditions (H1: fresh spring soil from Batch Experiment I, red triangles, H2: stored spring soil, grey circles, H3: fresh summer soil, dark red squares) in liquid phase with all triplicates displayed individually. Data for As 1 h - 3 d are missing for H1 due to measurement problems. One outlier has been removed in H3_wo_d3.

S.8 Results from additional incubation experiment

Table S6. Total amount of CO₂ formed and total dissolved Fe concentration after 7 d of incubation of spring and summer soil at 3 different temperatures from an additional incubation experiment for proof of microbial Fe(III) reduction. Values are given as range between two replicates.

| Soil | temp. [°C] | CO ₂ [μmol] | Fe [mg L ⁻¹] |
|--------------------|------------|------------------------|--------------------------|
| <i>spring soil</i> | 12 | 2.5 - 2.6 | 0.11 - 0.12 |
| | 21 | 4.5 - 5.2 | 0.18 - 0.48 |
| | 35 | 7.0 - 9.5 | 1.47 - 1.67 |
| <i>summer soil</i> | 12 | 5.7 - 6.7 | 0.07 - 0.17 |
| | 21 | 8.3 - 11.1 | 0.10 - 3.81 |
| | 35 | 20.8 - 22.6 | 14.98 - 15.45 |

Table S7. Correlation coefficients r_s between incubation temperature, total CO₂, and dissolved Fe concentration for the additional 7 d incubation experiment. Significance level is indicated by stars with * $P < 0.05$, ** $P < 0.01$.

| | both soils | | spring soil | | summer soil | |
|------------------------------|------------------------|--------------------------|------------------------|--------------------------|------------------------|--------------------------|
| | CO ₂ [μmol] | Fe [μg L ⁻¹] | CO ₂ [μmol] | Fe [μg L ⁻¹] | CO ₂ [μmol] | Fe [μg L ⁻¹] |
| <i>temp. [°C]</i> | 0.74** | 0.80** | 0.96** | 0.96** | 0.96** | 0.84* |
| <i>CO₂ [μmol]</i> | - | 0.69* | - | 0.94** | - | 0.83* |

S.9 Sulfur results for Batch Experiment I and II

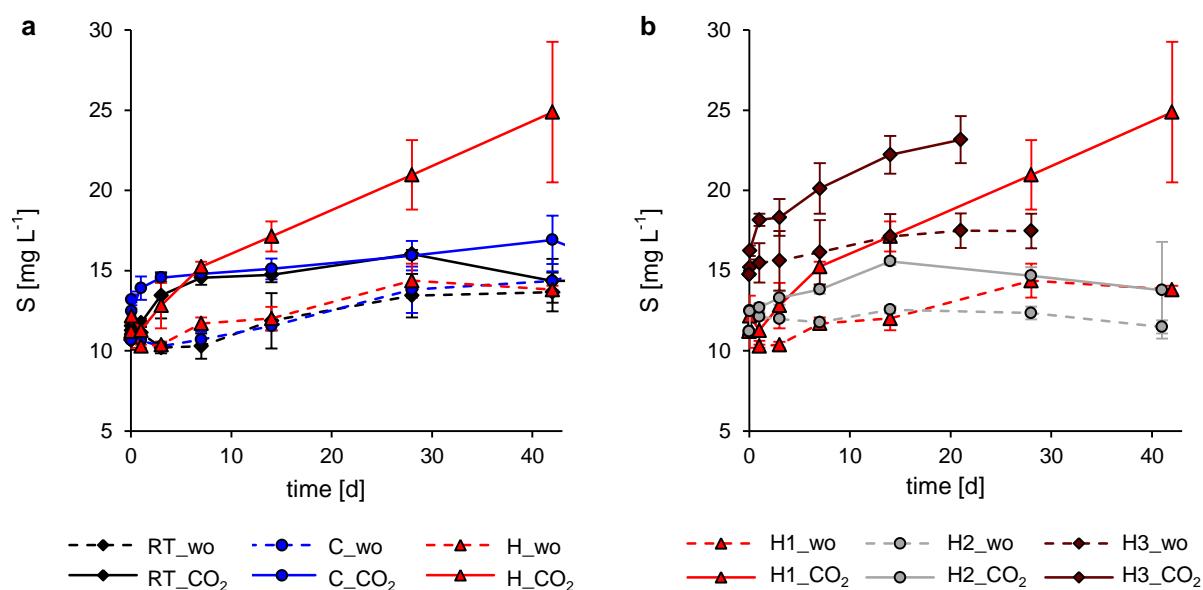


Fig. S5. Changes in total dissolved concentration (evaporation corrected) of S with (solid line) and without (abbreviation “wo”, dashed line) CO₂ (a) during Batch Experiment I at room temperature (RT, 22 °C, black squares), cooled (C, 16 °C, blue circles), and heated (H, 35 °C, red triangles) and (b) during Batch Experiment II with different start soil conditions (H1: fresh spring soil, red triangles; H2: stored spring soil, grey circles; H3: fresh summer soil, dark red squares) in liquid phase.

Table S8. Total dissolved concentration (evaporation corrected) of S for water blanks of all batch experiments (single measurements).

| time [d] | 0 | 0.04 | 1 | 3 | 7 | 14 | 21 | 28 | 41 | 42 |
|-----------------|--------------------------------|------|----|----|----|----|----|----|----|----|
| | <i>S</i> [mg L ⁻¹] | | | | | | | | | |
| <i>C_blank</i> | 11 | 10 | 10 | 10 | 10 | 11 | | 13 | | 14 |
| <i>RT_blank</i> | 11 | 11 | 11 | 10 | 10 | 11 | | 14 | | 13 |
| <i>H1_blank</i> | 11 | 11 | 10 | 10 | 11 | 12 | | 13 | | 13 |
| <i>H2_blank</i> | 11 | 12 | 12 | 13 | 13 | 14 | | 14 | 13 | |
| <i>H3_blank</i> | 15 | 16 | 15 | 15 | 16 | 17 | 17 | 16 | | |

Table S9. Total soil concentrations of S before (“initial”) and after Batch Experiment I with incubation of fresh spring soil without (“wo_CO₂”) and with CO₂ (“CO₂”) at 3 different temperatures and after Batch Experiment II with incubation of stored spring soil (H2) and fresh summer soil (H3).

| | <i>S</i> [g kg ⁻¹] | | | | | | | |
|--------------------------|--------------------------------|-----------|-----------|-----------|----------------|-----------|----------------|-----------|
| | <i>initial</i> | <i>C</i> | <i>RT</i> | <i>H1</i> | <i>initial</i> | <i>H2</i> | <i>initial</i> | <i>H3</i> |
| | <i>H1</i> | (16 °C) | (22 °C) | (35 °C) | <i>H2</i> | (35 °C) | <i>H3</i> | (35 °C) |
| <i>wo_CO₂</i> | 2.0 | 2.1 ± 0.1 | 2.2 ± 0.1 | 2.2 ± 0.2 | 2.5 | 2.4 ± 0.1 | 2.6 | 2.7 ± 0.2 |
| <i>CO₂</i> | | 2.1 ± 0.1 | 2.3 ± 0.1 | 2.2 ± 0.1 | | 2.3 ± 0.1 | | 2.7 ± 0.2 |

References

- Berns, A., Philipp, H., Narres, H.-D., Burauel, P., Vereecken, H., Tappe, W., 2008. Effect of gamma-sterilization and autoclaving on soil organic matter structure as studied by solid state NMR, UV and fluorescence spectroscopy. *Eur. J. Soil Sci.* 59, 540-550.
- Caccavo, F., Lonergan, D.J., Lovley, D.R., Davis, M., Stolz, J.F., McInerney, M.J., 1994. *Geobacter sulfurreducens* sp. nov., a hydrogen- and acetate-oxidizing dissimilatory metal-reducing microorganism. *Appl. Environ. Microbiol.* 60, 3752-3759.
- De Man, J., 1975. The probability of most probable numbers. *Eur. J. Appl. Microbiol.* 1, 67-78.
- Drake, H.L., 1994. Acetogenesis, in: Reddy, C.A., Chakrabarty, A.M., Demain, A.L., Tiedje, J.M. (Eds.), *Chapman & Hall Microbiology Series* Chapman & Hall, New York.
- Drake, H.L., Aumen, N.G., Kuhner, C., Wagner, C., Griesshammer, A., Schmittroth, M., 1996. Anaerobic microflora of everglades sediments: effects of nutrients on population profiles and activities. *Appl. Environ. Microbiol.* 62, 486-493.
- Herbert, R.B., Malmström, M., Ebenå, G., Salmon, U., Ferrow, E., Fuchs, M., 2005. Quantification of abiotic reaction rates in mine tailings: evaluation of treatment methods for eliminating iron- and sulfur-oxidizing bacteria. *Environ. Sci. Technol.* 39, 770-777.
- Lotrario, J., Stuart, B., Lam, T., Arands, R., O'Connor, O., Kosson, D., 1995. Effects of sterilization methods on the physical characteristics of soil: implications for sorption isotherm analyses. *Bull. Environ. Contam. Toxicol.* 54, 668-675.
- Postgate, J.R., 1979. *The sulphate-reducing bacteria*. Cambridge University Press, Cambridge.
- Trevors, J., 1996. Sterilization and inhibition of microbial activity in soil. *J. Microbiol. Methods* 26, 53-59.
- Weir, S.C., Lee, H., Trevors, J.T., 1996. Effect of selected disinfectants on the persistence and movement of a genetically engineered *Pseudomonas* sp. in soil. *Syst. Appl. Microbiol.* 19, 421-427.
- Wolf, D., Dao, T., Scott, H., Lavy, T., 1989. Influence of sterilization methods on selected soil microbiological, physical, and chemical properties. *J. Environ. Qual.* 18, 39-44.

STUDY 3: Copper mobilization and immobilization along an organic matter and redox gradient – insights from a mofette site

Judith Mehlhorn, Johannes Besold, Juan S. Lezama Pacheco, Jon Petter Gustafsson, Ruben Kretzschmar, Britta Planer-Friedrich

Reprinted with permission from

Environmental Science & Technology 52(23) (pp. 13698 – 13707)

Copyright 2018 American Chemical Society

ENVIRONMENTAL Science & Technology

December 4, 2018
Volume 52
Number 23
pubs.acs.org/est

CO₂ Exhalations: Natural Laboratories to Study Cu Mobility



ACS Publications
Most Trusted. Most Cited. Most Read.

www.acs.org

Copper Mobilization and Immobilization along an Organic Matter and Redox Gradient—Insights from a Mofette Site

Judith Mehlhorn,[†] Johannes Besold,[†] Juan S. Lezama Pacheco,[‡] Jon Petter Gustafsson,[§] Ruben Kretzschmar,^{||} and Britta Planer-Friedrich^{*,†,||}

[†]Environmental Geochemistry, Bayreuth Center for Ecology and Environmental Research (BayCEER), University of Bayreuth, D-95440 Bayreuth, Germany

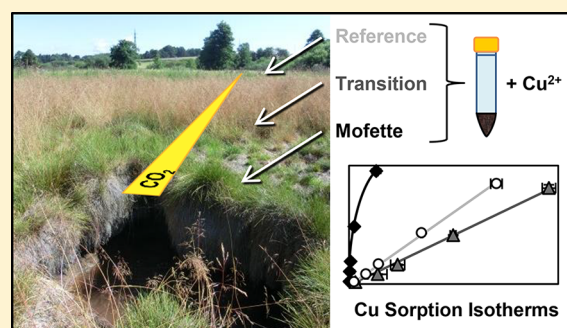
[‡]Department of Environmental Earth System Science, Stanford University, Stanford, California 94305, United States

[§]Department of Soil and Environment, Swedish University of Agricultural Sciences, 75007 Uppsala, Sweden

^{||}Soil Chemistry Group, Institute of Biogeochemistry and Pollutant Dynamics, ETH Zurich, CHN, CH-8092 Zurich, Switzerland

S Supporting Information

ABSTRACT: Mofettes (natural geogenic CO₂ exhalations) represent excellent sites to study the behavior of Cu in soils and the co-occurrence of different mobilization and immobilization processes since they exhibit both a gradient in redox conditions (oxic to permanently anoxic) and in soil organic matter (SOM; low to high contents). Soil and pore water samples from an 18 m-transect over a mofette showed a complex behavior of Cu, with highest mobility in the transition between oxic and anoxic conditions. Cu(II) sorption experiments on SOM-rich topsoil revealed that Cu mobility under oxic conditions was confined by adsorption to SOM while in the oxygen-free mofette center reduction and precipitation of sulfides was the dominating Cu-sequestering process. In transition areas with low amounts of oxygen (<10%), there was no mineral precipitation, instead high dissolved-to-soil organic carbon ratios strongly increased Cu mobility. Our results show that low stability of SOM formed under oxygen-limited conditions leads to increased Cu mobility unless sulfur-reducing conditions cause Cu sequestration by sulfide precipitation. The interplay of these (im)mobilization processes and especially the unexpectedly high mobility under suboxic conditions have to be considered when assessing Cu mobility along spatial or temporal redox gradients, e.g., at contamination sites or periodically flooded soils.



INTRODUCTION

Copper (Cu) is an essential trace element for most living organisms since it is an important component in many enzymes and proteins.¹ In higher concentrations, however, it can become toxic to microorganisms and plants and is therefore considered a contaminant.²

In oxic soils, Cu is primarily present as bivalent Cu(II) and its mobility is mainly controlled by sorption to soil organic matter (SOM).^{3–8} Closely spaced carboxylic and hydroxylic (or amine) groups in SOM form very stable five- to six-membered ring chelates with Cu(II) ions.^{9,10} Cu(II) can also adsorb to other soil constituents like clay minerals^{11,12} and Fe, Mn, or Al (oxyhydr)oxides.^{13–15} However, SOM seems to be the preferred binding partner.^{4,16}

Under (temporarily) reducing conditions, e.g., in floodplain soils or in peatlands, Cu(II) can be reduced to Cu(I) or Cu(0) directly by microorganisms^{17–20} and abiotically, e.g., by reaction with Fe²⁺ in solution²¹ or by redox active functional groups in SOM,^{22–24} which strongly affects Cu solubility.^{25–27} Metallic Cu(0) can precipitate in reducing soils, as has been already observed in early studies for peatlands^{28,29} and more recently also in contaminated periodically flooded

soils.^{20,22,30,31} If microbial sulfate reduction occurs, then Cu(II) can also be reduced by sulfide and precipitate as Cu(I) sulfides,^{32–34} a process that can occur even at low available sulfide concentrations.^{20,31,35} Dissolved Cu(I) disproportionates rapidly into Cu(0) and Cu(II)^{36,37} unless it is stabilized by complexation with suitable ligands such as sulfide or chloride.³⁸ Recently, it was shown that Cu(I) can also form complexes with SOM by coordination to at least one thiol group,^{22,30} a process that was up to then only described for estuarine waters and seawater.^{39,40}

In environments influenced by temporal or spatial gradients in redox conditions, like periodically flooded soils^{20,30,35} or anthropogenically influenced soils, (e.g., soils over landfills, organic contaminant spills, leaking pipelines or geologic carbon storage sites),^{41,42} the processes described above could coexist. For assessment of Cu mobility in such soils, it is important to understand how different sorption and precipitation processes

Received: May 18, 2018

Revised: September 5, 2018

Accepted: September 10, 2018

Published: September 10, 2018

Table 1. Overview of Selected Physical and Chemical Soil Parameters of the Untreated Soil Used in the Experiments^{a,b}

| | Mofette A | Transition A1 | Transition A2 | Reference A | Mofette B | Reference B |
|-----------------------------------|-------------|----------------|---------------|--------------|-------------|----------------|
| distance (m) ^c | 0 | 4 | 8 | 18 | 0 | 12 |
| $p(\text{CO}_2)$ (-) ^d | 0.972 | 0.556 | 0.072 | 0.016 | n.d. | n.d. |
| $p(\text{O}_2)$ (-) ^d | 0.000 | 0.089 | 0.198 | 0.205 | n.d. | n.d. |
| pH (-) ^e | 4.1 ± 0.04 | 3.7 ± 0.02 | 4.2 ± 0.03 | 4.5 ± 0.02 | 4.0 ± 0.04 | 4.6 ± 0.01 |
| C (g kg ⁻¹) | 202.0 ± 6.6 | 190.7 ± 2.5 | 148.3 ± 0.6 | 112.3 ± 0.6 | 127.7 ± 4.5 | 161.7 ± 2.5 |
| C/N ratio (-) | 16.7 ± 0.1 | 15.7 ± 0.1 | 12.8 ± 0.1 | 12.7 ± 0.03 | 16.0 ± 0.6 | 12.8 ± 0.1 |
| Cu (mg kg ⁻¹) | 23 ± 1 | 26 ± 1 | 36 ± 0 | 33 ± 1 | 12 ± 0 | 21 ± 0 |
| Fe (mg kg ⁻¹) | 6847 ± 164 | 75 697 ± 8,927 | 60 247 ± 889 | 30 041 ± 722 | 6679 ± 414 | 42 312 ± 1,794 |
| S (mg kg ⁻¹) | 4086 ± 26 | 3149 ± 141 | 2981 ± 38 | 2698 ± 41 | 2651 ± 29 | 3052 ± 194 |

^aSamples were taken from approx. 5–15 cm depth. Contents of Cu, Fe, and S were determined in aqua regia digests. ^bMean ± standard deviation, $n = 3$. ^cDistance from degassing center at Mofette A and B, respectively. ^dPartial pressure of CO₂ and O₂, respectively. ^eMeasured in 0.01 M CaCl₂

interact. Mofettes, which are characterized by degassing of mainly CO₂, represent excellent sites for studying the co-occurrence of Cu mobilizing and immobilizing processes in soils. Mofettes form in volcanic or seismic areas, where geogenic CO₂ ascends via faults and fissures toward the surface. Due to their diffuse spatial structure, a permanent gradient in soil conditions can be studied within only some meters from the mofettes. While the soil is completely anoxic right up to the top in degassing centers with CO₂ partial pressures ($p(\text{CO}_2)$) of up to almost 1, the CO₂ influence decreases sharply with distance,^{43,44} leading to a gradient in redox conditions over the mofette area. SOM is accumulating on mofette sites as a result of decreased decomposition under permanently anoxic conditions,^{45–48} creating an additional gradient in SOM content. Also, SOM composition differs along mofettes with accumulation of less degraded material and less interaction of SOM with soil minerals at higher $p(\text{CO}_2)$.^{48–50}

In the present study, we evaluated the influence of different Cu sequestering processes on the overall Cu mobility along the redox and SOM gradient of a mofette site. We studied Cu distribution in soil and pore water along a transect over a wetland mofette and conducted laboratory experiments determining Cu sorption isotherms for SOM-rich topsoil from two mofette sites. The aim of this study was to elucidate the interplay of the processes causing Cu immobilization (adsorption to SOM, reduction and sulfide precipitation) and mobilization (complexation with dissolved organic matter, DOM) in redoximorphic soils.

MATERIALS AND METHODS

Sampling Site. Samples were collected in February and September 2017 from two wetland mofettes (A and B) at a site in northwestern Czech Republic considered the seismic center of the Cheb Basin⁵¹ (detailed site description in Mehlhorn et al.⁵²). We sampled 18 soil samples over a transect of Site A (former site 2⁵²) in 0, 2, 4, 8, 12, and 18 m distance from the degassing center and from approximately 5–10, 25–35, and 55–65 cm depth with an auger and immediately shock-froze them on dry ice. Beulig et al.⁵³ characterized the mofette soil as a Hemic Histosol with reductimorphic properties due to the influence of upstreaming geogenic gas. The surrounding, non-CO₂-influenced soil was characterized as a Gleyic Fluvisol.⁵³ From the same spots, we collected pore water samples using 60 cm long pore water peepers type Hesslein⁵⁴ (50 individual chambers with a 1 cm depth resolution located in 10–60 cm depth). Peeper preparation and recovery after 9 weeks of equilibration time followed a previously described procedure.⁵²

Pore water from 5 chambers was combined to obtain sufficient sample volume. Samples were filtered (cellulose-acetate, 0.2 μm) and stabilized in 0.45% H₂O₂ and 0.65% HNO₃ for total Cu analysis and with 2% (w/v) zinc acetate (Grüssing, p.a.) for photometrical sulfide determination. Additional 2 mL of unfiltered pore water sample were stabilized in nitrogen-purged septum bottles for analysis of dissolved CO₂.

For laboratory sorption studies, four additional soil samples were taken from the transect of Site A: degassing center (“Mofette A”), transition with decreasing CO₂ influence (“Transition A1” and “Transition A2,” in approximately 4 and 8 m distance), and non-CO₂-influenced (“Reference A” in approximately 18 m distance from Mofette A). Locations were chosen based on vegetation changes as well as $p(\text{CO}_2)$ and $p(\text{O}_2)$ in soil air, determined in approximately 10 cm depth with a portable gas analyzer (BIOGAS 5000, Geotech). For comparison, additional samples were taken from the degassing center of a second mofette (“Mofette B”) and a non-CO₂-influenced reference (“Reference B” in approximately 12 m distance from Mofette B) (former site 1⁵²). If present, vegetation and root mats were removed and approximately 300 g of organic-rich topsoil (A/O-horizon, 5–15 cm depth) were sampled into bags and immediately shock-frozen on dry ice. Soil samples were stored in a freezer at –20 °C.

The sampled soils are generally characterized by decreasing soil pH, C and S contents, and an increasing C/N ratio with increasing $p(\text{CO}_2)$ (Table 1). This is in line with other studies from this site showing a CO₂-triggered soil acidification and a decreased C turnover in the mofettes.^{47,48,52} At Site B, the contents of C and S were higher in Reference than in Mofette, most likely because its location in a small depression and a smaller distance of Reference B to the CO₂-influenced area (approximately 1 m versus >3 m at site A) caused SOM translocation from the mofette and accumulation. The previously described negative effect of high $p(\text{CO}_2)$ in mofettes on the formation of Fe (oxyhydr)oxides^{48,55–57} is reflected by strongly decreased Fe contents in samples from degassing centers and accumulation of Fe in transition zones (Table 1).

Copper Sorption Experiment. All experiments were conducted in triplicate inside an anaerobic chamber (Coy, 95% N₂/5% H₂) using nitrogen-purged solutions prepared with ultrapure deionized water (Millipore, 18.2 MΩ cm) and chemicals of analytical grade. Soil samples (approximately 300 g per sample) were thawed inside the anaerobic chamber overnight and roots and stones were removed by pressing the well-mixed soil through a nylon sieve (1 mm mesh size). The wet soil was weighted immediately into centrifuge vials

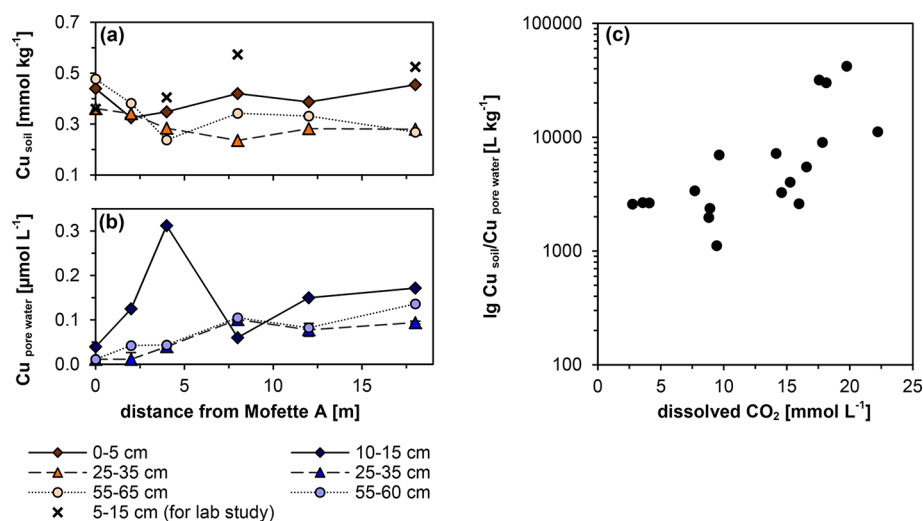


Figure 1. (a) Solid-phase Cu contents on a transect across Site A, going eastward from the degassing center (Mofette A) at 0 m, determined in aqua regia digests from freeze-dried soil samples taken at three depths per sampling point. Crosses mark samples taken for the laboratory sorption study. (b) Corresponding pore water Cu concentrations from three selected depths. Depth 25–35 cm shows mean value with error bars representing minimum and maximum value. (c) Distribution coefficients between Cu solid-phase content and Cu pore water concentration versus pore water CO₂ concentrations in the transect over Site A. Note the logarithmic scale of y-axis. Additional information on calculation of dissolved CO₂ concentrations can be found in [Section S.3, SI](#).

(equivalent to approximately 0.27 g dry weight) and 8 mL of 5 mM NaCl (Merck, p.a.) solution were added as background electrolyte leading to a soil-to-solution-ratio of approximately 1:30. All vials were wrapped in aluminum foil to exclude light influence. Suspensions were well-mixed, pH was adjusted to 4.5 ± 0.1 (approximately pore water pH of this mofette site⁵²) using 1 M NaOH or 1 M HCl, and suspensions were pre-equilibrated for 24 h with occasional shaking (permanent shaking might promote colloid formation). Afterward, 0–400 μL of 7.87 mM CuCl₂ (Grüssing, p.a.) stock solution, pH 4.5, were spiked to the suspensions, yielding spike concentrations of 0, 0.23, 1.16, 2.33, 5.83, and 11.65 mmol kg⁻¹. The suspensions were well-mixed and pH was adjusted to 4.5 ± 0.1 , then samples were left to equilibrate for 24 h with occasional shaking. The time required for achieving equilibrium conditions was determined in a kinetic study prior to this experiment (see [Section S.1, Supporting Information \(SI\)](#)). After equilibration, pH was measured in soil suspensions, then vials were centrifuged (5 min at 4500g, outside the glovebox) and the supernatant was removed with needle and syringe, filtered (0.2 μm , cellulose-acetate), and stabilized for total Cu analysis in 0.45% H₂O₂ and 0.65% HNO₃.

Analyses of Collected Samples. The remaining soil from the sorption experiment and the additional 18 soil samples from Site A were freeze-dried, pestled, and digested in aqua regia (soil-to-solution-ratio 1:100, microwave assisted digestion, MARS Xpress, CEM). Total Cu concentrations in filtered and diluted liquid phase samples and aqua regia digests were measured with a quadrupole inductively coupled plasma mass spectrometer (ICP-MS, X-Series 2, Thermo Scientific) at m/z 65 to avoid interferences with ArNa⁺ at m/z = 63. Aqua regia digests of the initial soil samples were additionally analyzed for total Fe and S concentrations by ICP-MS.

Total C and N contents in the initial, freeze-dried and pestled soil samples were determined with a CHN elemental analyzer (Thermo Quest, Flash EA, 1112). The amounts of organic matter mobilized from solid into liquid phase were determined in triplicate for samples with highest Cu(II) spike.

Due to limited sample amounts, the Cu sorption experiment was repeated for these samples, suspensions were centrifuged, and supernatants were filtered (0.45 μm , polyamide) and analyzed for total dissolved organic carbon (DOC) and nitrogen by thermo-catalytic oxidation with a TOC-VCPN Analyzer (Shimadzu).

Dissolved CO₂ concentrations in pore water samples collected from Site A were calculated from head space concentrations in the septum bottles applying Henry's law ($k_{\text{H,CO}_2} = 0.03344 \text{ mol L}^{-1} \text{ atm}^{-1}$ from Sander,⁵⁸ details in [Section S.3, SI](#)). Gaseous head space concentrations were measured with a gas chromatograph (SRI Instruments 8610C, U.S.) equipped with a methanizer and a flame ionization detector.

Sulfide concentrations in pore water samples were determined photometrically using the methylene blue method,⁵⁹ measuring the absorbance at 650 nm with a multiplate reader (Infinite 200 PRO, Tecan). With the same method, we checked for sulfide formation in selected samples from Cu sorption experiment using filtered soil suspensions. In the Cu(II)-spiked samples we also checked whether Cu(I) formation occurred, using the bathocuproine method^{24,60} with absorbance measured at 492 nm.

Characterization of SOM and Mineral Phases.

Characterization of SOM was done for samples from Mofette A, Transition A1, and Reference A by solid-state ¹³C nuclear magnetic resonance spectroscopy (NMR, details in [Section S.4, SI](#)). Further, we characterized DOM by Fourier-transform infrared spectroscopy (FTIR). Extraction of DOM was done with ultrapure deionized water at a soil-to-solution-ratio of 1:5 for 24 h on a horizontal shaker. Absorption band assignments are based on Artz et al.⁶¹ and Rennert et al.⁴⁸ Details on FTIR analysis can be found in [Section S.5, SI](#).

Samples from Transition A1 and Reference A were analyzed by X-ray powder diffraction (XRD) to gain information on mineralogy using a Philips X'Pert Pro diffractometer operating in reflection mode with Fe filtered CoK α_1 radiation, step size

0.03° 2θ , range 5–50°, and scan speed of 1.8°/min. Sample spectra can be found in Section S.6, SI.

One Cu-loaded sample of Mofette A was analyzed by scanning electron microscopy energy-dispersive X-ray spectrometry (SEM-EDS) to detect potential Cu precipitates (details in Section S.7, SI).

X-ray Absorption Spectroscopy. Copper *K*-edge X-ray absorption near edge structure (XANES) and extended X-ray absorption fine structure (EXAFS) spectra were collected at beamlines 4–1 and 4–3 at the Stanford Synchrotron Radiation Lightsource (SSRL, Stanford, U.S.A.). Spectra were collected for samples from Site A and for one sample from a peat lens at approximately 2 m depth beneath the degassing center of Site A (originating from the sampling in February, further information on physicochemical properties of this peat lens can be found in Mehlhorn et al.⁵²). We collected XANES only for initial soil samples, XANES and EXAFS for samples with the highest Cu spike from the sorption experiment and for the peat lens sample. Sample measurements were performed in fluorescence mode at 25 K using a 4-element solid-state Si drift detector (HTA Hitachi) and a liquid He cryostat at beamline 4–3 (samples Transition A1, A2, Reference A, and peat lens) or at 77 K using a 32-element solid-state Ge detector (Canberra) and a liquid nitrogen cryostat (samples Mofette A). The following published spectra were used as reference compounds: *Cu(II)-humic* (Cu(II) adsorbed to a soil humic acid solution),³⁰ *Cu(II)-malate* ($\text{Cu}(\text{C}_4\text{H}_5\text{O}_5)_2(\text{H}_2\text{O})_2$),³⁰ *Cu(II)-carboxyl* (Cu(II) adsorbed to carboxyl resin Bio-Rex 70 (Bio-Rad)),²² *Cu(II)-clay* (Cu(II) adsorbed to montmorillonite),³⁰ *Cu(I)-thiol* (Cu(I) adsorbed to thiol resin Ambersep GT74 (Supelco)),²² *Cu(I)-GSH* (Cu(I) adsorbed to L-Glutathione),³⁰ $\text{Cu}_{1.8}\text{S}$,²⁰ CuS ,³⁰ and *Cu(II)-ferrihydrite* (30 μM Cu(II) adsorbed to 0.3 mM ferrihydrite,¹⁵ kindly provided by Charlotta Tiberg, Swedish Geotechnical Institute, Stockholm). Additionally, *metallic Cu(0)* (Cu foil), measured in transmission mode, was used as a reference compound. Further details on data collection and evaluation can be found in Section S.8, SI.

RESULTS AND DISCUSSION

Natural Distribution of Solid and Liquid Phase Copper Along the Mofette-Reference Site Gradient.

Compared to the non- CO_2 -influenced reference in 18 m distance, Cu soil contents in the degassing center (0 m distance) were similar or slightly increased while Cu pore water concentrations were decreased (Figure 1a,b). Similar trends were reported previously by Mehlhorn et al.⁵² who observed a relationship ($r = 0.59$, $P < 0.005$) between total soil Cu and organic carbon (C_{org}). This observation led to the conclusion that Cu immobilization in mofettes is caused by adsorption to SOM.⁵² However, Cu data from the transect between the two end points Mofette and Reference did not just show a linear decrease or increase. Copper soil contents decreased sharply with increasing distance from the degassing center, reaching minima after 2–8 m and then slowly increasing again with further distance (Figure 1a). By contrast, Cu pore water concentrations sharply increased with distance reaching (local) maxima at 4 m distance, followed by local minima at 8 m, then slightly increasing again with further distance (Figure 1b). Distribution coefficients between Cu soil content and pore water concentration increased with dissolved CO_2 , with Cu being strongly shifted toward the solid phase at the highest CO_2 concentrations (Figure 1c). To clarify the

mechanisms that caused this behavior, we determined Cu sorption isotherms for soil samples from this mofette site.

Copper Sequestration Potential of Mofette, Transition, and Reference Soil. Copper sorption isotherms of the soils measured by batch experiments at $\text{pH } 4.5 \pm 0.1$ differed strongly between the samples, with highest Cu sequestration occurring in mofette centers (Figure 2a).

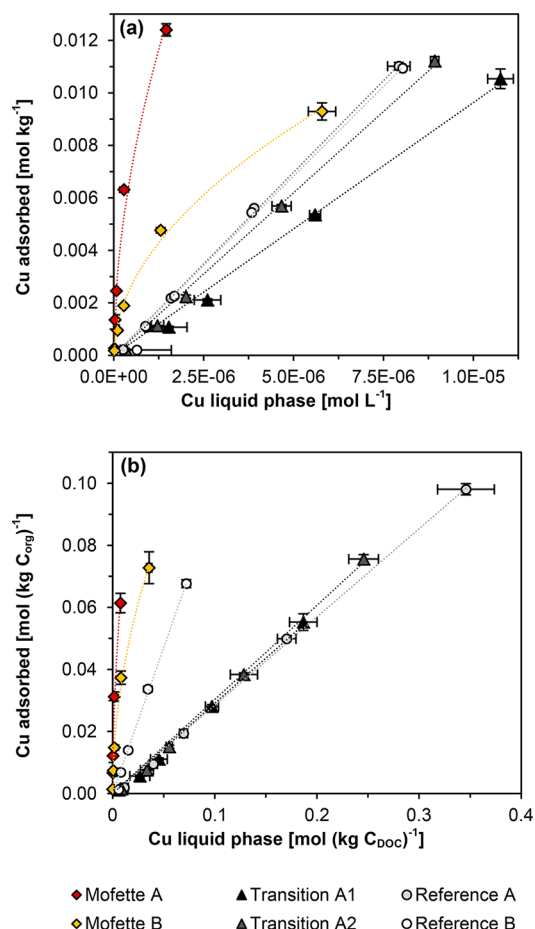


Figure 2. (a) Cu sorption isotherms determined at $\text{pH } 4.5 \pm 0.1$ at a soil-to-solution-ratio of approximately 1:30 with 5 mM NaCl as background electrolyte under anoxic conditions. Initial Cu soil concentrations are not included. (b) Same Cu sorption isotherms plotted normalized against the DOC concentration for the liquid phase and against total soil C_{org} for the solid phase. Symbols are measured data, dashed lines are calculated isotherms.

Isotherms for Mofette A and B were best fitted using a Freundlich isotherm with $q = K_F \times c^N$ (where q is the adsorbed Cu content in mol kg^{-1} , c is the dissolved Cu concentration in mol L^{-1} , N is a parameter describing the curvature of the isotherm, K_F is the Freundlich coefficient; $N = 0.53$ and 0.51 , $K_F = 16.7$ and 4.6 L kg^{-1} for Mofette A and B, respectively). Samples from the Transition and Reference sites showed linear adsorption behavior ($N = 1$; linear adsorption coefficients $K_{\text{linear}} = 963, 1238, 1395,$ and 1365 L kg^{-1} for Transition A1, A2, Reference A, and B, respectively). Interestingly, Cu adsorption was lowest at moderate CO_2 soil concentrations, i.e., in Transitions A1 ($p(\text{CO}_2) 0.556$, $p(\text{O}_2) 0.089$) and A2 ($p(\text{CO}_2) 0.072$, $p(\text{O}_2) 0.198$), which at first glance contradicts the hypothesis of stronger Cu adsorption in soils with higher

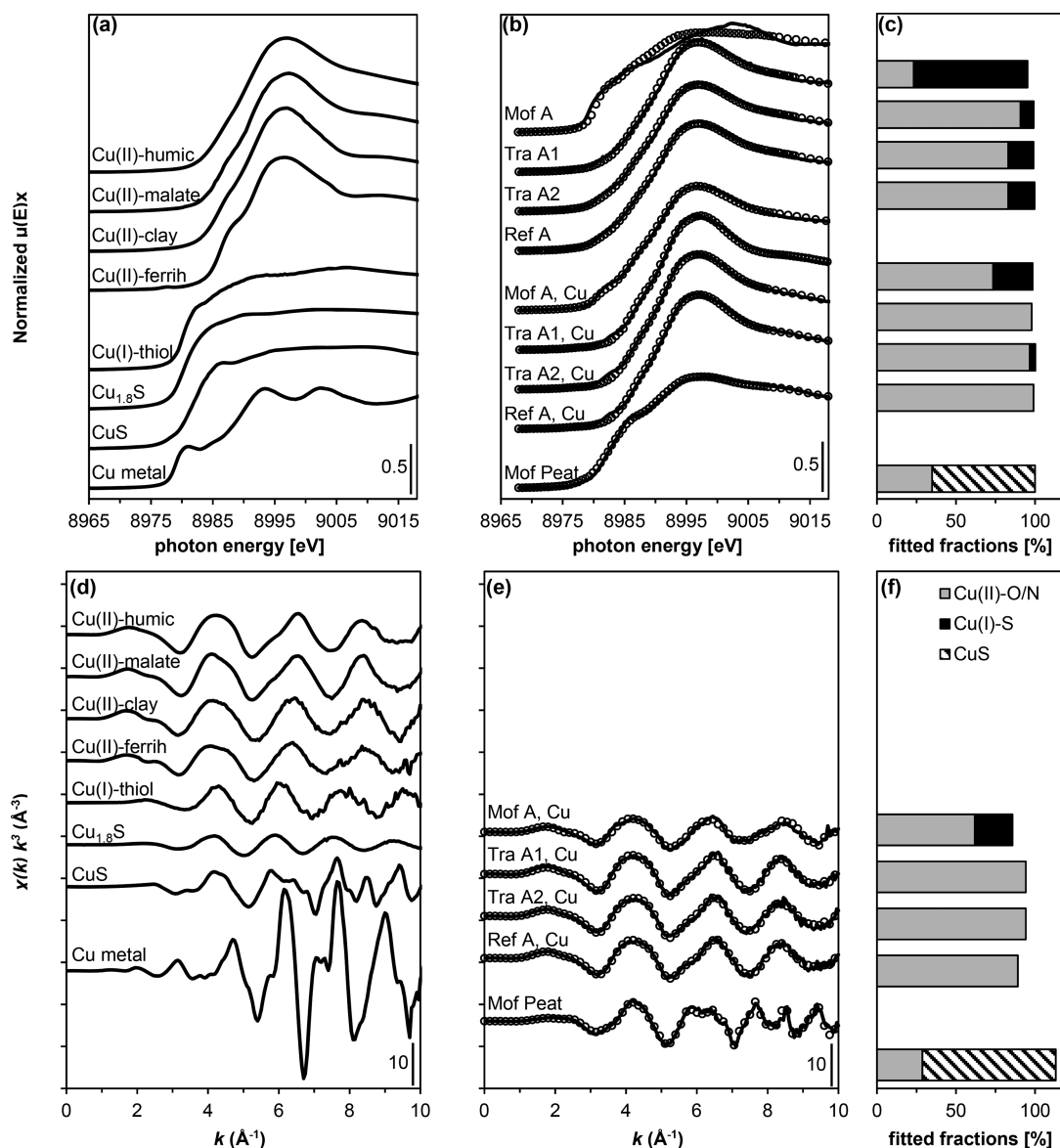


Figure 3. (a,b) Normalized Cu K-edge XANES spectra and (d,e) k^3 -weighted EXAFS spectra of Cu reference compounds (a,d) and sample spectra (d,e) with best LCF spectra (symbols). (c,f) Cu redox speciation in samples based on LCF of normalized XANES spectra in the energy range 8968–9018 eV (c) and of k^3 -weighted EXAFS spectra in the k -range 2.5–10 \AA^{-1} (f) (detailed results in Table S4, SI). Individual fractions were constrained to values between 0 and 1, the sum of fractions was not constrained. Cu(II)-ferrih = Cu(II)-ferrihydrite, Mof = Mofette, Tra = Transition, Ref = Reference, and Cu = Cu(II)-spiked samples.

SOM content. The two References A and B, however, plotted almost exactly on the same line.

Replotting the isotherms normalized against C_{org} content in soil solid phases and DOC concentration in the liquid phases, assuming organic matter to be the dominating binding partner for Cu, showed even more pronounced differences between mofette centers and all other soils (Figure 2b, C_{org} and DOC concentrations in Figure S3, SI). While the difference between Mofettes A and B became smaller, the isotherms of Transitions A1, A2, and Reference A even plotted on the same line having more or less identical adsorption coefficients ($K_{\text{linear}} = 0.291, 0.303, \text{ and } 0.285 \text{ kg } C_{\text{DOC}} (\text{kg } C_{\text{org}})^{-1}$). This observation implies that Cu adsorption to SOM is the most important sorption mechanism in all samples outside the mofette center investigated here. Copper sorption followed a linear isotherm, and no saturation occurred at the Cu loadings tested in this experiment. Maximum Cu loadings used in this study were well

below literature values of sorption capacities reported for humic substances (e.g., in Christl and Kretzschmar⁶² 3.1 and 2.7 mol kg^{-1} for humic, and 6.0 and 2.7 mol kg^{-1} for fulvic acid, for low and high affinity sites, respectively, according to the NICA-Donnan model). In this study, we did not distinguish between free and complexed Cu in the liquid phase. Thus, the presence of free Cu^{2+} in solution cannot be excluded, especially for samples with high Cu spikes. However, the almost identical sorption isotherms when normalizing Cu sorption data to C_{org} and DOC (Figure 2b) imply that Cu-DOM complexes played a dominant role. Only Reference B did not fit to Transitions A1, A2, and Reference A, showing a higher K_{linear} ($0.925 \text{ kg } C_{\text{DOC}} (\text{kg } C_{\text{org}})^{-1}$) than the other soils. Since Site B was sampled in September while Site A was sampled in February, seasonal differences in DOM quantity and quality (compare Table S1, Figures S3 and S4, SI) might

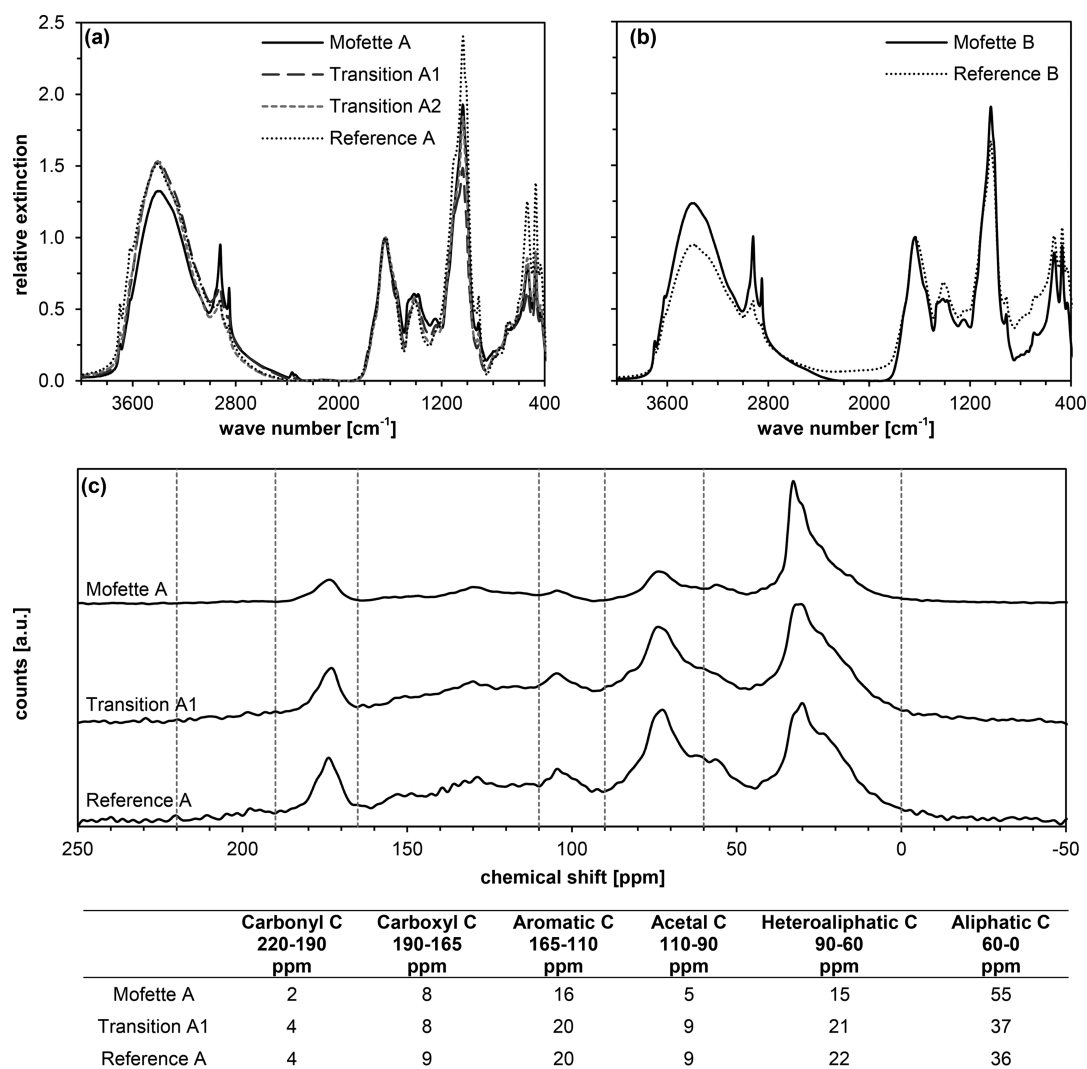


Figure 4. Organic matter quality: (a,b) FTIR spectra of freeze-dried DOM water extracts from Site A (a) and Site B (b) normalized to the peak at 1635 cm^{-1} . A detail from the spectra wavenumber region $1000\text{--}1800\text{ cm}^{-1}$ can be found in Figure S4, SI. (c) ^{13}C NMR spectra of soil from Mofette A, Transition A1, and Reference A with the respective relative contents of organic species derived from integrating areas of ^{13}C NMR spectra.

contribute to this discrepancy, but further research is needed to elucidate the exact processes.

To clarify which processes caused the completely different Cu sorption behavior in Mofette A and B compared to the other soils, we investigated the Cu solid-phase speciation.

Copper Binding to SOM and Mineral Precipitation. As already expected from their similar sorption behavior, the Cu solid-phase speciation in Transitions A1, A2, and Reference A was more or less identical. All XANES spectra showed an absorption maximum around 8988 eV (Figure 3a) indicative of the $1s \rightarrow 4p$ transition in Cu(II) coordinated to 6 oxygen/nitrogen atoms in a Jahn–Teller-distorted tetragonal configuration.⁶³ Principal component analysis of both XANES and EXAFS spectra indicated the dominance of one component ($>98.7\%$ for XANES, Table S3, SI). The best fits with normalized sum-squared residuals (NSSR) $< 0.2\%$ for XANES and $\leq 3\%$ for EXAFS were achieved with references of Cu(II) adsorbed to organic matter (*Cu(II)-humic*, *Cu(II)-malate*, *Cu(II)-carboxyl*, Figure 3c,f). However, for EXAFS fitting the difference to linear combination fits (LCF) including other oxygen/nitrogen-coordinated Cu(II) compounds was not

significant according to the Hamilton test,^{64,65} (cf. Section S.8, SI). This confirmed that Cu(II) bound to SOM was the dominating Cu species in natural soil samples from these sites and that the experimentally spiked Cu(II) was also predominantly adsorbed to SOM. The importance of SOM for Cu(II) sorption in soils is well-known.^{4,16,66–68} The Cu(II) binding mainly occurs via five- to six-membered ring chelates formed by closely spaced hydroxylic and carboxylic groups, building an octahedron of oxygen ions around the Cu(II) ion, which geometrically fits perfectly into this structure.^{9,10} The fact that the Cu sorption isotherms did not show any evidence for saturation, even at the highest Cu loadings, shows that there were still potential sorption sites on the SOM. Thus, moderate $p(\text{CO}_2)$ did not affect qualitative SOM composition in a way that influenced Cu adsorption potential directly. Small amounts ($<17\%$) of $\text{Cu}_{1.8}\text{S}$ in LCFs of these samples might be an artifact from radiation-induced Cu reduction, which mainly occurred during measurements at beamline 4–3 (details in Section S.8, SI).

In Mofette A the Cu solid-phase speciation differed from that of the other soils: XANES fitting of the initial sample

revealed the presence of 72% sulfur-coordinated Cu(I). Also the spiked Cu(II) seems to have been partially reduced, leading to 25% sulfur-coordinated Cu(I) besides Cu(II) binding to oxygen/nitrogen in the Cu-spiked sample (Figure 3c). Due to the complex sample matrix, there was no statistically significant difference between fits including $Cu_{1.8}S$ or *Cu(I)-thiol* as reference compound for sulfur-coordinated Cu(I). However, the effective removal of Cu from the liquid phase despite high DOC concentrations (Figure S3, SI) suggests that precipitation of Cu(I) sulfide minerals was more important than Cu(I) adsorption to thiol groups on SOM. We also analyzed a peat sample from 2 m depth of Mofette A, which had shown an enrichment with several metal(loid)s, including Cu, in a prior study.⁵² Linear combination fitting of XANES and EXAFS spectra now revealed that Cu(II) binding to SOM was not the dominating Cu sequestering process but that most Cu was instead present as CuS (covellite, 65% according to XANES LCF, Figure 3c). This can be seen in the XANES spectrum by a shift of the main absorption edge to lower energies around 8982–8984 eV^{9,63} (Figure 3b).

The formation of Cu(I) sulfide minerals requires prior reduction of Cu(II) and the presence of sulfide.³⁴ We could detect free sulfide concentrations of 60 μ M in the pore water sample from 10 to 15 cm depth of Mofette A (data not shown). The presence of sulfate-reducing bacteria has previously been shown for this mofette site.^{53,69} Even if we could neither detect free sulfide nor Cu(I) photometrically during the sorption experiment, it is likely that Cu(II) reduction occurred, however, liquid phase concentration might have remained low due to fast precipitation. Formation of Cu sulfides has been shown to occur in soils even at low available sulfide levels, which is attributed to the low solubility of Cu sulfide minerals.^{20,31,35} We also detected a small metallic Cu particle in the Cu-loaded Mofette A sample by SEM-EDS (details in Section S.7, SI). Precipitation of metallic Cu(0) can occur if aqueous Cu(I) formed by (microbial) reduction of Cu(II) is not stabilized by complexation, e.g., with sulfide, but disproportionates into Cu(II) and Cu(0).^{18,20,31,70} However, since LCFs of this sample did not confirm the presence of metallic Cu(0), contributions must have been low.

A mixture of adsorption and precipitation processes can explain the differing shape of the sorption isotherms of Mofette A and B in comparison to transitions and references (Figure 2), assuming a dominance of Cu reduction and following precipitation at low spikes and a mixture of precipitation and adsorption at higher spikes.

Effects of Organic Matter Quality on Cu Mobility. To further clarify the reasons for differing Cu sorption behavior despite similar XAS solid-phase speciation in soils with low (References) and moderate (Transitions) $p(CO_2)$ (Figure 2a), we further investigated organic matter quality, both for DOM and SOM.

Differences between FTIR spectra of DOM water extracts were relatively small (Figure 4a,b). Especially Transition A1, A2, and References A and B followed almost the same line (detailed band assignments in Section S.5, SI). The same accounted for SOM, where areal contributions of C in different functional groups determined by ¹³C NMR for Transition A1 and Reference A were almost equal (Figure 4c).

Both DOM and SOM, however, differed in samples from degassing centers (Mofette A and B) compared to transitions and references. In FTIR spectra of DOM water extracts, bands indicative of aromatic structures (1720, 1240 cm^{-1}), aliphatic

structures (1450 cm^{-1}), and polypeptides (1550 cm^{-1}) were more pronounced whereas the band at 1090 cm^{-1} , indicative of polysaccharides, was less pronounced compared to the other samples. The ratio of the peak heights at 2960 and 2920 cm^{-1} (asymmetric stretching of R–CH₃ and R–CH₂, respectively), which can be used as a measure of aliphatic chain length,⁷¹ was lower for Mofette A and B indicating longer aliphatic chains due to decreased decomposition.⁴⁸ Accordingly, we detected a higher relative fraction of aliphatic C in the ¹³C NMR spectrum of Mofette A soil in comparison to Transition A1 and Reference A (Figure 4c). Rennert et al.⁴⁸ observed accumulation of less degraded plant material (alkyl C like in lignin) under higher $p(CO_2)$ and less transfer of SOM into the clay fraction. They also showed that microbial formation of polysaccharides and polypeptides and their accumulation in the clay fraction is reduced. A less pronounced shoulder indicative of polysaccharides and more pronounced features indicative of aromatic structures such as lignin and of longer aliphatic chain lengths could also be observed in our study in the FTIR spectra of DOM from mofette centers. Aliphatic compounds in DOM have a lower binding affinity for Cu⁷² which may have contributed to lower dissolved Cu concentrations in mofette samples. Very recently, Rennert⁷³ reported a negative correlation between $p(CO_2)$ and the abundance of carboxyl groups in particulate SOM in a transect from a mofette site, an observation that could be relevant for Cu(II), since carboxylic groups are involved in its complexation by SOM.^{9,10} However, SOM quality differences do not seem to have affected Cu sorption in the concentration range tested in this study since XAS solid-phase speciation showed the same mode of Cu(II) binding. Therefore, the strongly increased Cu sequestration in mofette centers was likely caused by additional Cu(II) reduction and precipitation as Cu(I) sulfides.

Since the qualitative composition of both SOM and DOM in samples from low to moderate $p(CO_2)$ showed no significant differences, the observed differences in K_{linear} for Cu sorption (Figure 2a) must have been exclusively caused by different ratios of dissolved to solid-phase organic matter. Rennert and Pfanz⁴⁹ observed a strong relationship between the amount of particulate SOM and $p(CO_2)$. From this fact and from the previously mentioned decreased accumulation of SOM in the clay fraction they concluded that the reactivity of SOM is decreased, even under moderate $p(CO_2)$, which would facilitate potential release of DOM. Also lower contents of Fe (oxyhydr)oxides and clay minerals (Table 1, Section S.6, SI), which are able to stabilize SOM by surface interactions,⁷⁴ might contribute to an increasing DOM release with increasing $p(CO_2)$.^{48,49} This is in line with observations in our sorption study where DOM formation during the experiment as well as DOC:SOC ratio increased in the order: Reference A < Transition A1 < Transition A2 < Mofette A (Figure S3, SI). The reported negative effect of CO₂ on the interaction of SOM with soil minerals^{48,49} and a resulting higher proportion of Cu(II)-DOM complexes thus explains the observed decrease of Cu sorption coefficients in the order Reference A > Transition A1 > Transition A2 (Figure 2a). All isotherms plotted on the same line when sorption was normalized against total organic C (Figure 2b). These findings are in line with the observations of Degryse et al.⁷⁵ who showed that Cu partitioning between the solid phase and the pore water can be modeled quite well just using the DOC:SOC ratio in natural soils. The fact that Reference B did not follow the same

adsorption isotherm could indicate a seasonal influence on both DOM and SOM quality and quantity and, thus, on Cu mobility.

Implications for Copper Mobility in Mofettes and in Other Soils. The general assumption that higher SOM content increases Cu adsorption also holds true for mofette soils, but an increased release of DOM under high $p(\text{CO}_2)$ and the formation of Cu-DOM complexes can enhance overall Cu mobility. Formation of DOM in our experiment might have been overestimated compared to natural conditions, where cation bridging to clay minerals by exchangeable aluminum was recently proposed to be involved in SOM stabilization.⁷³ Cu adsorption did not seem to be affected by bulk structural SOM quality, which was rather similar at moderate to low $p(\text{CO}_2)$. Differences concerning functional groups, especially the recently described reduced content of carboxylic groups in particulate SOM formed under increased $p(\text{CO}_2)$,⁷³ might, however, become relevant at higher Cu loadings or in the presence of competing divalent cations, since these groups are known to be the dominant binding site for Cu(II).⁹

In degassing centers, the formation of Cu(I) mineral phases limited Cu mobility rather than adsorption to SOM due to the permanently anoxic conditions at $p(\text{CO}_2)$ of almost 1. It is likely that other chalcophilic metal(loid)s (e.g., Cd, Pb, Hg, at increased sulfide contents also Fe and As) can precipitate in mofettes as well. The presence of pyrite in deeper layers of mofettes has already been evidenced^{47,76} and the comparably high As concentrations in the peat lens in 2 m depth of Mofette A observed in Mehlhorn et al.⁵² might be partly caused by (co)precipitation of As sulfide minerals³³ or binding via thiol groups of SOM.⁷⁷

The estimated potential maximum Cu sequestration along the transect from low to high $p(\text{CO}_2)$, presented in a conceptual model in Figure 5, fits well to the observations

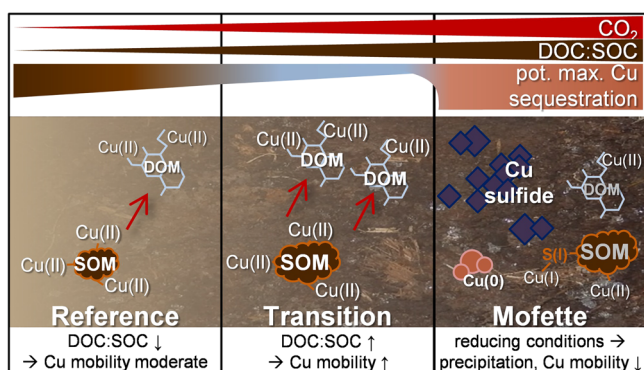


Figure 5. Conceptual model of Cu behavior in soils under the influence of geogenic CO_2 , going from low (Reference, left) to high soil CO_2 contents (Mofette, right). DOC:SOC = dissolved to solid-phase ratio of organic carbon, pot. max. Cu sequestration = potential maximum Cu sequestration including adsorption and precipitation processes.

from our field study: lowest Cu soil contents were detected in the transition zone, where Cu is most mobile (highest pore water Cu concentrations) due to complexation with DOM at high DOC:SOC ratios (Figure 1, Figure 5). Permanent Cu sequestration due to precipitation should, however, have led to even higher Cu soil contents in the degassing center than observed in our study. It is likely that Cu, released by weathering processes in deeper sediment layers and then

transported upward with groundwater flow, is already sequestered at greater depths, e.g., in the mentioned, sulfide-rich peat lens, limiting the Cu supply toward the topsoil. However, further research is needed to clarify the influence of translocation processes on Cu sequestration.

Similar processes influencing Cu mobility might occur at other sites exhibiting a temporal or spatial redox and/or SOM gradient. A decreased Cu bioavailability due to mineral precipitation under permanently anoxic conditions, as they may occur, e.g., in the center of organic contaminant spills or during flooding of wetland soils, can become a problem for certain microbes with an essential need for Cu, e.g., for methane-oxidizing bacteria.⁷⁸ An increased Cu mobility due to Cu-DOM complexation may become problematic at Cu-contaminated sites. According to our study, the highest Cu mobility can be expected in transition zones or transition times between oxic and permanently anoxic conditions. There, SOM decomposition and stabilization is slowed down due to limited oxygen supply and Cu-DOM complexes can form, but suboxic conditions hinder effective Cu sequestration by precipitation of sulfide minerals. Besides oxygen availability, numerous other factors can influence DOC:SOC ratios and sulfide occurrence along redox gradients, making the assessment of Cu mobility in such soils a complex issue and necessitating further research on interactions and influencing processes.

■ ASSOCIATED CONTENT

Supporting Information

The Supporting Information is available free of charge on the ACS Publications website at DOI: 10.1021/acs.est.8b02668.

Details on kinetics of Cu sorption, pH, DOM mobilization, organic acids in DOM, calculation of CO_2 concentrations, ^{13}C NMR analyses, FTIR analyses of DOM extracts, soil mineralogy determined by XRD, SEM-EDS analyses, SEM image of the Cu(0) particle and corresponding EDS spectra, and additional information on XAS measurements (PDF)

■ AUTHOR INFORMATION

Corresponding Author

*Phone: +49 921 55 3999; e-mail: b.planer-friedrich@uni-bayreuth.de (B.P.-F.).

ORCID

Britta Planer-Friedrich: 0000-0002-0656-4283

Notes

The authors declare no competing financial interest.

■ ACKNOWLEDGMENTS

We acknowledge financial support for a PhD stipend to Judith Mehlhorn from the German Academic Scholarship Foundation as well as by a DAAD mobility grant (No. 57315737) for travels to the U.S.A. We acknowledge the Stanford Synchrotron Radiation Lightsource (SSRL), SLAC National Accelerator Laboratory, supported by the U.S. Department of Energy, Office of Science, Office of Basic Energy Sciences under Contract No. DE-AC02-76SF00515. We are grateful to Matthew Latimer and Eric Nelson for support at beamline 4-3. From University of Bayreuth, we thank Beate Bojer (Inorganic Chemistry III) for NMR measurements, Dorothea Wiesner (BGI) for help with SEM-EDS, Tiziana Boffa Ballaran (BGI) for XRD measurements, Benjamin Gilfedder and Silke

Hammer (Hydrology) for providing access to GC, Heidi Zier (Hydrology) for FTIR measurements, Oliver Schmidt and Anita Gössner (Ecological Microbiology) for organic acid analysis, Manfred Fischer (Geomorphology), Ruth Freitag and Nicolas Weithmann (Process Biotechnology) for borrowing equipment, Nadja Knauer, Esther Breuninger, and Lukas Gerber for assistance during sampling and experiments. We acknowledge helpful discussions with Egbert Matzner (Soil Ecology) and Martin Obst (Experimental Biogeochemistry).

REFERENCES

- Rubino, J. T.; Franz, K. J. Coordination chemistry of copper proteins: how nature handles a toxic cargo for essential function. *J. Inorg. Biochem.* **2012**, *107* (1), 129–143.
- Flemming, C.; Trevors, J. Copper toxicity and chemistry in the environment: a review. *Water, Air, Soil Pollut.* **1989**, *44* (1–2), 143–158.
- McBride, M.; Sauve, S.; Hendershot, W. Solubility control of Cu, Zn, Cd and Pb in contaminated soils. *Eur. J. Soil Sci.* **1997**, *48* (2), 337–346.
- McLaren, R. G.; Crawford, D. V. Studies on soil copper II. The specific adsorption of copper by soils. *J. Soil Sci.* **1973**, *24* (4), 443–452.
- McLaren, R.; Williams, J.; Swift, R. Some observations on the desorption and distribution behaviour of copper with soil components. *J. Soil Sci.* **1983**, *34* (2), 325–331.
- Hering, J. G.; Morel, F. M. Humic acid complexation of calcium and copper. *Environ. Sci. Technol.* **1988**, *22* (10), 1234–1237.
- Kinniburgh, D. G.; van Riemsdijk, W. H.; Koopal, L. K.; Borkovec, M.; Benedetti, M. F.; Avena, M. J. Ion binding to natural organic matter: competition, heterogeneity, stoichiometry and thermodynamic consistency. *Colloids Surf., A* **1999**, *151* (1), 147–166.
- Flogeac, K.; Guillon, E.; Aplincourt, M. Surface complexation of copper (II) on soil particles: EPR and XAFS studies. *Environ. Sci. Technol.* **2004**, *38* (11), 3098–3103.
- Manceau, A.; Matynia, A. The nature of Cu bonding to natural organic matter. *Geochim. Cosmochim. Acta* **2010**, *74* (9), 2556–2580.
- Karlsson, T.; Persson, P.; Skyllberg, U. Complexation of copper(II) in organic soils and in dissolved organic matter – EXAFS evidence for chelate ring structures. *Environ. Sci. Technol.* **2006**, *40* (8), 2623–2628.
- McBride, M. Reactions controlling heavy metal solubility in soils. In *Adv. Soil Sci.*; Springer: 1989; pp 1–56.
- Strawn, D. G.; Palmer, N. E.; Furnare, L. J.; Goodell, C.; Amonette, J. E.; Kukkadapu, R. K. Copper sorption mechanisms on smectites. *Clays Clay Miner.* **2004**, *52* (3), 321–333.
- Parkman, R.; Charnock, J.; Bryan, N.; Livens, F.; Vaughan, D. Reactions of copper and cadmium ions in aqueous solution with goethite, lepidocrocite, mackinawite, and pyrite. *Am. Mineral.* **1999**, *84* (3), 407–419.
- Fischer, L.; Brümmer, G. W.; Barrow, N. J. Observations and modelling of the reactions of 10 metals with goethite: adsorption and diffusion processes. *Eur. J. Soil Sci.* **2007**, *58* (6), 1304–1315.
- Tiberg, C.; Sjöstedt, C.; Persson, I.; Gustafsson, J. P. Phosphate effects on copper(II) and lead(II) sorption to ferrihydrite. *Geochim. Cosmochim. Acta* **2013**, *120*, 140–157.
- Strawn, D. G.; Baker, L. L. Speciation of Cu in a contaminated agricultural soil measured by XAFS, μ -XAFS, and μ -XRF. *Environ. Sci. Technol.* **2008**, *42* (1), 37–42.
- Sugio, T.; Tsujita, Y.; Inagaki, K.; Tano, T. Reduction of cupric ions with elemental sulfur by *Thiobacillus ferrooxidans*. *Appl. Environ. Microbiol.* **1990**, *56* (3), 693–696.
- Hofacker, A. F.; Behrens, S.; Voegelin, A.; Kaegi, R.; Lösekann-Behrens, T.; Kappler, A.; Kretzschmar, R. *Clostridium* species as metallic copper-forming bacteria in soil under reducing conditions. *Geomicrobiol. J.* **2015**, *32* (2), 130–139.
- Wakatsuki, T. Metal oxidoreduction by microbial cells. *J. Ind. Microbiol.* **1995**, *14* (2), 169–177.
- Weber, F.-A.; Voegelin, A.; Kaegi, R.; Kretzschmar, R. Contaminant mobilization by metallic copper and metal sulphide colloids in flooded soil. *Nat. Geosci.* **2009**, *2* (4), 267–271.
- Matocha, C.; Karathanasis, A.; Rakshit, S.; Wagner, K. Reduction of copper(II) by iron(II). *J. Environ. Qual.* **2005**, *34* (5), 1539–1546.
- Fulda, B.; Voegelin, A.; Maurer, F.; Christl, I.; Kretzschmar, R. Copper redox transformation and complexation by reduced and oxidized soil humic acid. 1. X-ray absorption spectroscopy study. *Environ. Sci. Technol.* **2013**, *47* (19), 10903–10911.
- Pham, A. N.; Rose, A. L.; Waite, T. D. Kinetics of Cu(II) reduction by natural organic matter. *J. Phys. Chem. A* **2012**, *116* (25), 6590–6599.
- Maurer, F.; Christl, I.; Fulda, B.; Voegelin, A.; Kretzschmar, R. Copper redox transformation and complexation by reduced and oxidized soil humic acid. 2. Potentiometric titrations and dialysis cell experiments. *Environ. Sci. Technol.* **2013**, *47* (19), 10912–10921.
- Borch, T.; Kretzschmar, R.; Kappler, A.; Cappellen, P. V.; Ginder-Vogel, M.; Voegelin, A.; Campbell, K. Biogeochemical redox processes and their impact on contaminant dynamics. *Environ. Sci. Technol.* **2010**, *44* (1), 15–23.
- Du Laing, G.; Vanthuyne, D.; Vandecasteele, B.; Tack, F.; Verloo, M. Influence of hydrological regime on pore water metal concentrations in a contaminated sediment-derived soil. *Environ. Pollut.* **2007**, *147* (3), 615–625.
- Kirk, G. *The Biogeochemistry of Submerged Soils*; John Wiley & Sons: 2004.
- Lettr, R.; Fletcher, W. Syngenetic sulphide minerals in a copper-rich bog. *Miner. Deposita* **1980**, *15* (1), 61–67.
- Lovering, T. S. *Organic Precipitation of Metallic Copper*; US Government Printing Office: 1927.
- Fulda, B.; Voegelin, A.; Ehlert, K.; Kretzschmar, R. Redox transformation, solid phase speciation and solution dynamics of copper during soil reduction and reoxidation as affected by sulfate availability. *Geochim. Cosmochim. Acta* **2013**, *123*, 385–402.
- Hofacker, A. F.; Voegelin, A.; Kaegi, R.; Weber, F.-A.; Kretzschmar, R. Temperature-dependent formation of metallic copper and metal sulfide nanoparticles during flooding of a contaminated soil. *Geochim. Cosmochim. Acta* **2013**, *103*, 316–332.
- Patrick, R.; Mosselmann, J.; Charnock, J.; England, K.; Helz, G.; Garner, C.; Vaughan, D. The structure of amorphous copper sulfide precipitates: An X-ray absorption study. *Geochim. Cosmochim. Acta* **1997**, *61* (10), 2023–2036.
- Morse, J.; Luther, G. Chemical influences on trace metal-sulfide interactions in anoxic sediments. *Geochim. Cosmochim. Acta* **1999**, *63* (19), 3373–3378.
- Luther, G. W.; Theberge, S. M.; Rozan, T. F.; Rickard, D.; Rowlands, C.; Oldroyd, A. Aqueous copper sulfide clusters as intermediates during copper sulfide formation. *Environ. Sci. Technol.* **2002**, *36* (3), 394–402.
- Weber, F.-A.; Voegelin, A.; Kretzschmar, R. Multi-metal contaminant dynamics in temporarily flooded soil under sulfate limitation. *Geochim. Cosmochim. Acta* **2009**, *73* (19), 5513–5527.
- Sharma, V. K.; Millero, F. J. Oxidation of copper(I) in seawater. *Environ. Sci. Technol.* **1988**, *22* (7), 768–771.
- Fenwick, F. The equilibrium between cupric ion, cuprous ion and metallic copper. *J. Am. Chem. Soc.* **1926**, *48* (4), 860–870.
- Yuan, X.; Pham, A. N.; Xing, G.; Rose, A. L.; Waite, T. D. Effects of pH, chloride, and bicarbonate on Cu(I) oxidation kinetics at circumneutral pH. *Environ. Sci. Technol.* **2012**, *46* (3), 1527–1535.
- Leal, M. F. C.; Van Den Berg, C. M. Evidence for strong copper(I) complexation by organic ligands in seawater. *Aquat. Geochem.* **1998**, *4* (1), 49–75.
- Laglera, L. M.; van den Berg, C. M. Copper complexation by thiol compounds in estuarine waters. *Mar. Chem.* **2003**, *82* (1), 71–89.

- (41) Blume, H.-P.; Felix-Henningsen, P. Reductosols: Natural soils and Technosols under reducing conditions without an aquatic moisture regime. *J. Plant Nutr. Soil Sci.* **2009**, *172* (6), 808–820.
- (42) Lewicki, J. L.; Birkholzer, J.; Tsang, C.-F. Natural and industrial analogues for leakage of CO₂ from storage reservoirs: identification of features, events, and processes and lessons learned. *Environ. Geol.* **2007**, *52* (3), 457–467.
- (43) Bräuer, K.; Kämpf, H.; Niedermann, S.; Strauch, G.; Weise, S. M. Evidence for a nitrogen flux directly derived from the European subcontinental mantle in the Western Eger Rift, central Europe. *Geochim. Cosmochim. Acta* **2004**, *68* (23), 4935–4947.
- (44) Kämpf, H.; Geissler, W. H.; Bräuer, K. Combined gas-geochemical and receiver function studies of the Vogtland/NW Bohemia intraplate mantle degassing field, central Europe. In *Mantle Plumes*; Ritter, J. R. R., Christensen, U. R., Eds.; Springer: Berlin Heidelberg, 2007; pp 127–158.
- (45) Maček, I.; Videmšek, U.; Kastelec, D.; Stopar, D.; Vodnik, D. Geological CO₂ affects microbial respiration rates in Stavešinci mofette soils. *Acta Biol. Slov* **2009**, *52* (2), 41–48.
- (46) Videmšek, U.; Hagn, A.; Suhadolc, M.; Radl, V.; Knicker, H.; Schloter, M.; Vodnik, D. Abundance and diversity of CO₂-fixing bacteria in grassland soils close to natural carbon dioxide springs. *Microb. Ecol.* **2009**, *58* (1), 1–9.
- (47) Flechsig, C.; Bussert, R.; Rechner, J.; Schütze, C.; Kämpf, H. The Hartoušov mofette field in the Cheb Basin, western Eger Rift (Czech Republic): a comparative geoelectric, sedimentologic and soil gas study of a magmatic diffuse CO₂-degassing structure. *Z. Geol. Wiss* **2008**, *36* (3), 177–193.
- (48) Rennert, T.; Eusterhues, K.; Pfanz, H.; Totsche, K. U. Influence of geogenic CO₂ on mineral and organic soil constituents on a mofette site in the NW Czech Republic. *Eur. J. Soil Sci.* **2011**, *62* (4), 572–580.
- (49) Rennert, T.; Pfanz, H. Geogenic CO₂ affects stabilization of soil organic matter. *Eur. J. Soil Sci.* **2015**, *66* (5), 838–846.
- (50) Ross, D. J.; Tate, K. R.; Newton, P. C. D.; Wilde, R. H.; Clark, H. Carbon and nitrogen pools and mineralization in a grassland gley soil under elevated carbon dioxide at a natural CO₂ spring. *Global Change Biol.* **2000**, *6* (7), 779–790.
- (51) Bankwitz, P.; Schneider, G.; Kämpf, H.; Bankwitz, E. Structural characteristics of epicentral areas in Central Europe: study case Cheb Basin (Czech Republic). *J. Geodyn* **2003**, *35* (1–2), 5–32.
- (52) Mehlhorn, J.; Beulig, F.; Küsel, K.; Planer-Friedrich, B. Carbon dioxide triggered metal(loid) mobilisation in a mofette. *Chem. Geol.* **2014**, *382*, 54–66.
- (53) Beulig, F.; Urich, T.; Nowak, M.; Trumbore, S. E.; Gleixner, G.; Gilfillan, G. D.; Fjelland, K. E.; Küsel, K. Altered carbon turnover processes and microbiomes in soils under long-term extremely high CO₂ exposure. *Nat. Microbiol* **2016**, *1*, 15025.
- (54) Hesslein, R. H. An in situ sampler for close interval pore water studies. *Limnol. Oceanogr.* **1976**, *21* (6), 912
- (55) Rennert, T.; Eusterhues, K.; De Andrade, V. D.; Totsche, K. U. Iron species in soils on a mofette site studied by Fe K-edge X-ray absorption near-edge spectroscopy. *Chem. Geol.* **2012**, *332*–333, 116–123.
- (56) Mehlhorn, J.; Byrne, J. M.; Kappler, A.; Planer-Friedrich, B. Time and temperature dependency of carbon dioxide triggered metal(loid) mobilization in soil. *Appl. Geochem.* **2016**, *74*, 122–137.
- (57) Beaubien, S.; Ciotoli, G.; Coombs, P.; Dictor, M. C.; Krüger, M.; Lombardi, S.; Pearce, J.; West, J. The impact of a naturally occurring CO₂ gas vent on the shallow ecosystem and soil chemistry of a Mediterranean pasture (Latera, Italy). *Int. J. Greenhouse Gas Control* **2008**, *2* (3), 373–387.
- (58) Sander, R. Compilation of Henry's law constants (version 4.0) for water as solvent. *Atmos. Chem. Phys.* **2015**, *15* (8), 4399
- (59) Cline, J. D. Spectrophotometric determination of hydrogen sulfide in natural waters. *Limnol. Oceanogr.* **1969**, *14* (3), 454–458.
- (60) Moffett, J. W.; Zika, R. G.; Petasne, R. G. Evaluation of bathocuproine for the spectro-photometric determination of copper-
- (I) in copper redox studies with applications in studies of natural waters. *Anal. Chim. Acta* **1985**, *175*, 171–179.
- (61) Artz, R. R.; Chapman, S. J.; Robertson, A. H. J.; Potts, J. M.; Laggoun-Défarge, F.; Gogo, S.; Comont, L.; Disnar, J.-R.; Francez, A.-J. FTIR spectroscopy can be used as a screening tool for organic matter quality in regenerating cutover peatlands. *Soil Biol. Biochem.* **2008**, *40* (2), 515–527.
- (62) Christl, I.; Kretzschmar, R. Relating ion binding by fulvic and humic acids to chemical composition and molecular size. 1. Proton binding. *Environ. Sci. Technol.* **2001**, *35* (12), 2505–2511.
- (63) Kau, L. S.; Spira-Solomon, D. J.; Penner-Hahn, J. E.; Hodgson, K. O.; Solomon, E. I. X-ray absorption edge determination of the oxidation state and coordination number of copper. Application to the type 3 site in *Rhus vernicifera* laccase and its reaction with oxygen. *J. Am. Chem. Soc.* **1987**, *109* (21), 6433–6442.
- (64) Hamilton, W. C. Significance tests on the crystallographic R factor. *Acta Crystallogr.* **1965**, *18* (3), 502–510.
- (65) Calvin, S. *XAFS for Everyone*; CRC Press: 2013.
- (66) Brown, P. A.; Gill, S. A.; Allen, S. J. Metal removal from wastewater using peat. *Water Res.* **2000**, *34* (16), 3907–3916.
- (67) Kumpiene, J.; Lagerkvist, A.; Maurice, C. Stabilization of Pb- and Cu-contaminated soil using coal fly ash and peat. *Environ. Pollut.* **2007**, *145* (1), 365–373.
- (68) Strawn, D. G.; Baker, L. L. Molecular characterization of copper in soils using X-ray absorption spectroscopy. *Environ. Pollut.* **2009**, *157* (10), 2813–2821.
- (69) Krauze, P.; Kämpf, H.; Horn, F.; Liu, Q.; Voropaev, A.; Wagner, D.; Alawi, M. Microbiological and geochemical survey of CO₂-dominated mofette and mineral waters of the Cheb Basin, Czech Republic. *Front. Microbiol.* **2017**, *8*, 2446.
- (70) Xia, B.; Qiu, H.; Knorr, K.-H.; Blodau, C.; Qiu, R. Occurrence and fate of colloids and colloid-associated metals in a mining-impacted agricultural soil upon prolonged flooding. *J. Hazard. Mater.* **2018**, *348*, 56–66.
- (71) Ibarra, J.; Munoz, E.; Moliner, R. FTIR study of the evolution of coal structure during the coalification process. *Org. Geochem.* **1996**, *24* (6), 725–735.
- (72) Brooks, M. L.; Meyer, J. S.; McKnight, D. M. Photooxidation of wetland and riverine dissolved organic matter: altered copper complexation and organic composition. *Hydrobiologia* **2007**, *579* (1), 95–113.
- (73) Rennert, T. Geogenic CO₂ affects inorganic soil properties and the composition of soil organic matter in physical fractions. *Soil Res.* **2018**, *56* (4), 396–403.
- (74) Lützw, M. v.; Kögel-Knabner, I.; Ekschmitt, K.; Matzner, E.; Guggenberger, G.; Marschner, B.; Flessa, H. Stabilization of organic matter in temperate soils: mechanisms and their relevance under different soil conditions—a review. *Eur. J. Soil Sci.* **2006**, *57* (4), 426–445.
- (75) Degryse, F.; Smolders, E.; Parker, D. Partitioning of metals (Cd, Co, Cu, Ni, Pb, Zn) in soils: concepts, methodologies, prediction and applications—a review. *Eur. J. Soil Sci.* **2009**, *60* (4), 590–612.
- (76) Bussert, R.; Kämpf, H.; Flechsig, C.; Hesse, K.; Nickschick, T.; Liu, Q.; Umlauf, J.; Vylita, T.; Wagner, D.; Wonik, T. Drilling into an active mofette: pilot-hole study of the impact of CO₂-rich mantle-derived fluids on the geo-bio interaction in the western Eger Rift (Czech Republic). *Sci. Drill.* **2017**, *23*, 13.
- (77) Langner, P.; Mikutta, C.; Kretzschmar, R. Arsenic sequestration by organic sulphur in peat. *Nat. Geosci.* **2012**, *5* (1), 66.
- (78) Glass, J.; Orphan, V. Trace Metal Requirements for Microbial Enzymes Involved in the Production and Consumption of Methane and Nitrous Oxide. *Front. Microbiol.* **2012**, *3*, Article 61.

Supporting Information

Environmental Science & Technology

Copper mobilization and immobilization along an organic matter and redox gradient – insights from a mofette site

Judith Mehlhorn,[†] Johannes Besold,[†] Juan S. Lezama Pacheco,[‡] Jon Petter Gustafsson,[§] Ruben Kretzschmar,^{||} Britta Planer-Friedrich,[†]*

[†]Environmental Geochemistry, Bayreuth Center for Ecology and Environmental Research (BayCEER), University of Bayreuth, D-95440 Bayreuth, Germany

[‡]Department of Environmental Earth System Science, Stanford University, Stanford, California 94305, United States

[§]Department of Soil and Environment, Swedish University of Agricultural Sciences, 75007 Uppsala, Sweden

^{||}Soil Chemistry Group, Institute of Biogeochemistry and Pollutant Dynamics, ETH Zurich, CHN, CH-8092 Zurich, Switzerland

(23 pages, 7 figures, 4 tables)

CONTENTS

| | | |
|------------|--|----|
| S.1 | Kinetic study on copper sorption | 2 |
| S.2 | Copper sorption isotherm – additional data | 5 |
| S.3 | Calculation of dissolved CO ₂ concentrations | 8 |
| S.4 | ¹³ C nuclear magnetic resonance (NMR) spectroscopy | 9 |
| S.5 | FTIR spectra of DOM extracts | 10 |
| S.6 | Soil mineralogy (XRD) | 12 |
| S.7 | SEM-EDS of Mofette A sample with highest Cu(II)-spike | 13 |
| S.8 | Information on XAS measurements and copper reference compounds | 15 |
| References | | 21 |

S.1 Kinetic study on copper sorption

Materials and Methods. Only Transition A1 and Reference A were used for the kinetic study. Soil was thawed overnight inside an anaerobic chamber (Coy, 95% N₂/5% H₂), then sieved and homogenized by pressing the wet soil through a 1 mm mesh size nylon sieve. The soil was weighted immediately into PP bottles in triplicate (dry weight equivalent approx. 3.4 g) and 100 mL of 5 mM NaCl (Merck, p.a.), pH 4.5, were added as background electrolyte (approx. soil-to-solution ratio of approx. 1:30). The suspensions were well-mixed, pH was adjusted to 4.5±0.1 with 1 M NaOH or 1 M HCl, and bottles were left to pre-equilibrate for 24 h with occasional shaking. Afterwards, 25 mL of the supernatant were removed and stabilized for total Cu determination by ICP-MS (0.2 µm cellulose-acetate filtration, stabilization in 0.45% H₂O₂ and 0.65% HNO₃) and dissolved organic carbon (DOC) analysis (0.45 µm polyamide filter, stored frozen till analysis) by thermo-catalytic oxidation with a TOC-V_{CPN} Analyzer (Shimadzu). The removed supernatant was replaced by 25 mL of a 1.57 mM CuCl₂ (Grüssing, p.a.) solution, pH 4.5, leading to a spike concentration of approx. 11.65 mmol kg⁻¹. The suspensions were well mixed and the pH was re-adjusted to 4.5±0.1 with 1 M NaOH or 1 M HCl. In addition to the triplicate sets of treatments, single soil blank samples (without Cu Spike) and a single chemical blank (without soil) were prepared. All bottles were wrapped in aluminum foil to exclude light.

Sampling took place after 10 min, 1, 3, 6, 12, 24, 48, 96, 167, and 365 h. First, pH and redox potential were determined directly in the suspensions. Except for the 10 min sampling, the bottles were centrifuged (5 min at 4500 g, outside glovebox) and between 2 and 3.5 mL of the supernatant were removed using needle and syringe. After filtration, the supernatant was stabilized for total Cu determination by ICP-MS. At the last sampling, additional 8 mL were stabilized for DOC analysis (stored frozen till analysis) to determine the amount of organic carbon that was mobilized during the course of the experiment. At 1, 24, and 365 h, we also tested whether a formation of Cu(I) had occurred during the experiment. We used an UV-vis spectroscopy method with bathocuproine as colorimetric reagent.^{1,2} However, no detectable amounts of Cu(I) could be determined over the course of the kinetic experiment. After the last sampling, the supernatant was removed completely and the remaining soil was freeze-dried, grinded, and analyzed on total Cu content after microwave assisted aqua regia digestion (MARS Xpress, CEM). The amount of Cu adsorbed was calculated from the difference between initial Cu spike and Cu concentration in solution.

Results and Discussion. Sorption equilibrium for both Transition A1 and Reference A was reached after 24–48 h, with a higher amount of Cu adsorbed in Reference A compared to Transition A1 (Figure S1a). Interestingly, the amount of Cu adsorbed decreased for Transition A1 and increased for Reference A during the course of the experiment. Concluding also from the other results of this study, two different processes seem to have occurred. The strong increase in dissolved organic carbon (DOC) of Transition A1 indicates that organic matter was mobilized from the solid phase. This was also optically visible by a strong brownish color of the filtered samples. Copper that was complexed with organic matter was remobilized by this process too which explains the observed decrease in Cu adsorbed for Transition A1. DOC increase also occurred for Reference A but to a way lower extent. However, the observed decrease in redox potential and increase in pH were stronger in Reference A (end pH: 6.1 ± 0.1 , end redox: 220 ± 3 eV) compared to Transition A1 (end pH: 5.4 ± 0.0 , end redox: 250 ± 6 eV, Figure S1b). Copper sorption increases with increasing pH due to decreasing protonation of sorption sites. Thus, the slow increase in pH could have led to the observed increase in Cu adsorbed. The same might have occurred in Transition A1 samples, however, the effect of Cu mobilization by DOC formation must have exceeded this process. Additionally, Cu reduction and precipitation in form of metallic Cu(0) or Cu sulfides, as observed for Mofette A and B in our sorption isotherm experiment, might have occurred under more and more reducing conditions in Reference A samples of the kinetic study as well.

Redox potential decrease and pH and DOC increase were even more pronounced for the soil blanks (redox potential at the end: -110 and -170 eV, end pH: 6.8 and 6.6, end TOC: 510 and 24 mg L^{-1} for Mofette and Reference blank, respectively; data not shown). This indicates an influence of microbial activity (proton consuming processes, like nitrate or Fe reduction), that was significantly slowed down in the Cu spiked samples due to the toxicity of Cu towards microorganisms.^{3,4}

Results from the kinetic study indicate that 24 h equilibration time were enough to achieve equilibrium conditions between solid phase and Cu^{2+} in solution. Longer equilibration times would additionally lead to changes in pH and redox potential, which would decrease comparability between soils.

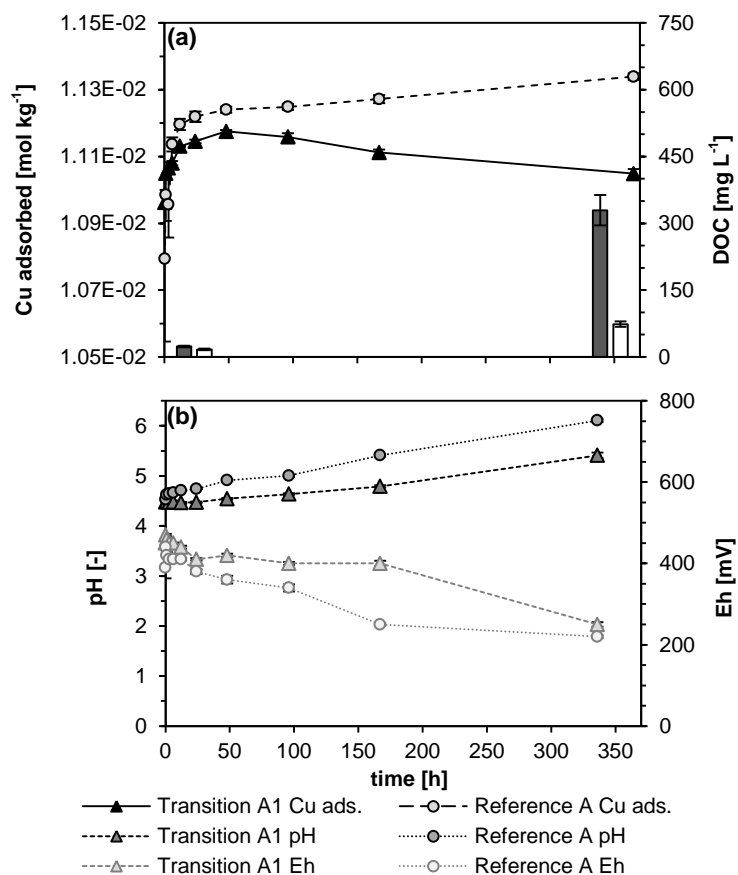


Figure S1. Results from kinetic study on Cu sorption to Transition A1 and Reference A soil. Experiments were conducted at pH 4.5 ± 0.1 at a solid-to-solution-ratio of approx. 1:30 with 5 mM NaCl as background electrolyte under anoxic conditions. Initial Cu soil concentrations are not included. **(a)** Amount of Cu adsorbed over time and DOC concentration in liquid phase for 0 and 365 h (bars). **(b)** Variation of pH and redox potential (Eh) in soil suspensions over time.

S.2 Copper sorption isotherm – additional data

pH in soil suspensions

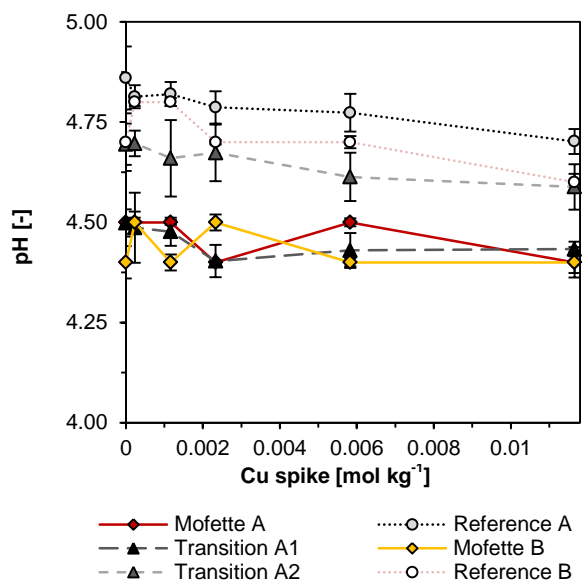


Figure S2. pH in soil suspensions after 24 h of equilibration with Cu(II) spike, initially adjusted pH of 4.5 ± 0.1 . Experiments were conducted at a solid-to-solution-ratio of approx. 1:30, with 5 mM NaCl as background electrolyte under anoxic conditions. Error bars represent standard deviation, $n=3$.

Organic C and N contents

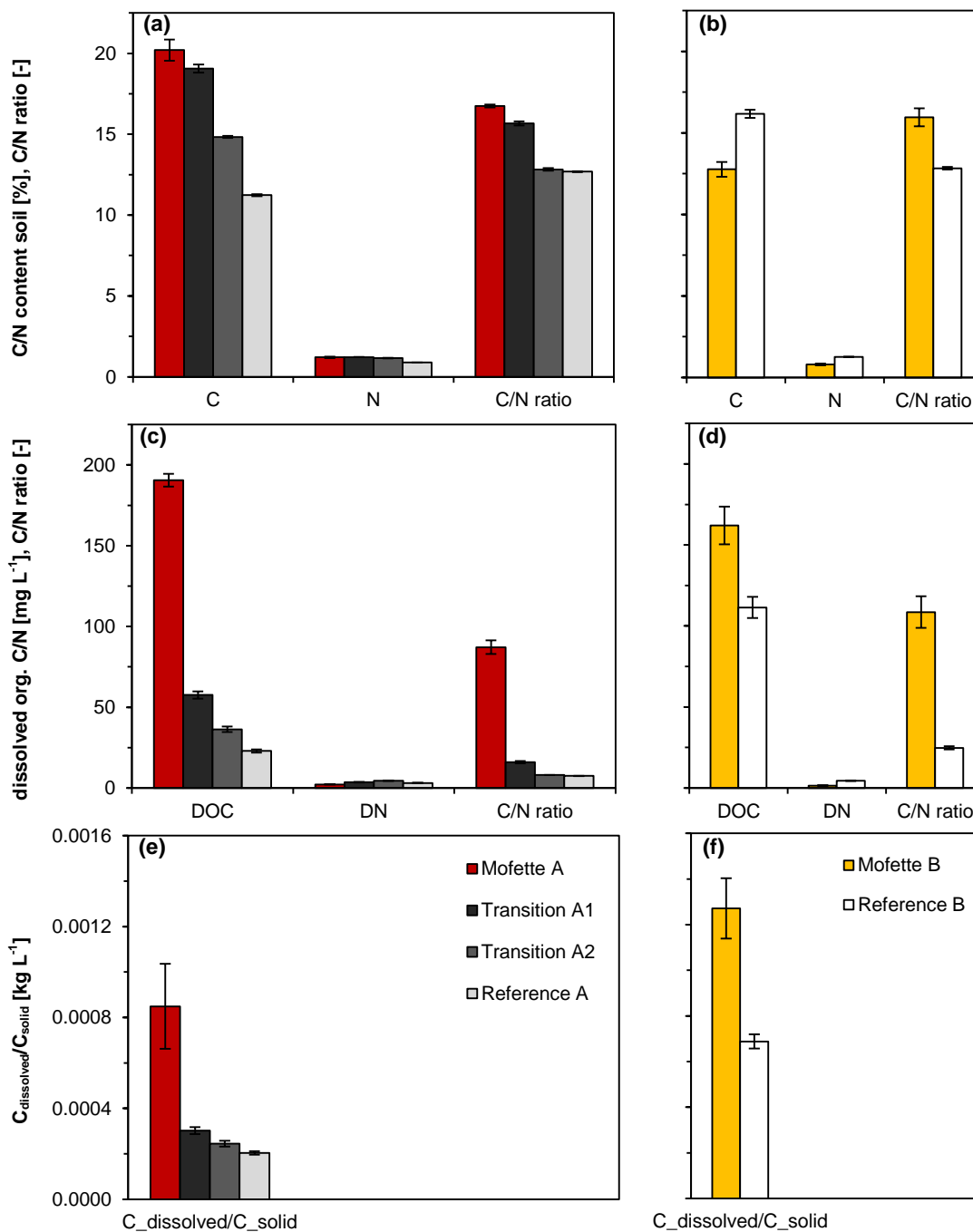


Figure S3. (a-b) Total organic C and N content and C/N ratio in soil samples of Site A and B. (c-d) Dissolved organic C (DOC) and N (DN) and C/N ratio determined after equilibration in liquid phase of soil suspensions that received the highest Cu(II) spike. (e-f) Molar ratio between DOC released into liquid phase during the isotherm experiment and total organic C in soil samples. Error bars represent standard deviation, n=3.

Organic Acids in Dissolved Organic Matter

The concentrations of the organic acids succinate, formiate, propionate, lactate, acetate, and butyrate were measured in single, filtered (0.2 μm , polyamide) liquid phase samples from the Cu sorption isotherm experiment for each soil. Since Cu might have caused interferences, the samples were already taken after the pre-equilibration step. Analysis was done with high performance liquid chromatography (1090 series II with RID detector, Hewlett Packard, Paolo Alto, USA) as described in Wüst et al.⁵

From the mentioned organic acids only lactate and acetate were present in low but detectable amounts (Table S1). Interestingly, we detected high amounts of a compound that according to retention time might have been ethanol, however, with the detector used, doubtless species identification was not possible. Differences between Site A and B might result from seasonal differences: while Site A was sampled directly after snowmelt in February 2017, Site B was sampled shortly after a relatively warm period in September 2017.

Table S1. Organic acid concentrations in liquid phase samples from Cu sorption isotherm experiment. The samples were taken after pre-equilibration but before Cu(II) spike addition to avoid Cu interferences.

| | Lactate [μM] | Acetate [μM] | Ethanol? [μM] |
|----------------------|---------------------------|---------------------------|----------------------------|
| <i>Mofette A</i> | 49 | 0 | 2023 |
| <i>Transition A1</i> | 55 | 44 | 379 |
| <i>Transition A2</i> | 48 | 134 | 262 |
| <i>Reference A</i> | 48 | 56 | 246 |
| <i>Mofette B</i> | 0 | 0 | 334 |
| <i>Reference B</i> | 0 | 192 | 2457 |

S.3 Calculation of dissolved CO₂ concentrations

The CO₂ concentrations in pore water samples from Site A were calculated from head space concentrations in septum bottles using Henry's law as described in the Materials and Methods section of the main text. This method worked well for samples from sites with low to moderate CO₂ influence (Transition and Reference) but CO₂ concentrations in pore water samples from the degassing center may have been underestimated due to the built-up of strong overpressure conditions in septum bottles containing these samples (observed during sampling of headspace gas phase). It is likely that the pore water in the degassing center was close to saturation or even oversaturated with regard to CO₂ due to permanent CO₂ purging, as observed in prior studies.^{6,7} Calculated concentrations of 18 to 22 mmol CO₂ L⁻¹ for samples from the degassing center are thus lower than expected (CO₂ saturation would correspond to approx. 33 mmol L⁻¹ assuming $k_{H,CO_2}=0.03344 \text{ mol L}^{-1} \text{ atm}^{-1}$ from Sander⁸). A correction of this potential error was not possible since the exact overpressure in every individual septum bottle remained unknown. However, despite this potential error, the overall trend presented in the main text (increasing Cu distribution coefficients with increasing dissolved CO₂ concentrations) remains unaffected.

S.4 ^{13}C nuclear magnetic resonance (NMR) spectroscopy

Two freeze-dried and pestled soil samples from “Transition A1” and “Reference A” were analyzed by solid-state ^{13}C nuclear magnetic resonance spectroscopy (NMR) using an Avance III HD spectrometer (Bruker) at a B_0 field 9.4 T. $^{13}\text{C}\{^1\text{H}\}$ (100.6 MHz) MAS spectra were obtained using a ramped cross-polarization (CP) experiment, where the nutation frequency ν_{nut} on the proton channel was varied linearly by 50%. The samples were spun at 12.5 kHz in a 4 mm MAS double resonance probe (Bruker). The corresponding ν_{nut} on the ^{13}C channel and the contact time were adjusted to 70 kHz and 3 ms, respectively. During acquisition proton broadband decoupling was applied using a spinal-64 sequence with $\nu_{\text{nut}}=70$ kHz. ^{13}C spectra are referenced indirectly with respect to tetramethylsilane (TMS) using adamantane as secondary reference. Relative contributions of various C groups were determined by integrating the signal intensity in the respective areas of chemical shift according to Hoffmann et al.⁹

S.5 FTIR spectra of DOM extracts

FTIR Materials and Methods. The DOM water extracts were filtered (0.45 μm , polyamide), freeze-dried, mixed with potassium bromide (KBr, Roth) in a ratio of 1:100, pressed into pellets, and analyzed for FTIR using a Vector 22 spectrometer (Bruker Optik). Measurements were conducted in transmission mode with a resolution of 2 cm^{-1} from 4500 to 300 cm^{-1} , 32 scans per sample were averaged and background corrected by subtracting the spectrum for pure KBr. Absorption band assignments are based on Artz et al.¹⁰ and Rennert et al.¹¹

Evaluation of FTIR spectra proved difficult since peak areas were partially influenced by mineral interferences. This made a semi-quantitative data evaluation, e.g. by calculation of humification indices as in Broder et al.¹² or by Lorentz peak fitting as in Rennert et al.¹¹, highly prone to errors. Therefore, we focused on differences between spectra concerning the occurrence and relative height of certain peaks and normalized all spectra to the peak at 1635 cm^{-1} (aromatic C=C stretching and asymmetric C-O stretching in COO^-), instead of using the mineral derived, highest peak at approx. 1030 cm^{-1} (stretching of Si-O), that differed strongly between samples.

FTIR band assignments. Transitions (A1, A2) and References (A, B) showed relatively similar spectra having main bands at approx. 1720 cm^{-1} (C=O stretching of carboxylic acids and aromatic esters), 1635 cm^{-1} (indicative for aromatics like lignin and aromatic or aliphatic carboxylates), 1550 cm^{-1} (carboxylic acids and amides), 1450 cm^{-1} (C-H deformations in phenolic and aliphatic structures), 1415 cm^{-1} (indicative for phenolic and aliphatic structures), 1380 cm^{-1} (stretching of deprotonated carboxyl or nitrate), 1245 cm^{-1} (indicative for C-O stretching and O-H deformation in phenols, like lignin), and 1095 cm^{-1} (C-O stretching and O-H deformation of polysaccharides). Spectra from Mofette A and B differed from the other soils: bands at approx. 1720 and 1240 cm^{-1} (indicative for lignin), 1450 cm^{-1} , and 1550 cm^{-1} were more pronounced whereas the band at 1095 cm^{-1} was less pronounced (Figure S4).

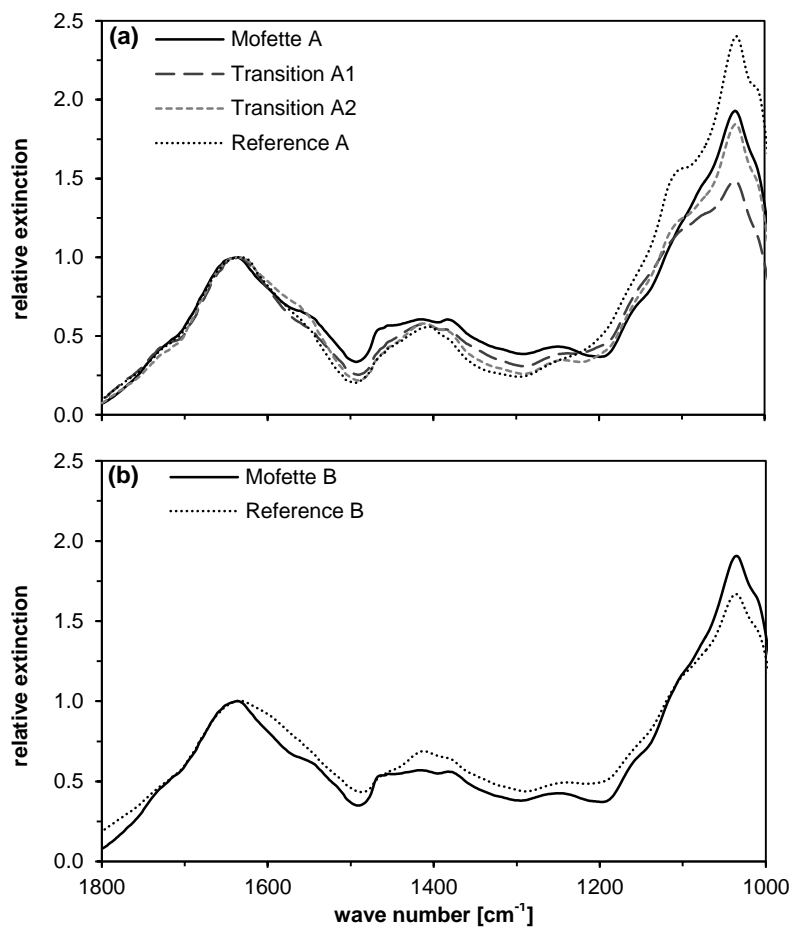


Figure S4. Detail from FTIR spectra of freeze-dried DOM water extracts from Site A (a) and Site B (b) normalized to the peak at 1635 cm⁻¹.

S.6 Soil mineralogy (XRD)

X-Ray diffractograms of samples from Transition A1 and Reference A showed similar peaks (Figure S5), indicating equal mineralogy in both samples, however with an overall higher mineral content in Reference A. We identified quartz, muscovite, feldspars (albite, anorthite, orthoclase), and clay minerals (kaolinite, chlorite), confirming results of former mineralogical analysis from this site.^{11,13}

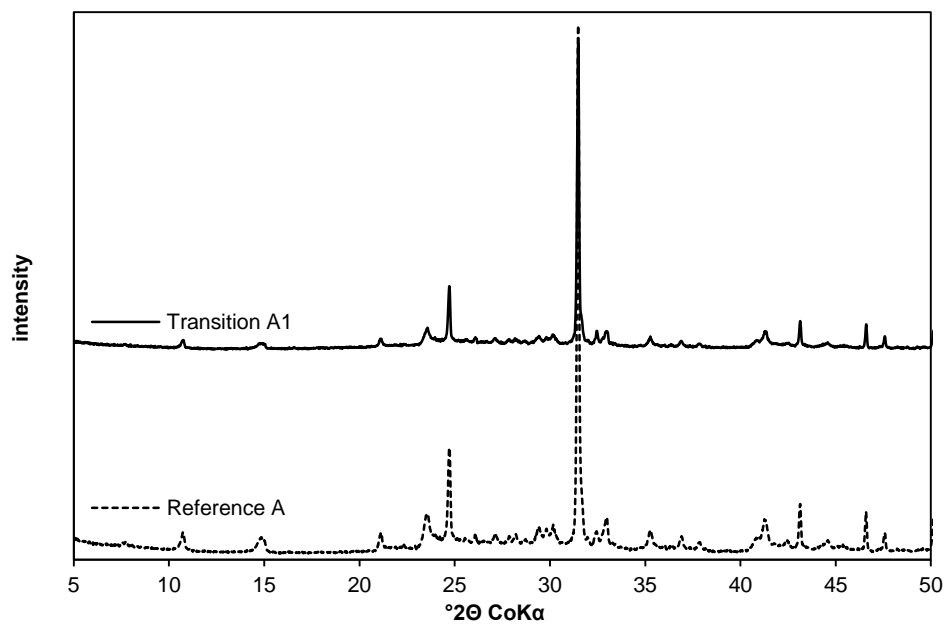


Figure S5. X-ray diffractograms of Transition A1 and Reference A.

S.7 SEM-EDS of Mofette A sample with highest Cu(II)-spike

One Cu-loaded sample of Mofette A was freeze-dried, homogenized, fixed on adhesive carbon tape, coated with carbon, and analyzed by scanning electron microscopy (SEM) in order to detect potential Cu precipitates using a Leo Gemini 1530 (Carl Zeiss, Germany) with a Schottky emitter. An accelerating voltage of 20.0 keV was used to produce images with a secondary electron as well as a backscatter electron detector. Elemental composition analysis was conducted by energy-dispersive X-ray spectrometry (EDS, Oxford X-Max 20, Oxford Instruments).

We could not detect any Cu sulfide minerals, probably because they would have still been in the nanosize fraction and/or in an amorphous state. However, we detected a small Cu-containing particle, that was most probably metallic Cu(0) according to its EDS spectrum (Figure S6). Other studies investigating the behavior of Cu in contaminated soils in response to flooding observed primarily the precipitation of metallic Cu(0), probably caused by microbially triggered reduction of Cu(II) to Cu(I) followed by disproportionation and precipitation of metallic Cu(0).¹⁴⁻¹⁷ Only later when microbial sulfate reduction started, Cu(I) was stabilized by complexation with sulfide or the previously formed Cu(0) was sulfidized and precipitated in form of Cu sulfides. The particle detected by SEM-EDS had a relatively large size when compared with the Cu nanoparticles observed in other studies¹⁴⁻¹⁷. Thus, it is likely that this particle was already present in the initial soil and did not form during our short-term (24 h) sorption experiment. X-ray absorption spectroscopy did not confirm the presence of metallic Cu in this sample, thus, contributions must have been small.

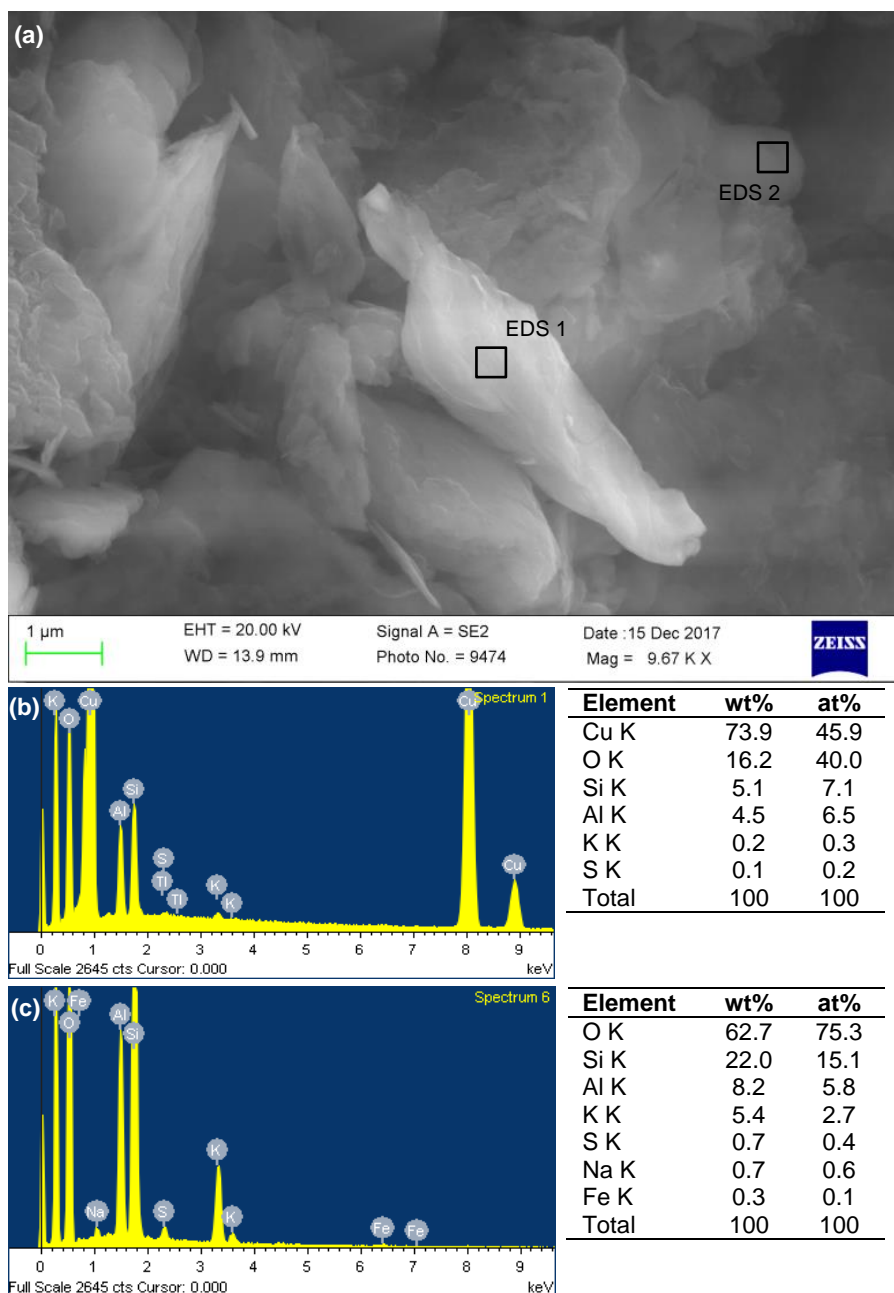


Figure S6. (a) SEM image of metallic Cu(0) particle in a sample from Mofette A after 24 h of equilibration with 11.65 mmol kg⁻¹ Cu(II). (b-c) Corresponding semi-quantitative EDS analyses from the Cu particle and the surrounding matrix. Due to small particle size mineral background in EDS 1 is still relatively high.

S.8 Information on XAS measurements and copper reference compounds

Sample Preparation. Samples for XAS analysis were freeze-dried, pestled, fixed in sample holders between Kapton® tape, and stored under anoxic conditions until analysis.

X-ray Absorption Spectroscopy. All spectra were collected at beamlines 4-1 and 4-3 at the Stanford Synchrotron Radiation Lightsource (SSRL, Stanford, USA). The measurements at beamline 4-3 (samples Transition A1, A2, Reference A, and peat lens) were performed at about 25 K using a closed cycle He-cryostat. The beamline was equipped with a 4-element solid-state Si drift detector (HTA Hitachi). Measurements at beamline 4-1 were done at 77 K using a 32-element solid-state Ge detector (Canberra) and a liquid nitrogen cryostat (samples from Mofette A). Detectors were calibrated by setting the first inflection of the K-absorption edge of a metallic Cu foil to 8979 eV. A combination of Ni and Al filters were used to reduce Fe fluorescence and scattering contributions. At beamline 4-1, we additionally used Soller slits and the monochromator was detuned to 70% of maximum intensity to reduce higher order harmonics in the beam. All sample spectra were collected in fluorescence mode (average of 1–2 scans per sample for XANES and 4–6 scans per sample for EXAFS, except peat lens: 12 scans), the metallic Cu foil was measured in transmission mode. In addition, published spectra were used as references for data analysis. The respective literature references, measurement conditions, and structural information can be found in Table S2.

XAS Data Processing. All spectra were processed using the software Athena¹⁸ and SixPACK.¹⁹ E_0 was fixed to 8988 eV. Background correction was performed by subtracting a first-order polynomial function fit to the pre-edge region (-150 to -40 eV) and subsequently dividing by a second-order polynomial fit to the post-edge region (80 to 490 eV for XANES; 80 to 700 eV for EXAFS). The background spline was adjusted using the Autobk algorithm (Rbkg=0.9; k -weight=3; k -range 0.5–14 Å⁻¹). Spectra were tested for the minimum number of components by principal component analysis (PCA) based on the empirical indicator function²⁰ and target transform was done for the significant components against the references library using the program SixPACK.¹⁹ SPOIL and chi-squared values as well as visual confirmation were used to evaluate whether a target was acceptable.^{20,21} Linear combination fitting (LCF) of the normalized XANES spectra in the energy range 8968–9018 eV and of the k^3 -weighted EXAFS spectra in the k -range 2.5–10 Å⁻¹ was done using the number of significant components (according to minimum of indicator value: 4 components for XANES and 2 components for

EXAFS LCF, Table S3) and reference spectra determined to be acceptable targets. Individual fractions were constrained to the range 0–1, the sum of fractions was not constrained. The best fit was chosen based on its normalized sum of squared residuals (NSSR), however, a fit with n components had to have a NSSR at least 10% lower than the respective fit with $n-1$ components, otherwise the fit with fewer components was considered.²² The quality of the combinations achieved with this method was tested using the Hamilton test²³ as described in Calvin²⁴. As proposed in Bennett et al.²⁵ we used the ‘information content’ value reported in Athena as estimate for the value a (half of the lower bound of the number of degrees of freedom of the closer fit) which is required for the Hamilton test. The ‘information content’ value is the magnitude of the fitted energy range divided by the core-hole lifetime of the absorption edge¹⁸ (28.1 eV in the case of the Cu K -edge). From the LCFs that did not differ significantly according to the Hamilton test, we chose the fit with the sum of components closest to 100% as best fit.

LCF of both XANES and EXAFS delivered contributions from reference compounds with the same oxidation state and coordination environment, however, in differing shares. Due to the better data quality of XANES (more data points, larger dataset), we focused our interpretation on XANES LCF results. Results from PCA can be found in Table S3, detailed results of LCF in Table S4.

Radiation Induced Reduction. In all measured samples, however, most pronounced for samples Transitions A1, A2, and Reference A, we observed radiation induced reduction (RIR) indicated by an increasing shoulder at 8982–8984 eV in the XANES spectra (exemplarily shown for Cu-loaded Reference A, Figure S7). This is, where oxygen bound Cu(I) would be expected to show a peak resulting from the $1s \rightarrow 4p$ transition.^{26,27} We cannot completely exclude that small amounts of Cu(I) were present in the initial soil samples, however, the height of this shoulder was increasing from scan to scan due to RIR which implies that Cu(I) in these three samples might be an artefact. We tried to reduce the effect of RIR on LCF by averaging only 1 to 2 scans per sample for evaluation of XANES data. Reduction of Cu(II) to Cu(I) due to beam damage has been observed in other studies as well,^{28,29} however, the problem mainly occurred when spectra collection was done at room temperature while our spectra were collected at 25 K. This implies that some Cu species highly sensitive to RIR must have been present in our samples.

Table S2. Structural information and literature references for Cu reference compounds used for LCF of XANES and EXAFS spectra. RT = room temperature.

| compound | measurement information | structural information from literature | | |
|-----------------------------|---|--|--------------|-------------------------------|
| | | coordination | distance [Å] | reference |
| <i>Cu metal</i> | SSRL beamline 4-1, RT | 12 Cu | 2.54 | Wyckoff ³⁰ |
| organic Cu(II)-O/N | | | | |
| <i>Cu(II)-humic</i> | spectrum from Fulda et al. ³¹ , 15 K | 4 O/N | 1.92–1.95 | Karlsson et al. ³² |
| <i>Cu(II)-malate</i> | spectrum from Fulda et al. ³¹ , 15 K | 4 O | 1.94 | Fulda et al. ³³ |
| <i>Cu(II)-carboxyl</i> | spectrum from Fulda et al. ³³ , 15 K | 4 O | 1.94 | Fulda et al. ³³ |
| inorganic Cu(II)-O/N | | | | |
| <i>Cu(II)-clay</i> | spectrum from Fulda et al. ³¹ , 77 K | 4 O | 1.95 | Strawn et al. ³⁴ |
| <i>Cu(II)-ferrihydrite</i> | spectrum from Tiberg et al. ³⁵ , RT | 4 O | 1.94–1.95 | Tiberg et al. ³⁵ |
| organic Cu(I)-S | | | | |
| <i>Cu(I)-thiol</i> | spectrum from Fulda et al. ³³ , 15 K | 2.9 S | 2.24 | Fulda et al. ³³ |
| <i>Cu(I)-GSH</i> | spectrum from Fulda et al. ³¹ , 77 K | 3 S 1 Cu | 2.26 2.69 | Poger et al. ³⁶ |
| inorganic Cu-S | | | | |
| <i>Cu_{1.8}S</i> | spectrum from Weber et al. ¹⁵ , RT | 3 S | 2.30 | Weber et al. ¹⁵ |
| <i>CuS</i> | spectrum from Fulda et al. ³¹ , 77 K | 3.67 S | 2.27 | Patrick et al. ³⁷ |

Table S3. Results from principal component analyses (PCA) of 9 normalized sample XANES spectra (energy range 8968–9018 eV) and 5 k^3 -weighted sample EXAFS spectra (k -range 2.5–10 Å⁻¹).

| compound | PCA XANES | | | PCA EXAFS | | |
|----------|-------------------|------------------------|-----------------------|------------|------------------------|------------------|
| | Eigenvalue | Cum. Var. ^a | IND ^b | Eigenvalue | Cum. Var. ^a | IND ^b |
| 1 | 1.97 | 0.987 | 1.30·10 ⁻⁴ | 28.66 | 0.842 | 0.149 |
| 2 | 0.02 | 0.999 | 1.23·10 ⁻⁵ | 4.74 | 0.981 | 0.026 |
| 3 | 10 ⁻² | 0.999 | 2.88·10 ⁻⁶ | 0.35 | 0.991 | 0.036 |
| 4 | <10 ⁻² | 0.999 | 1.52·10 ⁻⁶ | 0.15 | 0.996 | 0.131 |
| 5 | <10 ⁻² | 0.999 | 1.54·10 ⁻⁶ | 0.13 | 1.000 | NA |
| 6 | <10 ⁻² | 0.999 | 1.94·10 ⁻⁶ | | | |
| 7 | <10 ⁻² | 0.999 | 3.40·10 ⁻⁶ | | | |
| 8 | <10 ⁻² | 0.999 | 1.02·10 ⁻⁵ | | | |
| 9 | <10 ⁻² | 1.000 | NA | | | |

^acumulative variance

^bindicator function

Table S4. Comparison between Cu speciation in soil samples based on linear combination fitting (LCF) of Cu *K*-edge XANES and EXAFS. Individual fractions were constrained to values between 0 and 1, the sum of fractions was not constrained.

| XANES LCF | | | | | |
|-------------------|-------------------------------------|--------------------------------------|----------------|----------------|-----------------------------|
| | Cu(II)-O^a [%] | Cu(I)-S^b [%] | CuS [%] | SUM [%] | NSSR^c [%] |
| Mofette A | 23.3 (<i>humic</i>) | 72.0 (<i>thiol</i>) | - | 95.3 | 1.56 |
| Transition A1 | 90.8 (<i>humic</i>) | 8.4 (<i>Cu_{1,8}S</i>) | - | 99.2 | 0.14 |
| Transition A2 | 83.0 (<i>humic</i>) | 16.1 (<i>Cu_{1,8}S</i>) | - | 99.1 | 0.09 |
| Reference A | 83.0 (<i>humic</i>) | 16.7 (<i>Cu_{1,8}S</i>) | - | 99.7 | 0.07 |
| Mofette A, Cu | 73.4 (<i>humic, clay</i>) | 25.1 (<i>thiol</i>) | - | 98.5 | 0.06 |
| Transition A1, Cu | 97.9 (<i>mal</i>) | - | - | 97.9 | 0.04 |
| Transition A2, Cu | 96.7 (<i>humic, mal</i>) | 3.5 (<i>Cu_{1,8}S</i>) | - | 100.2 | 0.06 |
| Reference A, Cu | 99.1 (<i>humic, mal</i>) | - | - | 99.1 | 0.08 |
| Mofette A peat | 34.9 (<i>humic</i>) | - | 65.1 | 100.0 | 0.10 |
| EXAFS LCF | | | | | |
| | Cu(II)-O^a [%] | Cu(I)-S^b [%] | CuS [%] | SUM [%] | NSSR^c [%] |
| Mofette A, Cu | 61.9 (<i>clay</i>) | 23.9 (<i>Cu_{1,8}S</i>) | - | 85.5 | 5.6 |
| Transition A1, Cu | 94.2 (<i>humic, mal, carb</i>) | - | - | 94.2 | 2.5 |
| Transition A2, Cu | 94.2 (<i>humic, carb</i>) | - | - | 94.2 | 3.0 |
| Reference A, Cu | 89.1 (<i>humic, mal</i>) | - | - | 89.1 | 2.9 |
| Mofette A peat | 28.8 (<i>mal</i>) | - | 84.3 | 113.1 | 6.4 |

^a*humic*=Cu(II)-*humic*, *mal*=Cu(II)-*malate*, *carb*=Cu(II)-*carboxyl*, *clay*=Cu(II)-*clay*

^b*thiol*=Cu(I)-*thiol*, *GSH*=Cu(I)-*GSH*

^cnormalized sum of squared residuals = $\sum_i (\text{data}_{\text{exp}} - \text{data}_{\text{fit}})^2 / \sum_i (\text{data}_{\text{exp}})^2$

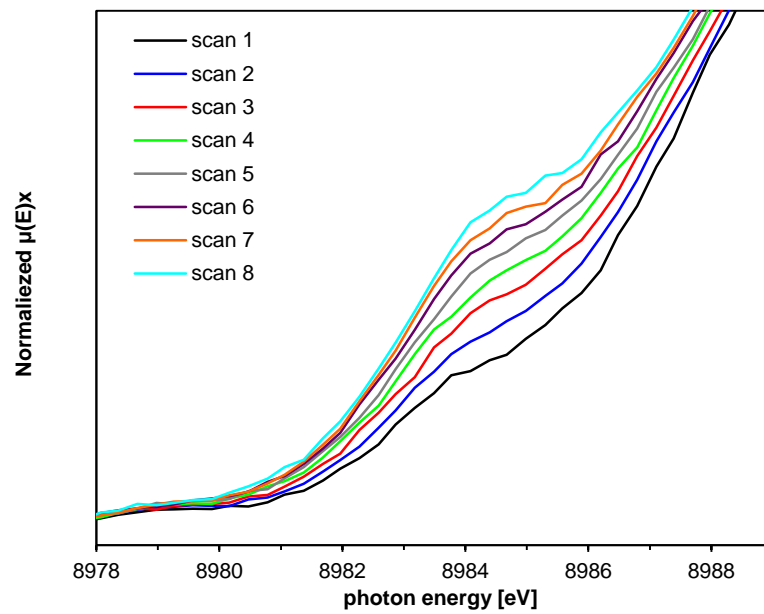


Figure S7. Detail from individual scans of the pre-edge region for Cu-loaded sample Reference A showing an increasing shoulder at 8982–8984 eV as a result of radiation induced reduction (RIR).

References

1. Maurer, F.; Christl, I.; Fulda, B.; Voegelin, A.; Kretzschmar, R., Copper redox transformation and complexation by reduced and oxidized soil humic acid. 2. Potentiometric titrations and dialysis cell experiments. *Environ. Sci. Technol.* **2013**, *47*, (19), 10912-10921.
2. Moffett, J. W.; Zika, R. G.; Petasne, R. G., Evaluation of bathocuproine for the spectrophotometric determination of copper(I) in copper redox studies with applications in studies of natural waters. *Anal. Chim. Acta* **1985**, *175*, 171-179.
3. Bååth, E., Effects of heavy metals in soil on microbial processes and populations (a review). *Water, Air, Soil Pollut.* **1989**, *47*, (3-4), 335-379.
4. Flemming, C.; Trevors, J., Copper toxicity and chemistry in the environment: a review. *Water, Air, Soil Pollut.* **1989**, *44*, (1-2), 143-158.
5. Wüst, P. K.; Horn, M. A.; Drake, H. L., In situ hydrogen and nitrous oxide as indicators of concomitant fermentation and denitrification in the alimentary canal of the earthworm *Lumbricus terrestris*. *Appl. Environ. Microbiol.* **2009**, *75*, (7), 1852-1859.
6. Beulig, F.; Heuer, V. B.; Akob, D. M.; Viehweger, B.; Elvert, M.; Herrmann, M.; Hinrichs, K.-U.; Küsel, K., Carbon flow from volcanic CO₂ into soil microbial communities of a wetland mofette. *ISME J.* **2015**, *9*, (3), 746-759.
7. Mehlhorn, J.; Beulig, F.; Küsel, K.; Planer-Friedrich, B., Carbon dioxide triggered metal(loid) mobilisation in a mofette. *Chem. Geol.* **2014**, *382*, 54-66.
8. Sander, R., Compilation of Henry's law constants (version 4.0) for water as solvent. *ACP* **2015**, *15*, (8).
9. Hoffmann, M.; Mikutta, C.; Kretzschmar, R., Bisulfide reaction with natural organic matter enhances arsenite sorption: insights from X-ray absorption spectroscopy. *Environ. Sci. Technol.* **2012**, *46*, (21), 11788-11797.
10. Artz, R. R.; Chapman, S. J.; Robertson, A. J.; Potts, J. M.; Laggoun-Défarge, F.; Gogo, S.; Comont, L.; Disnar, J.-R.; Francez, A.-J., FTIR spectroscopy can be used as a screening tool for organic matter quality in regenerating cutover peatlands. *Soil Biol. Biochem.* **2008**, *40*, (2), 515-527.
11. Rennert, T.; Eusterhues, K.; Pfanz, H.; Totsche, K. U., Influence of geogenic CO₂ on mineral and organic soil constituents on a mofette site in the NW Czech Republic. *Eur. J. Soil Sci.* **2011**, *62*, (4), 572-580.
12. Broder, T.; Blodau, C.; Biester, H.; Knorr, K., Peat decomposition records in three pristine ombrotrophic bogs in southern Patagonia. *Biogeosciences* **2012**, *9*, (4), 1479-1491.
13. Flechsig, C.; Bussert, R.; Rechner, J.; Schütze, C.; Kämpf, H., The Hartoušov mofette field in the Cheb Basin, western Eger Rift (Czech Republic): a comparative geoelectric, sedimentologic and soil gas study of a magmatic diffuse CO₂-degassing structure. *Z. Geol. Wiss.* **2008**, *36*, (3), 177-193.
14. Hofacker, A. F.; Voegelin, A.; Kaegi, R.; Weber, F.-A.; Kretzschmar, R., Temperature-dependent formation of metallic copper and metal sulfide nanoparticles during flooding of a contaminated soil. *Geochim. Cosmochim. Acta* **2013**, *103*, 316-332.
15. Weber, F.-A.; Voegelin, A.; Kaegi, R.; Kretzschmar, R., Contaminant mobilization by metallic copper and metal sulphide colloids in flooded soil. *Nat. Geosci.* **2009**, *2*, (4), 267-271.
16. Xia, B.; Qiu, H.; Knorr, K.-H.; Blodau, C.; Qiu, R., Occurrence and fate of colloids and colloid-associated metals in a mining-impacted agricultural soil upon prolonged flooding. *J. Hazard. Mater.* **2018**, *348*, 56-66.

17. Hofacker, A. F.; Behrens, S.; Voegelin, A.; Kaegi, R.; Lösekann-Behrens, T.; Kappler, A.; Kretzschmar, R., *Clostridium* species as metallic copper-forming bacteria in soil under reducing conditions. *Geomicrobiol. J.* **2015**, *32*, (2), 130-139.
18. Ravel, B.; Newville, M., ATHENA, ARTEMIS, HEPHAESTUS: data analysis for X-ray absorption spectroscopy using IFEFFIT. *J. Synchrotron Rad.* **2005**, *12*, (4), 537-541.
19. Webb, S., SIXpack: a graphical user interface for XAS analysis using IFEFFIT. *Phys. Scr.* **2005**, *2005*, (T115), 1011.
20. Malinowski, E. R., Determination of the number of factors and the experimental error in a data matrix. *Anal. Chem.* **1977**, *49*, (4), 612-617.
21. Beauchemin, S.; Hesterberg, D.; Beauchemin, M., Principal component analysis approach for modeling sulfur K-XANES spectra of humic acids. *Soil Sci. Soc. Am. J.* **2002**, *66*, (1), 83-91.
22. Jacquat, O.; Voegelin, A.; Kretzschmar, R., Soil properties controlling Zn speciation and fractionation in contaminated soils. *Geochim. Cosmochim. Acta* **2009**, *73*, (18), 5256-5272.
23. Hamilton, W. C., Significance tests on the crystallographic *R* factor. *Acta Crystallogr.* **1965**, *18*, (3), 502-510.
24. Calvin, S., *XAFS for Everyone*. CRC press: 2013.
25. Bennett, W. W.; Hockmann, K.; Johnston, S. G.; Burton, E. D., Synchrotron X-ray absorption spectroscopy reveals antimony sequestration by reduced sulfur in a freshwater wetland sediment. *Environ. Chem.* **2017**, *14*, (6), 345-349.
26. Manceau, A.; Matynia, A., The nature of Cu bonding to natural organic matter. *Geochim. Cosmochim. Acta* **2010**, *74*, (9), 2556-2580.
27. Kau, L. S.; Spira-Solomon, D. J.; Penner-Hahn, J. E.; Hodgson, K. O.; Solomon, E. I., X-ray absorption edge determination of the oxidation state and coordination number of copper. Application to the type 3 site in *Rhus vernicifera* laccase and its reaction with oxygen. *J. Am. Chem. Soc.* **1987**, *109*, (21), 6433-6442.
28. Strawn, D. G.; Baker, L. L., Speciation of Cu in a contaminated agricultural soil measured by XAFS, μ -XAFS, and μ -XRF. *Environ. Sci. Technol.* **2007**, *42*, (1), 37-42.
29. Strawn, D. G.; Baker, L. L., Molecular characterization of copper in soils using X-ray absorption spectroscopy. *Environ. Pollut.* **2009**, *157*, (10), 2813-2821.
30. Wyckoff, R. W. G., *Crystal structures*. Interscience New York: 1960; Vol. 2.
31. Fulda, B.; Voegelin, A.; Ehlert, K.; Kretzschmar, R., Redox transformation, solid phase speciation and solution dynamics of copper during soil reduction and reoxidation as affected by sulfate availability. *Geochim. Cosmochim. Acta* **2013**, *123*, 385-402.
32. Karlsson, T.; Persson, P.; Skyllberg, U., Complexation of copper(II) in organic soils and in dissolved organic matter – EXAFS evidence for chelate ring structures. *Environ. Sci. Technol.* **2006**, *40*, (8), 2623-2628.
33. Fulda, B.; Voegelin, A.; Maurer, F.; Christl, I.; Kretzschmar, R., Copper redox transformation and complexation by reduced and oxidized soil humic acid. 1. X-ray absorption spectroscopy study. *Environ. Sci. Technol.* **2013**, *47*, (19), 10903-10911.
34. Strawn, D. G.; Palmer, N. E.; Furnare, L. J.; Goodell, C.; Amonette, J. E.; Kukkadapu, R. K., Copper sorption mechanisms on smectites. *Clays Clay Miner.* **2004**, *52*, (3), 321-333.
35. Tiberg, C.; Sjöstedt, C.; Persson, I.; Gustafsson, J. P., Phosphate effects on copper(II) and lead(II) sorption to ferrihydrite. *Geochim. Cosmochim. Acta* **2013**, *120*, 140-157.
36. Poger, D.; Fillaux, C.; Miras, R.; Crouzy, S.; Delangle, P.; Mintz, E.; Den Auwer, C.; Ferrand, M., Interplay between glutathione, Atx1 and copper: X-ray absorption spectroscopy

determination of Cu(I) environment in an Atx1 dimer. *J. Biol. Inorg. Chem.* **2008**, *13*, (8), 1239-1248.

37. Patrick, R.; Mosselmans, J.; Charnock, J.; England, K.; Helz, G.; Garner, C.; Vaughan, D., The structure of amorphous copper sulfide precipitates: An X-ray absorption study. *Geochim. Cosmochim. Acta* **1997**, *61*, (10), 2023-2036.

LIST OF PUBLICATIONS

The following publications/manuscripts have been published or are submitted during the work on this thesis:

Mehlhorn, J., Gerber, L.A., Planer-Friedrich, B. (2018): Spatial distribution of metal(loid) depletion and accumulation zones around a natural carbon dioxide degassing site. *Chemical Geology*, 509: 64-76, DOI: 10.1016/j.chemgeo.2019.01.010.

Mehlhorn, J., Besold, J., Lezama-Pacheco, J.S., Gustafsson, J.P., Kretzschmar, R., Planer-Friedrich, B. (2018): Copper mobilization and immobilization along an organic matter and redox gradient – insights from a mofette site. *Environmental Science & Technology*, 52(23): 13698-13707, DOI: 10.1021/acs.est.8b02668.

Mehlhorn, J., Byrne, J.M., Kappler, A., Planer-Friedrich, B. (2016): Time and temperature dependency of carbon dioxide triggered metal(loid) mobilization in soil. *Applied Geochemistry*, 74: 122-137, DOI: 10.1016/j.apgeochem.2016.09.007.

Other publications:

Planer-Friedrich, B., Schaller, J., Wismeth, F., Mehlhorn, J., Hug, S. J. (2018): Monothioarsenate occurrence in Bangladesh groundwater and its removal by ferrous and zero-valent iron technologies. *Environmental Science & Technology*, 52(10): 5931-5939, DOI: 10.1021/acs.est.8b00948.

Suess, E., Mehlhorn, J., Planer-Friedrich, B. (2015): Anoxic, ethanolic, and cool – An improved method for thioarsenate preservation in iron-rich waters. *Applied Geochemistry*, 62: 224-233, DOI: 10.1016/j.apgeochem.2014.11.017.

Mehlhorn, J., Beulig, F., Küsel, K., Planer-Friedrich, B. (2014): Carbon dioxide triggered metal(loid) mobilisation in a mofette. *Chemical Geology*, 382: 54-66, DOI: 10.1016/j.chemgeo.2014.05.027.

SUPERVISED BACHELOR THESES

The following Bachelor theses have been co-supervised during the work on this thesis:

1. Metz, R. (2016): Influence of CO₂ on mobilization of Fe and As by abiotic and microbially triggered dissolution of ferrihydrite, Bachelor Thesis, University of Bayreuth, Environmental Geochemistry.

Results of this project are included in chapter 3.2 of this thesis.

2. Gerber, L. A. (2018): Räumliche Verteilungsmuster von Metall(oid)en im Bereich einer Mofette, Bachelor Thesis, University of Bayreuth, Environmental Geochemistry.

Results of this project are included in study 1 of this thesis.

(EIDESSTATTLICHE) VERSICHERUNGEN UND ERKLÄRUNGEN

(§ 8 Satz 2 Nr. 3 PromO Fakultät)

Hiermit versichere ich eidesstattlich, dass ich die Arbeit selbstständig verfasst und keine anderen als die von mir angegebenen Quellen und Hilfsmittel benutzt habe (vgl. Art. 64 Abs. 1 Satz 6 BayHSchG).

(§ 8 Satz 2 Nr. 3 PromO Fakultät)

Hiermit erkläre ich, dass ich die Dissertation nicht bereits zur Erlangung eines akademischen Grades eingereicht habe und dass ich nicht bereits diese oder eine gleichartige Doktorprüfung endgültig nicht bestanden habe.

(§ 8 Satz 2 Nr. 4 PromO Fakultät)

Hiermit erkläre ich, dass ich Hilfe von gewerblichen Promotionsberatern bzw. -vermittlern oder ähnlichen Dienstleistern weder bisher in Anspruch genommen habe noch künftig in Anspruch nehmen werde.

(§ 8 Satz 2 Nr. 7 PromO Fakultät)

Hiermit erkläre ich mein Einverständnis, dass die elektronische Fassung der Dissertation unter Wahrung meiner Urheberrechte und des Datenschutzes einer gesonderten Überprüfung unterzogen werden kann.

(§ 8 Satz 2 Nr. 8 PromO Fakultät)

Hiermit erkläre ich mein Einverständnis, dass bei Verdacht wissenschaftlichen Fehlverhaltens Ermittlungen durch universitätsinterne Organe der wissenschaftlichen Selbstkontrolle stattfinden können.

.....
Ort, Datum, Unterschrift